



**ASEAN-JAPAN COOPERATION
ON MATERIALS SCIENCE AND TECHNOLOGY**

**SEMINAR ON CORROSION
AND PROTECTION**

BANGKOK , THAILAND

17-19 OCTOBER 1990

b20-193
:b20-197
AS

SPONSORED BY: JAPAN INTERNATIONAL COOPERATION AGENCY

**ORGANISED BY: THAILAND INSTITUTE OF SCIENTIFIC
AND TECHNOLOGICAL RESEARCH**

LIST OF CONTENTS

Programme

Welcome address and Report by governor of TISTR

Address by the Embassy of Japan

Opening address by Minister of MOSTE

List of participants

List of papers

1. Atmospheric Corrosion Monitoring
2. The Use of Acoustic Emission in Monitoring Corrosion
3. Degradation of Coatings and Its Evaluation by AC Impedance and Photo Acoustic Methods
4. Atmospheric Roof Corrosion in the Communities that Surround the Makban Geothermal Facilities in the Philippines
5. Atmospheric Corrosion in Jakarta
6. Inhibition by Azelates on Contaminated Steel
7. Investigation on Anti - Corrosion Paint Coating Using Salt Evaluation Technique
8. New Type LB Films of Polyallylamine Containing Trifluoroacetic Acids by Ionic Bonds
9. A Study of the Permeability of Ions to Organic Coatings
10. The Overall Corrosion Monitoring System
11. The Determination of Film Resistance by Means of the Frequency at the Maximum Phase Angle and the Estimation of the Degradation of the Coating Film
12. Corrosion Resistance of Various Coating Materials on Steels Buried in Soil
13. Deterioration of Various Paints in Aqueous Acetic Acid Solution
14. Corrosion Problem in Petroleum Refinery
15. Ambient Acid Rain Precursor Concentration and Emission in Samutprakarn Industrial District
16. Corrosion of Steel Reinforcing Bars in Marine Environment

17. Effect of Crack Sizes on Corrosion of Reinforced Concrete Structures Subjected to Marine Environment
18. Material Selection of Fiber Reinforced Plastic (FRP) for Corrosion Resistance
19. The Chlorination and Oxidation Process of Nickel and Nickel Based Alloys at Elevated Temperature
20. Painting Systems for Heavy Duty Coatings
21. Stress Corrosion Cracking in Stainless Steel Piping Materials 304 and 321 and Weldment
22. Using of Amino Tri (Methylene Phosphoric Acid) and 1 - Hydroxy Ethylene - 1, 1 - Phosphoric Acid as Chemical Cleaning Condenser Tube
23. Paper from Brunei
24. Paper from Malaysia

PROGRAMME
ASEAN-JAPAN COOPERATION ON MATERIALS SCIENCE & TECHNOLOGY
SEMINAR ON CORROSION AND PROTECTION
ON
17-19 OCTOBER 1990
AT
PLEONCHIT HALL , IMPERIAL HOTEL
BANGKOK , THAILAND

DAY 1, WEDNESDAY 17 OCTOBER 1990

08:30 - 08:55	Registration of all Participants
09:00	Arrival of Guest of Honour
09:00 - 09:15	Welcome address and Report by governor of TISTR
09:15 - 09:30	Address by the Embassy of Japan
09:30 - 09:45	Opening address by Minister of MOSTE
09:45 - 10:00	Coffee Break
10:00 - 10.40	"Atmospheric Corrosion Monitoring" by Dr.Ladawal Chotimongkol, TISTR , <u>Thailand</u>
10:40 - 11:10	"The Use of Acoustic Emission in Monitoring Corrosion" by Dr. Winston Seah Kar Heng, National University of Singapore , <u>Singapore</u>
11:10 - 12:10	"Degradation of Coatings and Its Evaluation by AC Impedance and Photo Acoustic Methods" by Prof. Tooru Tsuru, Tokyo Institute of Technology , <u>Japan</u>
12:10 - 13:30	Lunch
13:30 - 14:00	"Atmospheric Roof Corrosion in the Communities that Surround the Makban Geothermal Facilities in the Philippines" by Dr. Ernesto S.Luis, Industrial Technology Development Institute, <u>Philippines</u>

- 14:00 - 14:30 "Atmospheric Corrosion in Jakarta" by Mr. Iing Musalam, R & D Centre for Metallurgy-Kompleks Puspiptek Serpong, Indonesia
- 14:30 - 15:00 "Inhibition by Azelates on Contaminated Steel" by Ms.Hasnah Abdul Wahab, Standard & Industrial Research Institute of Malaysia, Malaysia
- 15:00 - 15:20 Coffee Break
- 15:20 - 15:50 Paper from Malaysia
- 15:50 - 16:20 "Investigation on Anti-Corrosion Paint Coating Using Salt Evaluation Technique" by Dr.Sukumar Jana, Nanyang Technological Institute, Singapore
- 16:20 - 16:50 Paper from Brunei
- 16:50 - 17:20 "New Type LB Films of Polyallylamine Containing Trifluoroacetic Acids by Ionic Bonds" by Ms.Rungthip Chaiwattananone , TISTR , Thailand

DAY 2, THURSDAY 18 OCTOBER 1990

- 9:00 - 9:30 "A Study of the Permeability of Ions to Organic Coatings" by Ms. Cynthia R. Habana, Industrial Technology Development Institute, Philippines
- 9:30 - 10:00 "The Overall Corrosion Monitoring System" by Mr.Chaicharearn Atibaedya, Petroleum Authority of Thailand, Thailand
- 10:00 - 10:20 Coffee Break
- 10:20 - 11:20 - "The Determination of Film Resistance by Means of the Frequency at the Maximum Phase Angle and the Estimation of the Degradation of the Coating Film"
- "Corrosion Resistance of Various Coating Materials on Steels Buried in Soil"

- "Deterioration of Various Paints in Aqueous Acetic Acid Solution" by Mr. Isao Sekine, Science University of Tokyo, Japan
- 11:20 - 11:50 "Corrosion Problem in Petroleum Refinery" by Dr. Chanvootti Tangchitvittaya, ESSO Standard Thailand Ltd., Thailand
- 11:50 - 13:30 Lunch
- 13:30 - 14:00 "Ambient Acid Rain Precursor Concentration and Emission in Samutprakarn Industrial District" by Dr. Supat Wangwongwatana, Office of the National Environment Board, Thailand
- 14:00 - 14:30 "Corrosion of Steel Reinforcing Bars in Marine Environment" by Mr. Opad Orasaroaj, Jotun Thailand Co.,Ltd., Thailand
- 14:30 - 15:00 "Effect of Crack Sizes on Corrosion of Reinforced Concrete Structures Subjected to Marine Environment" by Dr. Ekasit Limsuwan, Chulalongkorn University, Thailand
- 15:00 - 15:20 Coffee Break
- 15:20 - 15:50 "Material Selection of Fiber Reinforced Plastic (FRP) for Corrosion Resistance" by Dr. Somsak Naviroj, Asia Glassfiber Industries Co.,Ltd. Thailand
- 15:50 - 16:20 "The Chlorination and Oxidation Process of Nickel and Nickel Based Alloys at Elevated Temperature" by Dr. Somchai Tongtem, Chiang-Mai University, Thailand
- 16:20 - 16:50 "Painting Systems for Heavy Duty Coatings" by Mr. Viniij La-onsuwan, T.O.A. Paint (Thailand) Co., Ltd., Thailand

DAY 3, FRIDAY 19 OCTOBER 1990

- 9:00 - 9:30 "Stress Corrosion Cracking in Stainless Steel Piping Materials 304 and 321 and Weldment" by Mr. Narong Sukapaddhi, Thai Oil Co.,Ltd., Thailand
- 9:30 - 10:00 "Using of Amino Tri(Methylene Phosphoric Acid) and 1-Hydroxy Ethylene-1, 1-Phosphoric Acid as Chemical Cleaning Condenser Tube" by Mr.Kasem Chudthong, EGAT, Thailand
- 10:00 - 10.20 Coffee Break
- 10:20 - 12.00 Discussion
- 12:00 - 17.00 Corrosion Laboratory and Factory Visit
(Lunch Box)

ASEAN JAPAN COOPERATION PROGRAMME ON
MATERIALS SCIENCE AND TECHNOLOGY
SEMINAR ON CORROSION AND PROTECTION
17th - 19th October 1990

LIST OF SPEAKERS

Dr. Ladawal Chotimongkol
Director of Metal and Material Technology Department
Thailand Institute of Scientific and Technological Research
Bangkhen, Bangkok 10900

Dr. Winston Seah Kar Heng
Senior Lecturer
Mechanical & Production Engineering
National University of Singapore

Mr. Tooru TSURU
Professor, Tokyo Institute of Technology

Dr. Ernesto S. Luis
Deputy Director
Industrial Technology Development Institute
Department of Science & Technology
P. Gil, Taft Ave., Manila Philippines

Mr. Iing Musalam
Chief of Atmospheric Corrosion Lab
R & D Centre for Metallurgy-Kompleks Puspiptek Serpong, Indonesia

Ms. Hasnah Abd. Wahab
Senior Research Officer Metal Protection and Finishing Unit
Standard & Industrial Research Institute of Malaysia (SIRIM)

Paper from Malaysia

Dr. Sukumar Jana

Senior Lecturer

Nanyang Technological Institute, Singapore 2263

Paper from Brunei

Ms. Rungthip Chaiwattananone

Researcher ,Chemical Formulation and Processing Lab.

Chemical Industry Department

Thailand Institute of Scientific and Technological Research

Bangkheng ,Bangkok 10900

Ms. Cynthia R. Habana

Specialist

Industrial Technology Development Institute

Department of Science & Technology

P. Gil, Taft Ave., Manila Philippines

Mr. Chaicharearn Atibaedya

Deputy Director of Technical Service Department

Petroleum Authority of Thailand

Petroleum Authority of Thailand Building, 17th floor

555 Vipavadee Rangsit Rd., Bangkok 10900

Mr. Isao SEKINE

Professor, Faculty of Science and Technology,

Science University of Tokyo

Dr. Chanvootti Tangchitvittaya
Project Implementation Manager
ESSO Standard Thailand Ltd.
P.O BOX 18, Sriracha, Cholburi 20110

Dr. Supat Wangwongwatana
Chief of Industrial Air Pool Section
Office of the National Environment Board
60/1 Soi Phibunwatana 7, Rama VI, Bangkok 10400

Mr. Opad Orasaroaj
Technical Service Manager
Jotun Thailand Ltd.
8th floor, Orakan Building, 26 Soi Chidlom, Ploenchit Rd., Bangkok

Dr. Ekasit Limsuwan
Professor, Chulalongkorn University, Bangkok

Dr. Somsak Naviroj
President of Asia Glassfiber Industries Co., Ltd.
80-86 Asok-dindaeng Rd., Huai-khwang, Bangkok 10310

Dr. Somchai Tongtem
Associate Professor
Faculty of Science, Chiang-Mai University, Chiang-Mai

Mr. Vinij La-ongsuwan
Technical Manager
T.O.A. Paint (Thailand) Co., Ltd.
104 Soi Pukmitr, Poochaosamingpri Rd, Samrongtai,
Samuthprakarn. 10270

Mr. Narong Sukapaddhi

Senior Metallurgist

Thai Oil Co., Ltd., Sriracha Refinery

Mr. Kasem Chudthong

Chemist, Electricity Generating Authority of Thailand

Bangkruay, Nonthaburi 11000

ASEAN JAPAN COOPERATION PROGRAMME ON
MATERIALS SCIENCE AND TECHNOLOGY
SEMINAR ON CORROSION AND PROTECTION
17th - 19th October 1990

LIST OF PARTICIPANTS

ASEAN

Mr. Mohamad Zin bin Awang Haji Selleh
Head of Structural Section
Public Works Department, Ministry of Development
Bandar Seri Begawan 2060, Brunei Darussalam

Mr. Hamiddon bin Hj Md Said
Research Engineer, Corrosion Unit of Structural Section
Public Works Department, Ministry of Development
Bandar Seri Begawan 2060, Brunei Darussalam

Mr. Hj Md. Jumin bin Hj. Marsal
Assistant Director (Development)
Public Works Department, Ministry of Development
Bandar Seri Begawan 2060, Brunei Darussalam

Ms. Lee Siow Hung
Research Engineer
Public Works Dept., Brunei Darussalam

Mr. Wahyudin
Head of Metal Technology Division
R & D Centre for Metallurgy, Jalan Cisitu kompleks LIPI,
Bandung 40135, Indonesia

Mr. Iing Musalam
Chief of Atmospheric Corrosion Lab
R & D Centre for Metallurgy-Kompleks Puspiptek Serpong, Indonesia

Mr. A. Sulaiman
Head of corrosion Division
R & D Centre for Metallurgy-LIPI
Jalan Cisit, Bandung 40135, Indonesia

Ms. Ratnawati Kardjana
Head of Section
Ir. Suprpto Sangkuriang 14, Bandung, Indonesia

Ms. Hasnah Abd. Wahab
Senior Research Officer Metal Protection and Finishing Unit
Standard & Industrial Research Institute of Malaysia (SIRIM)

Mr. Mohd Radzi Mohd Toss
Research officer
Standard & Industrial Research Institute of Malaysia (SIRIM)

Dr. Kamarudin Ab. Malek
Research officer
Rubber Research Institute of Malaysia (RRIM)

Mr. Mohd Zahri Bin Amat Sarbini
Technician
Standard & Industrial Research Institute of Malaysia (SIRIM)

Dr. Ernesto S. Luis
Deputy Director
Industrial Technology Development Institute
Department of Science & Technology
P. Gil, Taft Ave., Manila Philippines

Ms. Chona I. Dela Pena
Science Reseacher
Industrial Technology Development Institute
Department of Science & Technology
P. Gil, Taft Ave., Manila Philippines

Ms. Cynthia R. Habana
Specialist
Industrial Technology Development Institute
Department of Science & Technology
P. Gil, Taft Ave., Manila Philippines

Ms. Eden Luna Enriquez
Specialist, Industrial Technology Development Institute
Bicutan, Taguig M.M., Philippines

Dr. Tam Chat Tim
Associate Professor
Civil Engineering Dept., National University of Singapore
Lower Kent Ridge Crescent, Singapore 0511

Dr. Sukumar Jana
Senior Lecturer
Nanyang Technological Institute, Singapore 2263

Dr. Winston Seah Kar Heng
Senior Lecturer
Mechanical & Production Engineering
National University of Singapore

Mr. Loh Swee Heng
Exec structural Engrg., Structural Engrg. Dept.
Singapore

Dr. Ladawal Chotimongkol
Director of Metal and Material Technology Department
Thailand Institute of Scientific and Technological Research
Bangkhen, Bangkok 10900

Dr. Monthop Valayapetre
Chief of Metallurgical Development Section
Department of Mineral Resource
Rama VI, Bangkok 10400

Dr. Panya Srichan
Lecturer, Material Technology Department,
King Mongkut Institute of Technology Thorburi
Prachautip Rd., Bangmod, rachburana, Bangkok 10140

Mr. Wikrom Vajragapta
Lecturer, Metallurgical Engineering Department,
Chulalongkorn University
Phyatai Rd., Bangkok

Ms. Wanasri Samanasena
Thailand-COST Secretary,
National Research Council of Thailand
196 Phaholyothin Rd., Bangkhen, Bangkok 10900

JAPAN

Mr. Isao SEKINE

Professor, Faculty of Science and Technology,
Science University of Tokyo

Mr. Tooru TSURU

Professor, Tokyo Institute of Technology

Mr. Shigeki Kirihara

JICA Long-term Expert on Atmospheric Corrosion
JAPAN-ASEAN Cooperation on Science and Technology in Thailand

Ms. Mineko Sato

JICA Long-term Expert on Atmospheric Corrosion
JAPAN-ASEAN Cooperation on Science and Technology in Thailand

Mr. Hideo Nagai

JICA Long-term Expert on Atmospheric Corrosion
JAPAN-ASEAN Cooperation on Science and Technology in Thailand

Mr. Tetsuya Miwa

Assistant Resident Representative
JICA Thailand office

THAILAND

Dr. Siwa Bhongbhibhat

Managing Director

Siwa Testing Inspection and Consulting Co., Ltd.

17/1 St Louis Soi 3 South Sathorn Rd. Bangkok 10120

Mr. Viniij La-ongsuwan

Technical Manager

T.O.A. Paint (Thailand) Co., Ltd.

104 Soi Pukmitr, Poochaosamingpri Rd, Samrongtai,
Samuthprakarn. 10270

Mr. Narong Sukapaddhi

Senior Metallurgist

Thai Oil Co., Ltd., Sriracha Refinery

Mr. Chaicharearn Atibaedya

Deputy Director of Technical Service Department

Petroleum Authority of Thailand

Petroleum Authority of Thailand Building, 17th floor
555 Vipavadee Rangsit Rd., Bangkok 10900

Dr. Chanvootti Tangchitvittaya

Project Implementation Manager

ESSO Standard Thailand Ltd.

P.O BOX 18, Sriracha, Cholburi 20110

Dr. Supat Wangwongwatana

Chief of Industrial Air Pool Section

Office of the National Environment Board

60/1 Soi Phibunwatana 7, Rama VI, Bangkok 10400

Mr. Opad Orasaroaj

Technical Service Manager

Jotun Thailand Ltd.

8th floor, Orakan Building, 26 Soi Chidlom, Ploenchit Rd., Bangkok

Dr. Ekasit Limsuwan

Professor, Chulalongkorn University, Bangkok

Dr. Somsak Naviroj

President of Asia Glassfiber Industries Co., Ltd.

80-86 Asok-dindaeng Rd., Huai-khwang, Bangkok 10310

Dr. Somchai Tongtem

Associate Professor

Faculty of Science, Chiang-Mai University, Chiang-Mai

Mr. Kasem Chudthong

Chemist, Electricity Generating Authority of Thailand

Bangkruay, Nonthaburi 11000

Mr. Wirat Ngamsukhonratana
Engineer
SINO-THAI Pressure Vessel and Iron Works Co., Ltd.
40 Bangna-trad K.M. 4.5 Phrakanong, Bangkok

LT. Bodin Choochartchaikulkarn
Engineer
Bangchak Petroleum Co., Ltd.
210 Sukhumvit Soi 64, Bangna, Phrakanong, Bangkok 10260

Mr. Tanin Boonkobvijarn
Lab. Technician
I.C.I. Paint (Thailand) Co., Ltd.
34/5 Jangwattana Rd, Pangket, Nontaburi

Mr. Somsak Nimityont
Chief of Special Technique Section
Electricity Generating Authority of Thailand
Jaransanitwong Rd., Bangkrui, Nonthaburi

Dr. Rong Rujkorakarn
Material Technology Co-ordinator
Office of The Science and Technology Development Board.
6th floor, Jaran Insurance Building
401 Rachadaphisek Rd. Bangkok 10310

LT. Santirat Tharraketta RTN.
Scientist, Engineering Analysis Section
Naval Dock yard Department
Arunammarin Rd., Bangkok 10700

Ms. Patcharin Poosanaas
Engineer, National Center for Metal and Material Technology,
Ministry of Science Technology and Energy
Rama VI Rd., Phayatai, Bangkok 10400

Ms. Somjai Kajorncheappunngam
Lecturer, Chemical Engineering Department, Faculty of Engineering
Khonkaen University, Khonkaen 40002

Mr. Jiraphol Iamsudha
Administration Engineering
Port Authority of Thailand
Sunthonkosa Rd., Klongtei, Phrakanong, Bangkok 10110

Ms. Kalayanee Kooptarnond
Lecturer, Mining Engineer Department, Faculty of Engineering,
Songkhla University, Haadyai, Songkhla 90112

Mr. Pansa Buranawanich
Engineer, Metallurgy Division
Department of Mineral Resource
Rama VI Rd., Bangkok 10400

Mr. Adul Kaewlek
Technical Staff
Petroleum Authority of Thailand
Petroleum Authority of Thailand Building, 7th floor
555 Vipavadee Rangsit Rd., Bangkok 10900

Mr. Kiet Sakdejayont
Technical Staff
Technical Service Department
Petroleum Authority of Thailand
Petroleum Authority of Thailand Building
555 Vipavadee Rangsit Rd., Bangkok 10900

Mr. Chosit Pinsuwan
Engineer
Petroleum Authority of Thailand
Petroleum Authority of Thailand Building, 18th floor.
555 Vipavadee Rangsit Rd., Bangkok 10900

Mr. Chaiyo Suphantavee
Technical Staff
Petroleum Authority of Thailand
Petroleum Authority of Thailand Building
555 Vipavadee Rangsit Rd., Bangkok 10900

Ms. Arunwan Punyaporn
Engineer
Petroleum Authority of Thailand
Petroleum Authority of Thailand Building
555 Vipavadee Rangsit Rd., Bangkok 10900

LCDR Montree Choonamchai RTN
Head of Quality Control and Evaluation Department
Science Technology and Education Division
Naval Science Department, Wangderm Rd.,
Bangkokyai, Bangkok 10600

Mr. Komsak Tangkonchan

Sale Industrial

J.B.P. International Paint Co., Ltd.

34-3 Moo. 11 Soi Panichathon, Bangvak, Pasrichareon, Bangkok

Mr. Sumroeng Jongdeephaisal

Chief of Protective Coating Project

Jotun Thailand Ltd.

8th floor, Orakan Building

26 Soi Chidlom, Ploenchit Rd, Bangkok

Ms. Vilai Temsupasiri

Senior Chemist

Jotun Thailand Ltd.

8th floor, Orakan Building

26 Soi Chidlom, Ploenchit Rd, Bangkok

Mr. Oystien Rismyhr

Factory Manager

Jotun Thailand Ltd.

8th floor, Orakan Building

26 Soi Chidlom, Ploenchit Rd, Bangkok

Mr. Tuan Srikhum

Assistance technical manager

T.O.A. Paint (Thailand) Co., Ltd.

104 Soi Pukmitr, Poochaosamingpri Rd, Samrongtai,
Samuthprakarn. 10270

Mr. Pornchai Tharanatham

Director Environmental Quality Standard Division

Office of The National Environment Board

60/1 Soi Phibunwatana 7, Bangkok 10400

Sqn.Ldr Udom Ungsuwan
Head Assistance of Research and Testing Section
Directorate Aeronautical Engineering
Pradeepat Rd, Bangsue, Bangkok 10300

Mr. Pradit Pulputtpong
Engineer, Expressway and Rapid Transit Authority of Thailand
Phaholyothin Rd., Bangkok 10900

Mr. Naiyarat Amatayakul
Engineer i./c carried running gear and brake equipment repair section
The State Railway of Thailand
Krungkaseam Rd., Pratumwan, Bangkok 10500

Mr. Suripat Kamukamakul
Manager ,SIAM Steel Service Center Co., Ltd
51/3 Poochao Rd., Bangyaparak, Bangkok 10310

Mr. Surachai Piyakunakorn
Engineer
SIAM Steel Service Center Co., Ltd.
51/3 Poochao Rd., Bangyaparak, Bangkok 10310

Ms. Rungthip Chaiwattananone
Researcher ,Chemical Formulation and Processing Lab.
Chemical Industry Department
Thailand Institute of Scientific and Technological Research
Bangkhen ,Bangkok 10900

Mr. Phadoongkarn Hungsavaisya
Director of Training Division
Royal Irrigation Department
Samsen Rd., Bangkok 10300

Dr. Nongluck Pankurddee
Senior Researcher
Metal and Material Technological Department (MMTD)
Thailand Institute of Scientific and Technological Research (TISTR)

Ms. Ananya Tribumrungsuk

Mr. Pakomthep Migasena

Ms. Korrakoch Meechamnarn

Ms. Sutipa Masuthon

Ms. Rissara Ritkumrop

Mr. Sermkieat Kulkowit

Ms. Niramom Thanuddhanusilp

Mr. Kriengkrai Insompoch

Mr. Pongsak Buranasiri

Ms. Siriluck Kewdoknoi

Ms. Roongnapa Mettariganon

Ms. Suwalak Joosawat

Ms. Sriubol Hongcharoensri

Ms. Montanee Narkwichead

Ms. Wangam Thanawanichanam

Ms. Varaporn Paradamit

Mr. Niwat Sujaretrut

Mr. Suchat Suksawang

Atmospheric Corrosion Monitoring

Ladawal Chotimongkol, Phakomthep Migasena

Metal and Material Technology Department

Thailand Institute of Scientific and Technological Research

196 Phahonyothin Rd., Bang Khen, Bangkok, Thailand.

Introduction

The Kingdom of Thailand is situated in the Tropical zone (latitude from 6° to 21° N). As well as other countries in the tropical zone, corrosion of materials produce severely problems. Although there is a large volume of data relating corrosion of metals in different temperate climate environments, a relatively small amount of work has been conducted in this region, and much of that has been based on short term experiments. Most of atmospheric corrosion testing in tropical zone conducted in a low man-made atmospheric pollution area.⁽¹⁻¹²⁾ There are severe pollution problems in the city and many industrial areas in Thailand. The impact of these factors on atmospheric corrosion are increased dramatically in the past few years due to the increasing in industries. Many construction materials deteriorate much more rapidly in the tropics than in other parts of the world; this includes organic coatings that are used to protect metal.⁽²⁾

The comprehensive atmospheric Corrosion investigation in Thailand has been study by Thailand Institute of Scientific and Technological Research (TISTR), which aim to evaluate the durability of metal and organic coating metals by out door exposure test.

Exposure sites

There are 16 exposure sites were selected for installation of Exposure panels of atmospheric corrosion experiments in different climatic condition. since march 1987 as follows.

		Starting date
Site 1	Chumphon	(March 1987)
Site 2	TISTR (DECK)	(March 1987)
Site 3	Sakaerat	(April 1987)
Site 4	Pra-Padaeng	(May 1987)
Site 5	Si-Chang	(August 1987)
Site 6	Chiang-Mai	(September 1987)
Site 7	Phuket	(January 1988)
Site 8	Songkhla	(January 1988)
Site 9	Khonkaen	(March 1988)
Site 10	TISTR (ground)	(June 1989)
Site 11	Chiang Mai	(June 1989)
Site 12	Hua-Hin	(June 1989)
Site 13	TISTR	(June 1989)
Site 14	Pra-Padaeng	(June 1989)
Site 15	Maejo (Chiang Mai)	(October 1989)
Site 16	Prachuap Khirikhan	(October 1989)

The Exposure sites in Thailand are shown in Figure 1

Site 11, 12, 13, 14 were selected for ASEAN-JAPAN Project on Atmospheric Corrosion Organic Coatings, represented rural area, marine area, urban area, and industrial area respectively as follows:

1. Rural area, at Department of Physics, Faculty of Science, Chiangmai University, Ampor Muang, Chiangmai Province.
2. Marine area, at Police Training Rama VI Camp, Amphor Cha-am, Petchburi Province

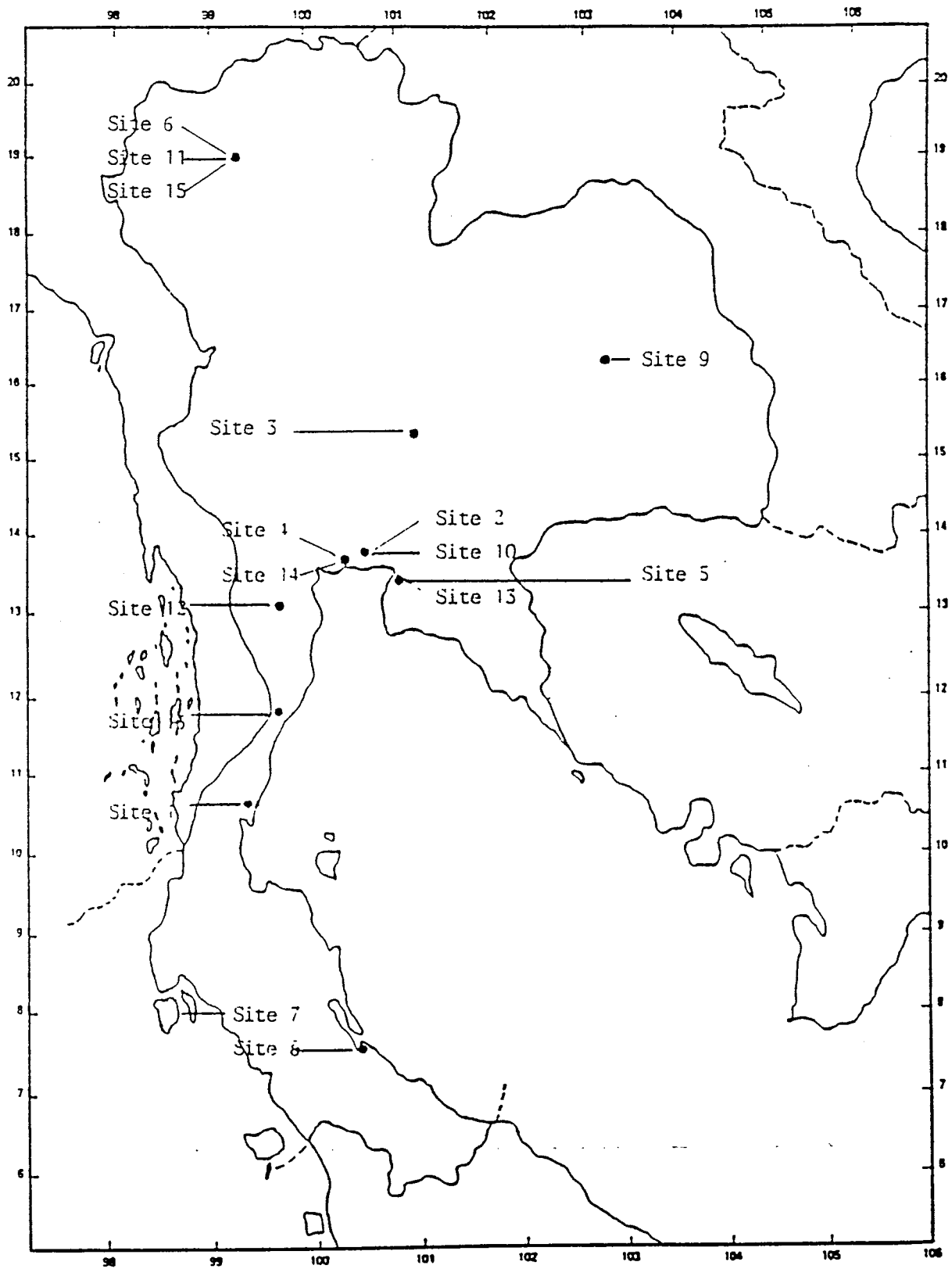


Figure 1 The exposure sites in Thailand

3. Urban area, at Thailand Institute of Scientific and Technological Research (TISTR), 196 Phahonyothin Road, Bangkok, Bangkok.
4. Industrial area, at Department of Mineral Resources (DMR), Phra-pradaeng, Samut-Prakarn Province

Exposure test programme

The exposure test programme follow the ASTM standard with a parital box design in which all of the specimens are exposed at the same starting point and then removals after exposed 1 month, 3 months, 6 months, 1 year, 2 years, 3 years, 4 years 5 years, 10 years, 15 years, and 20 years

Exposure stand

There are 2 types^{of} exposure stand, wooden frame and metal frame.

Specimens

Specimens were selected from the main local used types of materials and exposed at 0, 7, 30, 45, 90° to the horizontal facing south. First category is metallic Material as follows : carbon steel, Copper, Zinc, Aluminum, Stainless Steel 304, Stainless steel 430, Hot dip Galvanized Steel.

Result

Chemical composition of Aluminum (A), Copper (C), mild Steel (M) Steel for auto part (SPCEN), Stainless Steel 304 (ss 304) Stainless Steel 316 (ss 316), Hot dip Galvanized Steel (Z), Electro plating Galvanized Steel (ZC) are shown in table 1.

Table 1. Chemical Composition of bare metal and Galvanized Steel.

Type of Specimens	Chemical composition (% by weight)											
	Fe	Al	C	Cr	Cu	Mn	Mo	Ni	P	S	Si	Zn
A	-	9.71	-	-	-	-	-	-	-	-	-	-
C	-	-	-	-	-	-	-	-	-	-	-	-
M	*	-	0.15	-	-	0.29	-	-	0.014	0.020	0.23	-
SPON	*	-	0.11	-	-	0.13	-	-	0.013	0.020	0.20	-
SS 304	*	-	0.08	17.40	-	0.89	0.05	9.64	0.032	0.020	0.31	-
SS 316	*	-	0.05	16.73	-	0.99	1.49	13.33	0.029	0.021	0.38	-
Z	*	-	0.17	-	-	0.13	-	-	0.019	0.021	0.07	3.50
Ze	*	-	0.10	-	-	0.09	-	-	0.022	0.020	0.02	0.51

* Fe remainder

Second category was painted specimens and FRP. Six painting systems were selected as follows:

1. ss-oleoreginous painting system.
2. ss-Tar Epoxy system.
3. ss-Chlorinated rubber system.
4. ss-HB I/Z/P Epoxy Polyurethane system.
5. ss-HB I/Z/P Epoxy Fluorocarbon resin system
6. Zn. galvanized SS ~ Epoxy ~ Polyurethane system

More details of painting systems are shown in table 2.

Table 2. Painting System and Process for Outdoor Exposure test

Painting system	Test panel	1st Coat	2nd Coat	3rd Coat	4th Coat	5th Coat	Remark
		Common name	Common name	Common name	Common name	Common name	
1	Steel (Shotblast Rz = 60) 200x100x3.2	Long exposure wash primer film thickness 20 micron	Lead cyanamide rust preventive primer film thickness 35 micron	Same as left film thickness 35 micron	Long oil alkyd undercoat film thickness 35 micron	Long oil alkyd top coat film thickness 35 micron	-
2		Inorganic zinc shop primer film thickness 20 micron	Tar epoxy paint film thickness 20 micron	Same as left film thickness 20 micron	Same as left film thickness 20 micron	- -	- -
3		Epoxy zinc shop primer film thickness 20 micron	Chlorinated rubber primer film thickness 35 micron	Same as left film thickness 35 micron	Chlorinated rubber undercoat film thickness 35 micron	Chlorinated rubber top coat film thickness 35 micron	-
4		High-build inorganic zinc primer film thickness 75 micron	Epoxy primer film thickness 60 micron	Same as left film thickness 60 micron	Epoxy undercoat film thickness 35 micron	Polyurethane top coat film thickness 35 micron	Overthinned coat prior to 2nd coat film
5		High-build inorganic zinc primer film thickness 75 micron	Epoxy primer film thickness 60 micron	Same as left film thickness 60 micron	Fluoride undercoat film thickness 35 micron	Fluoride top coat film thickness 35 micron	Overthinned coat prior to 2nd coat
6		Hot dip galvanized steel 200x100x3.2	Epoxy primer film thickness 60 micron	Same as left film thickness 60 micron	Epoxy undercoat film thickness 35 micron	Polyurethane top coat film thickness 35 micron	-

Environment Factor Collection and Analysis

Data of temperature, relative humidity, amount of precipitation, measured time of wettness calculate time of wettness temp 0°C, RH 80%, amount of solar radiation, hours of sunshine and wind velocity were collected and analyzed. Some details of atmospheric condition of ASEAN - JAPAN project are shown in table 3-6. Gassous Pollutants, Sulfur dioxide, Hydrogen sulfide, Nitrogen dioxide. Chloride ion and Sea-Salt particle were analysed as follows:

Pollutant	Absorption	Determination
SO ₂	Lead Dioxide Cylinder ⁽¹⁴⁾	Turbidimetry ⁽¹⁵⁾
H ₂ S	Zinc Aeatate Filter Paper ⁽¹⁶⁾	Methylene blue Absorptimetry ⁽¹⁵⁾
NO ₂	Alkali Filter Paper ⁽¹⁷⁾	Saltzman,s Method ⁽¹⁷⁾
Cl ⁻	Alkali Filter paper ⁽¹⁷⁾	Mercury (II) this cyanate Absorptimetry ⁽¹⁵⁾
NaCl	Gauze Determination ⁽²⁾	Mercury (II) this cyanate Absorptimetry ⁽¹⁵⁾

The results are shown in Fig. 2-9.

TISTR 's previous work since 1987 on atmospheric Corrosion monitering has produced the results of atmospheric, pollutant data and corrosion rate of 7 types of metal as shown in Table 7 - 15 and Figure 10 - 17.

Conclusion

Results were obtained for one year period of experiment. The most corrosive region in Thailand for copper is the industrial area. Mild steel, steel for auto part and zinc galvanized steel are highly corroded in marine atmosphere. For aluminium, the corrosion rate was found to be high where mixed gaseous pollutants were produced such as the place near by chemical laboratory at TISTR. Further investigation will be carried out both in natural and given atmosphere for estimation life time of those materials.

Table 3 Yearly survey of environmental data
 Site 11 CHIANG-MAI Year 1989

Month	Temperature (°C)			Rel. humidity (%)		Calculate Wettness (hrs)
	Ave.	Max.	Min.	Ave.	Min.	
JUN'89	26.0	35.0	21.8	74.6	50.2	11.0
JUL.	26.0	31.8	22.5	80.1	56.8	13.0
AUG.	26.3	30.5	23.0	97.6	54.3	14.0
SEP.	26.3	31.4	22.9	82.5	57.8	14.2
OCT.	24.9	31.4	22.5	82.7	54.1	14.0
NOV.	24.0	30.7	20.8	75.1	46.0	12.0
DEC.	19.5	28.1	13.6	73.8	36.7	11.2

Table 4 Yearly survey of environmental data
 Site 12 HUA-MIN Year 1989

Month	Temperature (°C)			Rel. humidity (%)		Calculate Wettness (hrs)
	Ave.	Max.	Min.	Ave.	Min.	
JUL.	27.2	31.7	23.6	48.7	54.2	13.3
AUG.	26.9	32.1	23.7	80.0	54.1	13.9
SEP.	27.9	31.8	23.7	81.4	58.9	15.7
OCT.	25.4	28.7	22.7	87.8	73.2	18.0

Table 5 Yearly survey of environmental data

Test site: 13 TISR

Code:

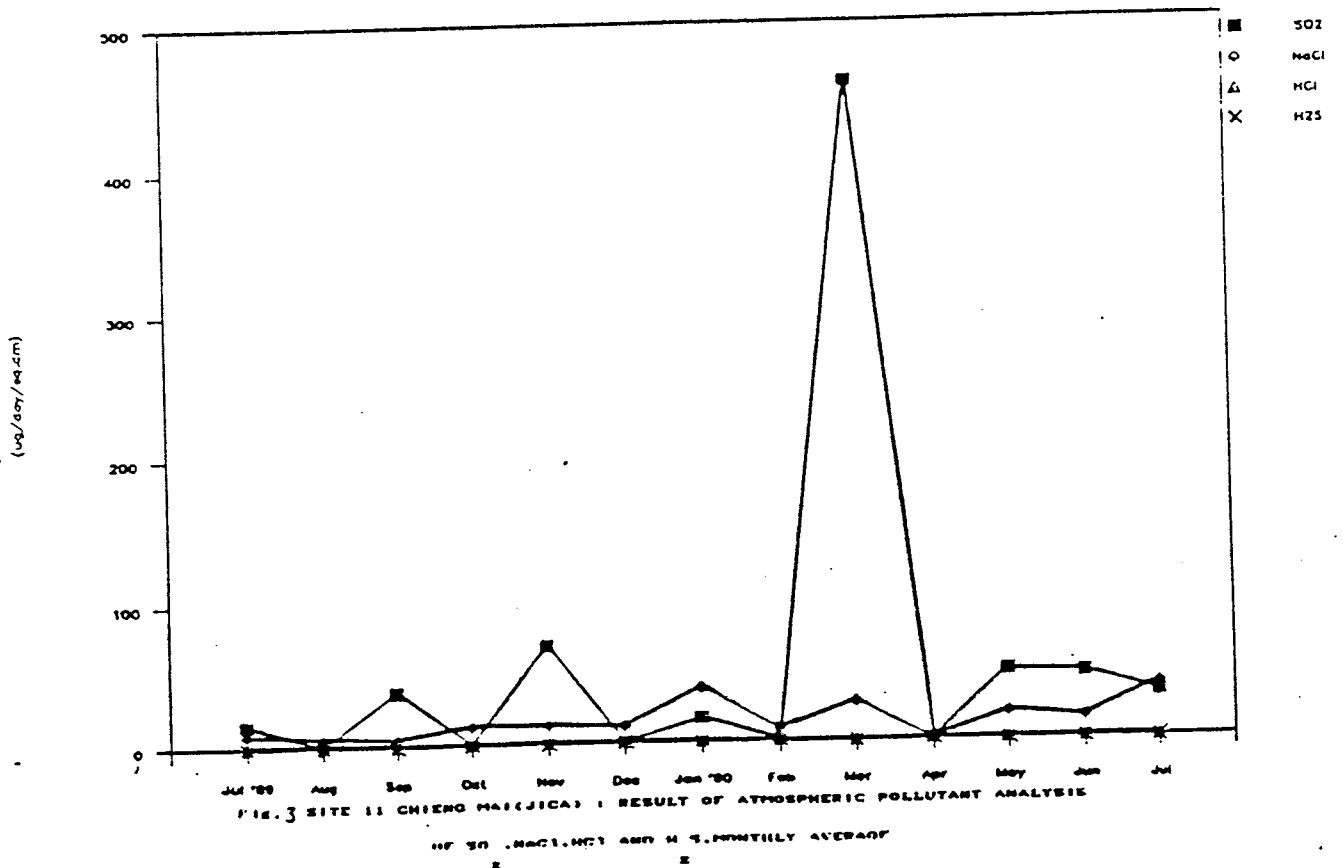
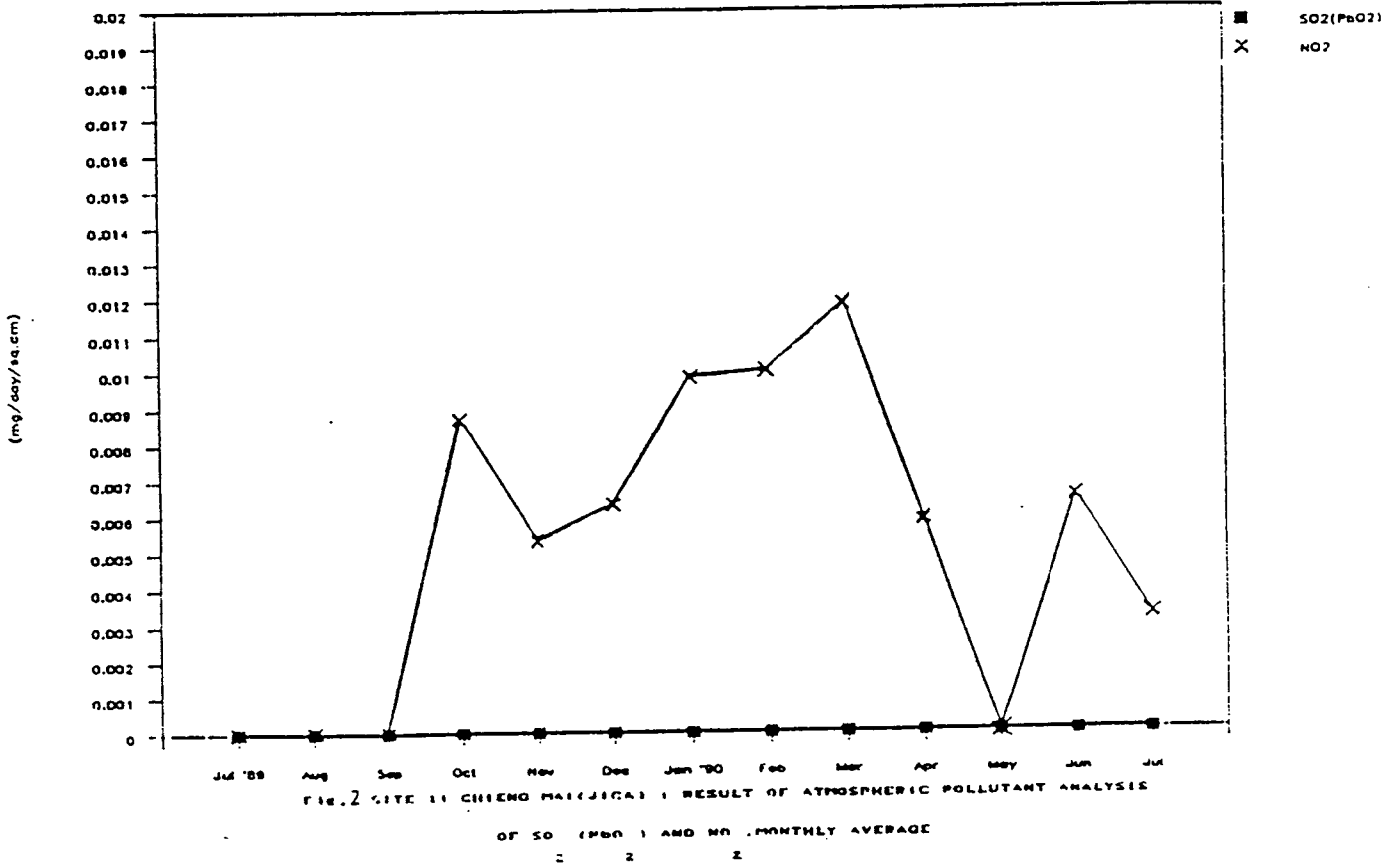
Contry:

Year: 1989

Month	Environmental characteristic (Meteorological factor)						
	Temperature (°C)	Rel. humidity (%)	precipitation Duration (hrs)	Amount of sun shine (MJ) m ²	Duration of sun shine (hrs)	Calculated time of wettness 0°C RH 80%	Measured time of wettness (hrs) --
JUL '89	29.4	75.20	84.16	572.12	381.90	10.50	150.18
AUG.	29.8	76.20	98.80	581.58	388.61	11.90	272.05
SEP.	29.2	79.90	91.80	165.19	400.82	13.70	283.60
OCT.	29.3	79.60	84.30	470.06	357.19	14.00	221.24
NOV.	29.3	73.90	10.95	202.17	122.68	10.30	2.76
DEC.	-	-	0.28	483.90	255.27	-	46.28

Table 6 Yearly survey of environmental data
 Site 14 PRA-PADAENG Year 1989

Month	Temperature (°C)			Rel. humidity (%)		Calculate Wettness (hrs)
	Ave.	Max.	Min.	Ave.	Min.	
JUN'89	28.0	33.2	24.3	72.6	45.6	11.4
JUL.	28.1	33.4	24.8	74.5	52.3	13.0
AUG.	-	-	-	-	-	-
SEP.	28.2	33.3	24.8	67.7	48.8	9.0
OCT.	27.9	33.1	24.6	75.4	50.1	12.0
NOV.	25.9	29.5	23.4	74.4	60.5	8.0
DEC.	24.0	30.4	19.8	71.4	49.3	10.0



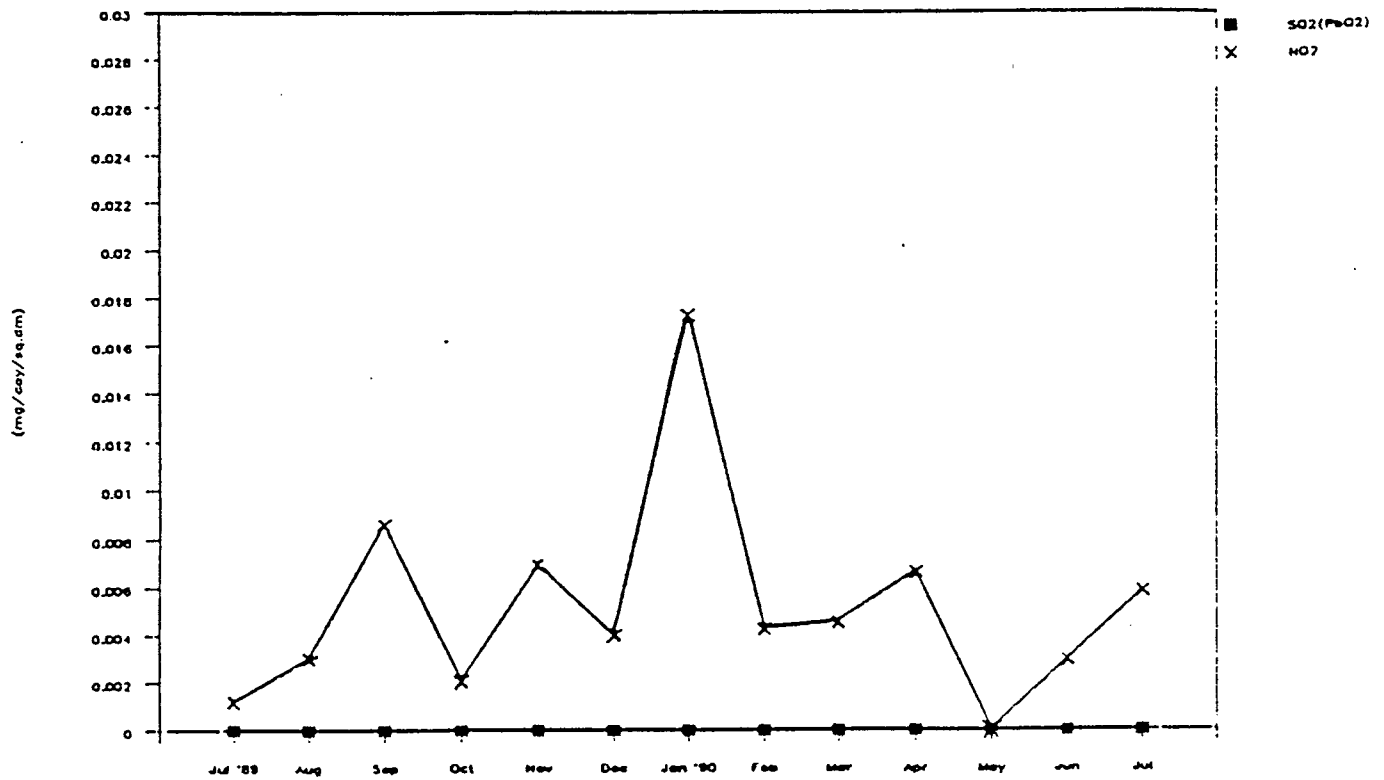


FIG. 4 SITE 12 HUA-NINIJICA : RESULT OF ATMOSPHERIC POLLUTANT ANALYSIS
OF SO₂ (PbO₂) AND NO₂ MONTHLY AVERAGE

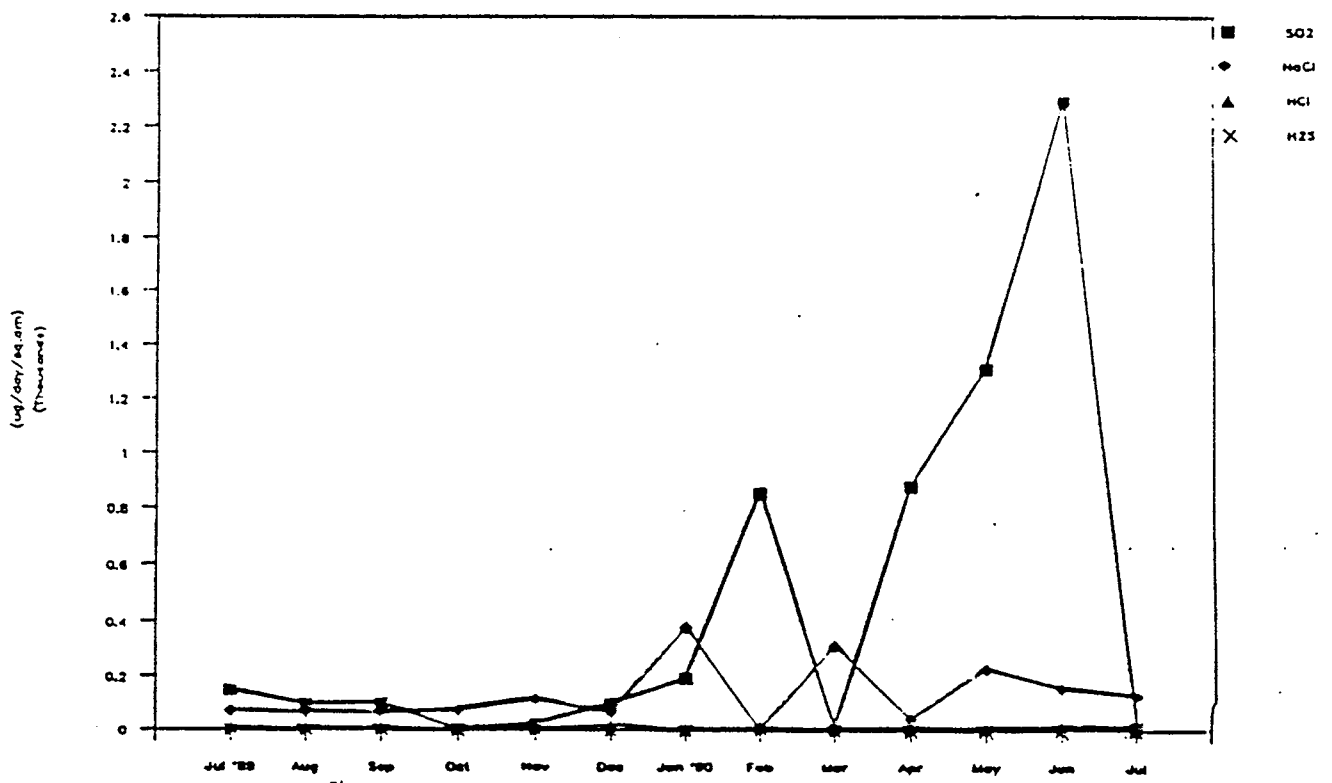
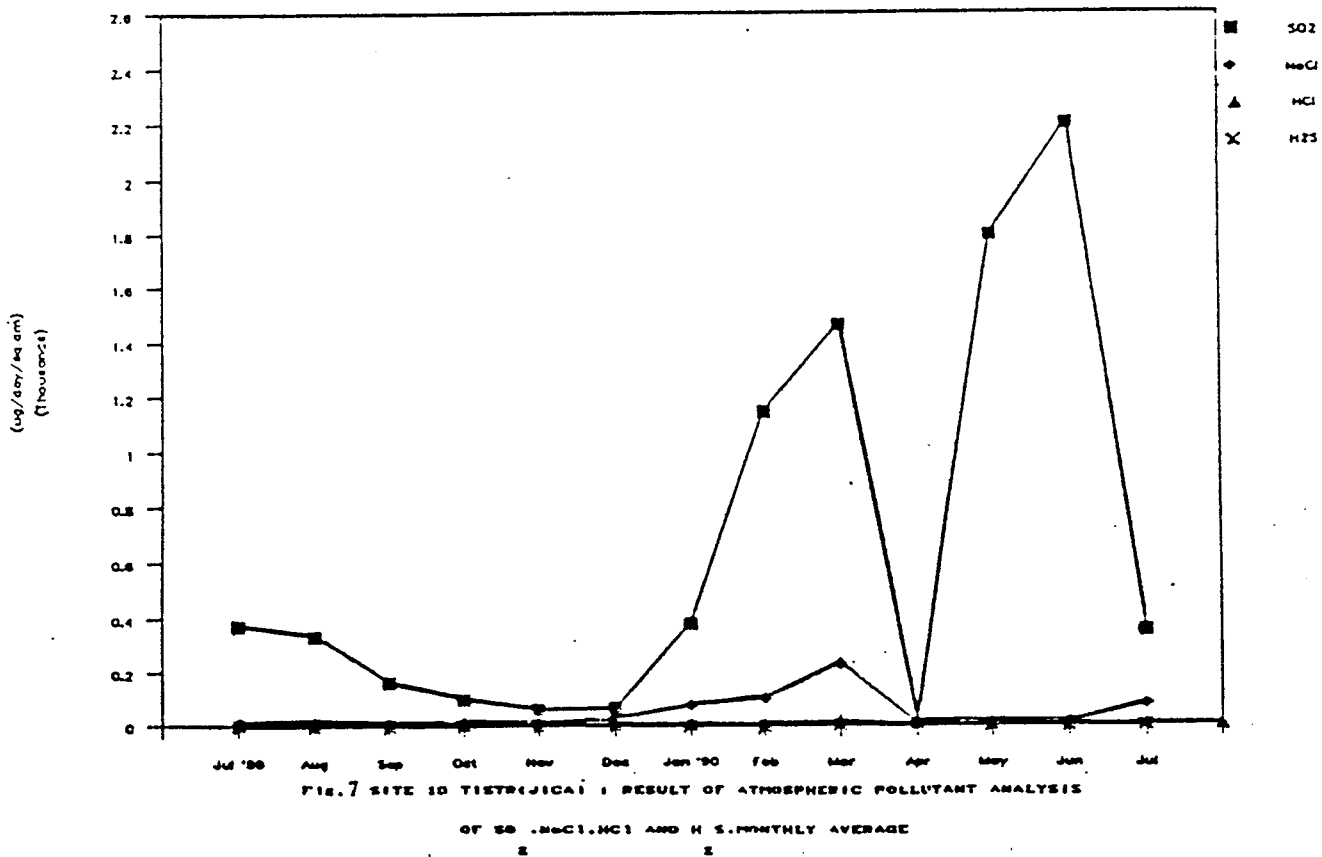
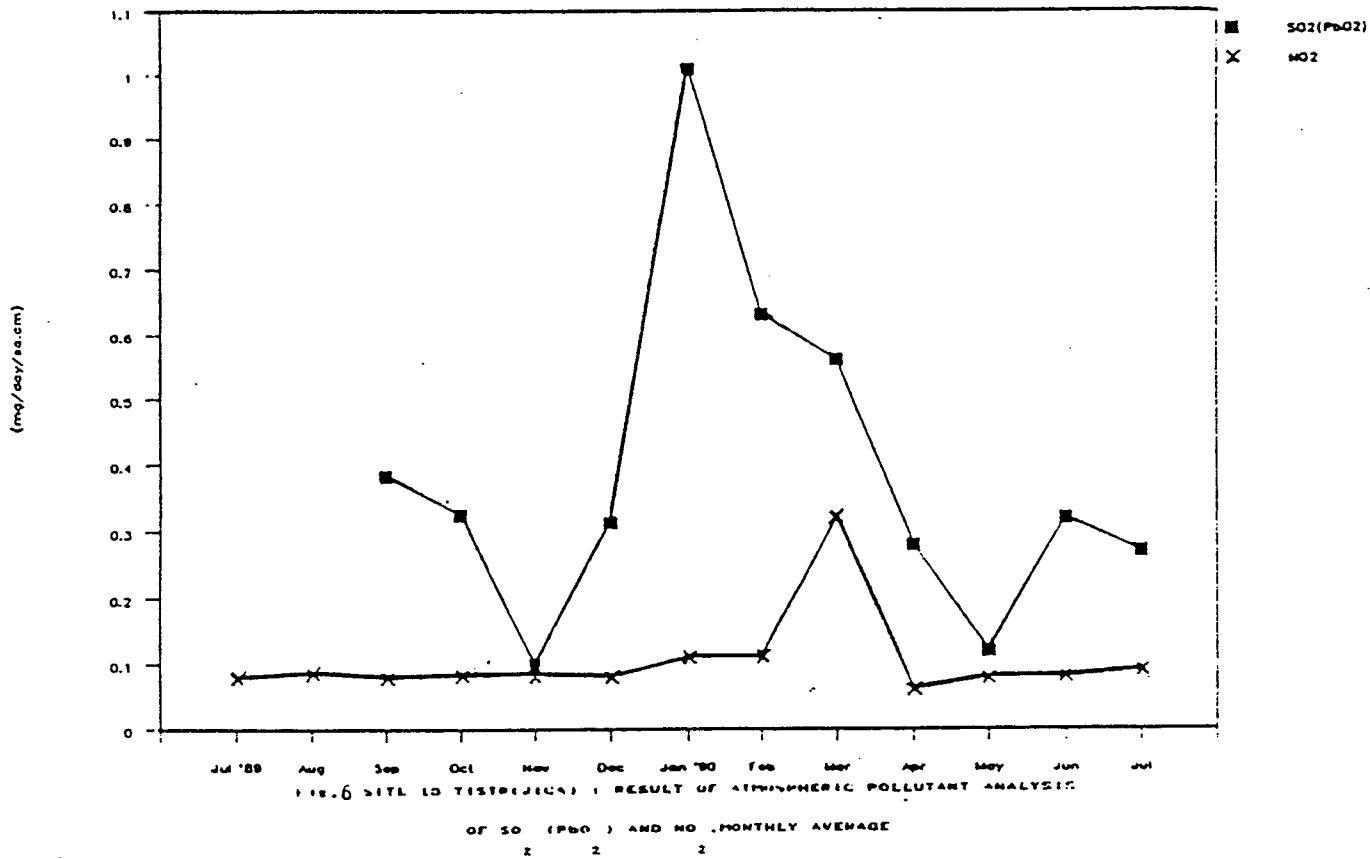


FIG. 5 SITE 12 HUA-NINIJICA : RESULT OF ATMOSPHERIC POLLUTANT ANALYSIS
OF SO₂, H₂S, HCl AND HClO MONTHLY AVERAGE



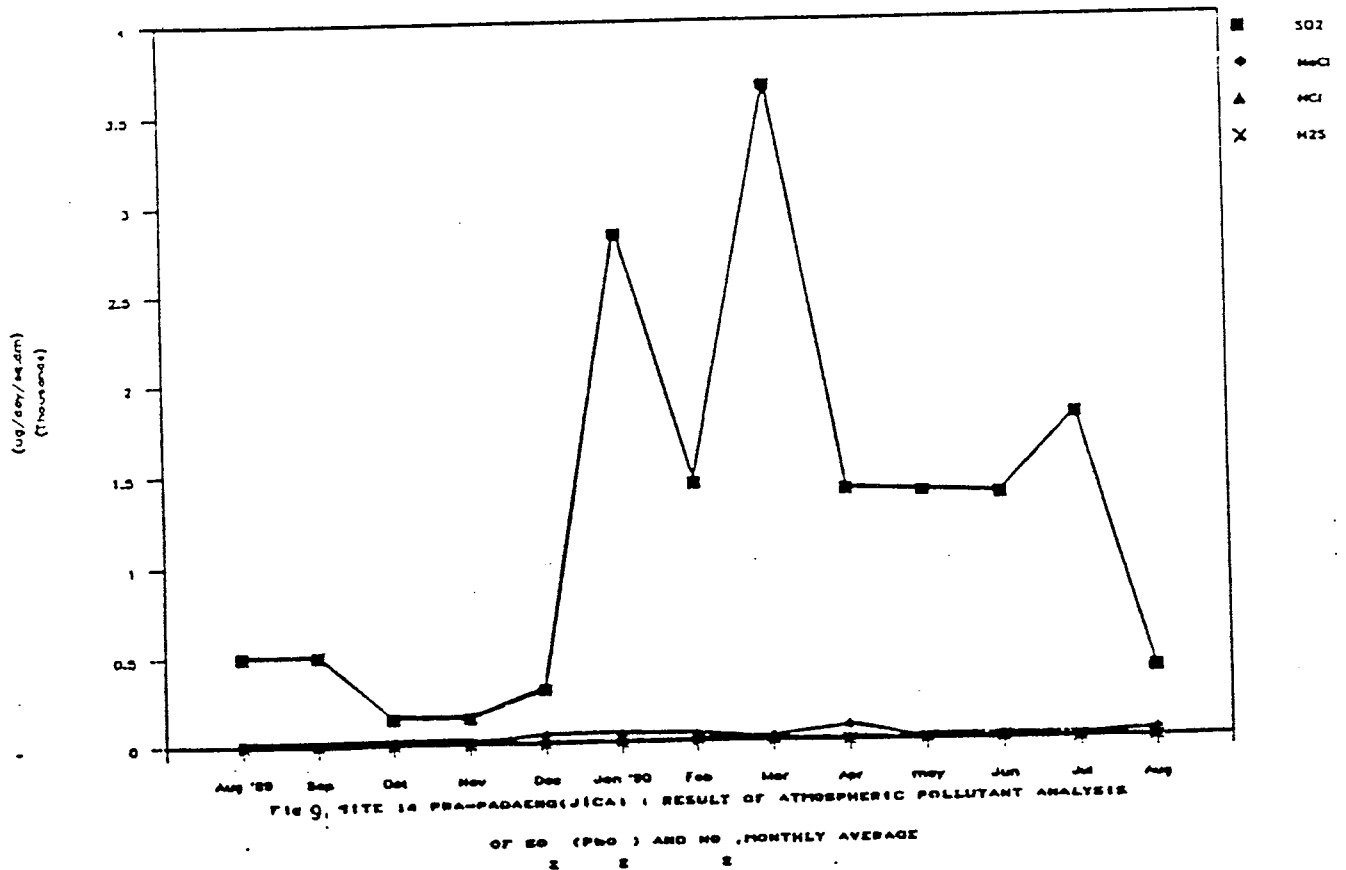
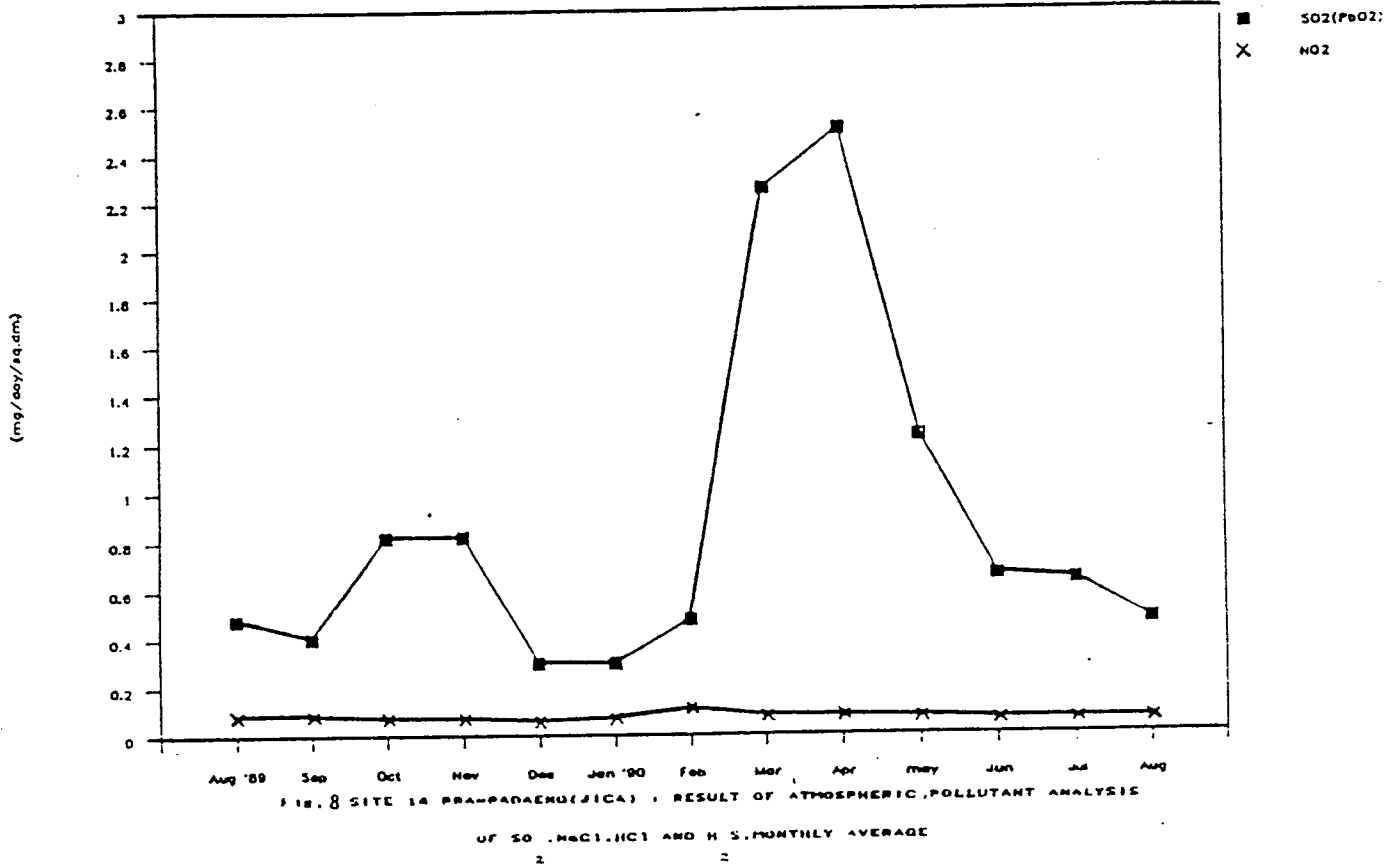


Table 7 RESULT OF ATMOSPHERIC POLLUTANT ANALYSIS

Location:02 TISTR

Year 1987 -1990

Environmental:Urban

Month	SO2 (ug.SO3/day/sq.dm)	NO2 (ppm)	NO2 (ug/day/sq.dm)	NaCl (ug/day/sq.dm)	HCl (ug.Cl/day/sq.dm)	H2S (ug/day/sq.dm)
Jan '87	-	-	-	-	-	-
Peb	-	-	-	-	-	-
Mar	-	-	-	-	12.34	-
Apr	155.99	0.0271	-	-	12.34	-
May	155.99	0.0271	-	-	80.79	-
Jun	155.99	0.0380	-	-	53.93	-
Jul	155.99	0.0446	-	-	53.93	-
Aug	155.99	0.0198	-	-	53.93	-
Sep	146.13	0.0275	-	-	35.52	-
Oct	166.73	0.0275	-	-	23.32	-
Nov	166.73	0.0187	-	-	9.11	-
Dec	98.40	0.0187	-	-	19.16	-
Jan '88	75.62	0.0460	-	-	30.58	-
Peb	519.55	0.0600	-	-	70.32	-
Mar	217.77	-	-	-	49.75	-
Apr	251.90	-	-	-	-	-
May	-	0.0380	-	-	22.17	-
Jun	288.18	0.0292	-	-	22.17	-
Jul	98.58	0.0310	-	-	34.45	-
Aug	150.77	0.0274	-	-	23.44	-
Sep	88.38	0.0292	-	-	32.12	-
Oct	0.00	0.0149	-	-	22.35	-
Nov	210.99	0.0368	-	-	-	-
Dec	43.56	-	-	-	-	-
Jan '89	229.35	0.0435	0.0171	32.38	18.15	0.07
Peb	590.40	0.0501	0.1297	51.51	21.29	0.05
Mar	1839.45	0.0506	0.1530	51.51	31.50	0.08
Apr	2718.16	0.0528	0.1058	76.48	17.24	0.02
May	534.78	0.0405	0.1312	45.33	15.26	0.04
Jun	3017.95	0.0407	0.2400	23.09	8.25	0.02
Jul	3017.95	0.0460	0.2400	23.09	8.25	0.02
Aug	505.72	0.0495	0.1200	32.46	8.35	0.04
Sep	3708.11	0.0143	0.0525	7.45	1.44	0.05
Oct	159.07	0.0209	0.1015	12.87	0.81	0.04
Nov	244.39	0.0220	0.0976	11.54	0.00	0.07
Dec	133.50	0.0220	0.0863	17.29	1.31	0.03
Jan '90	702.49	0.0435	0.1483	6.68	11.28	0.02
Peb	859.66	0.0517	0.1182	114.43	9.81	0.00
Mar	1131.96	0.0501	0.1155	93.84	14.92	0.01
Apr	3620.13	0.0550	0.0677	210.07	0.00	0.00
May	580.08	0.0539	0.1344	113.26	12.61	0.00
Jun	514.32	0.0253	0.0974	61.29	11.20	0.00
Jul	800.20	0.0902	0.1150	158.00	6.43	0.02

Table 8 RESULT OF ATMOSPHERIC POLLUTANT ANALYSIS

Location: 04 Pra - Padaeng

Year 1987 -1990

Environmental: Industrial

Month	SO2 (ug.SO2/day/sq.dm)	NO2 (ppm)	NO2 (ng/day/sq.dm)	NaCl (ug/day/sq.dm)	HCl (ug.Cl/day/sq.dm)	H2S (ug/day/sq.dm)
Jan '87	-	-	-	-	-	-
Feb	-	-	-	-	-	-
Mar	-	-	-	-	-	-
Apr	-	-	-	-	-	-
May	989.34	0.0154	-	-	49.31	-
Jun	989.34	0.0139	-	-	49.31	-
Jul	989.34	0.0139	-	-	32.54	-
Aug	898.19	0.0303	-	-	63.20	-
Sep	310.00	0.0143	-	-	17.34	-
Oct	320.00	0.0143	-	-	30.60	-
Nov	220.00	0.0187	-	-	14.17	-
Dec	770.00	0.0357	-	-	25.29	0.00
Jan '88	1200.00	0.0314	-	-	28.44	0.00
Feb	1200.00	0.0238	-	-	67.78	0.00
Mar	1400.00	0.0204	-	-	9.43	0.00
Apr	690.00	0.0314	-	-	20.53	0.00
May	690.00	0.0314	-	-	20.53	0.00
Jun	1980.00	0.0097	-	-	47.54	0.00
Jul	1050.00	0.0138	-	-	19.31	0.00
Aug	1210.00	0.0132	-	-	7.57	0.00
Sep	463.00	0.0192	-	-	17.58	0.00
Oct	540.00	0.0209	-	-	5.37	0.00
Nov	540.00	0.0452	-	-	5.37	0.00
Dec	262.00	-	-	-	-	0.00
Jan '89	1158.20	0.0302	0.0884	52.17	10.78	0.00
Feb	1158.20	0.0418	0.0884	29.73	10.78	0.01
Mar	1536.52	0.0185	0.0729	47.06	16.32	0.01
Apr	1536.52	0.0286	0.0124	47.06	16.32	0.01
May	5172.04	0.0186	0.0124	41.31	15.42	0.01
Jun	517.50	0.0188	0.0717	21.44	5.35	0.02
Jul	670.71	0.0231	0.0743	23.92	2.10	0.00
Aug	287.30	0.0231	0.0618	23.92	3.94	0.00
Sep	150.02	0.0132	0.1423	19.37	6.71	0.01
Oct	150.02	0.0297	0.0983	16.49	6.71	0.00
Nov	187.36	0.0186	0.0790	36.99	5.31	0.03
Dec	4362.54	0.0242	0.0959	30.80	15.42	0.03
Jan '90	4362.54	0.0264	0.0959	30.80	18.47	0.02
Feb	1530.55	0.0253	0.0181	8.51	18.47	0.02
Mar	5521.12	0.0479	0.0688	30.85	21.04	0.00
Apr	1802.52	0.0253	0.0719	116.93	13.01	0.00
May	2731.30	0.0220	0.0612	0.00	6.38	0.00
Jun	1266.33	0.0127	0.1014	5.82	5.07	0.00
Jul	2230.00	0.0121	0.0580	0.00	0.93	0.00
Aug						
Sep						
Oct						

Table 9 RESULT OF ATMOSPHERIC POLLUTANT ANALYSIS

Location:05 Si Chang

Year 1987 -1990

Environmental:Seaside

Month	SO2 (ug.SO3/day/sq.dm)	NO2 (ppm)	NO2 (mg/day/sq.dm)	NaCl (ug/day/sq.dm)	HCl (ug.Cl/day/sq.dm)	H2S (ug/day/sq.dm)
Jan '87	-	-	-	-	-	-
Feb	-	-	-	-	-	-
Mar	-	-	-	-	-	-
Apr	-	-	-	-	-	-
May	-	-	-	-	-	-
Jun	-	-	-	-	-	-
Jul	-	-	-	-	-	-
Aug	0.00	0.0046	-	-	136.65	-
Sep	0.00	0.0000	-	-	22.24	-
Oct	0.00	0.0024	-	-	48.51	-
Nov	5.20	0.0050	-	-	234.50	-
Dec	31.10	0.0036	-	-	147.40	-
Jan '88	31.10	0.0031	-	-	44.50	-
Feb	24.50	0.0039	-	-	98.30	-
Mar	48.10	-	-	-	98.30	-
Apr	48.10	-	-	-	98.30	-
May	0.00	0.0015	-	-	10.08	-
Jun	16.30	-	-	-	5.36	-
Jul	173.00	0.0022	-	-	15.43	-
Aug	128.00	0.0017	-	-	10.33	-
Sep	68.40	0.0036	-	-	17.56	-
Oct	68.40	0.0185	-	-	17.56	-
Nov	112.00	0.0066	-	-	20.25	-
Dec	141.00	-	-	-	-	-
Jan '89	13.18	0.0038	0.0000	12.21	24.35	0.00
Feb	124.21	0.0088	0.0000	9.64	5.74	0.00
Mar	0.00	0.0085	0.0000	0.71	10.53	0.00
Apr	0.00	0.0022	0.0000	0.71	10.53	0.00
May	46.12	0.0012	0.0000	10.70	37.72	0.00
Jun	46.12	0.0012	0.0000	86.39	37.72	0.01
Jul	26.35	0.0000	0.0016	11.93	9.45	0.00
Aug	46.12	0.0000	0.0052	9.61	8.70	0.00
Sep	85.03	0.0000	0.0067	42.61	19.19	0.00
Oct	0.00	0.0000	0.0000	38.93	7.96	0.00
Nov	0.00	0.0080	0.0077	51.14	7.96	0.00
Dec	94.16	0.0066	0.0097	17.11	3.86	0.00
Jan '90	76.56	0.0055	0.0097	17.11	0.00	0.00
Feb	50.60	0.0044	0.0021	6.70	0.73	0.00
Mar	82.67	0.0055	0.0031	43.78	1.12	0.00
Apr	190.50	0.0044	0.0090	37.87	0.00	0.00
May	110.07	0.0165	0.0000	0.00	17.00	0.00
Jun	124.21	0.0088	0.0016	10.08	24.95	0.00
Jul	150.00	0.0165	0.0030	21.44	6.30	0.00

Table 10 RESULT OF ATMOSPHERIC POLLUTANT ANALYSIS

Location: 06 Chiang Mai

Year 1987 -1990

Environmental: Rural

Month	SO2 (ug.SO3/day/sq.dm)	NO2 (ppm)	NO2 (ng/day/sq.dm)	NaCl (ug/day/sq.dm)	HCl (ug.Cl/day/sq.dm)	H2S (ug/day/sq.dm)
Jan '87	-	-	-	-	-	-
Feb	-	-	-	-	-	-
Mar	-	-	-	-	-	-
Apr	-	-	-	-	-	-
May	-	-	-	-	-	-
Jun	-	-	-	-	-	-
Jul	-	-	-	-	-	-
Aug	-	-	-	-	-	-
Sep	-	0.0033	-	-	3.22	-
Oct	-	0.0023	-	-	7.43	-
Nov	0.00	0.0022	-	-	9.35	-
Dec	0.00	0.0017	-	-	1.77	-
Jan '88	0.00	0.0028	-	-	19.56	-
Feb	0.00	0.0036	-	-	19.55	-
Mar	0.00	-	-	-	4.21	-
Apr	0.00	-	-	-	4.21	-
May	0.00	0.0024	-	-	0.30	-
Jun	0.00	0.0012	-	-	8.35	-
Jul	0.00	0.0010	-	-	0.55	-
Aug	0.00	0.0017	-	-	1.40	-
Sep	0.00	0.0012	-	-	11.51	-
Oct	74.90	0.0022	-	-	0.60	-
Nov	32.30	-	-	-	0.30	-
Dec	0.00	-	-	-	-	-
Jan '89	194.52	0.0065	0.0019	2.15	0.00	0.01
Feb	241.33	0.0060	0.0000	5.78	1.33	0.00
Mar	168.23	0.0031	0.0129	5.01	10.51	0.00
Apr	126.76	0.0066	0.0111	3.90	13.30	0.00
May	2045.04	0.0044	0.0039	12.55	6.30	0.00
Jun	14.32	0.0035	0.0000	7.52	0.00	0.00
Jul	0.00	0.0031	0.0000	5.96	0.00	0.00
Aug	37.51	0.0033	0.0000	4.40	0.00	0.00
Sep	69.25	0.0012	0.0053	4.40	0.00	0.00
Oct	0.00	0.0022	0.0087	13.29	0.00	0.00
Nov	788.61	0.0023	0.0103	12.58	0.00	0.00
Dec	74.90	0.0016	0.0000	39.34	1.33	0.28
Jan '90	74.90	0.0065	0.0000	38.23	0.00	0.00
Feb	386.04	0.0036	0.0104	0.00	0.00	0.00
Mar	458.68	0.0031	0.0119	27.11	0.00	0.00
Apr	0.00	0.0066	0.0058	0.00	0.00	0.00
May	48.10	0.0024	0.0000	18.19	0.00	0.00
Jun	45.67	0.0012	0.0065	14.11	0.00	0.00
Jul	31.75	0.0010	0.0032	37.95	0.00	0.00
Aug						

Table 11 Atmospheric and Pollutants Data

AVERAGE ATMOSPHERIC CONDITION
YEAR 1987-1988

Location	Temperature (°C)		Relative Humidity (%)	Rain Fall (mm)	Dew Point (°C)	Sun (HRS)	Windage (MPH)
	max.	min.					
CHIENMAI	31.79	22.91	81.59	4.84	23.23	7.00	4.8
KHONKAEN	32.90	24.50	76.56	4.96	22.25	6.51	4.91
SAKAERAT	32.03	22.02	79.19	5.39	22.44	4.89	1.34
TISTR, BKK	33.71	24.12	76.00	5.00	22.00	6.00	7.30
PRAPADAENG	31.89	25.22	75.79	4.80	23.12	7.88	7.67
SICHANG	32.09	20.23	70.99	3.86	19.63	7.25	3.58
CHUMFORN	31.78	23.39	80.79	8.63	23.73	6.33	9.40
SONGKHLA	32.24	25.08	73.25	6.00	23.00	6.00	7.00
PHUKET	34.72	22.91	71.83	4.01	21.15	6.34	3.19

Table 12 Corrosion rate of tested specimens at site 02 TISTR.

Corrosion rate of tested metal specimen

Location:02 TISTR

Start: March 31,1987

Environment:Urban

No.	Exposed Duration (months)	End of Exposure	Corrosion rate (mdd)							
			Aluminium (A)	Copper (C)	Mild steel (M)	SPCBW (SP)	Stainless steel 304 (SS)	Stainless steel 316L (SSL)	Zinc-coated (ZC)	Zinc-galvanized steel (Z)
1	1	Apr 87	0.00	6.80	10.60	12.92	0.00	0.00	0.11	0.33
2	3	Jun 87	0.00	2.29	6.69	9.69	0.00	0.92	0.10	0.24
3	6	Sep 87	0.15	1.08	6.40	10.44	0.47	0.56	0.65	0.60
4	9	Dec 87	0.00	2.01	5.05	7.91	0.14	0.05	0.15	0.29
5	12	Mar 88	0.02	2.25	4.19	6.23	0.03	0.12	0.15	0.39
6	24	Mar 89	0.01	0.93	4.17	6.31	0.10	0.10	0.24	0.23
7	36	Mar 90	0.01	0.86	3.11	4.98	0.01	0.01	0.54	0.37
8	48	Mar 91								

Table 13 Corrosion rate of tested specimens at site 04 Pra Pradaeng.

Corrosion rate of tested metal specimen

Location:04 Pra-Pradaeng

Start:May 29,1987

Environment:Industrial

No.	Exposed Duration (months)	End of Exposure	Corrosion rate (mdd)							
			Aluminium (A)	Copper (C)	Mild steel (M)	SPCBW (SP)	Stainless steel 304 (SS)	Stainless steel 316L (SSL)	Zinc-coated (ZC)	Zinc-galvanized steel (Z)
1	1	Jun 87	0.00	7.13	18.90	37.92	0.00	0.00	0.39	0.48
2	3	Aug 87	0.33	1.73	20.02	31.50	0.82	0.96	1.12	1.20
3	6	Nov 87	0.03	2.91	16.24	25.38	0.22	0.22	0.97	0.42
4	9	Mar 88	0.01	2.06	11.86	19.38	0.15	0.14	0.69	0.32
5	12	May 88	0.02	1.69	10.58	17.35	0.11	0.12	1.15	0.34
6	24	May 89	0.02	18.51	7.46	13.08	0.07	0.09	4.10	0.41
7	36	May 90	0.03	1.00	6.34	12.49	0.01	0.01	3.63	0.57
8	48	May 91								

Table 14 Corrosion rate of tested specimens at site 05 Si Chang.

Corrosion rate of tested metal specimen

Location:05 Si Chang

Start: August 11,1987

Environment:Seaside

No.	Exposed Duration (months)	End of Exposure	Corrosion rate (add)							
			Aluminium (A)	Copper (C)	Mild steel (M)	SPCRM (SP)	Stainless steel 304 (SS)	Stainless steel 316L (SSL)	Zinc-coated (ZC)	Zinc-galvanized steel (Z)
1	1	Sep 87	0.87	3.90	9.50	14.63	3.27	3.16	4.05	4.03
2	3	Nov 87		1.18		16.64				
3	6	Feb 88	0.03	3.41	30.66	26.33	0.25	0.23	0.77	1.51
4	9	May 88	0.03	2.48	15.27	21.05	0.18	0.17	0.43	1.01
5	12	Aug 88	0.03	1.81	10.92		0.02	0.03	0.37	0.76
6	24	Aug 89	0.05	1.02	19.45	26.99	0.08	0.04	0.26	0.73
7	36	Aug 90								
8	48	Aug 91								

Table 15 Corrosion rate of tested specimens at site 06 Chiang Mai.

Corrosion rate of tested metal specimen

Location:06 Chiang Mai

Start: September 12, 1987

Environment: Rural

No.	Exposed Duration (months)	End of Exposure	Corrosion rate (add)							
			Aluminium (A)	Copper (C)	Mild steel (M)	SPCRM (SP)	Stainless steel 304 (SS)	Stainless steel 316L (SSL)	Zinc-coated (ZC)	Zinc-galvanized steel (Z)
1	1	Oct 87	0.86	3.64	6.72	5.12	2.96	2.78	3.64	3.63
2	3	Dec 87	0	5.24	1.03	2.29	0.46	0.50	0.43	0.46
3	6	Mar 88	0.01	1.94	1.87	1.25	0.19	0.19	0.18	0.23
4	9	Jun 88	0.02	3.96	1.10	1.45	0.08	0.05	0.17	0.13
5	12	Sep 88	0.02	2.25	0.68	1.42	0.01	0.01	0.03	0.16
6	24	Sep 89	0.00	1.74	1.34	2.15	0.02	0.02	0.12	0.11
7	36	Sep 90	0.01	0.44	1.70	1.48	0.01	0.01	0.08	0.09
8	48	Sep 91								

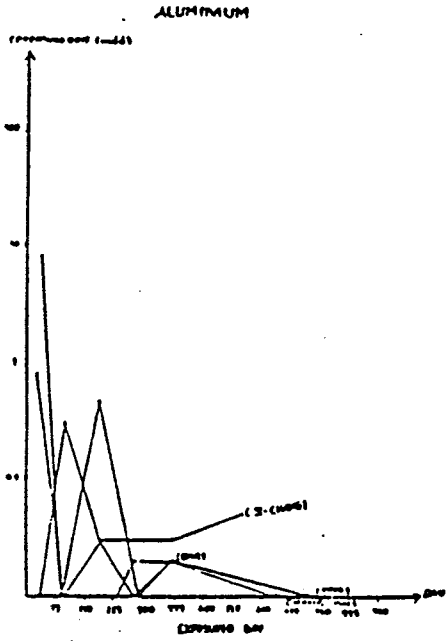


Figure 10 Corrosion rate of Aluminum
in various environment
(TISTR, IHR, CIHANG-HAI, SI-CIANG)

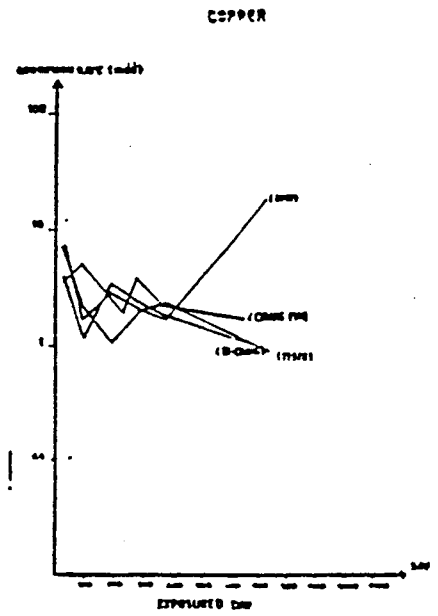


Figure 11 Corrosion rate of
Copper in various environment.
(TISTR, IHR, CIHANG-HAI, SI-CIANG)

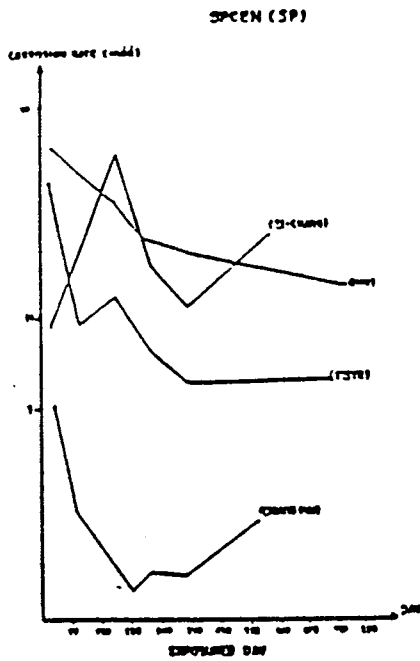


Figure 12 Corrosion rate of Steel for
rule part in various environment
(TISTR, IHR, CIHANG-HAI, SI-CIANG)

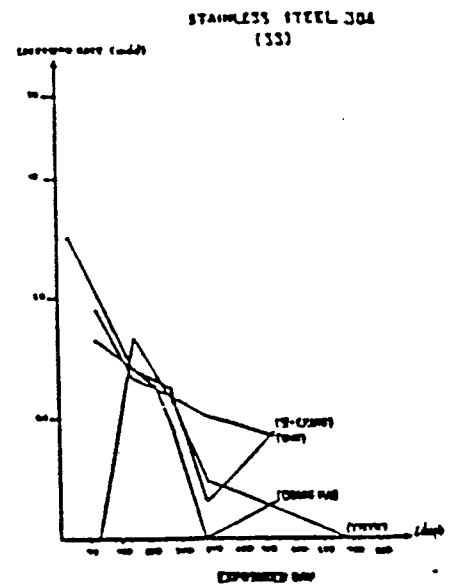


Figure 13 Corrosion rate of Stainless
Steel 304 in various environment
(TISTR, IHR, CIHANG-HAI, SI-CIANG)

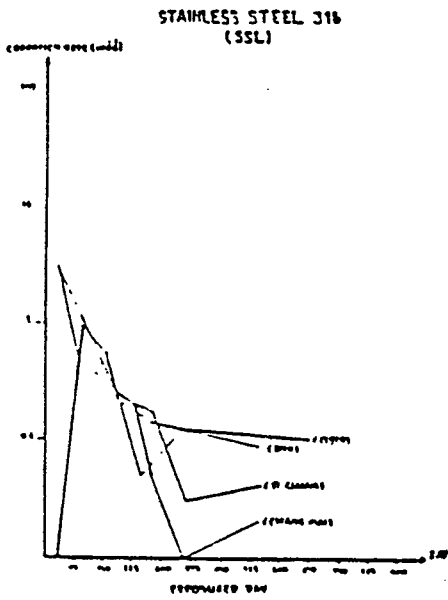


Figure 14 Corrosion rate of Stainless Steel 316 in various environment. (TISTR, IMR, CHIANG-MAI, SI-CHIANG)

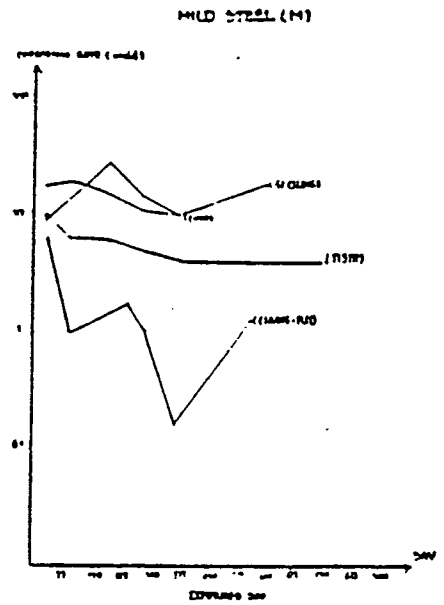


Figure 15 Corrosion rate of Mild Steel in various environment. (TISTR, IMR, CHIANG-MAI, SI-CHIANG)

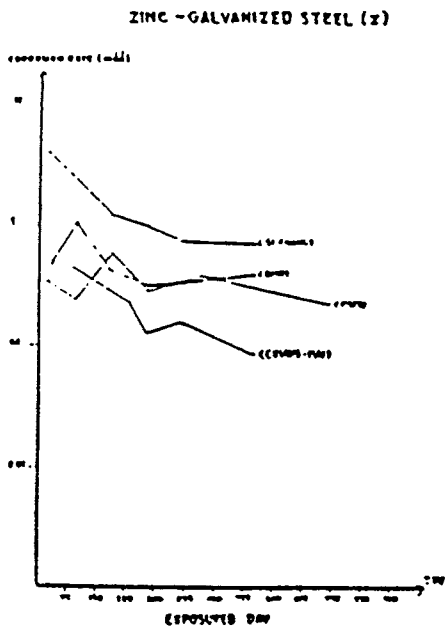


Figure 16 Corrosion rate of Hot dip Galvanized Steel (TISTR, IMR, CHIANG-MAI, SI-CHIANG)

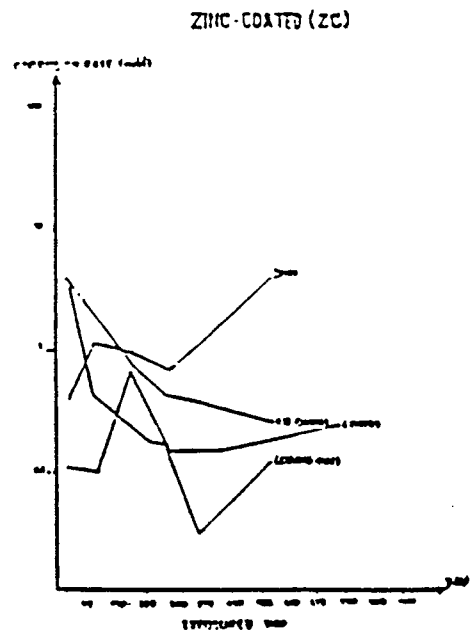


Figure 17 Corrosion rate of Electroplate Galvanized Steel (TISTR, IMR, CHIANG-MAI, SI-CHIANG)

REFERENCES

1. K. G. Compton, "Corrosion in the Tropics," Trans. Electrochem. Soc., 91, 705-714 (1947).
2. K.E. Wright, "Corrosion Problems at Navy Facilities on Tropical Pacific Islands," Proc. 14th Annual Conf. Natl. Assn. Corrosion Engineers (1958).
3. J. C. Hudson, "Corrosion, A Summary of the Work of the Joint Committee," Iron Steel, 20(6), 1-12 (1947).
4. H. R. Ambler and A.A. J. Bain, "Corrosion of Metals in the Tropics," J. Applied Chem., 5, 437-467 (1955).
5. G. I. Lawson, "Atmospheric Corrosion of Steel and Zinc in the Tropics," Tech. Memo. No.1/JTRU/64, Explosives Research and Development Establishment, Joint Tropical Research Unit, Ministry of Aviation, United Kingdom Dept. of Supply, Commonwealth of Australia (1964).
6. S. G. Clarke and E. E. Longhurst, "The Corrosion Behaviour of Metals and Protective Coatings in Tropical Atmospheric Exposure Tests," 1st Int. Conf. on Metallic Corrosion, 254-268 (1961).
7. K. S. Rajagopalan, P.L. Annamalai, M. Sundaram, and C. Rajagopal, "Atmospheric Corrosion of Steel in Some Tropical Locations in India," Proc. 3rd Int. Conf. on Metallic Corrosion, 4, 532-541 (1966).
8. F. Pearlstein and L. Teitell, "Corrosion of Aluminum in the Tropics," Proc. 7th Annual Natl. Conf. on Environmental Effects on Aircraft and Propulsion Systems, Inst. of Environmental Sciences, 161-171 (1970).

9. F. Pearlstein and L. Teitell, "Corrosion of Nickel Plated Steel at Tropical Environments," *Mat. Prot. Perf.*, 10(11), 30-32 (1971).
10. F. Pearlstein and L. Teitell, "Corrosion of Aluminum and Magnesium in the Tropics," *Mat. Perf.*, 13(3), 22-27 (1974).
11. S.K. Coburn, C.P. Larrabee, H. H. Lawson, and O. B. Ellis, "Corrosiveness of Various Atmospheric Test Sites as Measured by Specimens of Steel and Zinc," *ASTM STP 435*, 390-391 (1967).
12. W. H. Ailor, Jr., "Metal Exposures at Tropical and Marine Sites," 6th Annual Offshore Technology Conf., Paper No. OTC 1962 (1974).
13. ASTM G-1, Standard Practice for preparing, cleaning and evaluating corrosion Test specimens., American Society for testing and Materials,
14. JIS H 0521-1968, Testing Method for Atmospheric Corrosion of Aluminum and Aluminum Alloys
JIS Z 2381-1979, Recommended Practice for Weathering test
15. JIS K 0101-1979, Testing Method for Industrial Water
16. Y.Fakuda and T. Fukushima, Preprint for 73rd lecture Meeting of Metal Fin. Soc. Japan, p.214 (1986)
17. S. Fukui, *Japan Analyst*, 12 (1963), 1005

THE USE OF ACOUSTIC EMISSION IN MONITORING CORROSION

KHW Seah, KB Lim, CH Chew and SH Teoh
Department of Mechanical and Production Engineering
National University of Singapore
Kent Ridge
Singapore 0511
Republic of Singapore

ABSTRACT

This paper illustrates how acoustic emission can be used to monitor and predict corrosion. Results obtained in a series of experiments demonstrate that there is a striking correlation between acoustic emission activities and rate of corrosion in mild steel. It is also possible to use this method to detect the different stages of corrosion, such as uniform corrosion, pitting corrosion and intense localised corrosion. Moreover, the acoustic emission signals emitted from the corrosion activities were of sufficient magnitude to be easily detected by piezoelectric transducers.

INTRODUCTION

Acoustic emission (AE) is an elastic wave propagation generated by a rapid release of energy within a material. When energy is redistributed within a system, some of it might result in the generation of acoustic emission activities. For example, acoustic emission can be detected at the surface of a solid during deformation, as some energy appears as elastic waves which propagate at the speed of sound in the material. Similarly, metallic corrosion involves some chemical reactions which involve a redistribution of energy. Thus, any corrosion process is a potential source of acoustic emissions.

There has been some research and development of ultra-sensitive sensors since the early seventies and they have helped to make acoustic emission technology a good non-destructive testing tool. Dunegan (1975) described how the combination of acoustic emission and linear fracture mechanics could provide quantitative predictive information regarding structural failure. The important contribution of his work was the experimental proof of the correlation between acoustic emission activities and the mechanical deformation process.

Okada et al (1974) applied the technique to the study of stress corrosion cracking. They used the technique to differentiate between Active Path Corrosion and Hydrogen Embrittlement in the cracking of high strength steels and stainless steels. They also demonstrated the correlation between acoustic emission activities and the extent of crack growth, once again demonstrating the usefulness of acoustic emission technique in stress-corrosion related phenomena.

To apply the AE technique to the problem of corrosion proper, Rettig and Felsen (1976) developed some proprietary methods to follow corrosion reactions and to monitor corrosion of actual structures. In their work, one can clearly see the difference in AE activities for a metal immersed in various corrosive media.

Grossman (1984) also discussed the applicability of using an in-situ ultrasonic corrosion monitor to determine the relationship between the instantaneous corrosion rate and the weight loss of a material in a given corrosive environment.

Later on, Bassim and Piron (1982) made use of AE to monitor the corrosion of large structures under different corrosive environments whilst Chew et al (1984) used the technique to monitor the corrosion of steel pipes immersed in a corrosive medium.

The above literature survey describes some of the important contributions made so far in the development of the AE technique in corrosion monitoring. As corrosion is a complex phenomenon which usually involves the combination or interplay of various mechanisms, there is clearly a need to further explore this technique to detect the various stages of corrosion.

APPARATUS

The material tested in all the AE experiments was bright mild steel (AISI 1020) of composition 0.18%C, 0.22%Si, 0.55%Mn, 0.015%P and 0.014%S. The corrosive reagent used was dilute hydrochloric acid of various molarities ranging from 0.0005 to 0.01.

The acoustic emissions were monitored using a Dunegan/Endevco 8000 AE monitor and the results were printed using an Anadex DP-9500A AE printer. In addition, two 1801-190B AE pre-amplifiers, two S9204 AE transducers and a GOULD, OS 4000 Digital Storage Oscilloscope were also used.

A schematic diagram of the entire experimental set-up is shown in Fig. 1.

Test Specimen

The specifications for the test specimen were obtained from the American Society for Testing and Materials (ASTM) Standards for the Immersion Corrosion Test (Annual Book of ASTM Standards, 1984). However, in order to accommodate the AE transducer used in this phase of research, some modifications had to be made.

The ASTM standard recommends strip coupons of size 50 mm long, 25 mm wide and 3 mm thick (2 inch by 1 inch by 1/8 inch). In order for the transducer to be attached to it, the length was increased to 152.4 mm (6 inches). Of this length, only the original recommended length of 50 mm was exposed to the corrodent and the remainder of the length was insulated. The transducer was attached to this insulated portion.

Fig. 2 shows a diagram of the test specimen.

It is important to choose a material for insulation which neither corrodes nor attenuates the AE signals emitted during corrosion of the workpiece. A fast-setting epoxy adhesive (Araldite Rapid - maximum strength in 3 hours) was used. Since epoxy could not provide good surface contact for the transducer that was to be mounted on, only a short length of 38.1 mm (1 1/2 inches) above the exposed area was insulated with epoxy. The remaining portion of the strip was simply spray-painted with commercially available paint. In order to minimize the attenuation of the surface wave, only a very thin layer of paint was applied. This portion was not immersed in the reagent and hence the paint serves to prevent any possible atmospheric corrosion during the test.

Acoustic Emission Monitoring

The piezoelectric transducers used were undamped and had very high sensitivities at resonance. The frequency of an AE signal is broadband - up to several tens of a megahertz. A bandwidth of 100 to 300 kHz was selected for the transducers. This frequency range is a reasonable compromise because at low frequencies, there would be excessive mechanical noise interference and at high frequencies, there would be excessive signal attenuation.

Throughout the tests, the AE transducers would be picking up background noise due to vibrations from the equipment or from the surroundings. In order to minimize the amount of background noise picked up by the transducers, a threshold noise level was selected, below which the noise would not be recorded. This value was set at 26.5 dB since the background noise was largely below this level.

The method used for monitoring the AE signals is ring-down counting (Chew et al, 1984). A count is registered each time the signal waveform crosses the stipulated threshold level, as shown in Fig. 3. The data collected can be presented in terms of either the count rate or the total count for the whole test.

EXPERIMENTAL PROCEDURE

Fig. 1 shows a schematic diagram of the experimental set-up. The test method adopted was the Total Immersion Test (Annual Book of ASTM Standards, 1984) conducted in conjunction with the technique of Acoustic Emission.

A total of eight different tests were performed and two test specimens were used in each test. (The two transducers used for each pair of specimens were of slightly different frequency response for the purpose of determining if the frequency characteristics of the corrosion process varied with molarity of the reagent.) For each test, a different molarity of test solution, namely the reagent dilute hydrochloric acid, was used. The molarities used were 0.0005, 0.0007, 0.001, 0.0028, 0.0042, 0.0071, 0.008 and 0.01. The recommended minimum "solution volume to specimen area" ratio was 40 ml/cm² of specimen surface. From calculation, this gives 2.4 litres of acid. However 25 litres of acid were used since the molarity of the acid was very low.

The test duration was recommended as between 2 to 7 days (48 to 168 hours). For this series of experiments, a test duration of 48 hours was adopted since the weight losses measured in the specimens after the tests were large enough to be measured accurately.

After weighing the test specimens in a chemical balance, each specimen was clamped in place above the acid tank. Some Dunegan-Endevco AC-WS water soluble acoustic couplant was spread on to the transducer base plates to improve the contact and the latter were then mounted onto the specimens using adhesive tape. After submerging the specimens, the AE monitor was turned on.

Measurement of Corrosion Rate

The duration of each test was 48 hours (2 days). The corrosion rate was taken to be the total weight loss divided by 48 hours. This method is the weight loss method as recommended by the Annual Book of ASTM standards, 1984. The average corrosion rate throughout a predefined test period is expressed in milligrams per square decimeter per day (mdd) as follows:

$$[1] \quad \text{mdd} = \frac{\text{Weight Loss} \times 24}{\text{Area} \times \text{Time}}$$

where the weight loss is in milligrams, the area in square decimeters and the time in hours.

In the case of AE activities, it is the count rate of the AE signals that is used to assess AE activities and is expressed in count per square decimeter per day (cdd) as follows:

$$[2] \quad cdd = \frac{24 \times C}{A \times T}$$

where C is the total number of AE signal counts, A is the exposed area in square decimeters, and T is the time in hours.

The total AE count was collected over a period of 5 hours on the first day and another 5 hours on the second day. This was due to the limited storage capacity of the AE monitor. Only the results obtained from the 5 hours recorded on the second day were presented in this paper because the corrosion in the 5 hour duration on the first day had not stabilised enough for the results to be reliable.

RESULTS AND DISCUSSION

Fig. 4 is a plot of the corrosion rate and the AE count rate against the molarity of the reagent. The former two parameters are plotted on a logarithmic scale on the vertical axis and the latter parameter is plotted on a linear scale on the horizontal axis. For both specimens A and B, as molarity was increased from zero, the corrosion rate and AE count rate increased rapidly, but finally reached a limiting value when molarity exceeded 0.008.

There is a marked correlation between the corrosion rate and the AE count rate. Both show the same trend of monotonic increase with increasing molarity of the reagent. This is even more clearly seen in Fig. 5 in which the AE count rate is plotted against the corrosion rate, both on linear scales. The relationship between these two parameters is almost a linear one except for the probably spurious reading in transducer A in the region when the corrosion rate was about 200 mdd.

Fig. 6 is a linear plot of AE count rate against the molarity of the reagent. Three distinct regions can be seen in this graph. The first region is where molarity of the reagent is below 0.002 and the count rate is extremely low. In this region, the mild steel specimens experienced uniform corrosion as observed by visual inspection of the specimen. The second region is where molarity ranges from 0.002 to 0.004. Here the count rate increased slightly and pitting with some intensely corroded regions could be detected on the surface of the specimens. The third region is where molarity exceeds 0.004. In this region, the AE count rate rose rapidly and intensive localised corrosion was detected. Severe "streaking" could be seen on the surfaces of the specimens. These three different modes of corrosion, namely uniform corrosion, pitting corrosion and intense localised corrosion, which were observed in the mild steel specimens under different acid molarities represent typical corrosion behaviour as reported by Evans (1981).

CONCLUSIONS

The present research shows that there is a marked correlation between AE activities and corrosion rate. It is also possible to employ the observed AE count rate to detect the different stages of corrosion, such as uniform corrosion, pitting corrosion and intense localised corrosion.

REFERENCES

- Annual Book of ASTM Standards (1984), G31-72, pp 175-186.
- Bassim, M. N. and Piron, D. L. (1982), British Journal of Non-Destructive Testing, pp. 259-262.
- Chew, C.H., Lim, K.B., Seah, W. and Teoh, S.H. (1984), Proceedings of the 10th Canadian Congress of Applied Mechanics, Ontario, Canada, pp. E-107 to E-108.
- Dunegan, H. L. (1975), "Using Acoustic Emission Technology to Predict Structural Failure", Metals Engineering Quarterly, Feb 1975.
- Grossman, R.J. (1984), IEEE Transactions on Sonics and Ultrasonics, vol. SU-31, no. 1, pp. 25-31.
- Okada, H., Yukawa, K.I. and Tamura, H. (1974), Corrosion-NACE, vol. 30, no. 7, pp. 253-255.
- Rettig, T.W. and Felsen, M.J. (1976), Corrosion-NACE, vol. 32, no. 4, pp. 121-126.
- Ulick R. Evans (1981), "An Introduction to Metallic Corrosion", 3rd Edition, Chapter 2, pp 32-61.

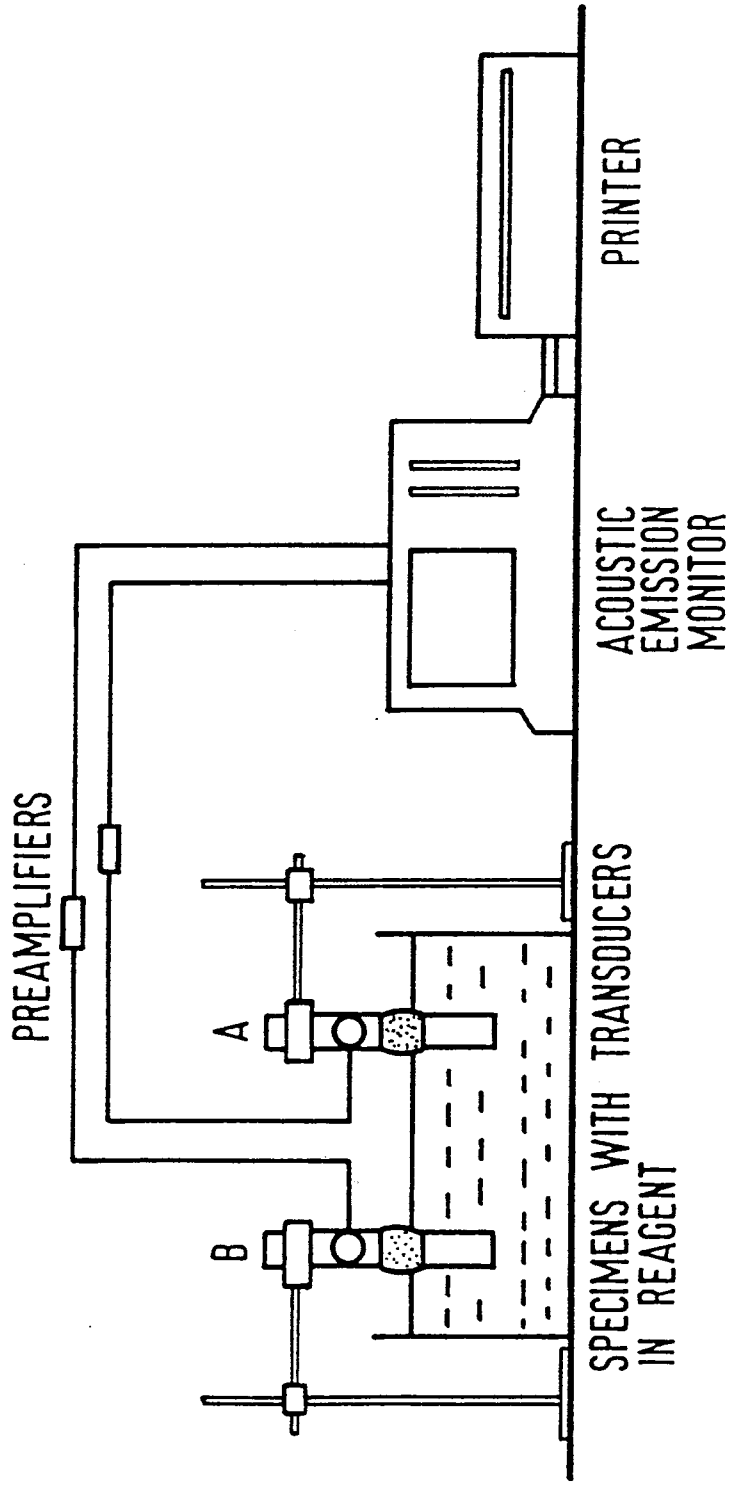


Fig.1 Experimental setup

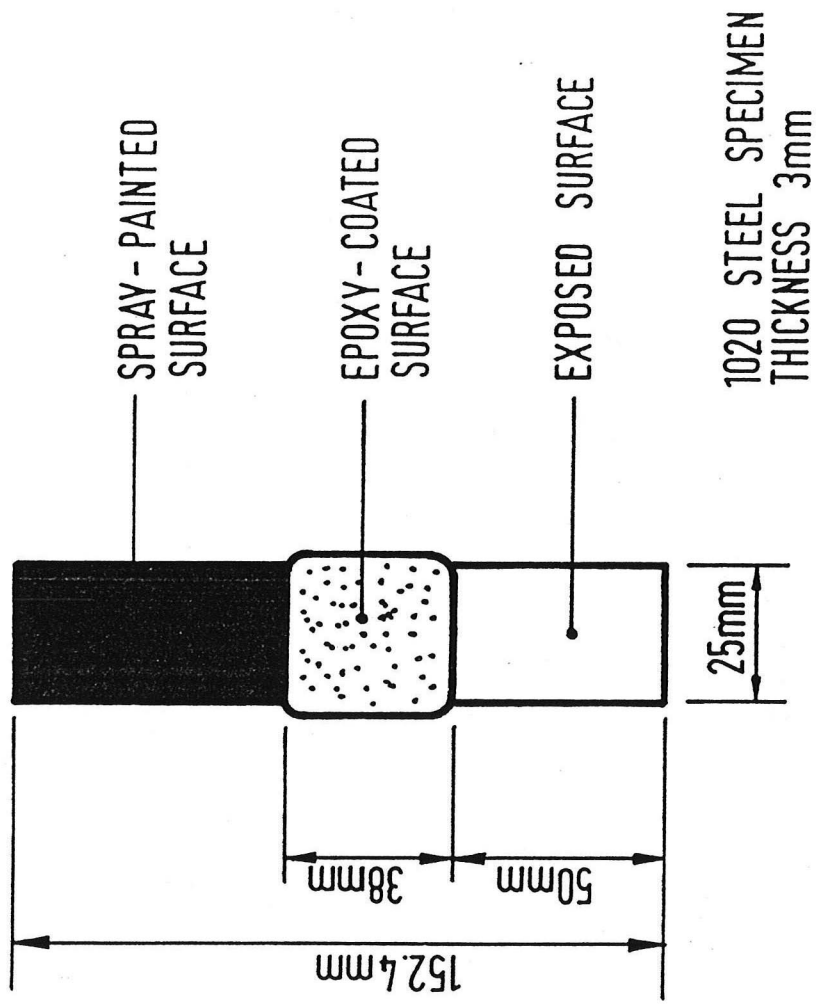


Fig. 2 Test specimen

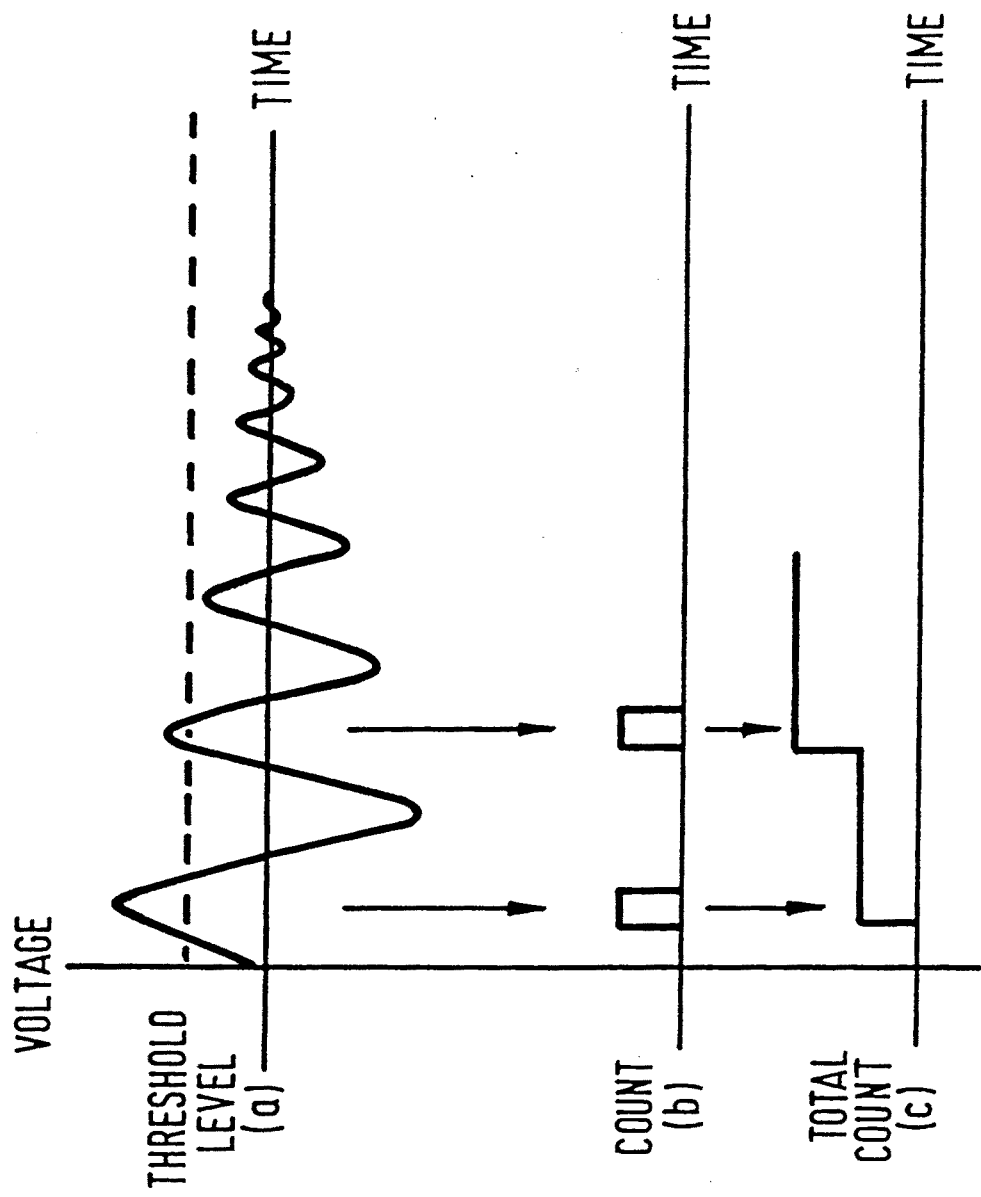


Fig. 3 Ring-down Counting

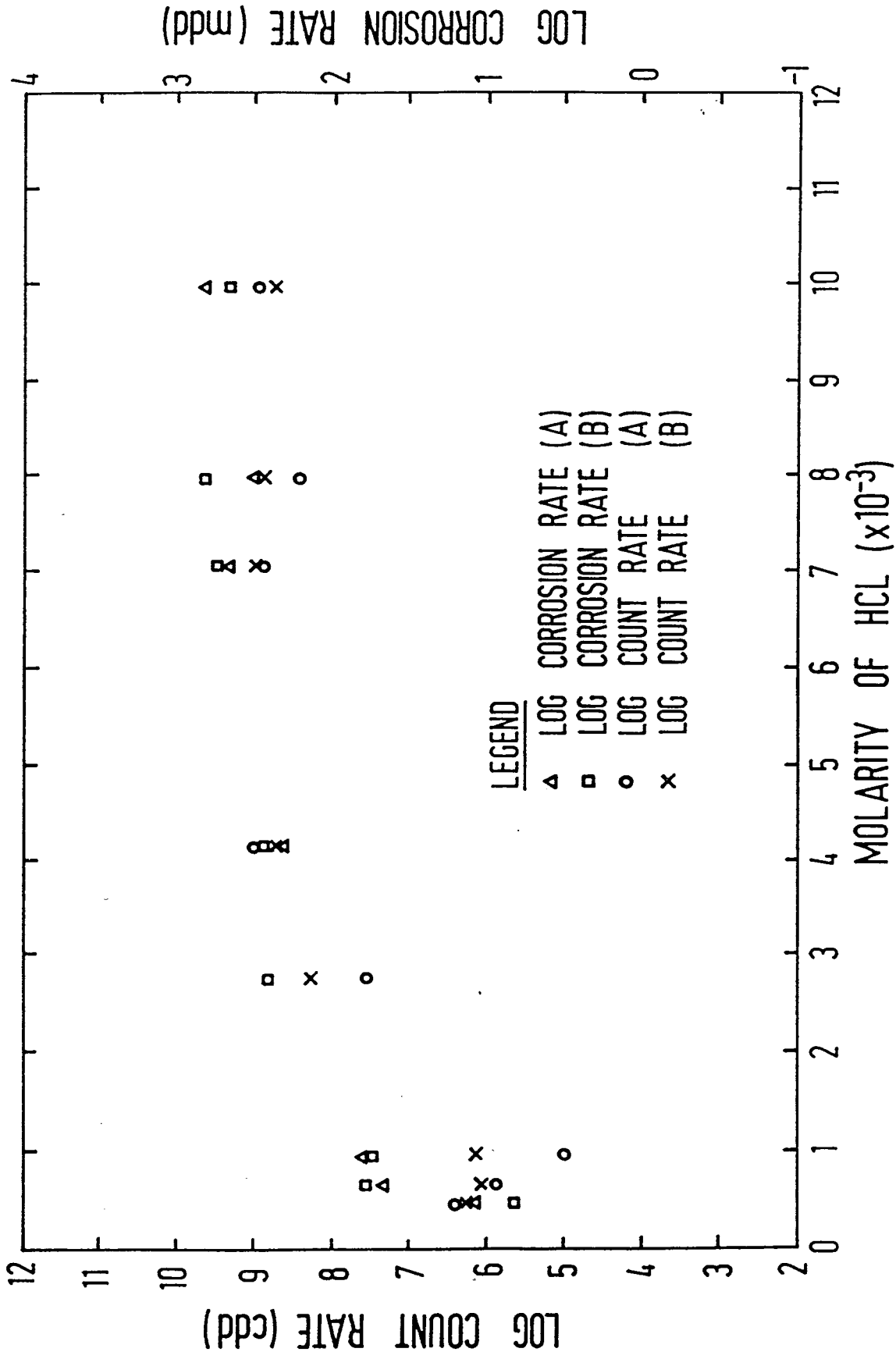


Fig.4 Log A.E. Count Rate And Log Corrosion Rate Vs Molarity Of Hydrochloric Acid

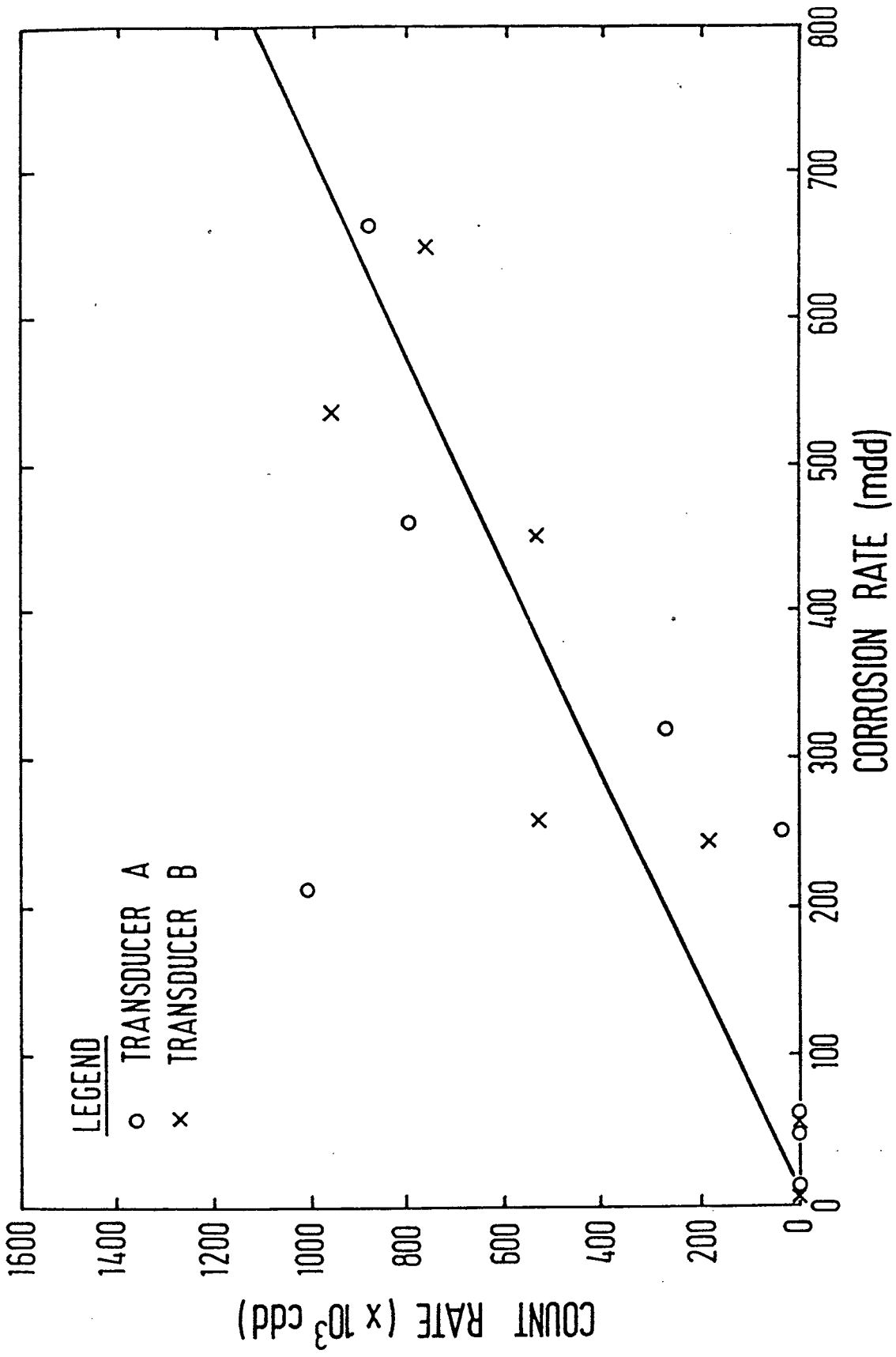


Fig.5 A.E. Count Rate Vs Corrosion Rate

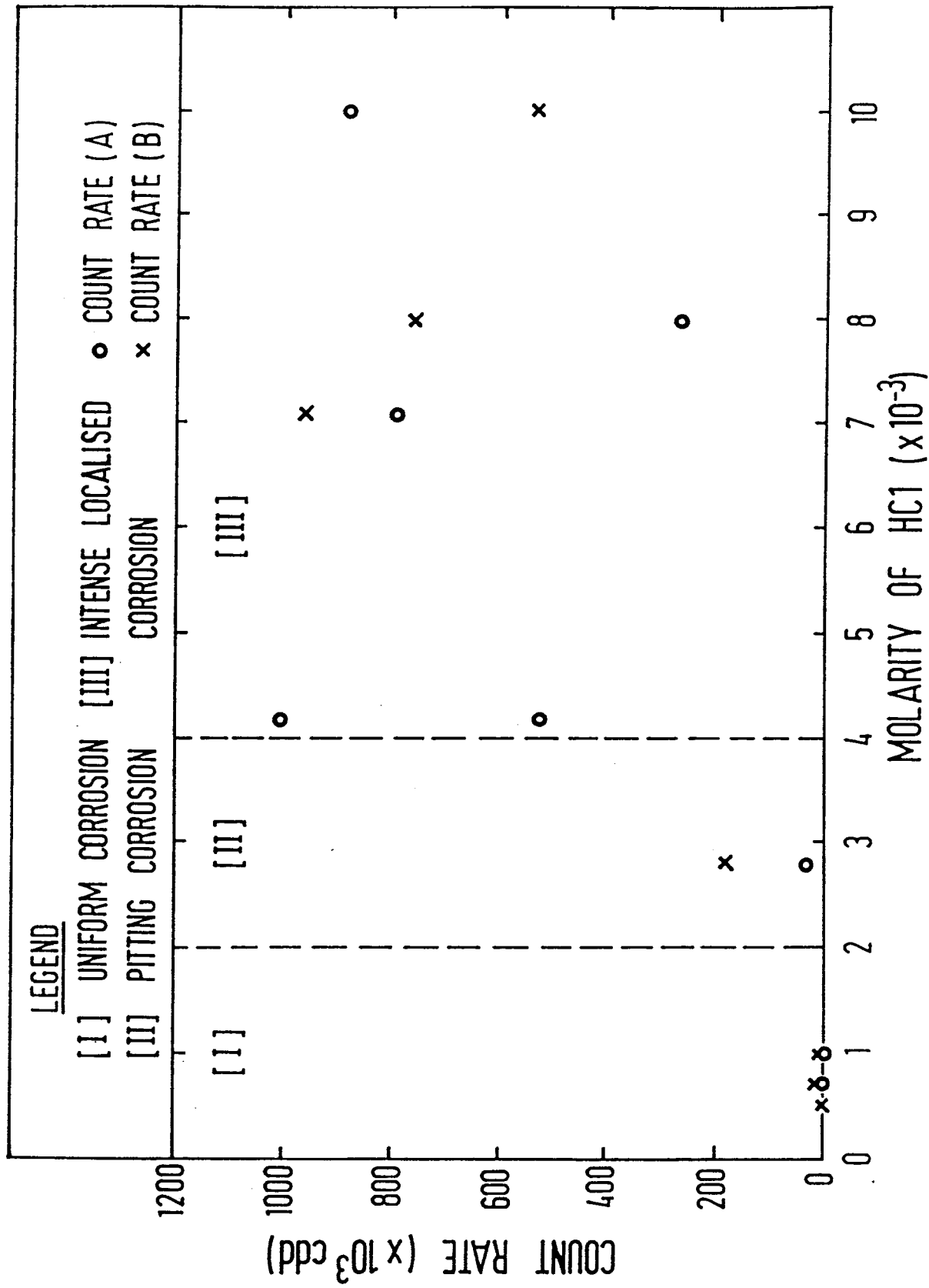


Fig. 6 A.E. Count Rate Vs Molarity Of Hydrochloric Acid

Degradation of Coatings and Its Evaluation by AC Impedance and Photo Acoustic Methods

Tooru TSURU

Department of Metallurgical Engineering
Tokyo Institute of Technology

2-12-1 O-okayama, Meguro-ku, Tokyo, 152 JAPAN

INTRODUCTION

Evaluation of coated steels degradation is very important subject to use organic coatings as a prevention of corrosion. Many investigations have been performed and proposed so many evaluation methods.

In this paper, three types of new approach, performed by the author, are summarized. Depending upon their characteristics, these new methods revealed the details of degradation mechanisms of coating films and proposed quantitative evaluation methods for the degradation.

DEGRADATION MECHANISMS OF COATINGS

A physico-chemical model for coating delamination has been proposed on some finely controlled experiments. Experimental details and the results will be seen in the following separated paper. It is summarized that the major part of the delamination is the cathodic one in which sodium ion accumulated to carry electricity, and that highly concentrated sodium ion leads the solution at the interface as very strong alkaline and increases the amount of water at the delaminated area by osmotic pressure.

EVALUATION BY AC IMPEDANCE METHOD

AC impedance method being popular now for electrochemical measurements has been applied for evaluation of coating degradation. The break-point frequency method was proposed to estimate the area of delamination and was successfully applied to practical coatings. The theoretical and experimental bases of the method are shown in another paper attached.

EVALUATION BY PHOTO ACOUSTIC METHOD

Backgrounds: An incidence of light beam cause many physical

and chemical effects. The major part of the energy of light beam absorbed converted to a thermal energy (production of heat). This means that an incidence of modulated or chopped light beam causes a synchronized heat production at the surface lighted and a heat wave propagates the sample. As schematically shown in Fig.1, modulated heat flux or temperature change will be observed at the opposite side of the sample. Increase in the thickness of the sample or insertion of a different materials into the sample, both will result a decrease in amplitude of cyclic change in temperature at the opposite surface and also result a increase in the duration or traveling time for the heat flux from its origin to the opposite surface.

Based on the idea mentioned above, new technique has been developed to evaluate coatings delamination and to detect the area of under film corrosion. Figure 2 illustrates the photo acoustic (PA) method. Chopped LASER light beam is scanned over the coating film and the heat flux passed across the coating film and steel is measured at the opposite side of the sample as PA signal by a PVDF (polyvinyliden difluoride) piezopolymer film sensor. The amplitude of PA signal decreases and the phase shift, which is an index of delay for traveling time of heat wave, increases when the light spot scanned over at the delaminated area or at the under film corrosion. So two types of data, PA amplitude image (mapping) and PA phase shift image, can be obtained.

Experimental Set up: The measurement system is shown in Fig.3, which was composed of Ar gas LASER for light source, chopper, X-Y stage controlled by stepping motors, and Lock-in-amplifier with referenced by light chopping signal. Whole the system was controlled by a desk top computer. The spacing of the scan was chosen mostly 20 μ m, and the beam spot size was about 20 μ m. The PVDF sensor was attached to the opposite side of the coated steel.

Spatial resolution of the PA signal images are limited by the beam spot size, spacing of scanning steps, and also the heat wave length (thermal diffusion length) λ ,

$$\lambda = \sqrt{\alpha/\pi f}, \quad \alpha = k/\rho C$$

where k ; the thermal conductivity (J/cm \cdot s \cdot K), ρ ; the density (g/cm 3), C ; the specific heat (J/g \cdot K), f ; the frequency (1/s), and α ; the thermal diffusivity. So higher chopping frequency leads higher spatial resolution. In the experiments, by the reason for signal/noise ratio, most of the experiments were conducted at 20 Hz.

Detection of Blisters: A steel sheet coated by black acrylic resin was immersed in a 3% NaCl solution to form blisters. After the immersion, the sample was examined by PA method. Figure 4 shows the amplitude image of PA signal in which upward direction corresponds the decrease in amplitude. The size of beam was about 100 μ m and the area shown in the figure was 10 mm square. It is readily seen that 5 to 6 blisters positioned at the central part

and their sizes were in the range of 1 to 2 mm in diameter. Most of these blisters were visible, because of their size, so the sizes and places were checked with the image. Using more sharp spot about 10 μ m and higher frequency of 60 Hz, more sharp resolution and images were obtained and a blister of 50 μ m in diameter was clearly detected.

Evaluation of Corrosion Depth from the Sample Edge: In usage of pre-coated steels, the edges of the sheet are usually not protected for corrosion. We have examined to estimate the corrosion depth from the edge using a latex coated steel in which the thicknesses of latex layers on both sides were 50 μ m. Making sure to detect the edge, the sample was placed on PVDF sensor as shown in Fig.5-(a). Figures 5-(b) and (c) show the results of the sample before and after the corrosion. In the PA image before corrosion, the edge of the sample is clearly shown at the 5th to 6th point from the left hand, and very shallow decrease in the right hand corresponding to bending of the sample. On the other hand, in Fig.5-(c), very sharp changes in image can be seen at the sample edge and 7 to 8th point from this edge. So the depth of corrosion was concluded from this as 1.4 to 1.6 mm from the edge of the sample. This was confirmed by a peeling off of the coating films after the measurement that the depth corresponded well to the front of the corrosion.

Evaluation of Under Film Corrosion Width During Corrosion Cycle Test: In practical corrosion tests for coated steels, the samples were damaged by a knife cut in shape of X, then examined by a salt spray test (SST) or a cyclic corrosion test (CCT). The results are usually evaluated by a visual rating for blisters and a peeling off test of coated films for estimation of corrosion width from the cut. Since these evaluation methods are qualitative and destructive, the PA method is proposed and examined as a quantitative and non-destructive evaluation.

Samples and Procedure: An electroplated zinc steel sheet, phosphated as pretreatment, coated by a cation electro-deposition of epoxy coating of 20 μ m thickness was damaged by a knife cut in usual way and used as a specimen. The samples before CCT and after CCT for 1, 3, 7 and 28 days were measured. The beam spot size and the step spacing were also 20 μ m.

PA Images before CCT: Cutting of the coated layer causes deformation of the substrate steel layer, as shown in Fig.6-(a) which was illustrated from an observation of scanning electron microscopy for the cross section. Changes in PA signals of amplitude and phase shift (Fig.6-(b)) just reflect the cross sectional image of the specimen. At the bottom of the X-cut, the PA amplitude was maximum and the phase shift was minimum, because of thinnest position of the sample. On the other hand, at the edge of the X-cut as the maximum thickness of the sample, the PA amplitudes decreased to a minimum and the phase shifts showed a maxi-

mum.

Figures 6-(c) and (d) show the PA signal images of the amplitudes and the phase shifts at the crossing point of the knife cut lines. It is very clearly seen the width of damage.

PA Images after CCT: After 7 days of CCT, as shown in Fig.7, especially clear in Fig.7-(c), an increase in the width of damaged coatings is readily seen. At the cut line, where metal surface exposed, a rust layer covered the metal surface, therefore, and the amplitudes and phase shifts of PA signals were decreased their contrast to the else. The front of coating delamination or under film corrosion was estimated by the width between the changing points from the rather flatten parts in Fig.7-(a). The bold curves in Fig.7-(c) show the fronts thus estimated.

The changes in the width of delamination or that of under film corrosion during a cyclic corrosion test were summarized in the Fig.8. The values of PA signal width correspond to them. The maximum value (○), the average (●) and the standard deviation (error bar) were calculated from the measurements of 40 times at different positions along with the cut line. From the figure, it is clear that the width increased with the duration of CCT and it is concluded that the delamination or under film corrosion can be quantitatively and non-destructively evaluated by the PA method.

CONCLUDING REMARKS

To evaluate the degradation of coated steels, three types of approach have been performed by the author. The AC impedance method, namely the break-point frequency method is powerful tool to estimate the area of delamination when the coating films are free from macroscopic defects. While the photo acoustic (PA) method is also useful in both the case with and without these defects. PA method can be combined with conventional degradation tests, such as salt spray test and cyclic corrosion test, because of its non-destructive inspection. For a practical use of these methods, it has to be selected considering the limitations and the advantages of these methods.

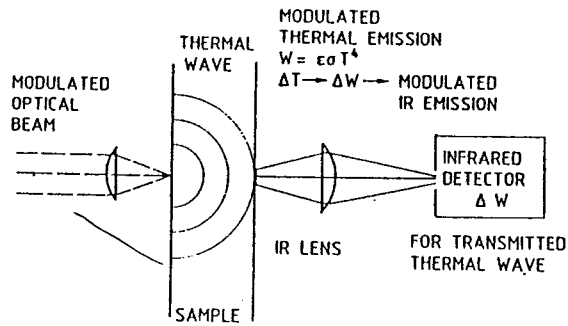


Fig.1 Scheme of photo acoustic method using infrared detector

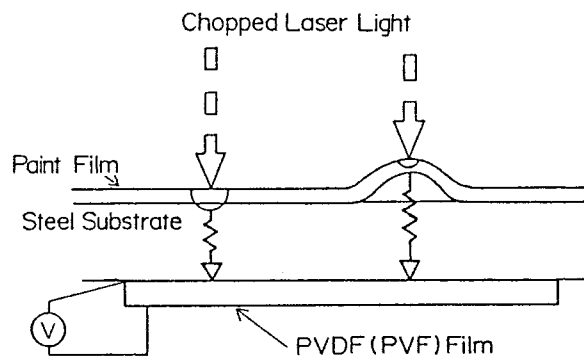


Fig.2 Application of photo acoustic method to evaluate degradation of coatings

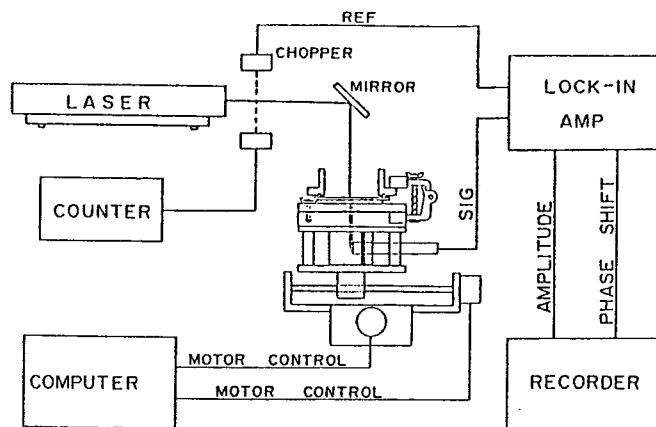


Fig.3 Illustration of the measurement system for PA method

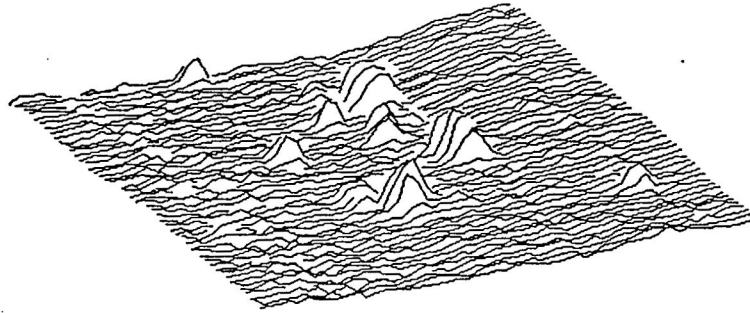


Fig.4 PA amplitude image of degraded coating steel with some blisters. (10 mm x 10 mm)

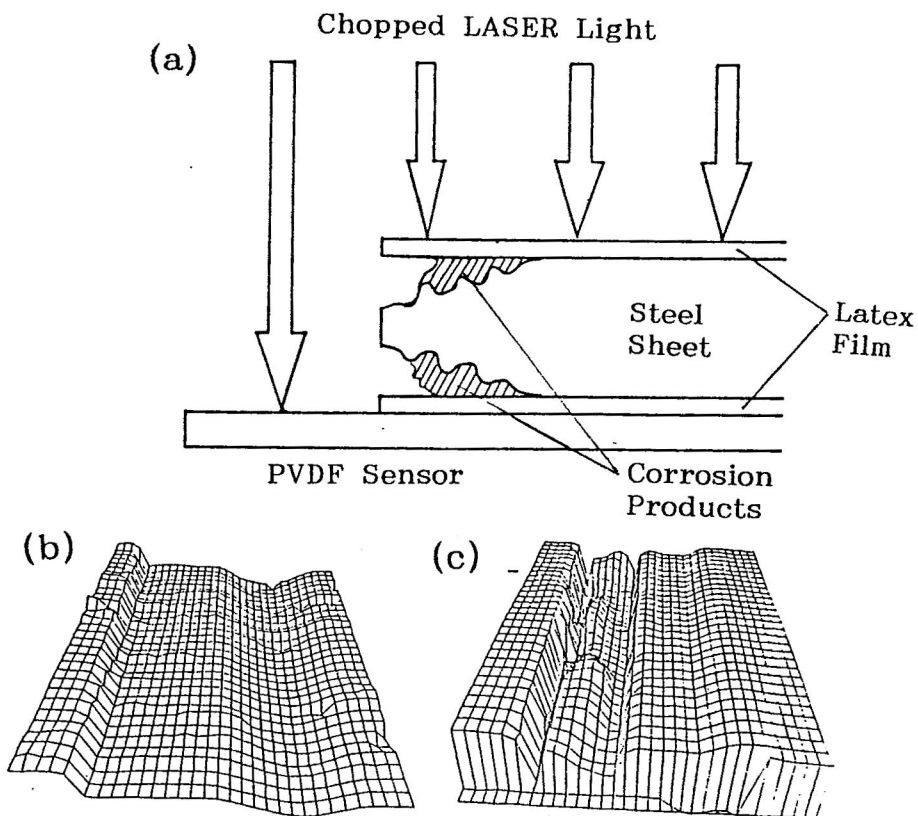


Fig.5 (a) Scheme of cross section of the latex coated steel corroded from the edge, (b) PA signal image before corrosion and (c) after corrosion.

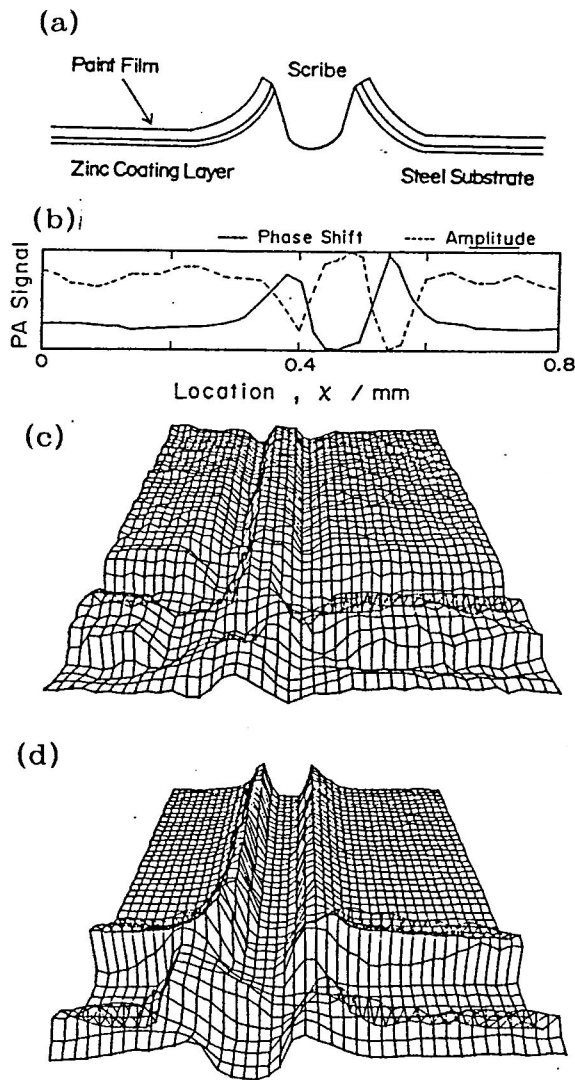


Fig.6 (a) SEM image of the cross section of the coated steel sample, (b) PA signals across the cut line, (c) amplitude and (d) phase shift image of PA signals. Before cyclic corrosion test. Spacing of grids; 20 μ m

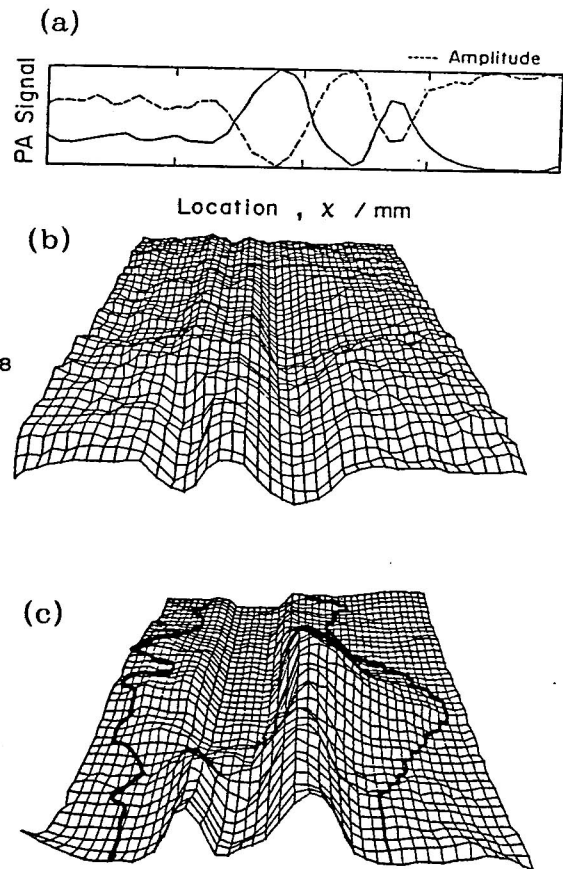


Fig.7 (a) PA signals across the cut line, (b) amplitude and (c) phase shift image of PA signals. After 7 days of CCT. Spacing of grids; 20 μ m

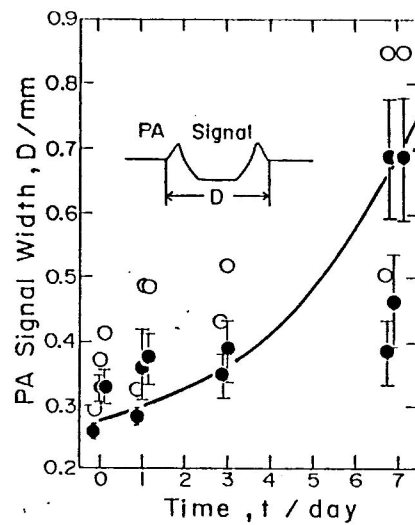


Fig.8 Change in the width of under film corrosion with duration of CCT estimated from PA signals

Reprint from "Corrosion Protection by Organic Coatings", Eds. M.W.Kendig & H.Leidheiser,Jr., The Electrochemical Society, Proc. Vol.87-2, 1988

MASS TRANSPORT IN BLISTERING OF COATED STEEL

Shiro Haruyama, Mitsuyori Asari and Tooru Tsuru
Tokyo Institute of Technology, Faculty of Engineering
O-okayama, Meguro-ku, Tokyo, Japan

ABSTRACT

Mass transport through a coating during blistering of epoxy-coated steel has been studied in a sodium chloride solution with or without the presence of electric current. In the presence of anodic or cathodic current, ferrous chloride or sodium hydroxide solutions are created beneath the coating respectively. The concentrations of the solutions in the blisters were found to be maintained at the level of 0.1 mol/kg, so that no appreciable osmotic pressure operates across coating. The water penetrated beneath coating by osmosis is utilized for hydrolysis reaction of ferrous ion in anodic blister and for dilution of sodium hydroxide in cathodic blister. Therefore, the amount of water penetrated into anodic blisters is an order of magnitude less than that in cathodic blisters.

INTRODUCTION

Blistering or delamination of organic coatings on a substrate is a very common phenomenon under service conditions. Although a large amount of literature exists on this subject,^{1,2} a quantitative explanation has been lacking up to the present time. This state of affairs is certainly due to the complexity of the phenomenon which involves a number of physico-chemical processes, such as penetrations of water, oxygen and ionic species, loss of adhesion, deformation of the coating and corrosion of the substrate.

The literature on the causes and the mechanism of blistering has been reviewed by Kresse.³ From the review it follows that osmosis often plays a role in blistering. Data about this phenomenon have been described by many workers⁴⁻⁸ nature. Influences of substrate and environment on the cathodic delamination of organic coatings are extensively studied by Leidheiser et al.⁹⁻¹¹ Van der Meer-Lerk et al.¹² and Perera et al.¹³ quantitatively studied the growth of blisters formed by water transport induced by dosed amount of salt.

The aim of this paper is to establish phenomenologically the mass transport through coating during blistering of coated-steel by means of chemical analysis of the solution in blisters.

EXPERIMENTAL DETAILS

Specimen

Specimens were cut from mild steel plate and abraded with emery paper. After soldering lead wire, the specimens were washed with ethanol and then coated with a transparent epoxy resin by brushing. The test surface was 32 cm² in area.

Procedure

The absorption of water by coated steel was studied in acidic 3% NaCl solution with or without the presence of electric current. Before the experiment, the specimens were kept in distilled water for 40 h in order to remove water-soluble substances in the coating, then dried in desiccator for 150 h, and kept under atmospheric condition. The counter electrode for the water absorption measurement was a platinized platinum wire 0.05 cm in diameter and 10 cm in length. Approximately constant current was supplied from dry batteries. Mass gain of the specimens was measured at appropriate time intervals. The experiments were conducted under atmospheric condition at 303.2 K.

Blistering of coated steel occurred in relatively short period under cathodic or anodic polarization, although anodic blisters are much smaller either in number or in size than cathodic blisters. Since the delaminated portion has an optical reflectivity difference from a sound portion, the delaminated area was measured by visual observation after photographing the surface. After appropriate experimental time, the specimens were washed with a jet of distilled water, then blisters were broken and the specimens were soaked in 20 ml of 2N H₂SO₄ for 20 s and washed with a jet of distilled water to recover the solution beneath the coating for chemical analysis. The amount of chloride was determined by potentiometric titration, and sodium and ferrous ions were analyzed by atomic absorption. The pH value of the solution in blisters was determined by a test paper.

EXPERIMENTAL RESULTS AND DISCUSSIONS

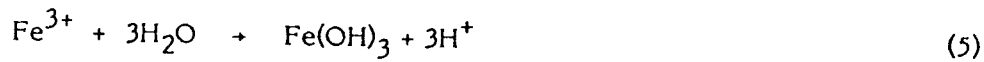
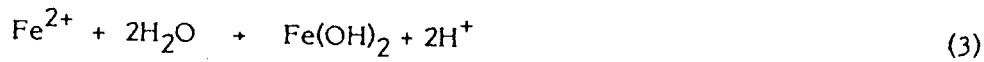
Penetration of Water

Figure 1 shows the mass increase of coated steels in acidic 3% NaCl solution with or without the presence of electric current. In the absence of electric current, the mass increased with time in the initial period, exhibiting an asymptotic behavior. The ratio of the mass increase to the mass of coating was approximately independent of the thickness of coating. Since no blister was observed up to this stage, the mass increase is mainly attributable to absorption of water by the coating. In the presence of cathodic current, however, a step-wise mass increase was observed together with the occurrence of blisters filled with aqueous solution. The rate of the mass increase decreased with increasing the thickness of coating. A similar experiment was conducted for an extended

period. It is the experimental fact that the transport of water through coating for blister formation is accelerated by application of cathodic current with the average rate of approximately 20-60 mol/F depending on the thickness of the coating. This high penetration rate of water is probably attributable to osmotic pressure across coating. On the other hand, the rate of the mass increase under anodic current is an order of magnitude less than that under cathodic current.

Ionic Transport Through The Coating

In order to simulate the partial cathodic and anodic reactions that would occur in corrosion of coated steel, the specimens were polarized in acidic 3% NaCl solution with constant anodic or cathodic current for an extended period. In anodic blister, the substrate anodically dissolves as ferrous ion and forms hydroxide or oxide by hydrolysis beneath the coating, thus



Water is transported through the coating mainly by osmosis. Electroneutrality in the blisters is maintained by migration of charge carriers through the coating. The possible charge carriers in anodic blisters are Fe^{2+} and Cl^- . On the other hand, in cathodic blister, hydroxyl ion is formed by cathodic reduction of oxygen, thus



Oxygen and water needed for the reaction are transported by diffusion and osmosis respectively. Possible charge carriers at cathodic area should be Na^+ and H^+ .

Total amounts of Fe^{2+} , Cl^- and Na^+ accumulated in the blisters are plotted against the amount of charge passed in Figs. 2, 3, and 4 respectively. In spite of an appreciable scattering in coating thickness of respective specimens, the graphs in Figs. 2, 3, and 4 exhibit straight lines. It is seen in Fig. 2 that ferrous ion accumulated in the anodic blisters is only 50% of that expected from the amount of electric charge passed. This means that the rest of ferrous

ion was lost by outward migration through coating. On the other hand, the amount of chloride is approximately 50% of that estimated assuming that the transport number of Cl^- through coating is unity, as shown in Fig. 3. Therefore, it is said that, at anodic sites, current is carried through the coating by Fe^{2+} and Cl^- at approximately equal rates. Owing to the hydrolysis reactions shown in Eqs. [3-5], the pH value of the solution in anodic blisters should decrease. Decrease in the pH value stimulates the outward migration of hydronium ion, which leads the pH value of the solution in anodic blisters to a stationary value of approximately 3.5.

In the cathodic blisters, Cl^- and Fe^{2+} were not detected and Na^+ was accumulated. The pH value of the solution in the blisters increases over 13.5 owing to OH^- ion created by reaction [6]. As is seen in Fig. 4, the apparent transport number of Na^+ is approximately 0.5 in the initial period and then decreases to zero in the final stage. It must be noted in Fig. 5 that almost the entire surface was delaminated by the cathodic charge of 2 C/32 cm². This means that, in the initial stage of blistering, 50 percent of the current through the coating is carried by Na^+ and the rest is probably attributable to migration of H^+ . Therefore, it is likely that the pH value of the solution under the coating increases over 13 in the initial short period, which stimulates delamination of coating. In the following stage, current is carried through the coating mainly by H^+ which forms water in the blisters, thus



However, the amount of water created by this mechanism is 2×10^{-3} g for 12 Coulomb, which is approximately 1/100 of that estimated either by visual observation of the blisters or by mass gain measurement. The outward migration of OH^- may be also possible because of high pH value of the solution in cathodic blister. Nevertheless, most of the water in the blisters should be transported by osmosis. In the stationary stage, the pH value in cathodic blisters may decrease gradually.

Blistering

Blistering of coated metal is caused by the accumulation of water between the coating and the substrate. This accumulation is the result of a unidirectional transport of water through the coating by osmosis. According to van der Meer-Leark et al (12), the transport of water through the coating, flux q , is determined by the modified osmosis law given by Eq. [8]

$$q = \frac{DC_w V_w}{dRT} (\Delta\pi - P_k) = \frac{DC_w}{d} \left(\ln \frac{a_2}{a_1} - \frac{P_k}{RT} \right) \quad (8)$$

where a_1 and a_2 are the activities of water in salt solutions inside and outside of blister respectively, and D is the mean diffusion coefficient, C_w the mean water concentration in the coating, V_w the partial molar volume of water, $\Delta\pi$ the osmotic pressure, d the thickness of film, P_k the compressive pressure, and the other symbols have their usual significances. The compressive pressure represents the forces of adhesion and rigidity of the coating. The activity of water vapor with pressure p is given by

$$a = p/p_0 \quad (9)$$

where p and p_0 represent vapor pressures of water above the salt solution and the pure water respectively.

According to Eq. [8], the susceptibility of coated steel to blistering depends on various parameters, such as D , C_w , d , P_k and a_1 and a_2 . For a given coated steel, the controlling factor for blistering is a_1 , the magnitude of which depends on the concentration of salt solution in the blister. The salt beneath the coating is created by corrosion of the substrate and migration of ionic species. The activity of water of salt solutions (14) is plotted against the concentrations in Fig. 6. It is seen that the activity decreases steeply above a threshold concentration of 2 mol/kg irregardless of the nature of salts. As can be seen in Eq. [8], the rate of blistering decreases with decreasing the activity of water outside the blister. It was observed by Leidheiser et al. (9) that the rate of cathodic delamination of coated steel decreases with increasing the concentration of NaCl solution.

It has been well known that blistering or delamination of coatings are predominant at cathodic sites compared with anodic sites. In anodic blisters, Fe^{2+} and Cl^- are introduced by anodic dissolution of the substrate and inward migration of Cl^- respectively and then forms green-black or red-brown precipitates, probably hydrated magnetite or ferric hydroxide. Therefore, it is likely that the salt concentration in the anodic blisters is limited below 1 mol/kg by the hydrolysis equilibria of Eqs. [3-5], where the activity of water is close to unity as is noted in Fig. 6. On the other hand, Pourbaix (15) claimed that the first precipitate in a similar occluded cell is $FeCl_2 \cdot 2H_2O$ at 5 mol/l and pH 3.5. The activity of water of this solution is 0.58 (Fig. 6). Nevertheless, the osmotic pressure across the coating in anodic blisters should not be so high, although the precipitation of oxide and hydroxide in the coating somewhat inhibits the penetration of water. Under stationary conditions, water is transported into anodic blister with the rate of approximately 1 mol/F, which is used for the hydrolysis reactions.

On the other hand, OH^- and Na^+ are concentrated in the cathodic blister owing to cathodic reduction of oxygen and migration of Na^+ . No hydrolysis reaction occurs in this case. Therefore, if the rate of transport of water through the coating is much lower than that of cathodic reduction of oxygen beneath the coating, the concentration of sodium hydroxide in cathodic blisters would increase up to the saturated value of 27 mol/kg, where the activity of water is below 0.07 (Fig. 6). If this is the case, the osmotic pressure across the

coating would exceed over 10 atmospheres of pressure as was claimed by several workers^{12,13}. As was mentioned above, however, water was transported into blisters through the epoxy coating with the rate of approximately 20-60 mol/F under cathodic current of 4×10^{-6} A/cm² depending on the thickness of the coating (Fig. 1). The average concentration of sodium chloride solution in the cathodic blisters is plotted against the amount of charge passed in Fig. 7. It is seen that the concentration of sodium hydroxide in cathodic blisters is maintained below 2 mol/kg during blistering exhibiting a fluctuation. Since the activity of water of this solution is over 0.9 as is noted in Fig. 6, it is likely that the transport of water through the epoxy coating is so rapid that only a little osmotic pressure appears across the coating. The osmotic pressure would increase under high cathodic current densities or high corrosion rates, which should not occur under usual service conditions. The osmotic pressure would be also increased with increasing the forces of adhesion and rigidity of the coating P_k in Eq. [8]. However, it seems likely that the forces are readily reduced by chemical attack caused by concentrated alkaline solution created beneath the coating. As can be seen in Fig. 7, the concentration of sodium hydroxide in cathodic blisters increases with increasing the thickness, probably resulting in an increase in the osmotic pressure across the coating.

Effect of The Nature of The Cation

Similar cathodic delamination experiments were made in various chloride solutions having different cation, e.g., CsCl, KCl, NaCl, LiCl, BaCl₂ and CaCl₂. The delaminated area of the epoxy-coated steels in respective solutions is plotted against the amount of cathodic charge passed in Fig. 8. The rate of delamination decreases only slightly with the order of CsCl, KCl, NaCl and LiCl, probably owing to relatively small differences in solubility and migration rate. On the other hand, delamination did not develop in the BaCl₂ and CaCl₂ solutions because the solubility limit of Ba(OH)₂ and Ca(OH)₂ is approximately 0.2 mol/kg and no appreciable osmotic pressure for water penetration will operate across the coating. In this case, a possible charge carrier across the coating is hydronium ion.

Summarizing the discussion, the rate of penetration of water through epoxy coatings by osmosis is so rapid that the concentration of the solutions beneath the coating is maintained at the level where the activity of water is close to unity. No appreciable osmotic pressure appears across the coating during blistering. The transport of chemical species across coating during blistering is illustrated in Fig. 9. The water penetrated is utilized for hydrolysis reactions in anodic blisters and for dilution in cathodic blisters. Therefore, the total amount of water penetrated into cathodic blisters is an order of magnitude larger than that in anodic blisters, so that the delamination occurs mainly at the cathodic area.

CONCLUSION

Blistering of coated steel is caused by the penetration of water through the coating by osmotic pressure, the magnitude of which increases with increasing the concentration of the salt solution beneath the coating. The salt solution is created by corrosion of the substrate and migration of ions. Electric current through the coating is carried by Fe^{2+} and Cl^- with equal rates in anodic blisters. Hydrolysis of Fe^{2+} in anodic blister results in precipitation of hydroxide and oxide which may inhibit penetration of water through the coating. The concentration of ferrous ion in anodic blisters is controlled below 1 mol/kg by the hydrolysis equilibria. The pH value in anodic blisters was approximately 3.5. On the other hand, in cathodic blisters, electric current through the coating is carried by Na^+ and H^+ with equal rates in the initial period, but only by H^+ in the stationary state. Therefore, it is likely that the pH value in cathodic blisters increases over 13.5 in the very initial period, which stimulates delamination of the coating.

Because of the rapid penetration rate of water in cathodic blisters and of hydrolysis equilibria of ferrous ion in anodic blisters, the concentrations of salt solutions in the blisters are maintained at the level where the activity of water is close to unity. Therefore, no appreciable osmotic pressure appears across the coating. The penetrated water is mainly utilized for dilution of sodium hydroxide in cathodic blisters and for hydrolysis reactions in anodic blisters. Therefore, the amount of water penetrated into anodic blisters is an order of magnitude less than that in cathodic blisters. Thus, the delamination of coated steels occurs mainly at the cathodic site.

Acknowledgement

This work was partially supported by General Research and Development Center of the Tohoku Electric Power Co. and the Nippon Steel Corporation. Thanks are also due to Mrs. Tomomi Watanabe of Nippon Paint Co. for coating material.

REFERENCES

1. W. Funke, Progr. In Organic Coatings, 9, 29 (1982).
2. H. Leidheiser, Jr., Corrosion, 38, 374 (1982).
3. P. Kresse, Farbe u. Lack, 72, 1179 (1966).
4. D.M. Brusher and T.J. Nurse, J. Appl. chem., 9, 96 (1959).
5. D.M. James, J. Oil Col. Chem. Assoc., 43, 653 (1960).
6. J.L. Prosser and T.R. Bullett, *ibid.*, 45, 836 (1962).
7. W. Funke, J. Oil Col. Chem. Assoc., 62, 63 (1979).

8. K.R. Gowers and J.D.Scantlebury, *Corros. Sci.*, 23, 935 (1983).
9. H. Leidheiser, Jr. and W. Wang, *J. Coatings Techn.*, 53, 77 (1981).
10. H. Leidheiser, Jr., *Corrosion* 38, 374 (1982).
11. H. Leidheiser, Jr., *Corrosion*, 37, 28 (1981).
12. L.A. van der Meer-Lerk and P.M. Heertjes, *J. Oil Col. chem. Assos.*, 58, 70 (1975).
13. D.Y. Perera and P.M. Heertjes, *ibid.*, 14, 313, 395, 546, 774 (1971).
14. W. Kangro and A. Groeneveld, *Z. Physik. Chem. (Frankfurt)*,32, 110 (1962).
15. M. Pourbaix, "Atomistics of Fracture," NATO Conference Series 6, (1983), p. 603.

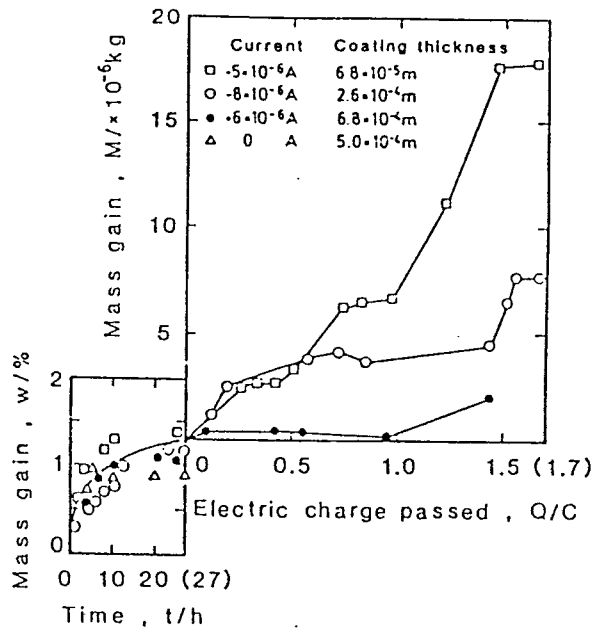


Fig. 1 Absorption of water by an epoxy-coated steel in 3% NaCl solution with or without the presence of electric current. Specimen : surface area ; 32 cm^2

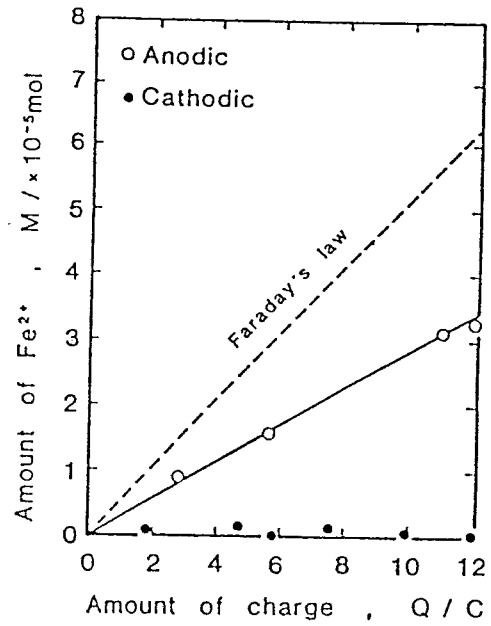


Fig. 2 Amount of Fe^{2+} accumulated in blisters formed on an epoxy-coated steel in 3% NaCl solution in the presence of electric current. Specimen : surface area ; 32 cm^2

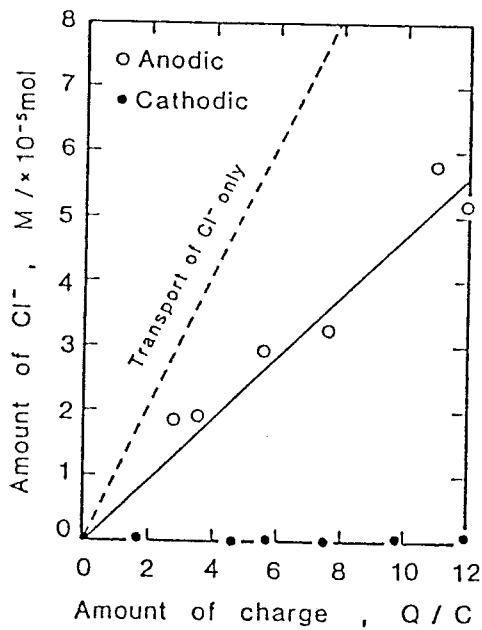


Fig. 3 Amount of Cl^- accumulated in blisters formed on an epoxy-coated steel in 3% NaCl solution in the presence of electric current. Specimen : surface area ; 32 cm^2

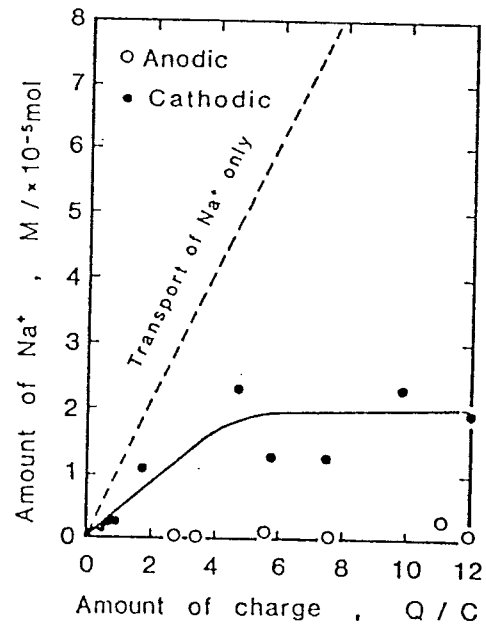


Fig. 4 Amount of Na^+ accumulated in blisters formed on an epoxy-coated steel in 3% NaCl solution in the presence of electric current. Specimen : surface area ; 32 cm^2

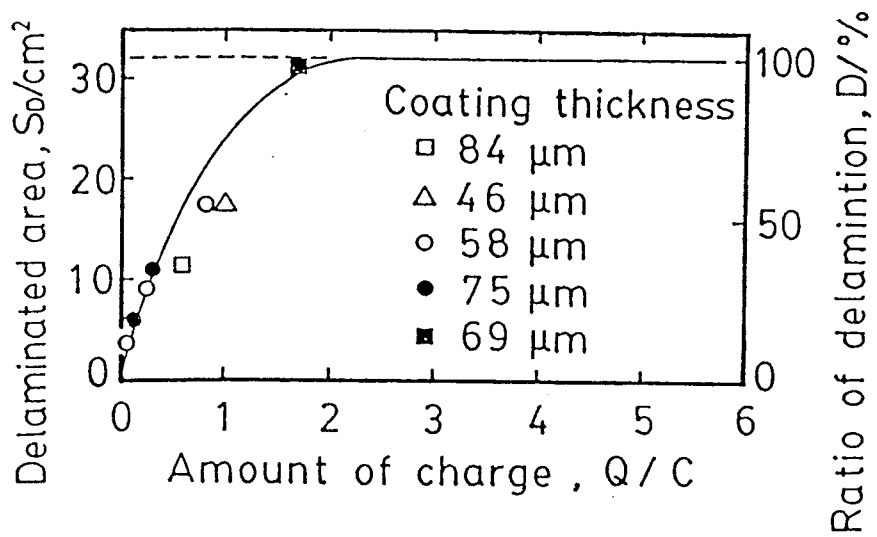


Fig.5 Delaminated area of epoxy-coated steel in 3% NaCl solution under cathodic current of 1×10^{-6} A . Surface area: $32cm^2$

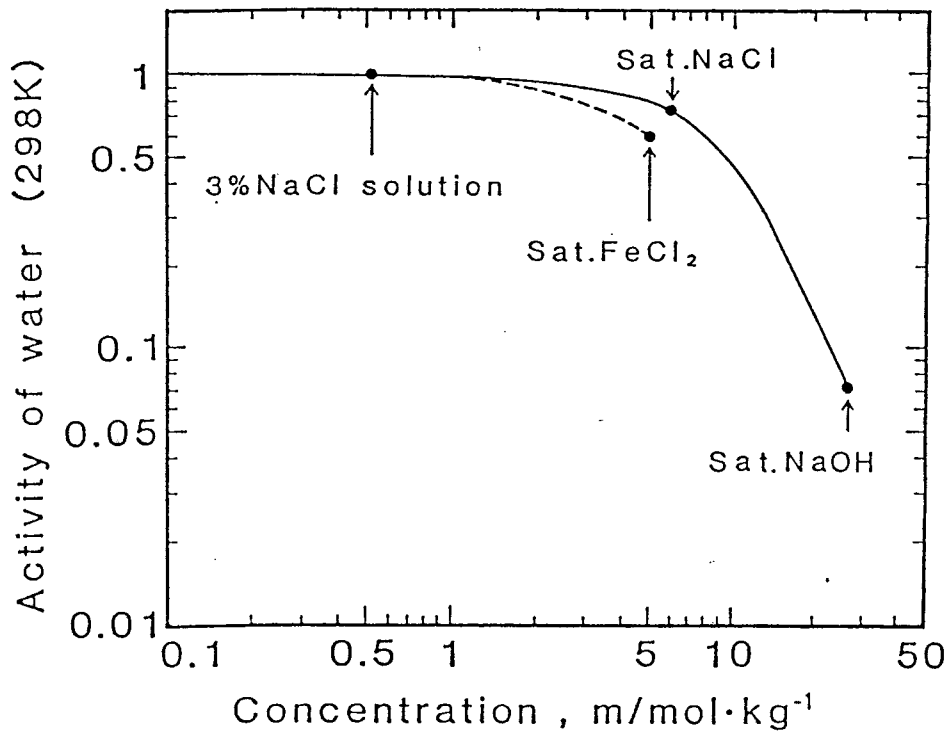


Fig.6 Activity of water NaOH, NaCl and FeCl₂ solutions.

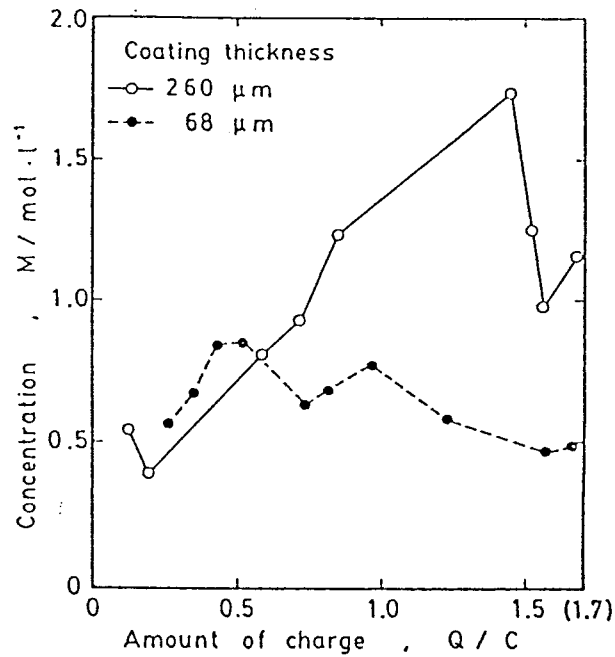


Fig.7 Average concentration of solution in the cathodic blisters versus amount of charge.

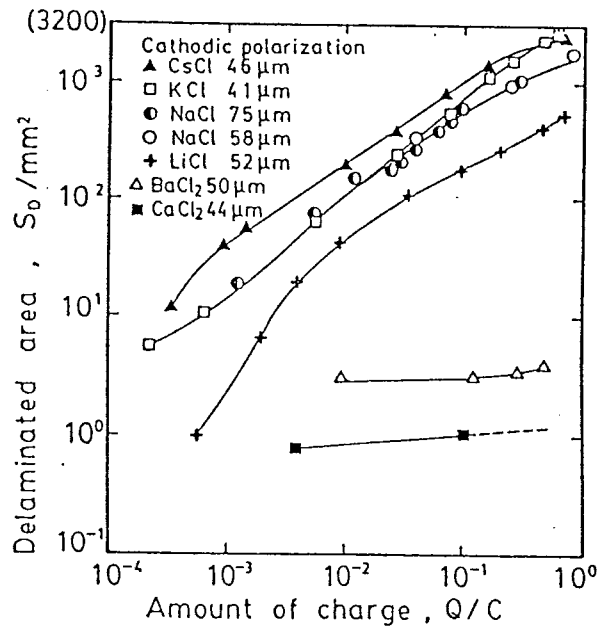


Fig.8 Cathodic delamination of epoxy-coated steel in CsCl, KCl, NaCl, LiCl, BaCl₂ and CaCl₂ solutions. Cathodic current; $0.1 \sim 1.0 \times 10^{-7}$ A. Surface area: 32 cm².

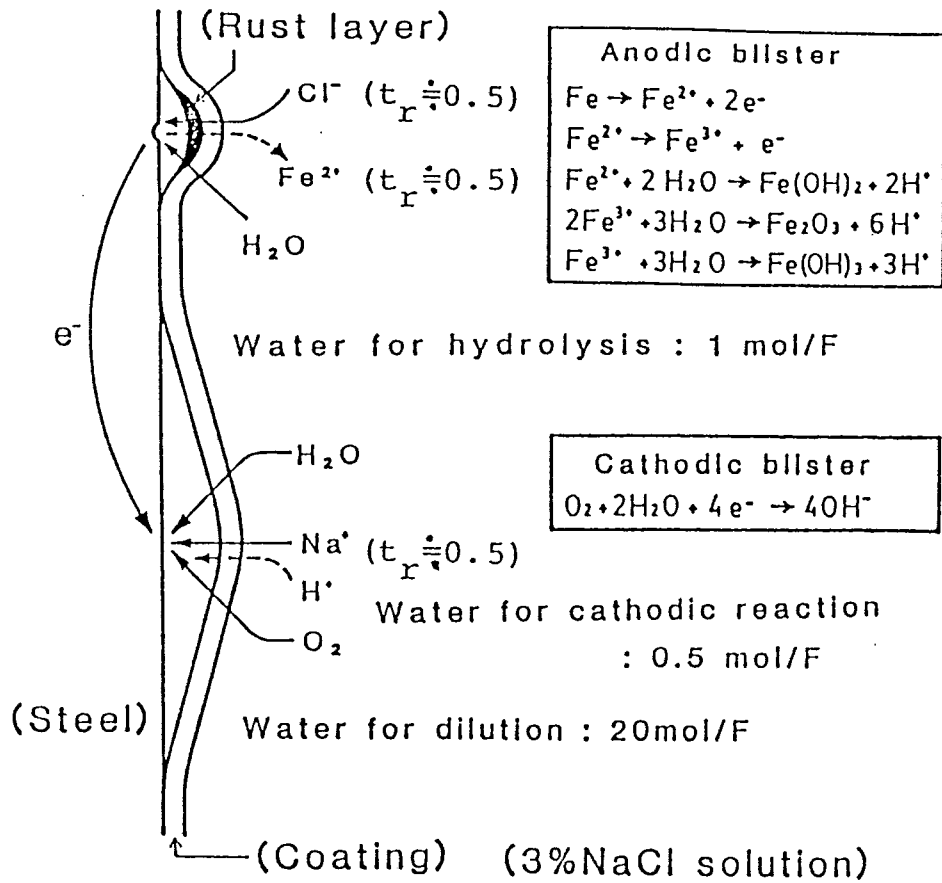


Fig.9 Transport of chemical species during blistering of coated steel.

Reprint from "Corrosion Protection by Organic Coatings", Eds. M.W.Kendig & H.Leidheiser,Jr., The Electrochemical Society, Proc. Vol.87-2, 1988

IMPEDANCE CHARACTERISTICS DURING DEGRADATION OF COATED STEEL

Shiro Haruyama, Mitsuyori Asari and Tooru Tsuru
Tokyo Institute of Technology, Faculty of Engineering
O-okayama, Meguro-ku, Tokyo 152, Japan

ABSTRACT

Degradation of coated steel in an acidic sodium chloride solution with or without the presence of electric current has been studied by means of impedance technique. The impedance of coated steel during degradation is well simulated by a simple equivalent circuit taking account of delaminated area as a parameter. Since the impedance of anodic blisters is an order of magnitude larger than that of cathodic blisters, the total impedance of coated steel under mixed potential control is substantially reduced to the impedance of cathodic blisters, unless the blisters are broken. It is found that the frequency of a break-point on the Bode diagram is proportional to the delaminated area in the initial period of degradation and serves as a reliable measure of the degradation of coated steels.

INTRODUCTION

Blistering of delamination of organic coating on metallic substrate is a very common phenomenon in service condition. The phenomenon involves several electrochemical processes such as corrosion of substrate and ionic migration through coating. Many studies of the electrical properties of polymer coatings reported in the past include measurements of the current response of an isolated film or a coated metal to an applied potential (1, 2). Mayne and co-workers (3, 4) have extensively investigated the dc conductivity of free polymer films, while the ac response of coated metals has been treated and discussed recently by several workers in terms of equivalent resistances and capacitances (5-12). Because of lack of a definite physiochemical model for this phenomenon, however, their investigations still remain at qualitative level.

Aims of this paper are to establish the correlation between the impedance characteristics and the degradation of coated steel, and to present a new method for evaluating the delamination of the coatings.

EXPERIMENTAL DETAILS

Specimen

Specimens were cut from mild steel plate and abraded with every paper. After soldering lead wire, the specimens were washed with ethanol and then coated with transparent epoxy resin by brushing. The edge and backside of

the specimens were covered with a silicone resin. The test surface was approximately 32 cm² in area.

Procedure

The coated steel specimens were placed in a 3% NaCl solution with or without the presence of electric current. The impedance measurement of coated steel was made at appropriate time intervals using a frequency response analyzer (NF Circuit Design Block, S-5720B). The measurement was made on two-electrode cell using a bare mild steel plate 230 cm² in area as counter electrode. The impedance of the counter electrode is so small that the total impedance of the two-electrode cell is substantially reduced to that of the coated steel specimens. The impedance measurements were carried out over the frequency range from 100k to 0.001 Hz. The impedance data are represented in the Bode diagram. All the experiments were conducted under atmospheric condition at 303.2K.

Equivalent Circuit for Coated Steel

Impedance characteristics of coated steel have been studied using the equivalent circuits shown in Fig. 1 (7, 9). The impedances $Z(j\omega)$ for the circuits are written as

$$Z(j\omega) = R_s + \frac{1}{jC_f\omega + \frac{1}{R_f + \frac{1}{jC_{dl}\omega + \frac{1}{R + W}}} \quad (1)$$

where ω represents angular frequency, R_s the solution resistance, C_f and R_f the electric capacitance and ionic resistance of coating respectively, and C_{dl} and R_t represent the double layer capacitance and the charge transfer resistance at substrate/coating interface respectively. The R_t value is inversely proportional to the rate of charge transfer or corrosion (13). The Warburg impedance designated as W in Eq. (1) is written as

$$W = \sigma(\omega^{-1/2} - j\omega^{-1/2}) \quad (2)$$

where for a simple redox electrode,

$$\sigma = \frac{RT}{2ZF^2} \frac{1}{C_o D_o} + \frac{1}{C_r D_r} \quad (3)$$

D is the diffusion coefficient, C_o and C_r indicate the concentrations of oxidant and reductant respectively, and the other symbols have their usual significances. The Warburg impedance that is observed on a degraded coated steel may be attributable to the diffusion of oxygen through coating or in electrolyte solution beneath coating, since it does not occur in the presence of anodic current as shown later. Occurrence of the Warburg impedance on a degraded coated steel is sometimes attributed to a distribution of the time constants owing to nonuniformity of the coating (8). A typical impedance diagram for Eq. (1) is shown in Fig. 1, where the calculations were made using the parameter values reasonable in degradation of coated steel. Correspondence between the parameter values and the characteristic points on the diagram is also indicated.

When a coated steel contacts with electrolyte solution, there is no electrolyte solution at metal/coating interface in the initial period. Therefore, no Helmholtz double layer exists and no electrochemical reaction takes place at the interface. This means that, in Fig. 1 C_{dl} and R_t are zero and infinite respectively, and hence the W value is also infinite. The only information obtained by impedance measurement in this stage is on C_f value. With the elapse of time, water and oxygen penetrate through the coating and corrosion of the substrate takes place together with the emergence of the electric double layer and then delamination of coating occurs forming blisters filled with electrolyte solution. Consequently, the magnitude of R_t decreases and the C_{dl} value increases in proportion to the delaminated area. The corrosion of the substrate is accompanied by migration of ionic species through the coating under the control of electroneutrality. Since ionic current through the coating is concentrated at the delaminated area, the magnitude of R_f also relates to the area, or more exactly the mantle area. Therefore, as a first approximation, the parameters in the equivalent circuit are written as

$$C_f = C_f^0 \cdot S_0 \quad (4)$$

$$C_{dl} = C_{dl}^0 \cdot S \quad (5)$$

$$R_t = R_t^0/S \quad (6)$$

$$R_f = R_f^0/S \quad (7)$$

$$\sigma = \sigma^0/S \quad (8)$$

where S_0 indicates the surface area of specimen, S the total delaminated area, and C_{dl}^0 , R_t^0 and R_f^0 represent the specific values, namely the magnitudes per unit area of respective parameters. The delaminated area in this model means the area of metal/coating interface where charge transfer reaction is ready to

occur. In practice, however, the specific values should be different for individual blisters and the thickness of the coating may not be uniform. This complication may give the impedance behavior an extra distributed dispersion at low frequencies. In this paper, however, the impedance data are discussed in terms of the equivalent circuits of Fig. 1 considering Eqs. (1) - (8). The values of impedance parameters in this study were determined from the impedance data by computer simulation.

RESULTS AND DISCUSSIONS

Impedance Measurement

Degradation of coated steel in a NaCl solution with or without the presence of electric current was traced with impedance measurement.

Figure 2 shows the change in impedance diagram of coated steel in the absence of electric current. Computer-simulated curves based on Eq. (1) are plotted in solid lines in the figure. In the initial period, the specimen is quite capacitive, namely, the impedance diagram exhibits a straight diagonal line and phase shift is close to 90 degrees over a wide frequency range. The capacitance value was 2×10^{-9} F/32 cm², which corresponds to that of the coating C_f . No blisters were observed in this stage. The impedance at high frequencies slightly decreases with time indicating an increase in C_f value owing to absorption of water. With the elapse of immersion time, both the impedance and phase shift at low frequencies decrease exhibiting undulation. Few small green-black blisters appeared, surrounded by many transparent blisters of various size. The former and latter correspond to the anodic and cathodic blisters respectively. The decrease in impedance at extremely low frequencies is attributable to occurrence of corrosion coupled with delamination of the coating. Referring to the equivalent circuit of Fig. 1, this impedance value corresponds to $R_t + R_f$ and should be proportional to the inverse of delaminated area. On the other hand, the impedance arrest at intermediate frequencies corresponds to the ionic resistance of the coating R_f at delaminated area. The capacitance value obtained at low frequencies corresponds to the double layer capacitance C_{dl} at delaminated area and should increase in proportion to the area. The impedance at high frequencies, hence C_f value, was not so much changed by occurrence of blistering.

In order to study the anodic and cathodic degradation separately, impedance measurements were made on the coated steel specimens after keeping in an acidic chloride solution in the presence of electric current for appropriate period. DC voltage of 9 V was supplied across two identical coated steel electrodes of 32 cm² in area, so that the two electrodes served as anode and cathode respectively. Current increased gradually and reached a stationary value of 1.5×10^{-7} A within 5 days. At appropriate time intervals, the impedance of each electrode was measured against a bare steel counter electrode 230 cm² in area, after disconnecting the dc source.

Impedance diagrams of the anode at appropriate experimental times are shown in Fig. 3. In the initial period, the impedance is highly capacitive, exhibiting the phase shift of 90 degrees over wide frequencies. With the elapse of time, namely increasing the amount of anodic charge passed, the impedance value at low frequencies decreases exhibiting an arrest at intermediate frequencies together with decrease in phase shift. The impedance characteristics in this stage is well explained by the circuit shown in Fig. 1, although the Warburg impedance are not observed. The decrease in impedance value is almost saturated after 3 days, where R_t , R_f and C_{dl} values are 3×10^7 ohm, 2×10^7 ohm and 2×10^{-6} F respectively. By comparing the results shown in Figs. 2 and 3, it is seen that coated steel is rather protected from delamination by the application of anodic current. This finding suggests the possibility of anodic protection of coated steel in the absence of pores. In this stage, few small green-black blisters were observed. The impedance at high frequencies, hence C_f value, is not substantially affected by application of anodic current.

Impedance diagrams of the cathode are shown in Fig. 4. Theoretical curves based on Eq. (1) are also plotted in solid lines. The impedance at low frequency decreases rapidly with time, exhibiting the Warburg impedance. The impedance arrest corresponding to transfer resistance is scarcely observed after cathodic polarization. In this stage, many large transparent blisters were observed on the surface. It is likely that the changes in R_f and C_{dl} and the occurrence of the Warburg impedance are attributable to delamination of the coating/metal interface. The R_f value of the anode is roughly 100 times larger than that of the cathode after 16 day experiment, even though a same amount of charge has passed through both the electrodes. If the specific resistance of the coating is assumed to be the same of anodic and cathodic blisters, the delaminated area of cathodic blisters is 100 times that of anodic blisters. It is said that the delamination of the coating is very much accelerated by the application of cathodic current. The C_f value did not change with time even in the presence of many cathodic blisters.

Changes in the magnitudes of R_f , R_t and C_{dl} during the cathodic degradation of epoxy-coated steel are plotted against the cathodic charge passed in Fig. 5. In the initial period, the R_f and R_t values decrease in proportion to $1/3$ power of the amount of charge passed. After an appreciable amount of charge passed, however, the R_f value reaches to a saturation, whereas R_t decreases steeply. This saturation of R_f value may be because only a part of the mantle surface of blisters serves as the path for ionic migration through the coating in the final stages of blistering.

Impedance of coated steel under mixed potential control as shown in Fig. 2 is represented by a parallel combination of the impedances of the cathode and anode. Since the impedance of cathodic blisters is always an order of magnitude less than that of anodic blisters, the total impedance of coated steel is substantially reduced to the impedance of cathodic blisters, unless the blisters are broken.

Assessment of Degradation of Coated Steels

As stated in the preceding section, the impedance of coated steel is well explained by the equivalent circuits shown in Fig. 1 and Eqs. (1) - (8), although some ambiguities still remain at low-frequency impedance probably because of distributed time constants.

The typical impedance diagram for the equivalent circuits has four break points which are indicated in Fig. 1 as f_s , f_h , f_m and f_l respectively. The break point f_s could not be observed in usual impedance measurement, since it appears at very high frequencies. The frequencies at the break points relate to the impedance parameters, thus

$$f_h = (1/2\pi C_f R_f) \left(\frac{S}{S_0} \right) \quad (9)$$

$$f_m = 1/2\pi C_{dl}^0 R_f^0 \quad (10)$$

$$f_l = 1/2\pi C_{dl}^0 (R_t^0 + R_f^0) \quad (11)$$

where it is assumed that $R_s \ll R_f$ or R_t , and $C_{dl} \gg C_f$. It must be noted that f_m and f_l are independent of the delaminated area, although, in practice, they may somewhat depend on the delaminated area due to the inconsistency in the effective area between the double layer on the metal surface and migration paths through the coating in a late stage of blistering. Generally, the impedance arrest corresponding to transfer resistance is not clearly observed due to the high resistance of the coating and the participation of the Warburg impedance.

The specific values C_f^0 and R_f^0 of the coating are written as

$$C_f^0 = \epsilon/2\pi d \quad (C_f^0 = \epsilon/2\pi d) \quad (12)$$

$$R_f^0 = \rho \cdot d \quad (13)$$

where ϵ , d and ρ represent the dielectric constant, the thickness and the specific ionic resistance of the hydrous coating respectively. Substitution of Eqs. (12) and (13) into Eq. (9) yields

$$f_h = (d/\epsilon\rho d) \left(\frac{S}{S_0} \right) = K_f (S/S_0) \quad (14)$$

where K_f is a characteristic constant of the coating material, which is independent of the thickness. It must be emphasized in Eq. (14) that the f_h

value is proportional to the ratio of delaminated area to the total area, without depending on the thickness or total area of the coating.

Computer simulation of the impedance of coated steels having different delaminated area was made on the basis of the circuit shown in Fig. 1 using Eqs. (1) - (8). The results shown in Fig. 6 well describe the change in the impedance characteristics of coated steel during degradation. The influence of the coating thickness on the impedance of a partially delaminated coated steel is simulated in Fig. 7, using Eqs. (12) and (13). With increasing the thickness, the magnitude of the impedance increases and the Warburg impedance and transfer resistance fade away, whereas the break frequency f_h is kept unchanged. It is noted in Figs. 6 and 7 that the values of R_t , C_{dl} and σ can not be experimentally obtained for thickly coated steel or in the initial period of degradation, where the rates of corrosion and delamination are controlled by ionic migration through the coating. The only data which can be obtained in these cases are on R_f and f_h values. Since the f_h value is proportional to delaminated area without depending on the thickness of the coating, it provides a most reliable information on the delamination of coated steel.

In order to confirm the feasibility of this approach, the values of the R_f , σ and C_{dl} obtained from Fig. 4 are plotted against the respective f_h values in Fig. 8. It is noted in Fig. 8 that R_f and R_t decrease and C_{dl} increases approximately proportional to f_h until the magnitudes of f_h and R_f reach a saturation. Occurrence of the saturation of R_f value indicates that an easy migration path was already formed in the delaminated part of the coating and afterward the R_f value remained constant regardless of further development of delamination. The K_f value can be determined either from Eq. (13) using the known values of the dielectric constant and ionic resistance of the coating or by a preliminary experiment. Since the phase shift is usually 45 degrees at the break point, the f_h value can be precisely determined from the phase shift. Accordingly, it is concluded that the break frequency f_h is utilized as a quantitative measure of the delaminated area especially in the initial stage of blistering.

Application of The Break-Point Frequency Method

Degradation of various coated steel in 3% NaCl solution was studied by means of the break-point frequency method described above. The specimens were the steel plates covered with epoxy resin after different surface treatments; e.g. as-received (A), as phosphated (B), as-plated with Ni-Zn alloy (C), as-phosphated after Ni-Zn plating (D), as-chromated after Zn plating. The surface area of the specimens were 32 cm². The details of the impedance measurement were similar to those described above. All the impedance diagrams obtained have the form similar to Figs. 2, 3 and 4. The break-point frequency f_h was obtained from Bode diagrams as the frequency at the phase shift of 45 degree.

The break-point frequencies of various coated steels are plotted against the time of immersion in Fig. 9. Since the break-point frequency is proportional to the delaminated area according to Eq. (14), the graphs in Fig. 9

represent substantially the time-course of delamination of coated steels. It is seen in Fig. 9 that the rate of delamination of specimen A is more than an order of magnitude larger than the other specimens. The rate of delamination of specimen D is very low in the initial period but it increases steeply after 10 h. The rate of specimen E is very low and fluctuates after 10 h. In this experiment, occurrence of delamination could be discriminated by visual observation only after the break-point frequency exceeded 200 Hz, where the delaminated area was approximately 10^{-2} of the total surface area. The minimum break-point frequency in Fig. 9 is 0.02 Hz which corresponds to the delamination ratio of 10^{-6} . Therefore, it is concluded that the break-point frequency method is four orders of magnitude more sensitive in detecting delamination than visual observation.

CONCLUSION

A fissure-free epoxy-coated steel is highly resistant to degradation in the presence of anodic current. Depression of the impedance value at low frequencies was not noticed over an extended period. This fact suggests the possibility of anodic protection of coated steels. On the other hand, the coated steel is degraded very quickly in the presence of cathodic current. The impedance value at low frequencies decreases in a short period and the Warburg impedance is usually observed.

The capacitance of the coating C_f does not change appreciably with time. The magnitudes of R_f , R_t and $1/C_{dl}$ decrease approximately in proportion to the delaminated area in the initial stage of delamination. Since the impedance of anodic blisters is an order of magnitude larger than that of cathodic blisters, the total impedance of coated steel under mixed potential control is substantially reduced to the impedance of cathodic blisters, unless the blisters are broken.

The impedance of coated steels during degradation is well simulated by a simple equivalent circuit taking account of the delaminated area as a parameter. The frequency of the break-point f_h on the Bode diagram is proportional to delaminated area in the initial stage of delamination and serves as a reliable quantitative measure of the delamination of coated steels.

Acknowledgement

This work was partially supported by General Research and Development Center of the Tohoku Electric Power Co., the Nippon Steel Corporation and Central Engineering Laboratory of the Nissan Motor Co.

REFERENCES

1. N.D. Tomashov, Yu.N. Mikhailovskii and V.N. Leonov, *Corrosion*, 20, 125C (1964)

- (2) M.W. Kendig and H. Leidheiser, Jr., J. Electrochem. Soc., 123, 982 (1976)
- (3) J.E.O. Mayne, Brit. Corrosion J., 5, 106 (1970)
- (4) E.M. Kinsella and J.E.O. Mayne, Brit. Polym. J., 1, 173 (1969)
- (5) L.M. Callow and J.D. Scantlebury, J. Oil Col. Chem. Assoc., 64, 83, 119, 140 (1981)
- (6) J.D. Scantlebury, A. Guiseppi-elie, D.A. Eden and L.M. Callow; Corrosion, 39, 108 (1983)
- (7) F. Mansfeld, M.W. Kendig and S. Tsai, Corrosion, 38, 478 (1982)
- (8) M.W. Kendig, F. Mansfeld and S. Tsai, Corros. Sci., 23, 317 (1983)
- (9) G.W. Walter, J. Electrochem. Soc., 118, 259 (1981)
- (10) J. Hubrecht, J. Vereecken and M. Piens, J. Electrochem. Soc., 131, 2010 (1984)
- (11) T. Tsuru, S. Sudo and S. Haruyama, Denki Kagaku, 51, 159 (1983)
- (12) L. Beaunier, I. Epelboin, J.C. Lestrade and H. Takenouchi, Surf. Technol., 4, 237 (1976)
- (13) S. Haruyama, Proceedings, 5th International Congress in Metallic Corrosion, National Association of Corrosion Engineers, (1972), p.82
- (14) W. Kangro and A. Groeneveld, Z. physik. Chem. (Frankfurt), 32, 110 (1962)

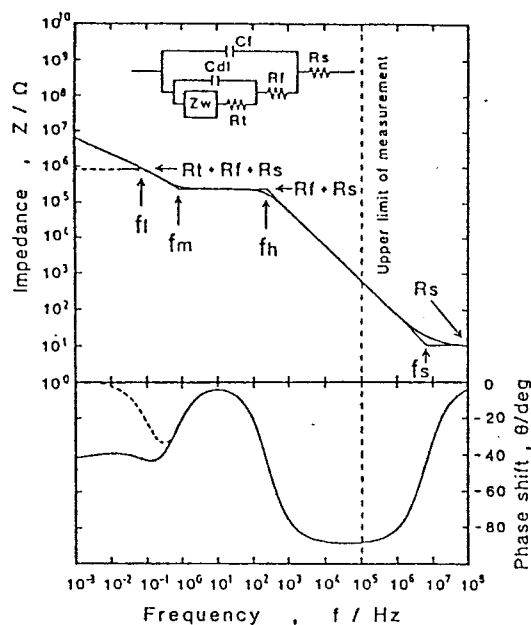


Fig. 1. Equivalent circuit for impedance diagram for degraded coated steel
 $R_s=10 \text{ ohm}$, $R_f=2.5 \cdot 10^5 \text{ ohm}$, $R_t=6.5 \cdot 10^5 \text{ ohm}$,
 $C_f=2.4 \cdot 10^{-4} \text{ F}$, $C_{d1}=1.6 \cdot 10^{-6} \text{ F}$, $\sigma=3.4 \cdot 10^5 \text{ ohm}$

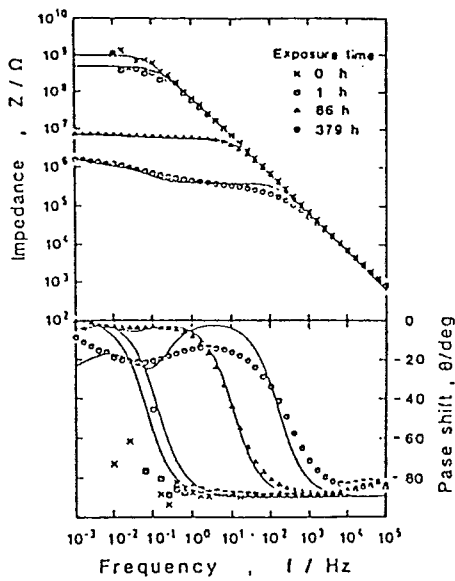


Fig. 2. Change in impedance characteristics of an epoxy-coated steel with time in 3% NaCl solution in the absence of electric current surface area: 32 cm^2 , coating: $7.8 \cdot 10^{-3} \text{ cm}$ solid line; computer-simulated curves

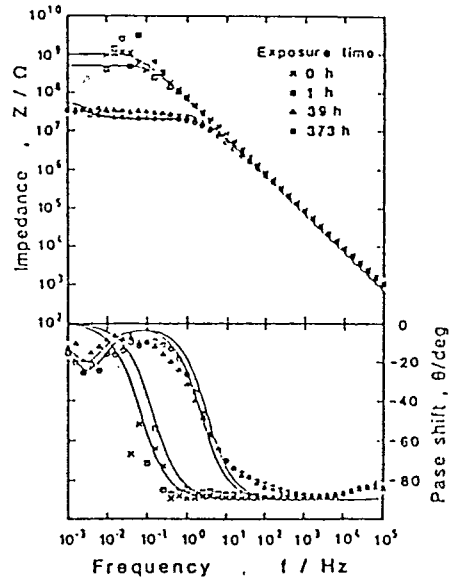


Fig. 3. Change in impedance characteristics of epoxy-coated steel with time in 3% NaCl solution in the presence of anodic current of $1.5 \cdot 10^{-7} \text{ A}$ surface area: 32 cm^2 , coating: $9.4 \cdot 10^{-3} \text{ cm}$ solid line; computer-simulated curves

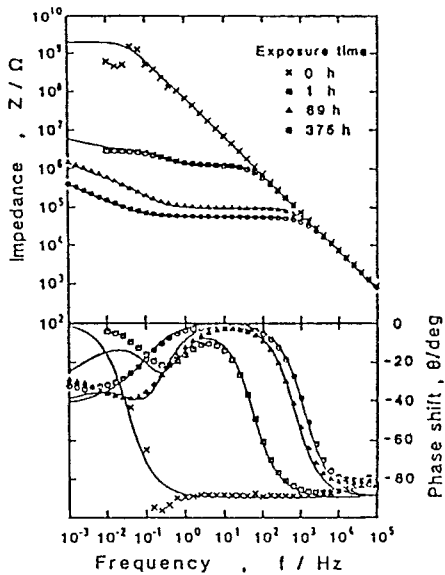


Fig. 4. Change in impedance characteristics of an epoxy-coated steel with time in 3% NaCl solution in the presence of cathodic current of $1.5 \cdot 10^{-7} \text{ A}$ surface area: 32 cm^2 , coating: $8.0 \cdot 10^{-3} \text{ cm}$ solid line; computer simulated curves

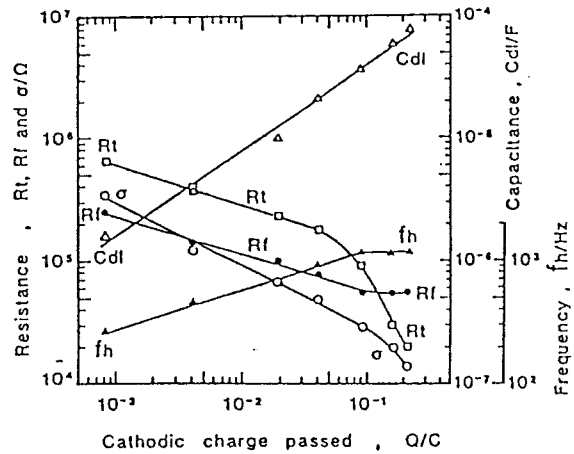


Fig. 5. Change in magnitude of R_f , R_t , C_{dl} , and σ of an epoxy-coated steel in 3% NaCl solution during cathodic delamination surface area: 32 cm^2 , coating: $8.0 \cdot 10^{-3} \text{ cm}$

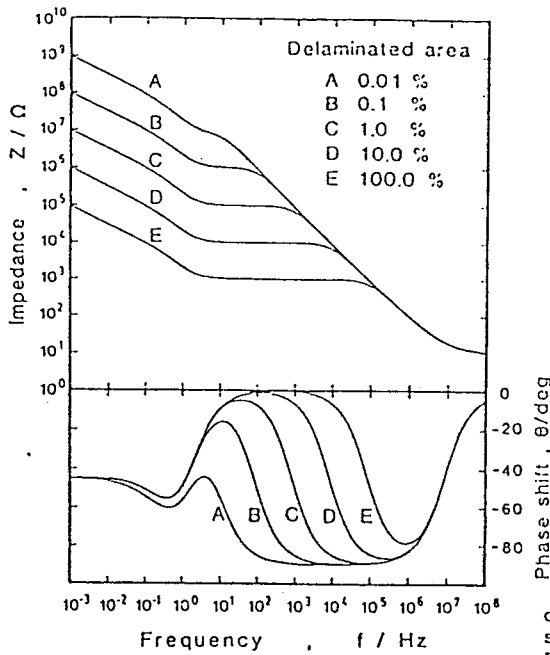


Fig. 6. Computer simulation of impedance characteristics of degraded coated steel $R_s=10 \text{ ohm}$, $C_{dl} S_0=2 \cdot 10^{-9} \text{ F}$, $C_{dl} S_0=1 \cdot 10^{-4} \text{ F}$, $R_f/S_0=1000 \text{ ohm}$, $R_t/S_0=5000 \text{ ohm}$, $\sigma_0/S_0=5000 \text{ ohm}$. Numbers indicate S/S_0

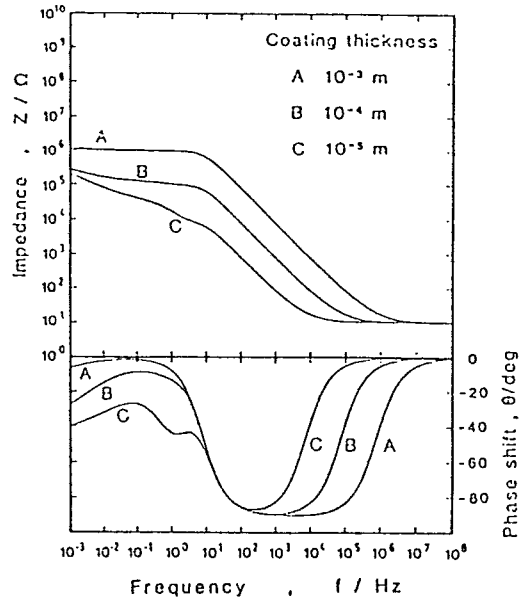


Fig. 7. Computer simulation of impedance characteristics of a partially delaminated steel having different coating thickness $R_s=10 \text{ ohm}$, $C_{dl}=1 \cdot 10^{-9} \text{ F}$, $R_t=2 \cdot 10^4 \text{ ohm}$, $\sigma=1 \cdot 10^4 \text{ ohm}$, $R_f=1 \cdot 10^7 \text{ (d/cm) ohm}$, $C_f=2 \cdot 10^{-9} \text{ (d/cm) F}$

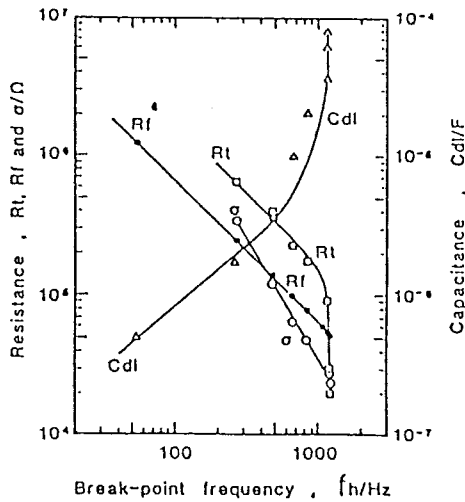


Fig. 8. Logarithmic plots of change in magnitude of R_f , R_t , C_{dl} and σ against f_h during cathodic delamination of an epoxy-coated steel in 3% NaCl solution surface area; 32 cm^2 , coating; $8.0 \cdot 10^{-3} \text{ cm}$

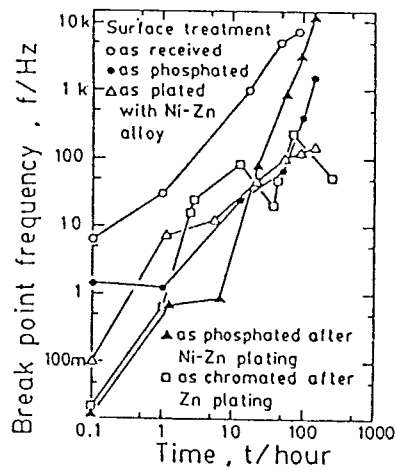


Fig. 9. Time course of break-point frequencies of various coated steels prepared after different surface treatments in 3% NaCl solution

Atmospheric Roof Corrosion in the Communities
that Surround the Makban Geothermal Facilities
in the Philippines

by DR. ERNESTO S. LUIS

ABSTRACT

This is a research project to study the corrosivity of the atmosphere and the corrosion behavior of galvanized steel specimens which is used as roofing materials in the Makban Geothermal Facilities in the Phil. This study was undertaken employing two main activities, (1) monitoring of environmental factors and (2) outdoor exposure testing. The monitoring activity was conducted having the following parameters: a) atmospheric pollutants, namely: SO_2 , H_2S , airborne salinity or NaCl and dustfall, and b) meteorological factors like relative humidity, temperature and wind direction. Outdoor exposure testing was employed in order to evaluate the corrosion rate of the exposed test specimens of galvanized steel sheet gauge 24 and gauge 26.

Atmospheric Corrosion in Jakarta

by Iing Musalam

ABSTRACT

Atmospheric corrosion tests have been carried out in Jakarta Metropolitan City, including marine, industrial, urban, trading and congested traffic areas.

Bare and coated specimens of mild steel were exposed for five months. In this test only SO_2 and chloride ion as corrosive agents were monitored. This paper discussed the results of the tests.

INHIBITION BY AZELATES ON CONTAMINATED STEEL

HASNAH ABDUL WAHAB
Senior Research Officer
Metal Protection and Finishing Unit
Standards & Industrial Research
Institute of Malaysia

ABSTRACT

This investigation indicates that lead azelate protects mild steel in fairly aggressive solution of sulphate, chloride and nitrate. It is more tolerant of increasing amounts of sulphate, chloride and nitrate than its sodium salt. The order of aggressiveness of the three anions studied are sulphate > chloride > nitrate.

It is suggested that the inhibitive nature of lead azelate on the aqueous corrosion of mild steel is not associated with it forming insoluble salts with aggressive anions but rather to it being cathodically deposited in metallic or hydroxide form.

INTRODUCTION

Lead salts have been used in anti-corrosive paints for many hundreds of years¹, the most common system currently used being red lead (Pb_3O_4) in linseed oil. Mayne² showed that this inhibitive effect is associated with the formation of water soluble material derived from the metallic soaps of the linseed oil fatty acids. Mayne and Van Rooyen³ analysed the aqueous extracts and concluded that inhibition was due to the degradation products of the acids. The main component of this degradation product has been shown⁴ to be azelaic acid. Lead soaps break down in the presence of water and oxygen to yield lead azelate, an effective anodic inhibitor.

The investigation work here investigates the effects of aggressive ions (chloride, sulphate, nitrate) on the inhibition by sodium and lead azelate.

EXPERIMENTAL TECHNIQUES

Specimen Material

Commercially pure cold rolled mild steel in the form of a sheet with thickness of 1mm

Preparation of Specimens

Specimens in the form of 1 x 5cm rectangles were fitted with wires. Lacomit was applied over all cut edges and one specimen side. The specimens were then flat polished, successively with 120 μ m and 600 μ m emery papers. They were finally washed, degreased and then stored in a desiccator over silica gel before use.

Test solutions

- i) 10^{-3} M sodium azelate + 10^{-3} M sulphate solution
- ii) 10^{-3} M sodium azelate + 10^{-2} M sulphate solution
- iii) Saturated lead azelate + 10^{-3} M sulphate solution
- iv) 10^{-3} M sodium azelate + 10^{-3} M chloride solution
- v) 10^{-3} M sodium azelate + 10^{-2} M chloride solution
- vi) Saturated lead azelate + 10^{-3} M chloride solution
- vii) 10^{-3} M sodium azelate + 10^{-3} M nitrate solution
- viii) 10^{-3} M sodium azelate + 10^{-2} M nitrate solution
- ix) Saturated lead azelate + 10^{-3} M nitrate solution
- x) 10^{-3} sodium azelate solution

Methods of Analysis

- i) Rest potential measurements

The specimens were immersed individually in beakers containing their test solution. Their potentials, relative to a saturated calomel electrode, were measured at 1/2 hourly intervals over a period of 20 hours. Their potential/time curves are shown in Fig. 1 - 3.

ii) Scanning Electron Microscope (S.E.M.)

The immersed specimens were then carbon coated and relevant micrographs of tested specimen surfaces along with analysis of their surfaces by means of the Energy Dispersive X-ray Analytical Unit (E.D.A.X) attached to the S.E.M. were conducted.

iii) Auger Spectroscopy

The immersed specimens were washed and degreased. The lacomite layer was then scrapped off with a clean razor blade and the specimens cut carefully with a guillotine to a size 10mm square maximum. These specimens were then stored in a desiccator over silica gel and analysis carried out as soon as possible to prevent contamination.

RESULTS AND DISCUSSIONS

Potential time measurements of polished specimen

Potential time readings were taken immediately after immersion of the specimens under stationary conditions.

Figure 1 shows the potential-time curves of mild steel immersed in 10^{-3} M sodium azelate solution containing sulphate ions. The curve of the 10^{-3} M sodium azelate + 10^{-3} M sulphate is at a higher potential than that immersed in 10^{-3} M sodium azelate + 10^{-2} M sulphate. The two curves

decreases rapidly and remained constant at about -530mV and -690mV respectively. The sudden drop in potential would presumably be due to film breakdown. Both the specimens show some form of local attack on its surface and rust left in solution after immersion but the specimen in the more concentrated sulphate solution was more severely attacked since more rust was found in the beaker.

The curve of saturated lead azelate + 10^{-3} M sulphate is at a much higher potential than that of sodium azelate containing the same amount of sulphate ions. This large difference in potential (280mV) suggest that lead azelate is a far better inhibitor of iron and that it is more tolerant towards sulphate aggressive ions in solution than sodium azelate. The specimens immersed in saturated lead azelate + 10^{-3} M sulphate show a passivated clean surface.

Figure 2 show the curves plotted from potential-time readings of the immersion of mild steel specimens in chloride containing solutions. There is a slight yellow stain on both the specimens after immersion. From the appearance of the specimen and the declining tendency of the curve it would suggest a slow breakdown of the passive film.

The lead azelate + 10^{-3} M chloride curve on the average show a negligible drop in potential (+ 15mV). The curve progress in a wave form. The specimen after immersion showed a

passivated clean surface. This suggest that the film remained protective for some time.

The curve of saturated lead azelate + 10^{-3} M chloride is at a much higher potential than that of sodium azelate containing the same amount of chloride. This large difference in potential (325mV after 20 hours immersion) suggests that lead azelate is a far better inhibitor of iron and that it is more tolerant towards chloride aggressive ions in solution then sodium azelate.

Figure 3 shows the potential time curves of mild steel immersed in saturated lead azelate and sodium azelate solution containing nitrate aggressive ions. All the specimens showed passivated clean surfaces after immersion. The difference in potential suggest that lead azelate is a better inhibitor of iron than sodium azelate and is more tolerant towards nitrate ions.

From the order of the potential of the immersed specimens it would suggest that the order of aggressiveness of anions towards lead and sodium azelate are sulphate > chloride > nitrate. Specimens immersed in lead azelate containing 10^{-3} M aggressive ions all show passivated clean surfaces.

Scanning Electron Microscopic Studies (S.E.M.)

Figures 4 and 5 show scanning electron micrographs of mild steel immersed in 10^{-3} M sodium azelate + 10^{-3} M sulphate solution and saturated lead azelate + 10^{-3} M sulphate solution respectively. The micrographs clearly show that the surface of the specimen immersed in sodium azelate corroded while that immersed in saturated lead azelate solution remained passive. The nature of surface attack by the sulphate ion is a localised form of attack.

The surface of these two specimens were analysed by E.D.A.X. but no lead could be detected. An E.D.A.X. of the white particles shown in Figure 6 showed the presence of lead and iron.

Further micrographs (figure 7) of a specimen immersed in a solution of saturated lead azelate + 10^{-3} M chloride were taken. The surface of this specimen in general show a passivated surface but a pit with some corrosion products surrounding it was found. The pit was present in a stained area. This specimen had been examined by Auger Spectroscopy.

Auger Spectroscopic Studies

The Auger spectras for a specimen immersed in saturated lead azelate + 10^{-3} M chloride solution are shown in Figures 8 to 12.

Figure 8 is the spectra of the white particles found on the surface of this specimen. These particles were also similar to those found on the surface of the specimen immersed in saturated lead azelate + 10^3 M sulphate (figure 5). No such particles were observed on specimens immersed in sodium azelate solutions. Figure 8 showed the presence of lead (peak at 91eV). Other peaks that could be identified were carbon, nitrogen and oxygen which were probably due to atmospheric contaminants.

The spectra of the ion substrates (Figure 9) indicate that lead, sulphur, chlorine, carbon, oxygen and iron were present. This spectra is typical of a passivated clean surface having iron oxide on its surfaces. The lead could either exist in the form of a metallic or hydroxide, $Pb(OH)_2$. No chloride ion was shown on the spectra, suggesting that the inhibitive properties is not connected with the lead forming a precipitate with the chloride ion. The other elements present i.e. sulphur, chlorine, carbon and oxygen could be just atmospheric contaminants, iron being the metal itself.

Figure 10 is the spectra of the corrosion product around a pit while Figure 11 is a spectra of the dark stain surrounding the pit. The two spectras are similar, the

sulphur, chlorine, carbon, nitrogen and oxygen peaks are probably due to atmospheric contaminants. This suggest that the dark stain are actually the spread of corrosion products over the surface arising from the localised attack (pit).

When the dark stain was etched its Auger spectra (Figure 12) identifies the presence of lead. This spectra is similar to that of the spectra for the ion substrate which suggests a passivated surface.

No chloride ion was shown on the spectra. This therefore suggests that the inhibitive properties is not associated with the lead forming a precipitate with the chloride and that it could either be in the metallic or hydroxide form $Pb(OH)_2$.

No lead was detected on areas of the specimen that had corroded or just begun to corrode. Areas that were passive and resist attack contained lead. Only certain areas were locally attacked. This suggests that the aggressive ion had attacked at weak sites, in the passive film probably brought about by various inhomogeneities on the metal surface.

CONCLUSION

It can be concluded from the various experiments and surface analytical techniques carried out that lead azelate is a more efficient inhibitor for iron than sodium azelate.

Lead azelate seems to be more tolerant of increasing amounts of sulphate, nitrate and chloride anions than sodium azelate. The order of aggressiveness of the three anions studied is sulphate > chloride > nitrate. With sulphate and chloride anions, breakdown in the presence of insufficient inhibitors leads to localised attack.

The inhibitive properties of lead azelate is not associated with it forming insoluble salts with aggressive anions.

REFERENCES

- 01) Bailey R.C., 'The Elder Pliny's Chapters on Chemical Subjects', Part 2, Edward Arnold, London, p. 61 (1932)
- 02) Mayne, J.E.O., JOCCA, 34, 473 (1951)
- 03) Mayne, J.E.O. and Van Rooyen, D., J.Appl. Chem. 4, 384 (1954)
- 04) Mayne, J.E.O. and Ramshaw E.H., J.Appl. Chem. 13, 553 (1963)

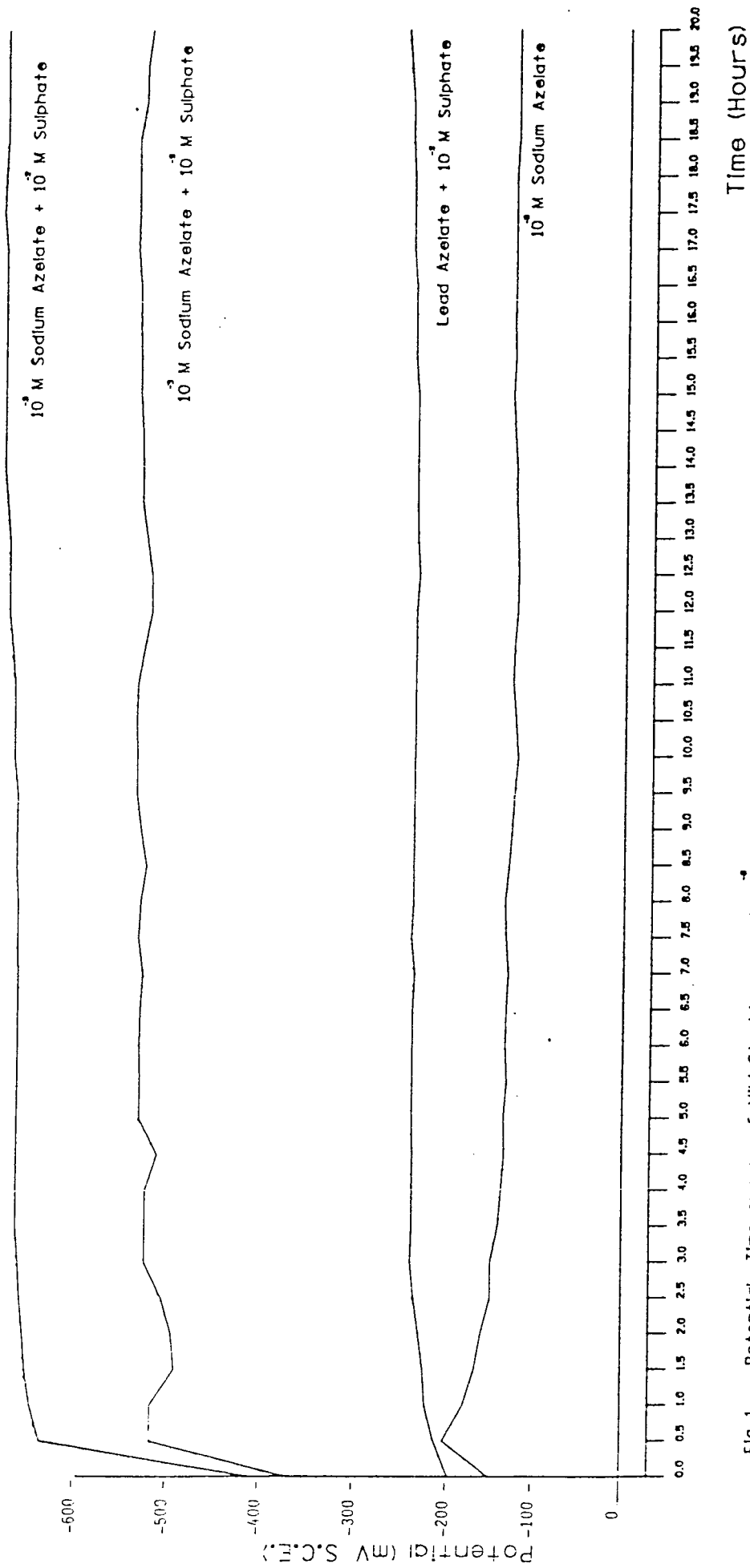


Fig 1 Potential-Time curves of Mild Steel immersed in 10^{-3} M Sodium azelate solution and sulphate containing solution

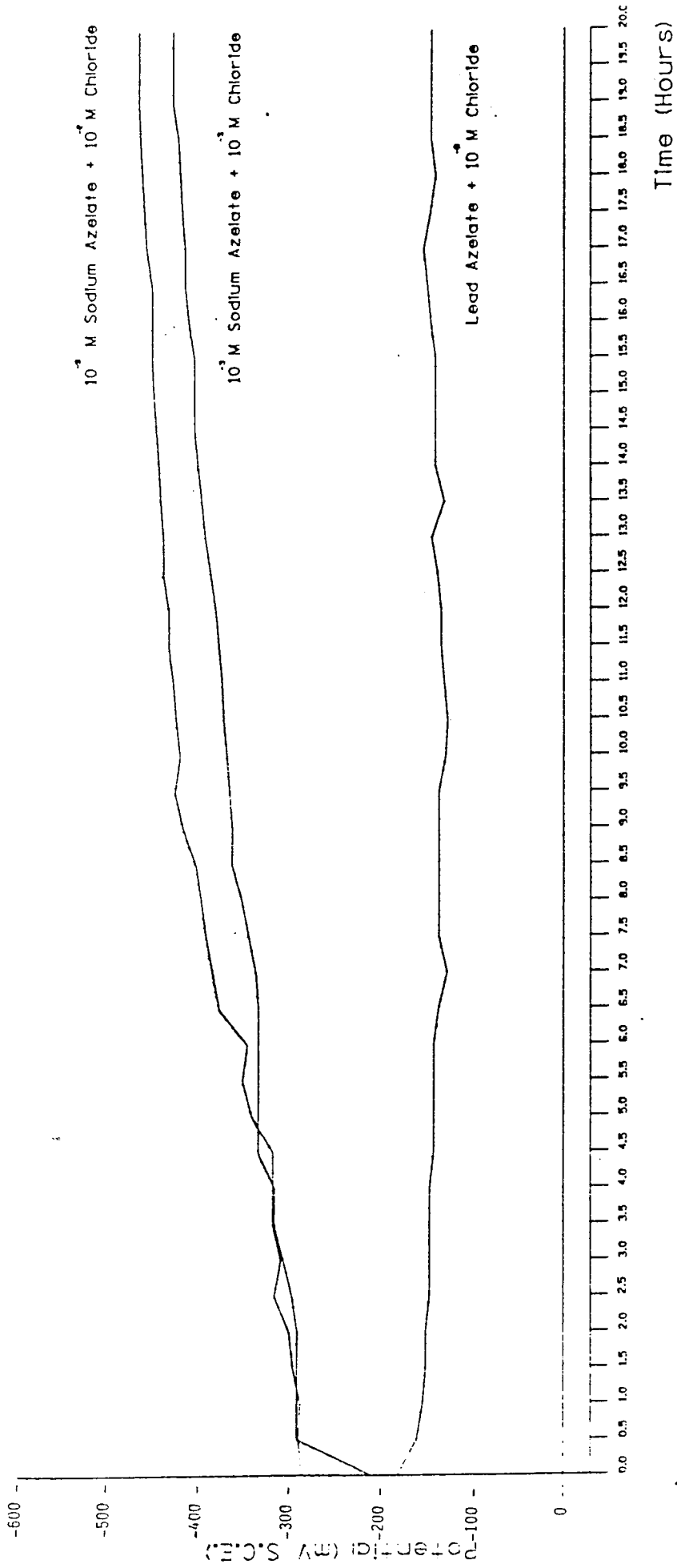


Fig 2 Potential-Time curves of Mild Steel immersed in chloride Solutions

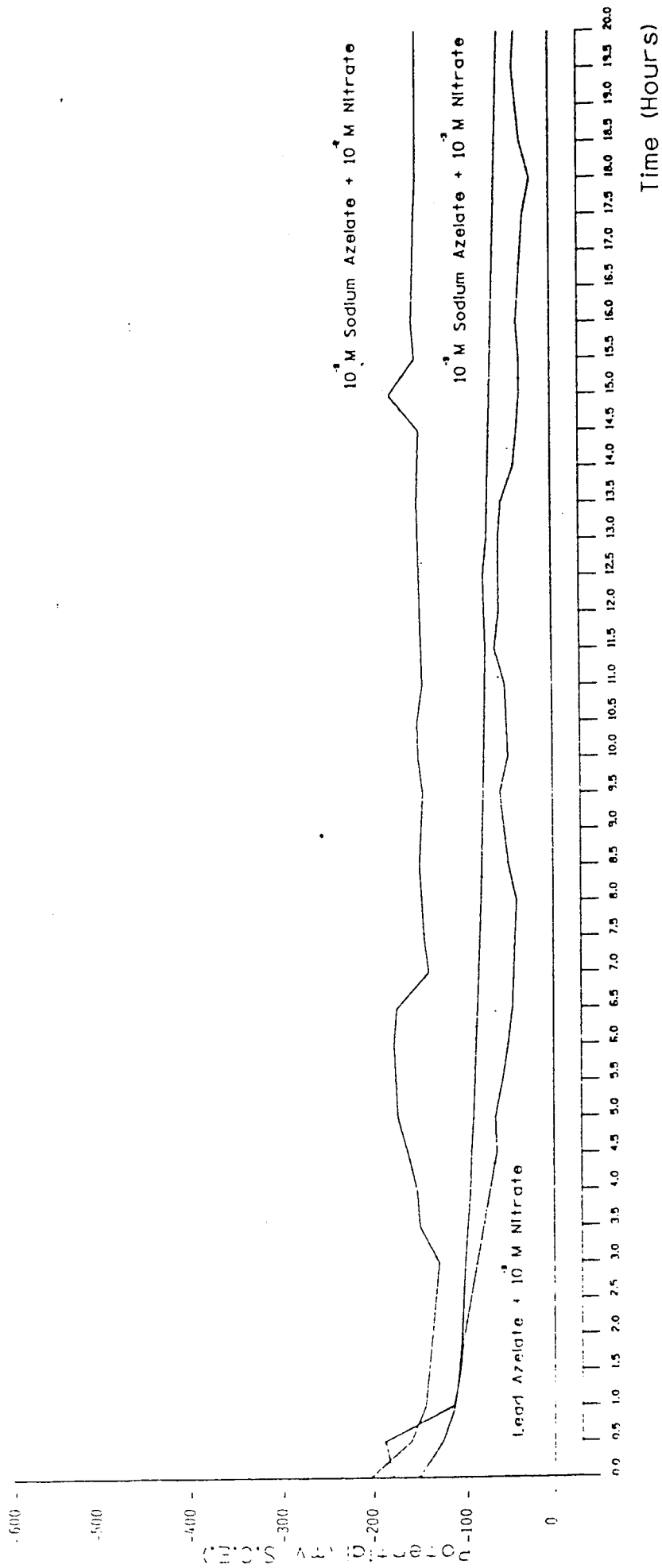


Fig 3 Potential time curves of Mild Steel immersed in Nitrate containing Solutions

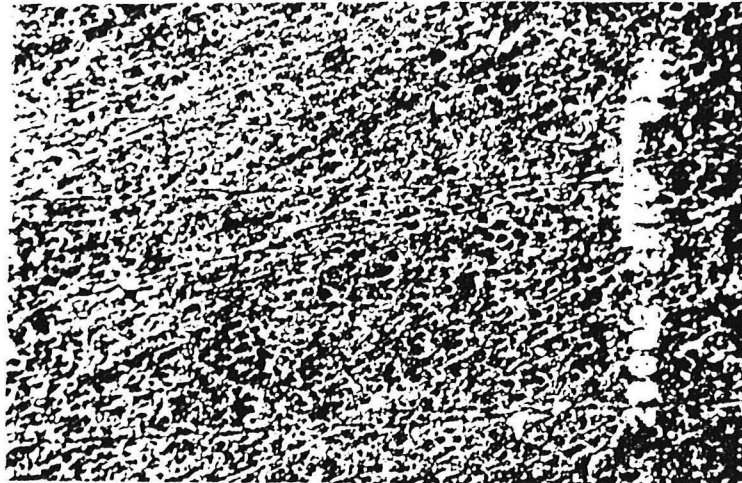


Fig. 4 : Scanning Electron Micrograph of Mild Steel Immersed for 20 Hours in 10^{-3} M Sodium Azelate + 10^{-3} M Sulphate Solution. ($\times 360$)

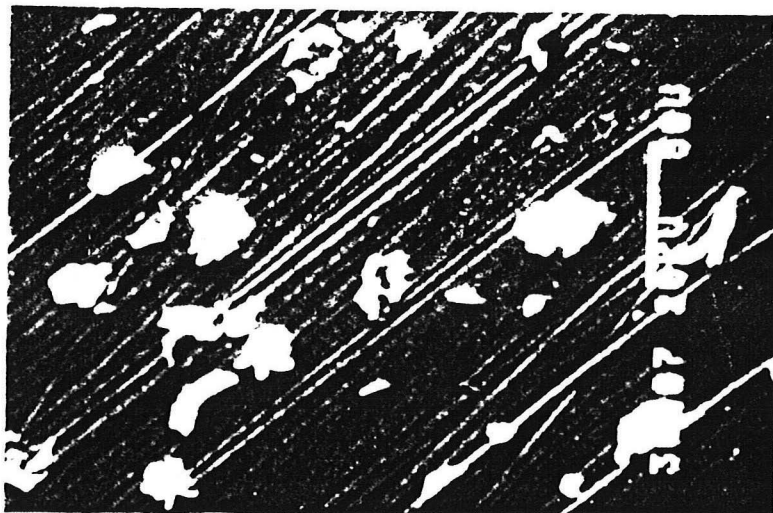


Fig. 5 : Scanning Electron Micrograph of Mild Steel Immersed for 20 Hours in Saturated Lead Azelate + 10^{-3} M Sulphate Solution. ($\times 360$)

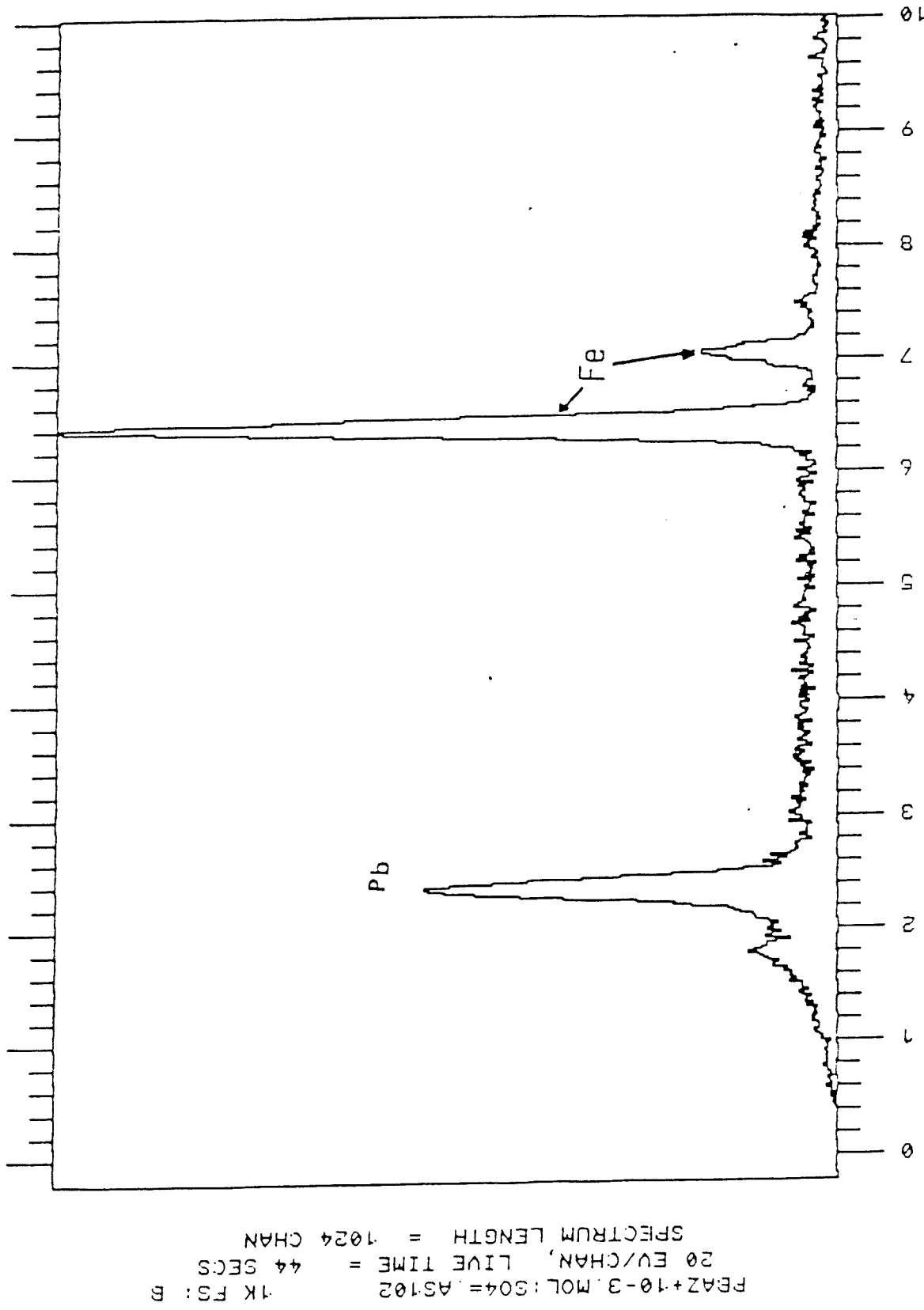
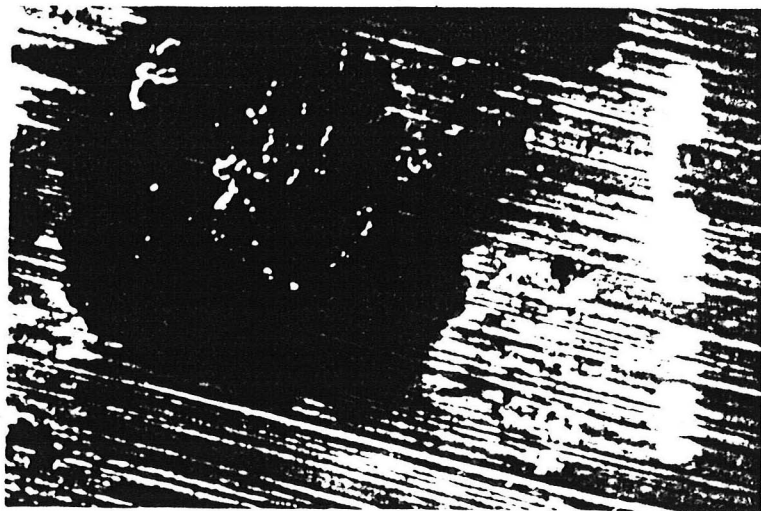


Fig. 6 : E.D.A.X. Spectra of Mild Steel Immersed in a Solution of Saturated Lead Azelate + 10^{-3} M Sulphate.
(Particle)



(ii) Pit Surrounded by Corrosion Products on Stained Area ($\times 380$)

Fig. 7 : Scanning Electron Micrographs of Mild Steel Immersed for 20 Hours in Saturated Lead Azelate + 10^{-3} M Chloride Solution.

A02202.AES Region 1 / . 1 Auger - Spectrum V.G.Scientific
 Level 1 / 1 Point 1 / 1

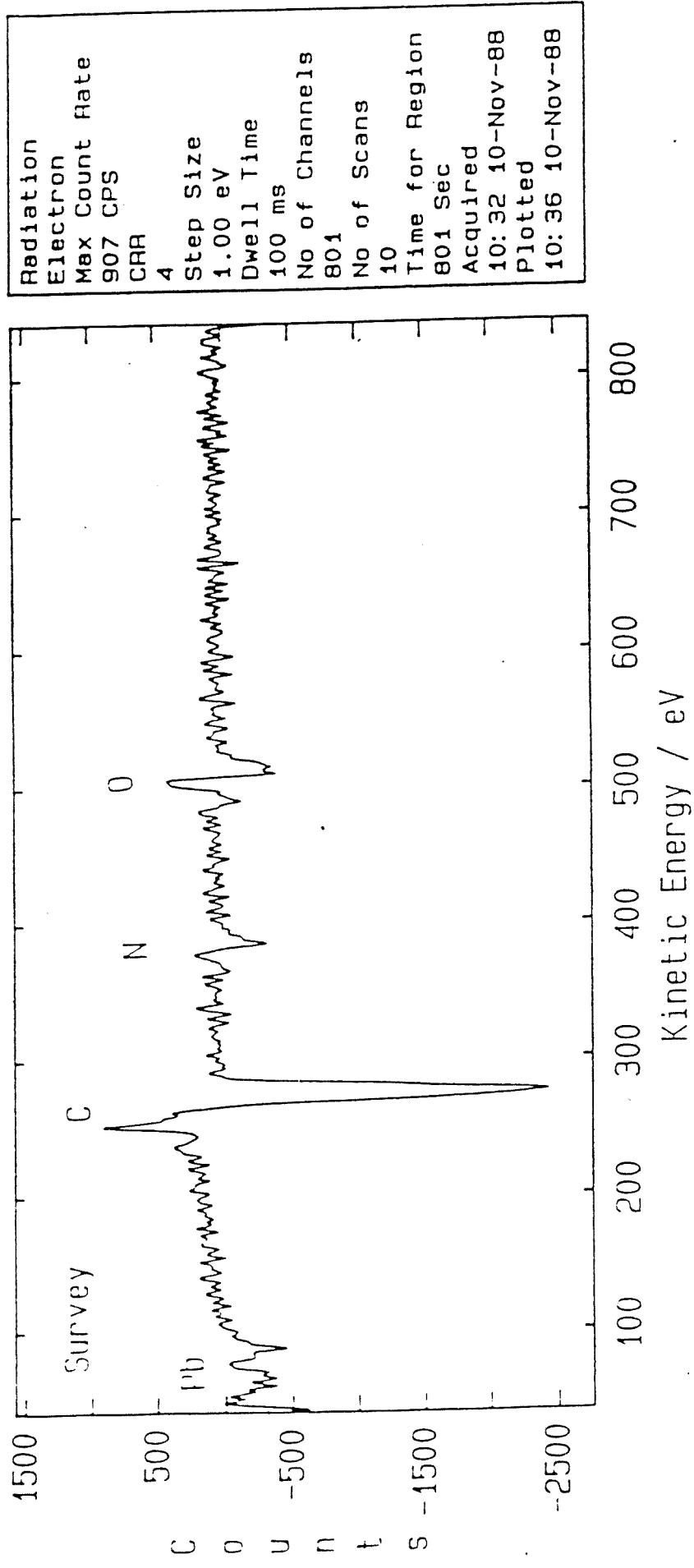


Fig. 8 : Analysis of the Particle on the Surface of Mild Steel Immersed in a Solution of Saturated Lead Azelate + 10⁻³M Chloride.

A02203.AES Region 1 / 1 Auger - Spectrum V.G. Scientific Point 1 / 1

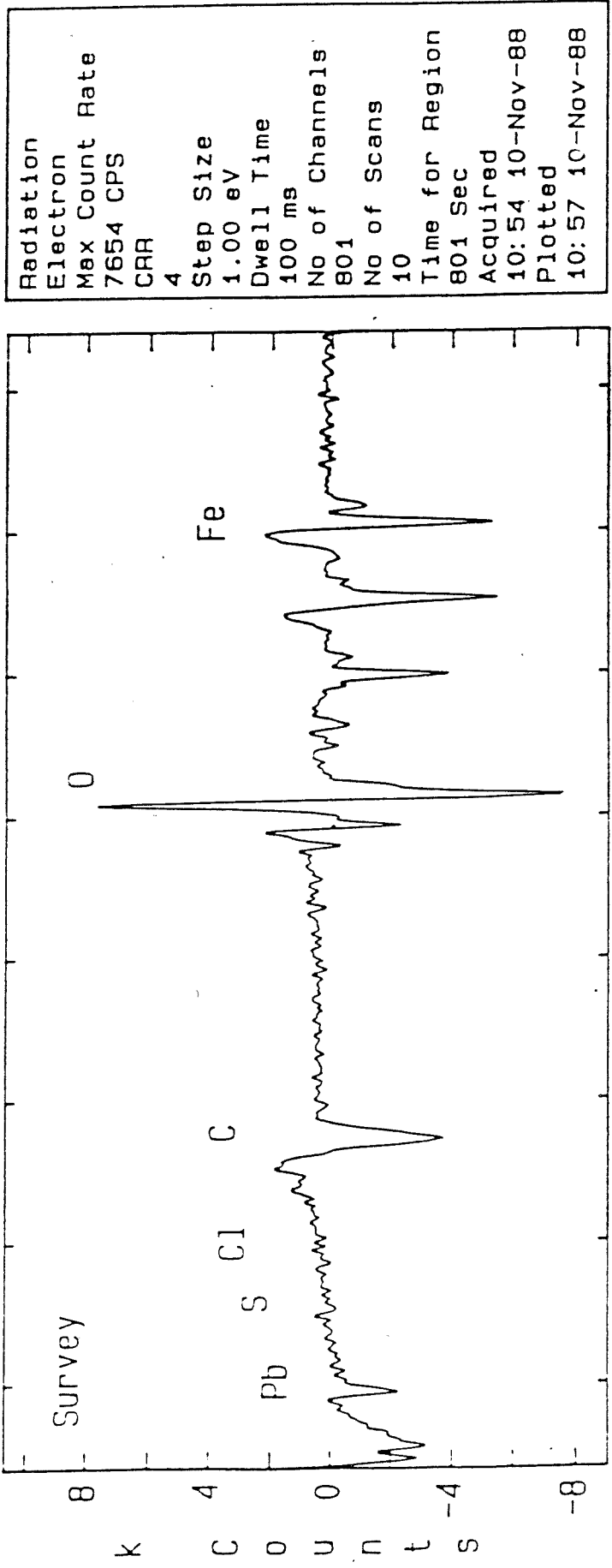


Fig 9 Analysis of the Surface of Mild Steel Immersed in a Solution of Saturated Lead Azelate + 10^{-3} M Chloride.
(for Substrate)

A02205.AES Region 1 / 1 Auger - Spectrum V.G.Scientific
 Level 1 / 1 Point 1 / 1

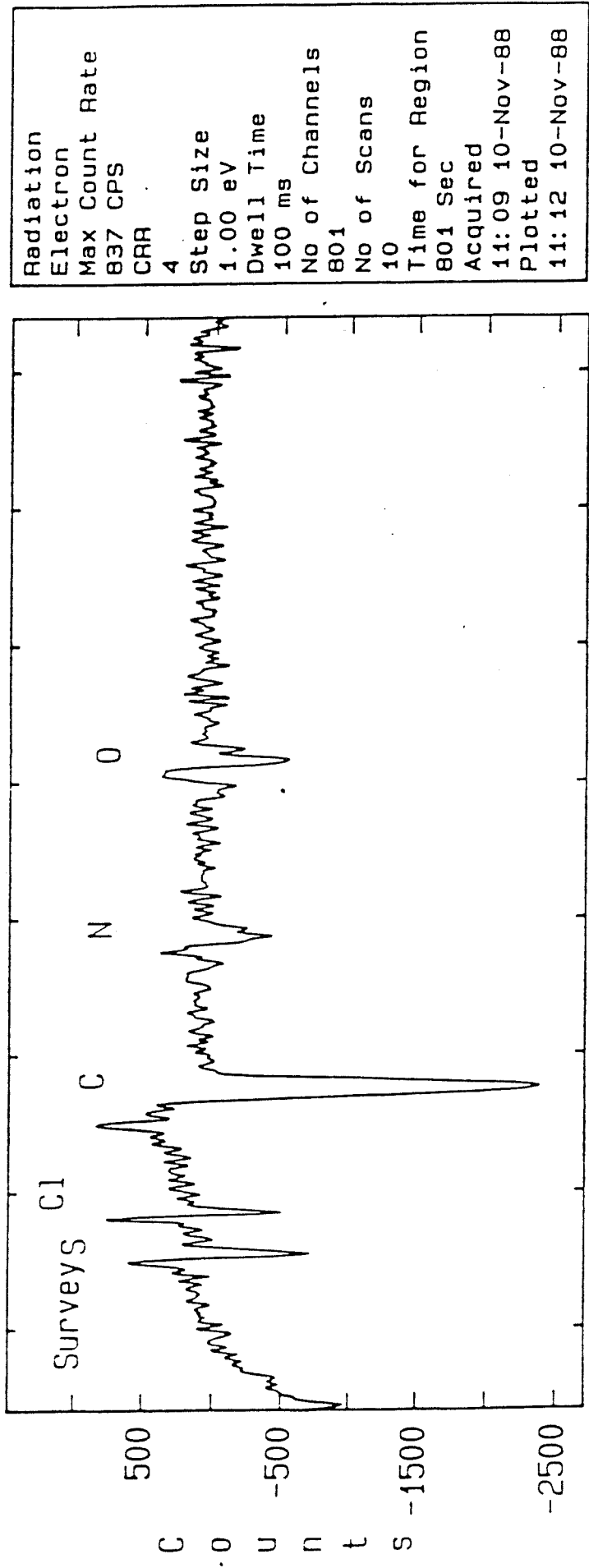


Fig. 10 : Analysis of the Surface of Mild Steel Immersed in a Solution of Saturated Lead Azelate + 10⁻³M Chloride.
 (Corrosion Product Around Pit)

A02206.AES Region 1 / 1 Level 1 / 1 Point 1 / 1 Auger - Spectrum V.G.Scientific

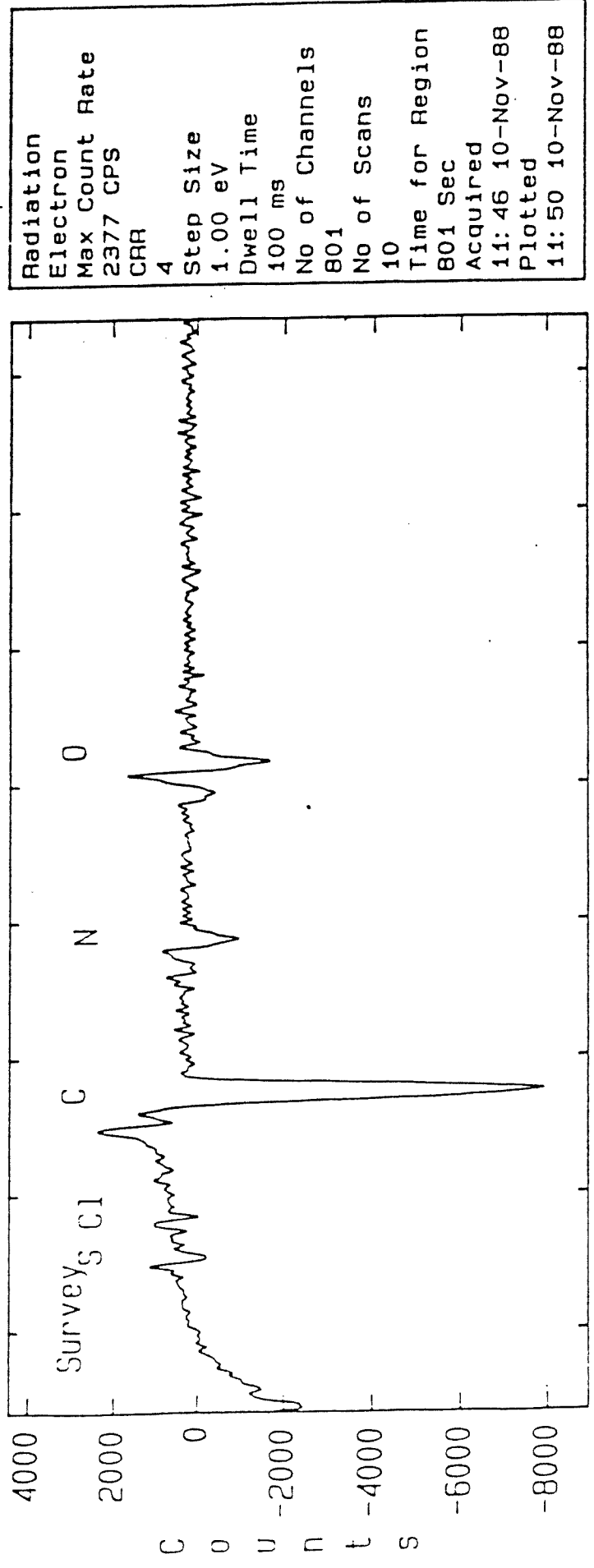


Fig. 11 Analysis of the Surface of Mild Steel Immersed in a Solution of Saturated Lead Azelate + 10^{-3} M Chloride.
(Dark Stain Surrounding Corrosion Pit)

A02214.AES Region 1 / 1 Auger - Spectrum V.G.Scientific Point 1 / 1
 Level 1 / 1

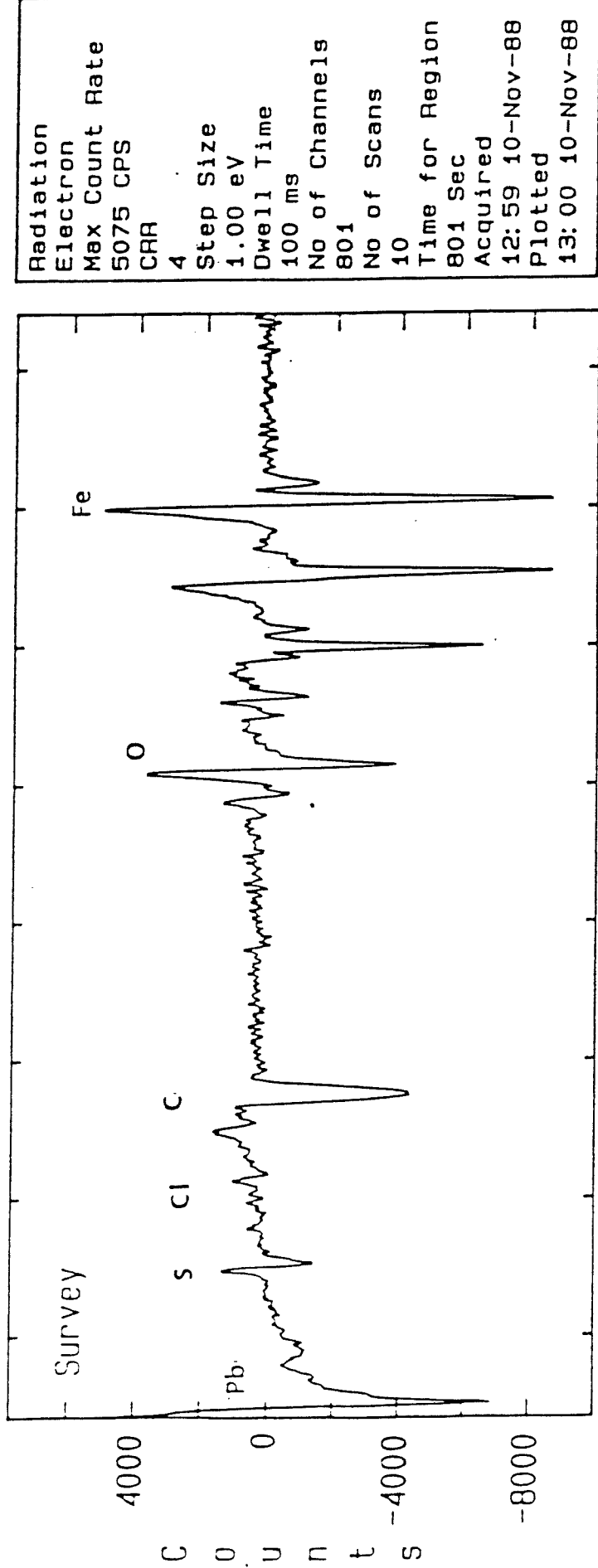


Fig. 12 : Analysis of the Surface of Mild Steel Immersed in a Solution of Saturated Lead Azelate + 10^{-3} M Chloride.
 (Dark Stain, After Light Etch)

INVESTIGATION ON ANTI-CORROSIVE PAINT COATINGS USING SALT SPRAY EVALUATION TECHNIQUE

DR S JANA*

ABSTRACT

Salt spray corrosion test is considered to be a very useful technique for evaluating corrosion behaviour under marine atmosphere since it simulates the basic conditions with some acceleration. Such accelerated corrosion tests, though not fully representative of real life corrosion situation, do, nevertheless, show general trends and often serve as a basis for comparison among different materials and coatings. The present paper documents the extent of corrosion in a Singapore port warehouse structure and evaluates by salt spray exposure the various paint systems that could possibly be applied to retard the warehouse corrosion.

* Senior Lecturer, School of Mechanical & Production Engineering, Nanyang Technological Institute, Singapore.

1. INTRODUCTION

Salt spray test is often used for evaluating materials, in particular, paints and electroplatings. It is intended to reproduce the corrosion that occurs in atmosphere containing salt spray or splash. Specimens are exposed in a cabinet containing a fog of salt solution. It is a useful technique for simulating the basic conditions of marine atmosphere. These tests may not be directly related to the intended services but are often incorporated in specifications as acceptance tests. Although some doubts persist on such accelerated corrosion tests, they do provide a reasonable assessment of the protective properties of paint films in marine atmospheres on the whole. The present paper first documents the extent of corrosion in a Singapore port warehouse steel structure and then describes the evaluation by salt spray exposure of the various paint systems that could possibly be applied to retard the warehouse structural corrosion.

2. SURVEY OF PORT WAREHOUSE CORROSION

The warehouse (approx. 200 m length, 80 m width and 50 m height in dimensions) stores bulk materials such as industrial salts and fertilizers. A repackaging operation is also carried out from time to time within the warehouse itself. The fumes from the engine together with the floating materials contaminate the inside air. Poor ventilation, humid atmosphere and proximity to the sea further aggravate the conditions. The contaminants settle on the steel structure of the warehouse and over the years become the starting points of corrosion.

Corrosion in the warehouse steel structure took various forms. Flaking off of loose paint, formation of deposits, severe blistering and under-deposit corrosion were all observed to various degrees. Figs. 1 through 7 show the extent and the nature of corrosion.

The choice of a coating on a general steelwork depends to a large extent on the type of structure and the environment of exposure. Sprayed metal coatings, like sprayed zinc or sprayed aluminium, would be clearly unsatisfactory in the present case because of their porous nature. Most steelwork is protected with paint. In many ways paint is a more flexible material and can be applied more easily. The facilities for applying are also far more widely available than for other types of coating.

As a preventive measure against further deterioration due to corrosion, several paint systems were, therefore, considered for application. These paints were applied on small corroded specimens taken from warehouse structures and then subjected to different surface preparation and finally evaluated in accelerated salt spray test.

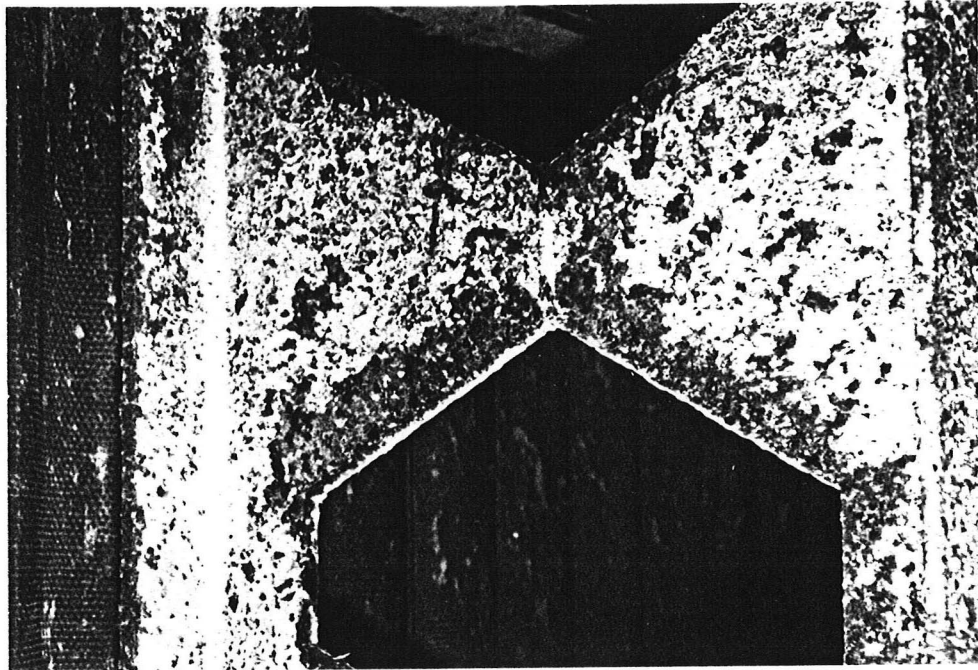


Fig. 1 Flaking off of loose paint



Fig. 2 Severe blistering in steel structure

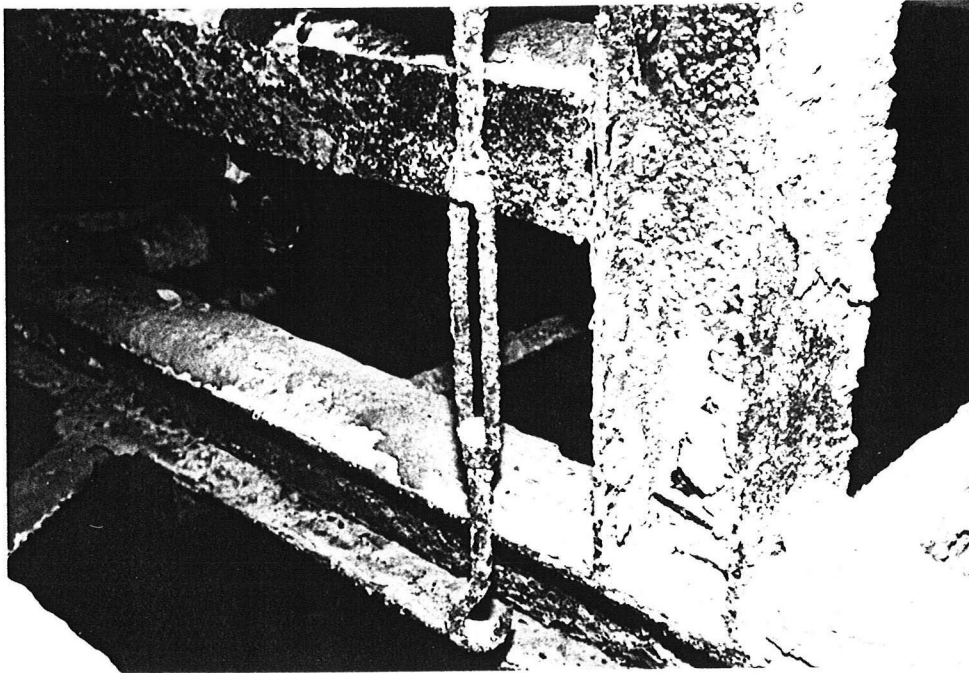


Fig. 3 Formation of depositions on the steel structure to the right

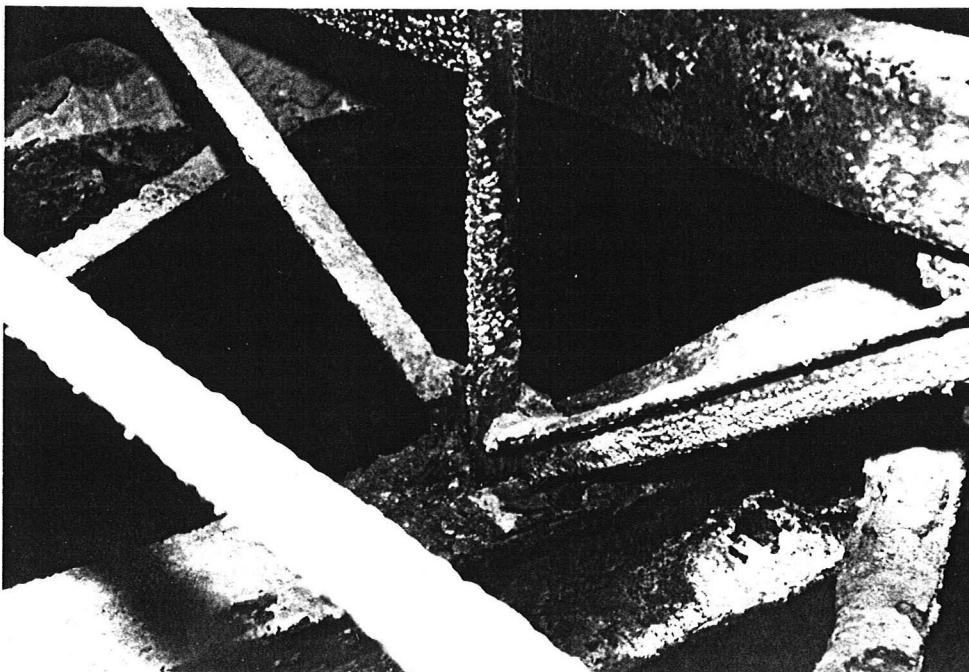


Fig. 4 Corrosion at the joints due to collection of dirt, moisture and contaminants

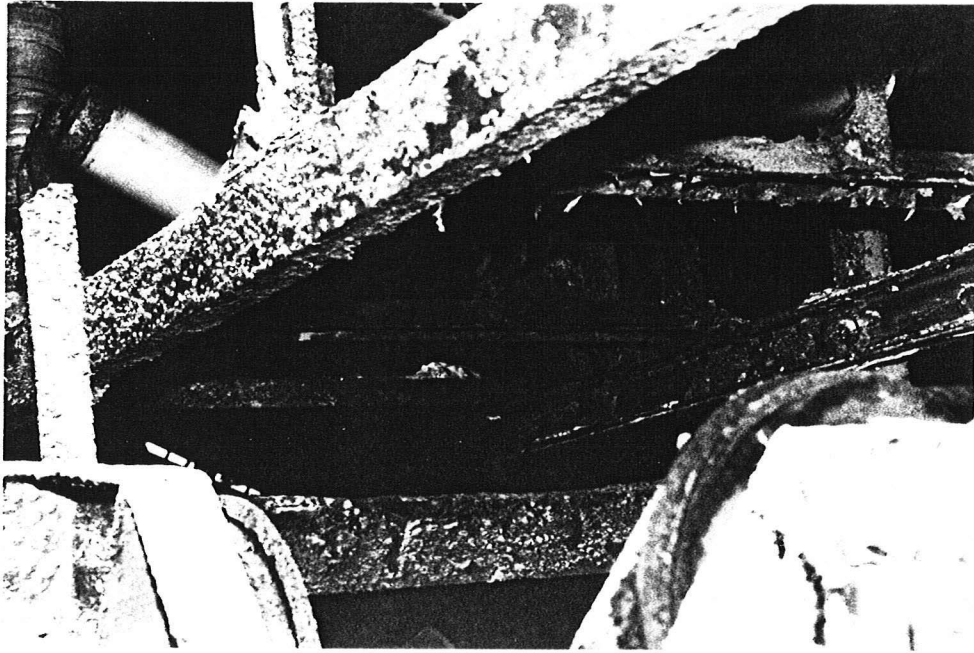


Fig. 5 Corrosion occurring below the conveyor belt

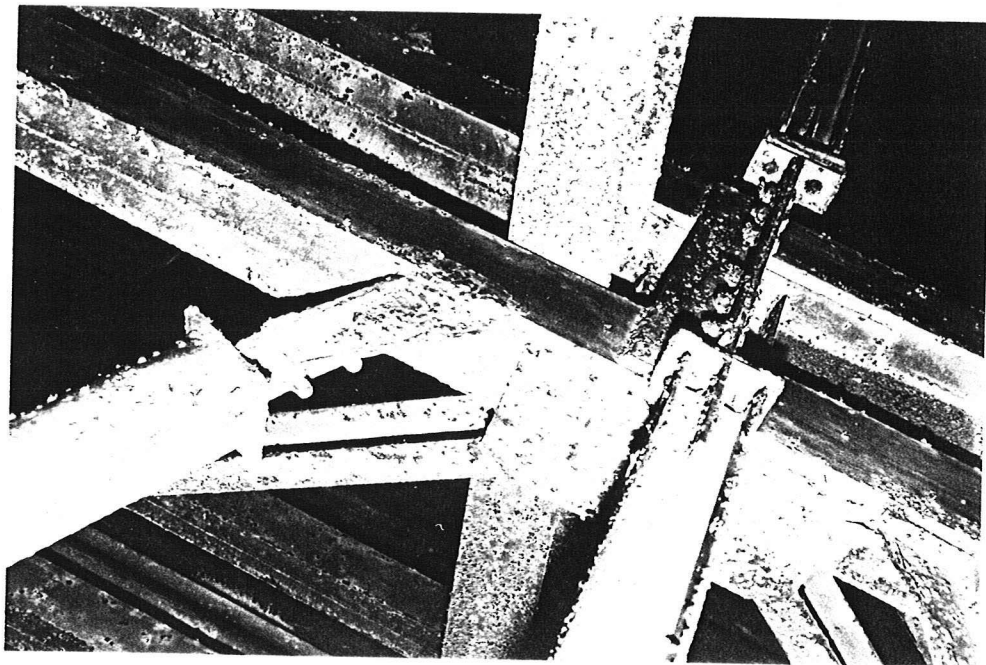


Fig. 6 Joints provided ideal sites for corrosion

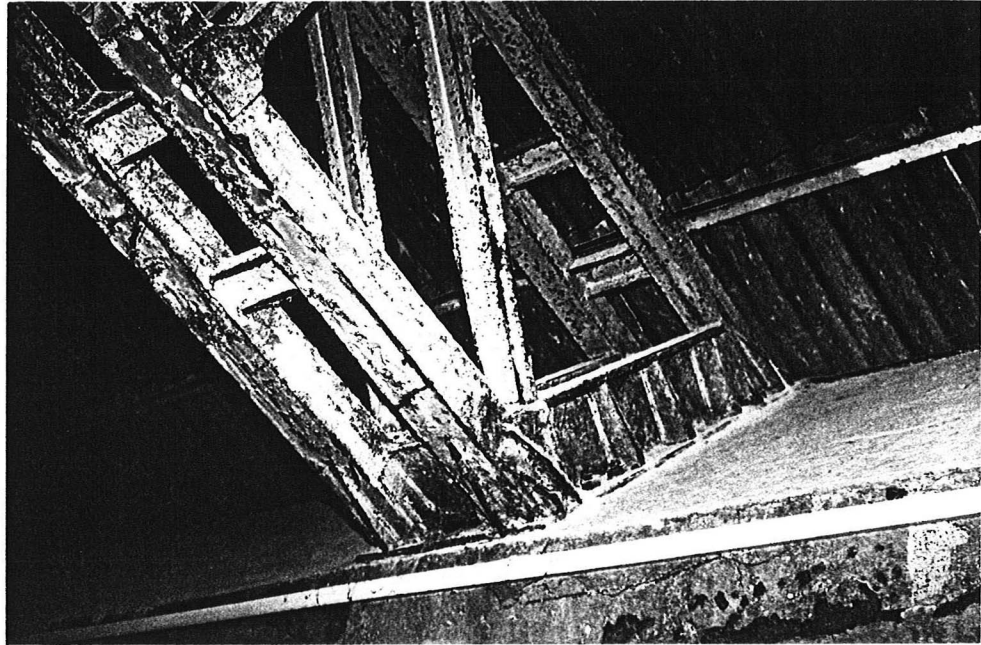


Fig. 7 Corrosion on the roof support framework

3. APPLICATIONS AND TYPES OF SALT SPRAY TESTING

Salt spray tests have received very wide acceptance for determining the corrodibility of ferrous and non-ferrous metals as well as the degree of protection afforded by inorganic and organic coatings on a metallic base. The most commonly used and accepted salt spray test is the method outlined in ASTM - B117 (1), although some companies and governmental agencies are known to have their own standards and procedures of such tests. A salt solution, usually containing a specified percentage of NaCl or sometimes more complex mixtures, is sprayed as a mist or atomised into droplets, which reach the painted steel surface. Many new salt spray test procedures and modifications of earlier procedures have been developed in the recent past. These include an acetic acid salt spray test (ASTM G85, Annex A1), a copper accelerated acetic acid salt spray test (ASTM B368), a cyclic acidified salt spray test (ASTM G85, Annex A2), an acidified synthetic seawater spray test (ASTM G85, Annex A3) and a salt-sulphur dioxide spray test (ASTM G85, Annex A4).

These modified procedures have extended the application of such tests to newer areas, e.g., the evaluation of susceptibility of various aluminium alloys to exfoliation corrosion and production control of exfoliation resistant heat treatments (4).

4. FACTORS AFFECTING CORROSION OF PAINTED STEEL

Several factors can influence the corrosion rate of painted steel. These are:

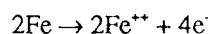
- discontinuity (eg, a scribe) on the coating
- mechanical properties of the coating
- exposure environment
- hydroxide ion formation during cathodic corrosion
- adhesion of the coating

Discontinuities in the paint coating are the sites where corrosion initiates beneath the paint film. Such discontinuities form crevices and cause delamination of paints adjacent to the discontinuities (5). In salt spray tests, specimens are, therefore, often scribed with a scriber to produce an artificial discontinuity and monitor its influence on the progress of corrosion.

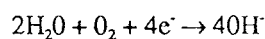
Once corrosion begins beneath a paint film, the buildup of the corrosion products starts to exert stress on the coating. As a result, defects begin to appear on the coating and eventually the coating fractures at several areas. Elastomeric coatings able to withstand high elongation before fracturing are thus useful as corrosion resistant coatings. In other words, the mechanical properties of the coatings, in particular its elastic properties, influence its corrosion resisting ability. Also organic coatings such as paints usually dry to a reasonably hard film within a matter of hours. However, changes occur in the properties of the dry film over a period of time. In particular, films may harden and become brittle in some circumstances. These changes that occur with time also add to the difficulties of testing in the laboratory. Often tests carried out within a few days of coating a panel may give a false impression of the performance of the coating.

The environment has an effect on the coating material and may determine the type that can be satisfactorily used. Traditional salt spray corrosion tests involve exposure of samples to sodium chloride environment. While evaluation of coatings for marine environment can be unquestionably made by such salt spray tests, other environments and atmospheric pollutants, in particular SO₂ levels and humidities, need different studies (6).

Corrosion of steel in the atmosphere generally involves an anodic reaction:



and a cathodic reaction:



It is well documented (7,8) that in salt spray testing of painted steel, the anodic and the cathodic corrosion reactions are well separated. The anodic reaction is localized at the scribe while the cathodic reaction takes place beneath the paint coating. Oxygen diffuses through the paint film and hydroxide ions form. These hydroxide ions degrade both the paint film and also the underlying metal pretreatment, if any performed, eg, phosphatizing, and cause delamination of the coating.

As corrosion proceeds, corrosion products build up at corroded sites and act as wedge along the coating/steel interface. It is here that the adhesion of the coating to the underlying steel, in particular its peel strength, is important. The coatings very often lose their peel strength when wet and corrosion crack propagation is most rapid during periods of wetness (9). Also, to achieve adhesion, the steel surface must be clean and devoid of loose matter before the coating is applied. Furthermore, it must be roughened sufficiently to provide a mechanical key.

Most salt spray tests are carried out on coated steel samples where the paint coatings are applied on pretreated (eg. phosphatized or chromate rinsed) or carefully ground steel surface. In the present instance, the in-situ nature of the existing old port warehouse structure precludes such surface treatments. Thus the underlying steel may just have to be "wire-brushed" before any paint coating can be applied. In some difficult-to-access areas, a chemically "stabilized rust" or even "loose" old paint may have to be left behind before fresh paint coating is applied. It is these additional influencing factors that make the present investigation necessary and relevant. It was felt that the corrosion performance of paint coatings on relatively unpretreated and corroded substrate needs to be looked into using accelerated salt spray tests in view of evidence indicating that the roughness and cleanliness of the substrate determine to a great extent the coating performances (10).

5. EXPERIMENTAL

5.1 Salt Spray Exposure System

The salt spray exposure system used in the current investigation produced uniform free falling spray mists with uniform collection rate. A schematic diagram of the salt spray system is shown in Fig. 8 and an overall view of the equipment in Figures 9 and 10.

It essentially consisted of the following:

1. Salt fog cabinet made of steel with a vinyl lining and an acrylic cover.
2. Self regulating level control comprising a distilled water reservoir and a salt solution reservoir.
3. Bubble tower through which the air is sent into the chamber saturated with water vapour.
4. Dispersion tower inside the fog chamber providing salt fog.
5. Control box.

5.2 Paint Coatings

The two types of paints utilized for this study were:

1. Chlorinated rubber paint.
2. Two-pack epoxy paint.

The chlorinated rubber paint is a one-pack chemical resistant product. The films produced are brittle and so a plasticizer is added in amounts varying from 20 to 50%. Ideally, these paints should not be used at temperatures above 60°C. Being a one-pack paint, it is easier to apply, there being no intercoat adhesion problem. The particular chlorinated rubber paint used in this experimentation was Rubbertight-300 HB obtained from M/S DNT Pte Ltd, Singapore 2260.

The two-pack epoxy paints come in two separate containers and are mixed in specified proportions for applications. The hardening agent is either a polyamide or a polyamine. Polyamides produce materials with a longer pot life, (i.e. the period after mixing during which the epoxy can be used) and its mixing proportion is less critical than the amines. Coatings produced from polyamide epoxies are more flexible and durable than polyamine epoxies but they take longer time to cure. Also the chemical and solvent resistance of polyamide cured epoxies is inferior to amine cured epoxies. Of the four epoxy paints used for this experimentation, the Epoxy White and the Epoxy Bar Rust were obtained from M/S DNT Pte Ltd while the Epoxy A 390 and Epoxy AM 66 were obtained from M/S DIMET Singapore Ltd, Singapore 2261.

5.3 Test Conditions

Conditions set forth under ASTM B117 and ASTM D1654 (1, 2) were adhered to as closely as possible during experimentation. These were as follows:

1. The specimens were supported between 15° and 30° to the vertical (see Fig. 11).
2. A 35% concentrated salt solution with a pH in the range of 6.5 to 7.2 was used to promote rapid corrosion.
3. The air supply to the nozzle for atomization was maintained at 15 psi (equivalent to 103 kPa).
4. The exposure zone was maintained at 35 ± 1°C.

5.4 Test Specimens

The specimens were sheet steels approximately of 130 mm x 70 mm size obtained from corroded structures inside the warehouse. These specimens were given different surface preparation as follows prior to applying the paint coating.

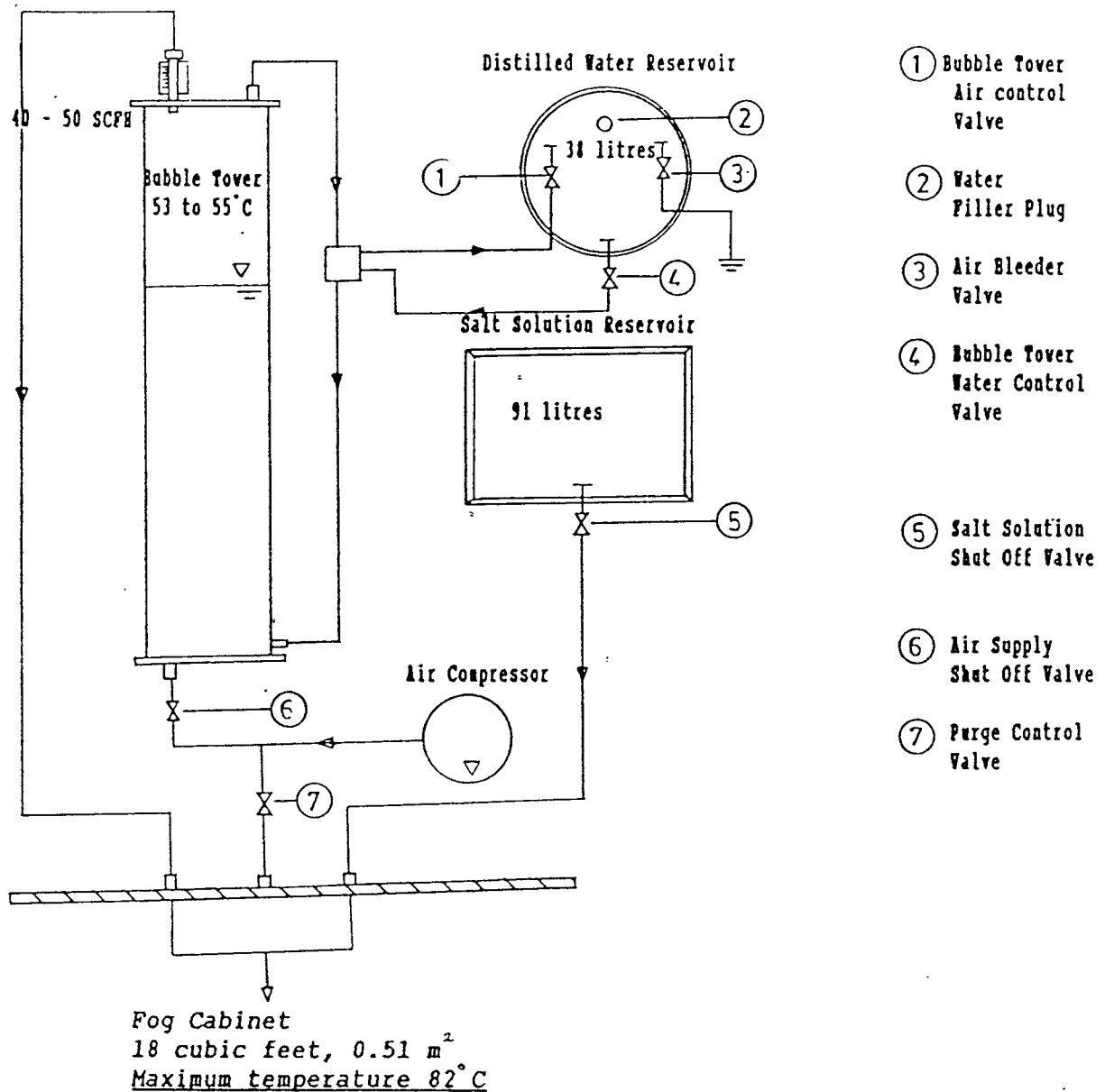


Fig. 8 Schematic diagram of the salt spray exposure system

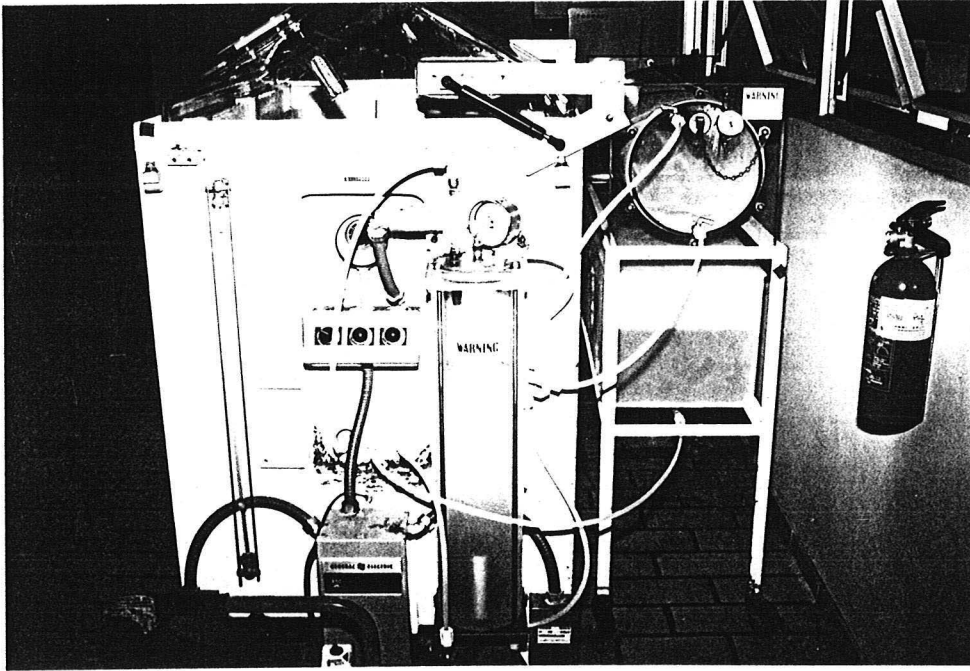


Fig. 9 An overall view of the corrosive fog exposure system

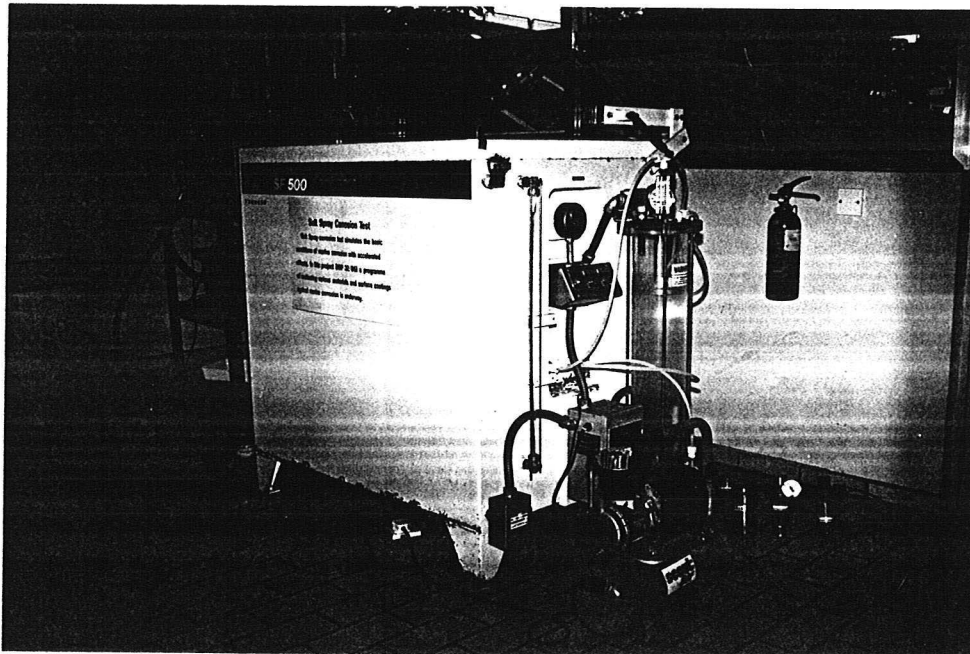


Fig. 10 Another view of the salt spray system

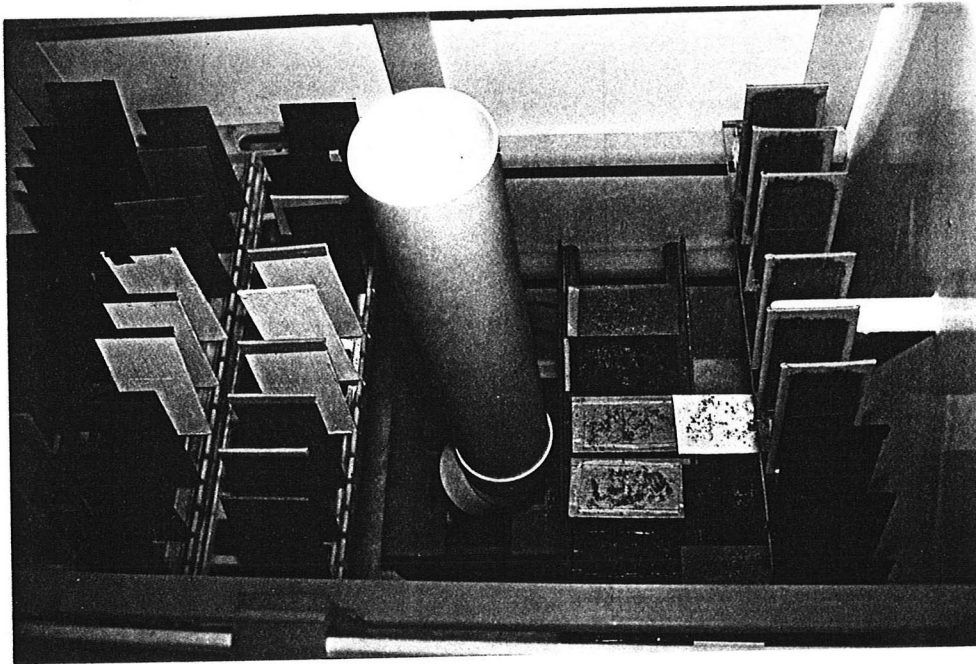


Fig. 11 Test specimens in the salt fog cabinet

1. SA 2 surface finish: It demands almost complete removal of rust from the corroded surface. Sandblasting the corroded specimens was carried out for this purpose.
2. Wirebrush surface finish: Due to complexity of building structures, sandblasting may not be always possible. Wirebrushing the surface will remove only loose rust.
3. "Loose" paint surface finish: In some specimens old paint was left as it is before fresh paint coating was applied over it.
4. Stabilized rust surface finish: In some specimens, the rusted surface was coated with a rust converter first. The rust converter reacted chemically with the rust converting it into a complex organic iron compound. The compound forms a film that is impervious to water or oxygen. New paint was subsequently applied on such a rust stabilized surface.

Following the surface preparation, the paint coatings were applied by brush.

The specimens were then masked with thick muslin tape on one side to restrict corrosion only to the unmasked side. The edges of the specimen were further dipped in wax to prevent selective edge corrosion. The coated

test specimen was scribed with a scribe across the width. The scribe penetrated the full coating thickness. Corrosion originated from the scribed surface and depending on the quality of the coating proceeded at a fast or slow pace. After exposure in the salt fog, the specimens were cleaned in Clark's solution (20 g of antimony trioxide and 50 g of stannous chloride in 1 litre of HCl) and dried and weighed.

Corrosion rate was calculated as:

$$\text{Millimetres/yr (mmpy)} = \frac{87.6 \times W}{DAT}$$

- W = weight loss, mg
D = density of specimen/coating, g/cm³
A = area of specimen, cm²
T = time of exposure, hr.

Blistering was observed in some of the specimens. These were rated by comparing with the photographic reference standards of ASTM D 714 (3). Blistering was recorded as a number indicating the size of the blisters (0 to 10, 0 indicating biggest blisters) and also as a qualitative term indicating frequency of their occurrence (dense D, medium dense MD, medium M and few F).

6. TEST RESULTS

Tests were carried out in salt spray mist for three durations of time with three different specimens, eg, 168 hrs, 336 hrs and 510 hrs. The corrosion rates and the blister formations were noted. Table I gives the summary of the results. Figures 12 through 16 show the physical appearance of some of the specimens after salt spray testing and indicate the size and frequency of blisters formed.

7. DISCUSSION

The chlorinated rubber and the Epoxy AM 66 performed poorly in the salt spray evaluation as either few large sized blisters or numerous small sized blisters formed during exposure. Three such specimens are shown in Figs. 12, 13 and 14. These two paints also generally show an increasing rate of corrosion with increasing exposure with the exception perhaps of Epoxy AM 66 applied with a rust stabilizer. However, the blister formation phenomenon rules out the effectiveness of these coatings.

Among the rest of the paint coatings, the Epoxy Bar Rust applied over a SA 2 surface appeared most promising. The corrosion rate in its case actually decreased with increasing time of exposure. The blister formation was also minimal (Fig. 15). Epoxy A 390 applied over loose paint also showed decreasing corrosion rate; however the overall corrosion

rate was much higher in this case. Also with loose paint, the adhesion of the new paint will greatly depend on the nature of the underlying loose paint and hence its effectiveness should be viewed with caution. Figure 16 shows Epoxy A390 over wire brushed surface. Although the blister formation here is minimal, the corrosion rate in this case appeared to increase with increasing time.

A decreasing corrosion rate with increasing exposure would indicate that the corrosion products formed on the surface are providing a measure of protection to the surface and thereby inhibiting corrosion to some extent. Based on this criterion, among all the paint coatings studied, the epoxy Bar Rust applied on a SA 2 surface appeared to be the best paint to apply on the corroded warehouse structure. Since sand blasting may be difficult to apply, the next best approach would be to use a hand-held motorised rotating disc grinder to remove millscale and corrosion products

Table I: Corrosion Evaluation of Painted Specimens

S/No	Paint Type	Paint Thickness (microns)	Surface Finish	Corrosion Rate mmpy			Blister Rate
				168 hrs	336 hrs	510 hrs	
1	Epoxy White	100	SA 2	.007	.011	.028	6, Few
2	Epoxy White	100	Stabilized rust	.014	.018	.031	8, Few
3	Epoxy Bar Rust	110	SA 2	.136	.074	.028	8, Few
4	Epoxy Bar Rust	110	Wire brush	.124	.131	.143	6, Few
5	Epoxy Bar Rust	110	Loose paint	.012	.012	.057	8, Few
6	Epoxy A 390	110	SA 2	.012	.024	.037	4, Few
7	Epoxy A 390	110	Wire brush	.012	.031	.037	8, Few
8	Epoxy A 390	110	Loose paint	.500	.297	.163	6, Few
9	Epoxy AM 66	110	SA 2	.012	.052	.062	2, Few
10	Epoxy AM 66	110	Stabilized rust	.014	.011	.014	8, Dense
11	Chlorinated rubber	80	SA 2	.072	.118	.149	2, Dense
12	Chlorinated rubber	80	Stabilized rust	.079	.043	.057	8, Med Dense

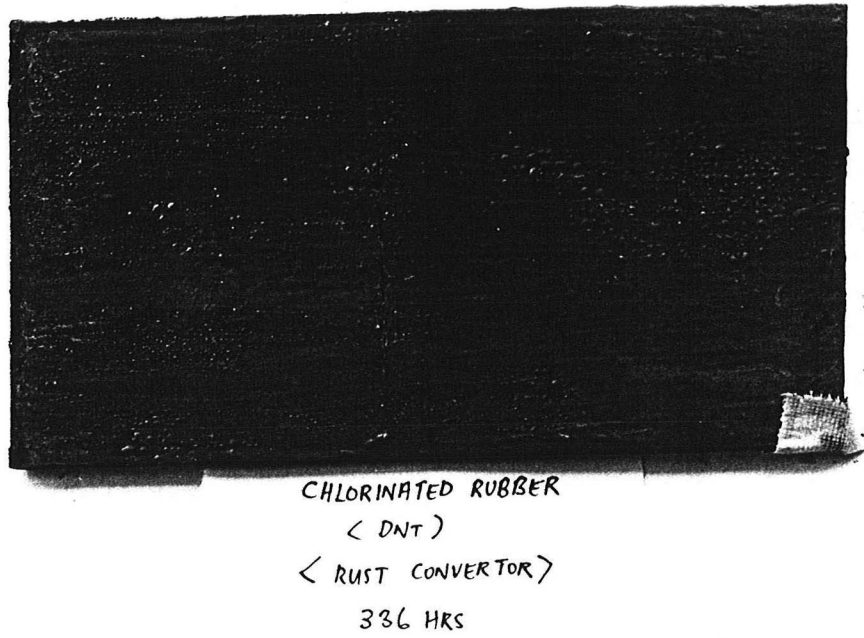


Fig. 12 Formation of blisters on salt spray exposure. Chlorinated rubber paint coating on stabilized rust surface after 336 hrs

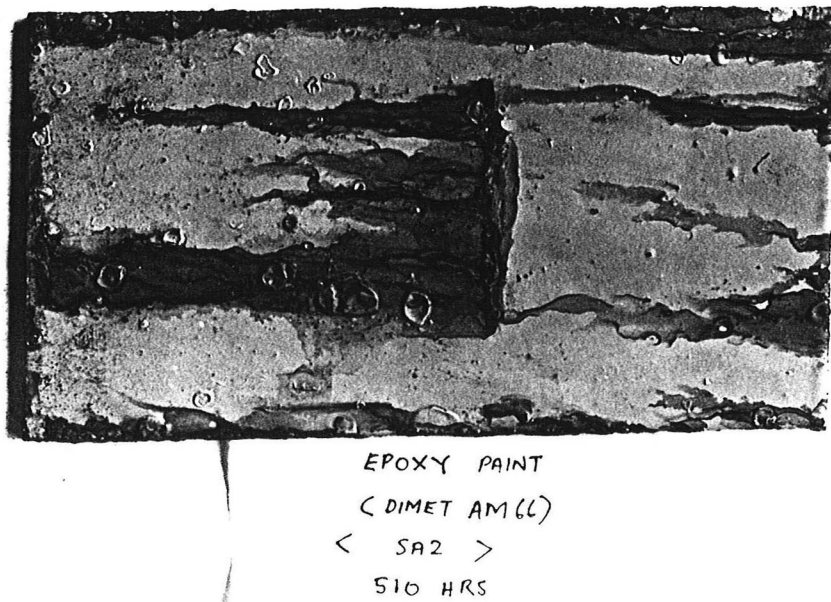


Fig. 13 Formation of blisters on salt spray exposure. Epoxy AM 66 paint coating on a SA 2 surface after 510 hrs

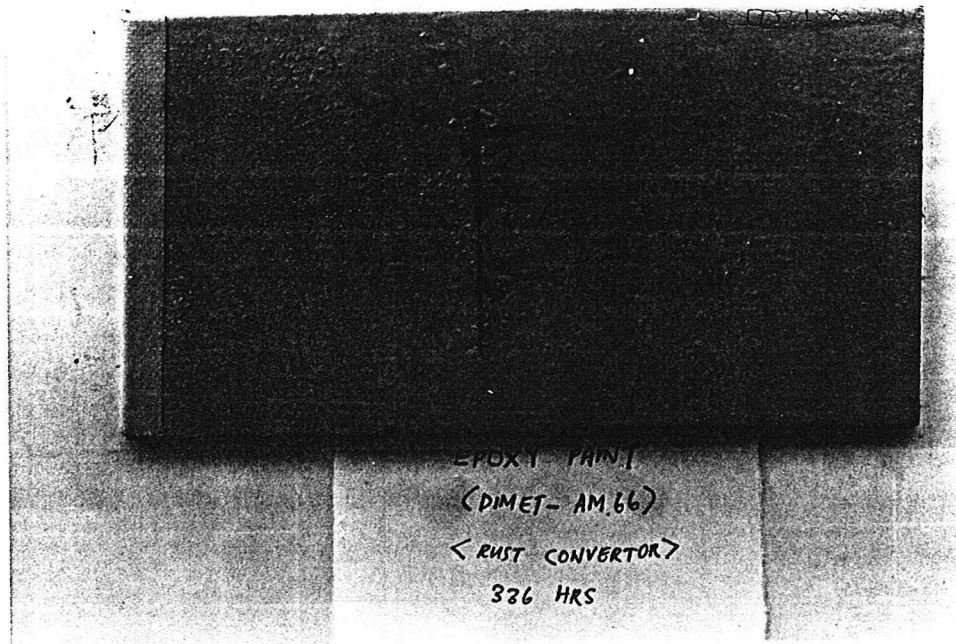


Fig. 14 Epoxy AM 66 paint coating on stabilized rust surface after 336 hrs.
Formation of numerous small sized blisters

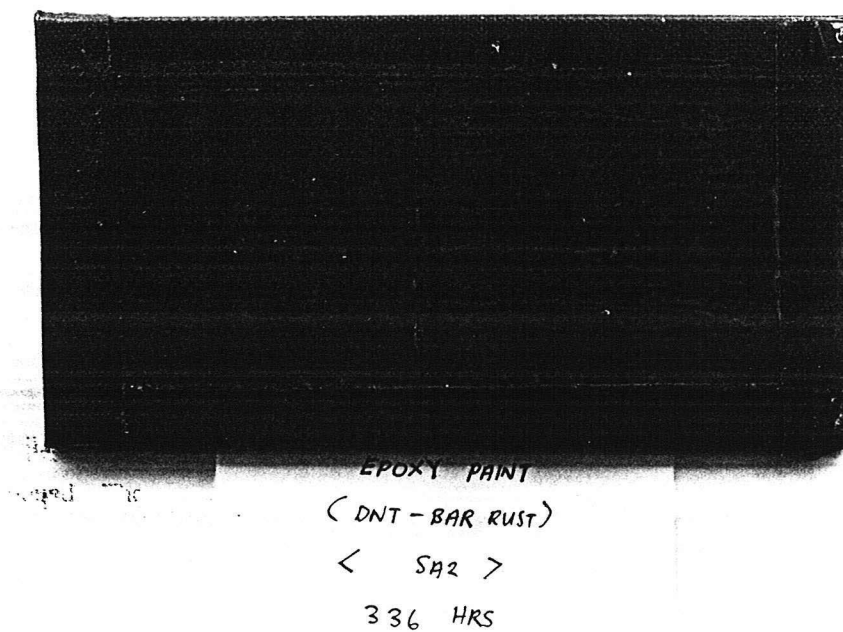


Fig. 15 Epoxy bar rust paint coating on a SA 2 surface finish after 336 hrs of salt spray exposure.
Minimal blistering effect

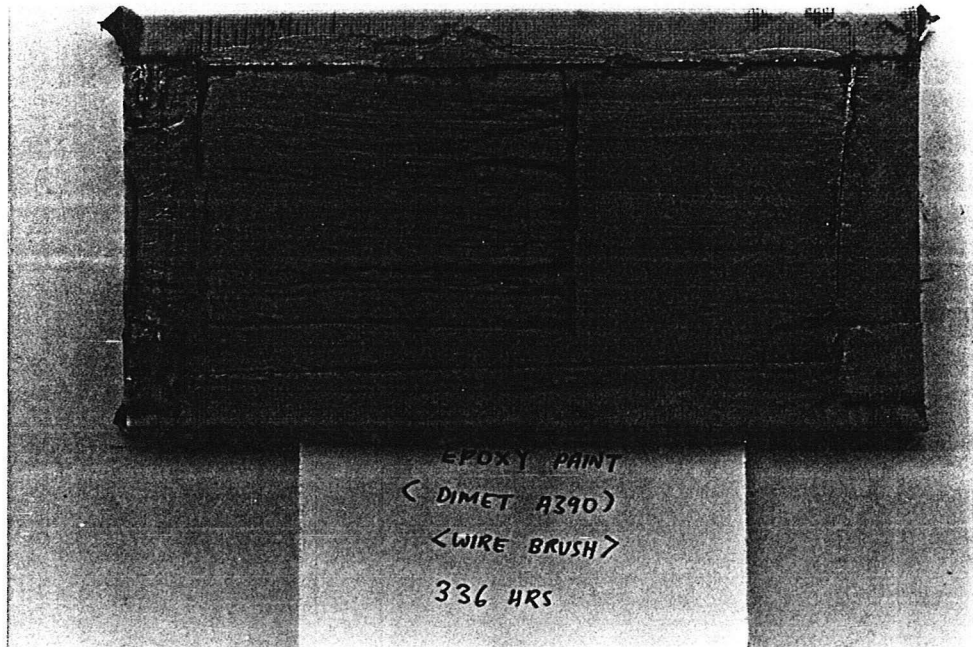


Fig. 16 Epoxy A 390 paint coating on a wire-brushed surface after 336 hrs of salt spray exposure. Minimal blistering effect but increasing corrosion rate with increasing time.

mechanically. Clearly, surface preparation before application of paint coating is very important since the same Epoxy Bar Rust applied over a "wire-brushed" or a "loose-paint" surface was not as effective.

Though salt spray test is an established method of evaluation of paint coatings in a short span of time, its findings should be corroborated by a more realistic exposure test under actual service conditions spread over a period of time. Trial test with the paint applied on a small selected area within the warehouse for, say, six months should be carried out before full scale paint work.

8. CONCLUSION

The warehouse structure was suffering from severe corrosion in the form of flaking paints, blistering, formation of deposits and under-deposit corrosion. Several paint systems which could possibly be applied on the existing warehouse structure under different surface preparations were evaluated using salt spray exposure tests. An epoxy bar rust paint applied over a sand blasted surface appeared to be the most effective under the test conditions.

9. ACKNOWLEDGEMENT

The work was partially supported by Nanyang Technological Institute's Applied Research Grant (RP 32/86) and the support is gratefully acknowledged. The major part of the experimental investigation was carried out by Mr Juan

Hee Teng in partial fulfilment toward his Bachelor's Degree in Engineering. His contribution is acknowledged and appreciated.

10. REFERENCES

1. Standard Method of Salt Spray (Fog) Testing - ASTM Designation B 117-85, ASTM Annual Book of Standards, Vol 03.02, 1987.
2. Standard Method for Evaluation of Painted or Coated Specimens Subjected to Corrosive Environments - ASTM Designation D 1654-84, ASTM Annual Book of Standards, Vol 06.01, 1987.
3. Standard Method of Evaluating Degree of Blistering of Paints - ASTM Designation D 714-81, ASTM Annual Book of Standards, Vol 06.01, 1987.
4. S.J. Ketcham and I.S. Shaffer, "Exfoliation Corrosion of Aluminium Alloys", Localized Corrosion - Cause of Metal Failure, STP 516, American Society for Testing and Materials, 1972, p. 3.
5. J.V. Standish, "Atmospheric Corrosion Mechanisms of Painted Steel", The Study and Prevention of Corrosion, SP-538, Society of Automotive Engineers, 1983, p. 1.
6. J.R. Walton, J.B. Johnson and G.C. Wood, British Corrosion Journal, Vol. 17, 1982, p. 59.
7. R.A. Dickie and A.G. Smith, Paper No. 126, Corrosion 80, National Association of Corrosion Engineers, 1980.
8. R.A. Iezzi and H. Leidheiser, Journal of Corrosion, Vol. 37, 1981, p. 28.
9. A.J. Kinloch, Journal of Adhesion, Vol. 10, 1979, p. 193.
10. R.W. Drisco, L.K. Schwab, "Effect of Steel Profile and Cleanliness on Coating Performance", Metallic Corrosion - Proceedings 8th International Congress, on Metallic Corrosion, Vol. II, Deutsche Gesellschaft fur Chemisches Apparatewesen, 1981, p. 1062.

New Type LB Films of Polyallylamine Containing
Trifluoroacetic Acids by Ionic Bonds

Rungthip Chaiwattananone

Thailand Institute of Scientific and Technological Research
(TISTR)

ABSTRACT

Syntheses of polyallylamine containing long-chain perfluoroalkyl groups by covalent bonds and trifluoromethyl groups by ionic bonds were carried out. Various new type LB films of the polymers containing trifluoroacetic acids by ionic bonds were successfully prepared and the monolayers could be deposited onto hydrophilic glass slides, forming Y-type films, using Langmuir-Blodgett (LB) technique. Measurements of surface pressure-surface area (F-A) isotherms, contact angles of water, critical surface tensions (γ_c) and monolayers' thicknesses were performed to investigate characterization of these LB films. The results indicate that trifluoromethyl groups, short-chain perfluoroalkyl groups, introduced by ionic bonds could be arranged on the LB film surface and also had an effect on conformation of polyallylamine chain and properties of the films.

1. INTRODUCTION

Langmuir-Blodgett(LB) technique is a method for forming thin ordered multilayers of amphiphilic molecules onto inorganic substrates.¹⁻⁹

Recently, study on polymeric LB films with functional group as long perfluoroalkyl group on the surface which shows excellent properties, such as water- and oil- repellence, has been carried out.¹⁶

Many investigations of polymeric LB films with long perfluoroalkyl groups by covalent bonds have been reported.¹⁷⁻²⁵ And ^{also} polymeric LB films with long perfluoroalkyl groups by covalent bonds and ionic bonds was studied.²⁶

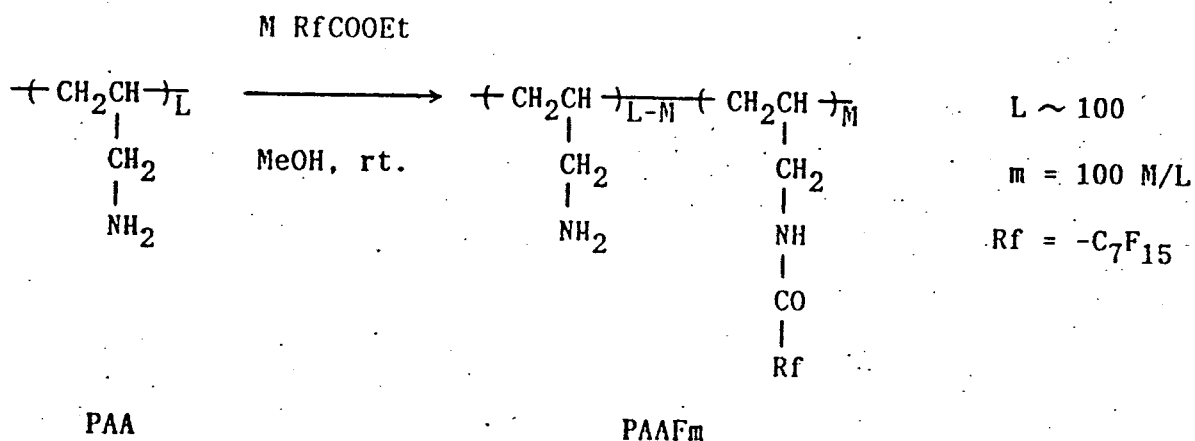
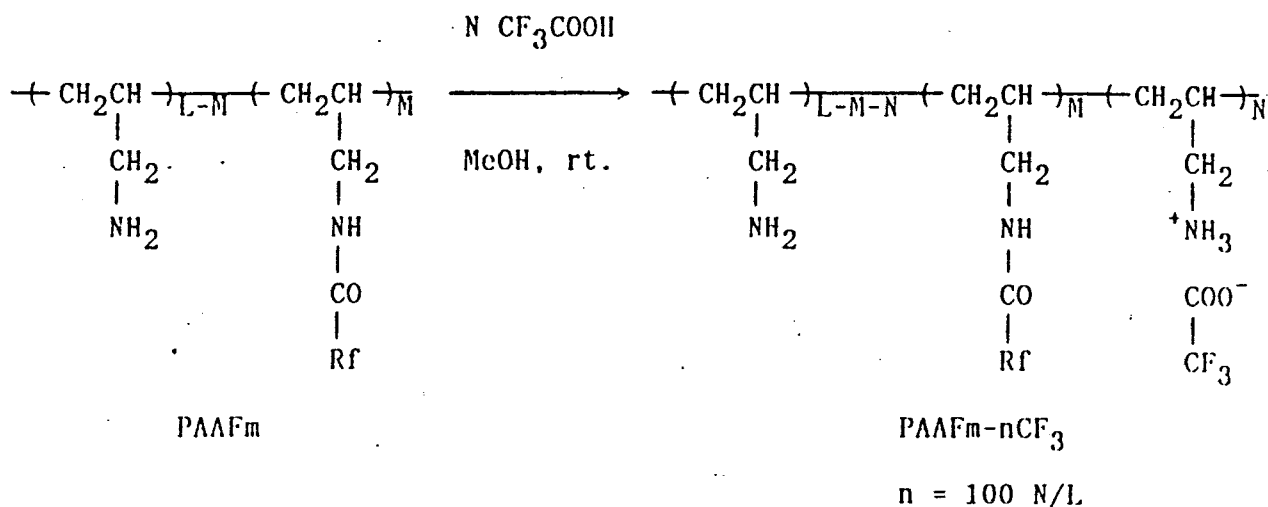
In general, trifluoroacetic acid, short-chain organic acid, cannot be prepared stable LB film. At this point, the LB film of polymers containing trifluoroacetic acids has been expected to study.

This present paper focuses on investigation of LB films of polyallylamine containing long-chain perfluoroalkyl groups by covalent bonds and trifluoroacetic acids by ionic bonds and also describes the characterization of the films.

2. EXPERIMENTAL

2.1. Syntheses of polymers

Synthesis of polymer modified with long-chain perfluoroalkyl groups by covalent bonds and trifluoromethyl groups by ionic bonds was carried out by the reaction between PAAFm, polyallylamine modified by perfluoroacylation,²⁰ and trifluoroacetic acid in methanol. The synthetic sequences used for preparing various polymers are as follows:



Then these polymers were dissolved in the methanol-benzene solution (1:1 by volume) and were spread on a pure water using Lauda film balance at 17°C. The monolayers of these polymers were formed and surface pressure-area (F-A) isotherms were measured.

3. RESULTS AND DISCUSSION

3.1. Syntheses of polymers

The various polymers of polyallylamine containing Rf groups by amide bonds and $-\text{CF}_3$ groups by ionic bonds, PAAFm-nCF₃ (m = mol% of Rf groups to amino groups in PAA, and n = mol% of $-\text{CF}_3$ groups to amino groups in the modified PAA), could be synthesized and also could dissolved in methanol. The LB films of PAAF10-nCF₃, PAAF15-nCF₃ and PAAF20-nCF₃ were prepared and investigated.

The LB films of PAAF10 containing acetic acids (PAAF10-nCH₃) and the LB films of PAAF10 containing octanoic acids (PAAF10-nC₇H₁₅) were prepared for comparison with the LB films of PAAFm-nCF₃. But attempts to prepare the LB films of either PAAF10 containing succinic acids (PAAF10-nC₂H₂) or PAAF10 containing eicosanedioic acids (PAAF10-nC₁₈H₃₆) were unsuccessful because both of these polymers could not dissolve in the methanol-benzene solution.

3.2. Surface pressure-area (F-A) isotherms

F-A isotherms of PAAF10-nCF₃ (0 < n < 90), PAAF15-nCF₃ (0 < n < 85) and PAAF20-nCF₃ (0 < n < 80) are shown in Figure 1. They indicate that the monolayers of the polymer containing $-\text{CF}_3$ groups by ionic bonds were stable at air-water interface up to more than 60 mN m.⁻¹ Also they

illustrate that when the modification ratio of ionic bonds n increased, the area decreased as can be seen clearly from the curves which moved from the right to the left.

Table 1 shows the limiting area (A_0) of PAAFM- nCF_3 , that is, the limiting area of fluorocarbon unit at zero pressure, designed as A_0 (Rf+ CF_3); the limiting area of an amide unit at zero pressure, designed as A_0 (amide); and the limiting area of an allylamine unit at zero pressure, designed as A_0 (allylamine). According to the data, as the modification ratio of ionic bonds n increased, the A_0 (Rf+ CF_3) values tended to decrease. But the A_0 (amide) values and the A_0 (allylamine) values increased and then decreased.

Clearly, this can be seen from Figure 2 which shows relationship between A_0 (amide) and modification ratio of ionic bonds n as well as Figure 3 which shows relationship between A_0 (allylamine) and modification ratio of amide bonds and ionic bonds $m+n$. The results indicate that $-CF_3$ groups could be arranged on the film surface, so that when the modification ratio of ionic bonds n increased, the PAA chains of polymer expanded to increase the values of A_0 (amide) and A_0 (allylamine). However, when n increased beyond some point, the PAA chains of polymer could not expand but was bent and folded as a whole to decrease the values.

The deposition of monolayers of the decided polymers was attempted onto hydrophilic slide glasses under surface pressure of 20 mN m^{-1} . The monolayers of all cases were able to readily adhere to the glasses as Y-type films, head-tail-tail-head arrangement.

3.3. Critical surface tensions (γ_c) and contact angles of water

Measurement of critical surface tensions (γ_c) and contact angles of water on the deposited LB film surface of PAAFM- nCF_3 was carried out. The critical

surface tensions (γ_c) were calculated from the Zisman plot of contact angles²⁷ of liquid n-alkanes on the film surface: a plot of cosine of the contact angle (θ) versus surface tension for the various liquids applied to the surface of 1-layer PAAF10-20CF₃ LB film shown as the representative polymeric film, which yielded a critical surface tension, γ_c (point where $\cos \theta = 1$). The Zisman plot of each LB film of PAAFm-nCF₃ was straight line. The values of γ_c and the contact angles of water on 1- and 5-layer LB films of PAAFm-nCF₃ are listed in Table 2.

According to the data, the 1-layer LB films showed higher γ_c values compared with the 5-layer LB films. This is because the glass surface influenced the thinner films.²⁴ On the other hand, when the modification ratio of ionic bonds n increased, the γ_c values increased and then decreased. This result can be explained that the tendency of the γ_c values corresponded to A_0 (amide) which means the limiting area per Rf unit. As mentioned above when the modification ratio of ionic bonds n increased, the values of A_0 (amide) increased at some point and then became decreased. This means that increase of the modification ratio of ionic bonds n made Rf density smaller at some point and then became larger. Therefore, the γ_c values depended on Rf density. From the result, it is reasonable to say that Rf groups had an effect on the film surface much more than the influence of -CF₃ groups because it is supposed that -CF₃ group is a small group.

In the case of contact angles of water, the 1-layer LB films showed smaller contact angles of water compared with the 5-layer LB films because of the influence of the glass surface.²⁴ On the other hand, when the modification ratio of ionic bonds n increased, the values of 5-layer LB films increased and then decreased. This may be because of two effects, one is that increase of fluorocarbons made water repellence of the films increase. The other is that increase of ionic bonds n made water repellence of the films

decrease owing to the affinity of ionic bond to water.

To support the above results, polymers of PAAFm containing acetic acid (PAAF10-nCH₃) and polymers of PAAFm containing octanoic acid (PAAF10-nC₇H₁₅) were synthesized. Preparation of LB films of these polymers were carried out to measure F-A isotherms, Λ_0 values, γ_c and contact angles of water. Comparison of the limiting area (Λ_0) among PAAF10-nCF₃, PAAF10-nCH₃ and PAAF10-nC₇H₁₅ are shown in Table 3 and comparison of γ_c and contact angles of water among these polymers are listed in Table 4.

Referring to the data of Table 3 as well as Table 4, in the case of PAAF10-nCH₃, the data showed that as the modification ratios of ionic bonds n increased, the values of Λ_0 , γ_c and contact angles of water unchanged. In contrast, PAAF10-nC₇H₁₅ showed the change of these values as n increased. It means that only LB films of the polymers containing long-chain hydrocarbon groups could be prepared and long chain hydrocarbon groups were oriented on the film surface. This is because, in the case of PAAF10-nCH₃, acetic acid dissolved into the water even if the modification ratio of acetic acid increased, so that the values of Λ_0 , γ_c and contact angles of water unchanged. Considering the case of PAAFm-nCF₃, the data showed the change of the values of Λ_0 , γ_c and contact angles of water. Consequently, these experimental results supported the above results that new type LB films of polyallylamine containing trifluoroacetic acids could be prepared and short-chain per-fluoroalkyl groups could be arranged on the film surface.

3.4. LB films' thicknesses

Attempts in the measurement of LB films' thicknesses were performed by X-ray diffraction using 19-layer LB films of PAAFm-nCF₃. Indeed, only in the case of the LB films of the less modification ratio by ionic bonds ($n = 10$

mol%), broad peaks derived from diffraction between layer in the films were observed as X-ray diffraction patterns and the thicknesses of the films were calculated from the diffraction peaks by the mentioned equation. The calculated values of films' thicknesses are given in Table 5.

Obviously, the data show that LB film of PAAFm-10CF₃ were thinner than that of PAAFm-OCF₃. It is reasonable to explain that as the modification ratio of ionic bond n increased from 0 to 10, the PAA chains in polymers expanded to make the monolayers thinner.

4. CONCLUSIONS

Along with the mentioned results of the new type polymeric LB films investigation lead to the following conclusions:

1. The new type LB films of polyallylamine containing Rf groups by covalent bonds and -CF₃ groups by ionic bonds (PAAFm-nCF₃) can be successfully prepared at the air-water interface.

2. The monolayers of the all polymeric LB films are stable on the pure water surface, up to more than 60 mN.n.⁻¹ and can be deposited onto hydrophilic slide glasses as Y-type films.

3. -CF₃ groups, short-chain perfluoroalkyl groups, can be arranged on the LB film surface.

4. When the modification ratio of ionic bonds n increases, the polymer chains expand on the film surface showing increase of A₀ (amide) values and A₀ (allylamine) values. However, when the modification ratio increases beyond some point, the polymer chains can not expand but is buckled and folded as a whole showing decrease of A₀ (amide) values and A₀ (allylamine) values.

5. Increase of the modification ratio of ionic bonds n makes the film surface energy higher. However, if the modification ratio increases beyond

some point, the film surface energy becomes lower.

6. The water repellence of the multilayer LB films increases when the modification ratio of ionic bonds n increases till exceeds some point the water repellence becomes decreased.

REFERENCES

1. K.B. Blodgett, J. Am. Chem. Soc., 57, 1007 (1935).
2. T. Nakamura and Y. Kawabata, Techno Japan, 22, 8 (1989).
3. A. Momose, Y. Hirai, I. Waki, S. Imazeki, Y. Tomioka, K. Hayakawa and M. Naito, Thin Solid Films, 178, 519 (1989).
4. V. K. Agarwal, Thin Solid Films, 178, 155 (1989).
5. K.F. Fukuda and M. Sugi (Eds), Langmuir-Blodgett Films 4, Vol. 1, p. v, Elsevier Applied Science, London and New York, 1989.
6. L. Yajun, W. Xianxiu, P. Xiaomin, H. Yuling and F. Junqins, Thin Solid Films, 178, 525 (1989).
7. R. Popovitz-Biro, K. Hill, E. Shavit, D.J. Hung, M. Lahav, L. Leiseronitz, J. Sagiv, H. Hsiung, G.R. Meredith and H. Yanherzeele, J. Am. Chem. Soc., 112, 2498 (1990).
8. D.J. Sawalen, D.L. Allara, J.D. Andrade, E.A. Chandross, S. Garoff, J. Israelachvili, T.J. McCarthy, R. Murray, R.F. Peace, J.F. Rabolt, K.J. Wynn and H. Yu, Langmuir, 3, 932 (1987).
9. M. Sugi, J. Mol. Electron., 1, 3 (1985).
10. R.H. Tredgold, Thin Solid Films, 152, 223 (1987).
11. D. Lupo, W. Prass and U. Scheunemann, Thin Solid Films, 178, 403 (1989).
12. R.H. Tredgold and C.S. Winter, J. Phys. D: Appl. Phys., 15, L55 (1982).
13. P. Hodge, E. Khoshdel, R.H. Tredgold, A.J. Vickers and C.S. Winter, Br. Polym. J., 17, 368 (1985).

14. R. Elbert, A. Laschewsky and H. Ringsdorf, J. Am. Chem. Soc., 107, 4134 (1985)
15. S.T. Kowel, R. Selfridge, C. Eldering, N. Matloff, P. Stroeve, B.G. Higgins, M.P. Srinivasan and L.B. Coleman, Thin Solid Films, 152, 377 (1987).
16. W.A. Zisman, Adv. in Chem. Series, 43, 1 (1964).
17. R. Elbert, T. Folda and H. Ringsdorf, J. Am. Chem. Soc., 107, 7687 (1985).
18. N. Higashi, T. Kunitake and T. Kajiyama, Polym. J., 19, 289 (1987).
19. H. Yamada, Y. Goto and M. Fujihira, 54th National Meeting of the Chemical Society of Japan, Tokyo, April 1987, Abstr., No. 3VII42.
20. A. Sekiya, H. Ishida, M. Tamura and Watanabe, Chem. Lett., 1987, 1593.
21. A. Sekiya, M. Tamura, M. Watanabe and H. Ishida, Chem. Lett., 1988, 527.
22. A. Sekiya, M. Tamura and H. Ishida, Chem. Lett., 1988, 1223.
23. M. Tamura, H. Ishida and A. Sekiya, Chem. Lett., 1988, 1277.
24. M. Tamura, H. Ishida and A. Sekiya, Thin Solid Films, 178, 373 (1989).
25. M. Tamura and A. Sekiya, Chem. Lett., 1989, 231.
26. M. Tamura, A. Sekiya and B. Song, Chem. Lett., 1990, 1027.
27. Y. Kitazaki, Hyomen, 14, 116 (1976).

Table 1. Limiting area (Λ_0) of PAAFM- $n\text{CF}_3$.

PAAFM- $n\text{CF}_3$	$\Lambda_0(\text{Rf}+\text{CF}_3) / \text{\AA}^2$	$\Lambda_0(\text{amide}) / \text{\AA}^2$	$\Lambda_0(\text{allylamine}) / \text{\AA}^2$
PAAF10-0CF ₃	72	72	7
PAAF10-10CF ₃	47	95	9
PAAF10-20CF ₃	37	111	11
PAAF10-50CF ₃	22	131	13
PAAF10-70CF ₃	14	114	11
PAAF10-90CF ₃	10	104	10
PAAF15-0CF ₃	63	63	9
PAAF15-10CF ₃	44	74	11
PAAF15-20CF ₃	37	86	13
PAAF15-30CF ₃	31	93	14
PAAF15-70CF ₃	13	72	11
PAAF15-85CF ₃	11	70	11
PAAF20-0CF ₃	52	52	10
PAAF20-10CF ₃	44	66	13
PAAF20-20CF ₃	41	83	16
PAAF20-30CF ₃	36	89	18
PAAF20-70CF ₃	13	61	12
PAAF20-80CF ₃	11	56	11

Table 2. Critical surface tension (γ_c) and contact angles of water on the PAAF_m-nCF₃ LB films surface.

PAAF _m -nCF ₃	γ_c / dyn cm ⁻¹		contact angles of H ₂ O / deg	
	1 layer	5 layer	1 layer	5 layer
PAAF10-0CF ₃	18.4	16.3	100	98
PAAF10-10CF ₃	18.5	17.6	95	95
PAAF10-20CF ₃	19.0	18.6	94	98
PAAF10-50CF ₃	20.6	19.6	93	99
PAAF10-70CF ₃	18.8	18.7	86	97
PAAF10-90CF ₃	18.6	18.6	53	98
PAAF15-0CF ₃	17.6	15.3	100	97
PAAF15-10CF ₃	17.8	16.9	97	104
PAAF15-20CF ₃	18.1	17.8	98	107
PAAF15-30CF ₃	18.8	18.4	97	109
PAAF15-70CF ₃	18.2	18.1	94	102
PAAF15-85CF ₃	17.6	17.5	86	102
PAAF20-0CF ₃	16.9	14.6	103	106
PAAF20-10CF ₃	17.2	16.1	101	104
PAAF20-20CF ₃	17.6	16.3	101	104
PAAF20-30CF ₃	18.7	17.1	100	107
PAAF20-70CF ₃	17.5	16.9	96	104
PAAF20-80CF ₃	17.3	16.7	96	103

Table 3. Limiting area (Λ_0) of PAAF10- $n\text{CF}_3$, PAAF10- $n\text{CH}_3$ and PAAF10- $n\text{C}_7\text{H}_{15}$.

PAAF10-n	$\Lambda_0(\text{Rf}+\text{CF}_3) / \text{\AA}^2$	$\Lambda_0(\text{amide}) / \text{\AA}^2$	$\Lambda_0(\text{allylamine}) / \text{\AA}^2$
PAAF10- 0CF_3	72	72	7
PAAF10- 20CF_3	37	111	11
PAAF10- 50CF_3	22	131	13
PAAF10- 0CH_3	72	72	7
PAAF10- 20CH_3	21	62	6
PAAF10- 50CH_3	10	62	6
PAAF10- $0\text{C}_7\text{H}_{15}$	72	72	7
PAAF10- $20\text{C}_7\text{H}_{15}$	40	119	12
PAAF10- $50\text{C}_7\text{H}_{15}$	29	171	17

Table 4. Critical surface tension (γ_c) and contact angles of water on the polymeric LB films surface.

PAAF10-n	γ_c / dyn cm ⁻¹		Contact angles of H ₂ O / deg	
	1 layer	5 layer	1 layer	5 layer
PAAF10-0CF ₃	18.4	16.3	100	98
PAAF10-20CF ₃	19.0	18.6	94	98
PAAF10-50CF ₃	20.6	19.6	93	99
PAAF10-0CH ₃	18.4	16.3	100	98
PAAF10-20CH ₃	18.2	15.6	105	109
PAAF10-50CH ₃	18.3	15.7	103	108
PAAF10-0C ₇ H ₁₅	18.4	16.3	100	98
PAAF10-20C ₇ H ₁₅	18.9	17.5	100	109
PAAF10-50C ₇ H ₁₅	20.2	19.1	102	108

Table 5. The monolayer's thickness of the PAAF_m-nCF₃ LB films.

PAAF _m -nCF ₃	Monolayer thickness / Å
PAAF10-OCF ₃	19
PAAF10-10CF ₃	15
PAAF15-OCF ₃	17
PAAF15-10CF ₃	15
PAAF20-OCF ₃	16
PAAF20-10CF ₃	14

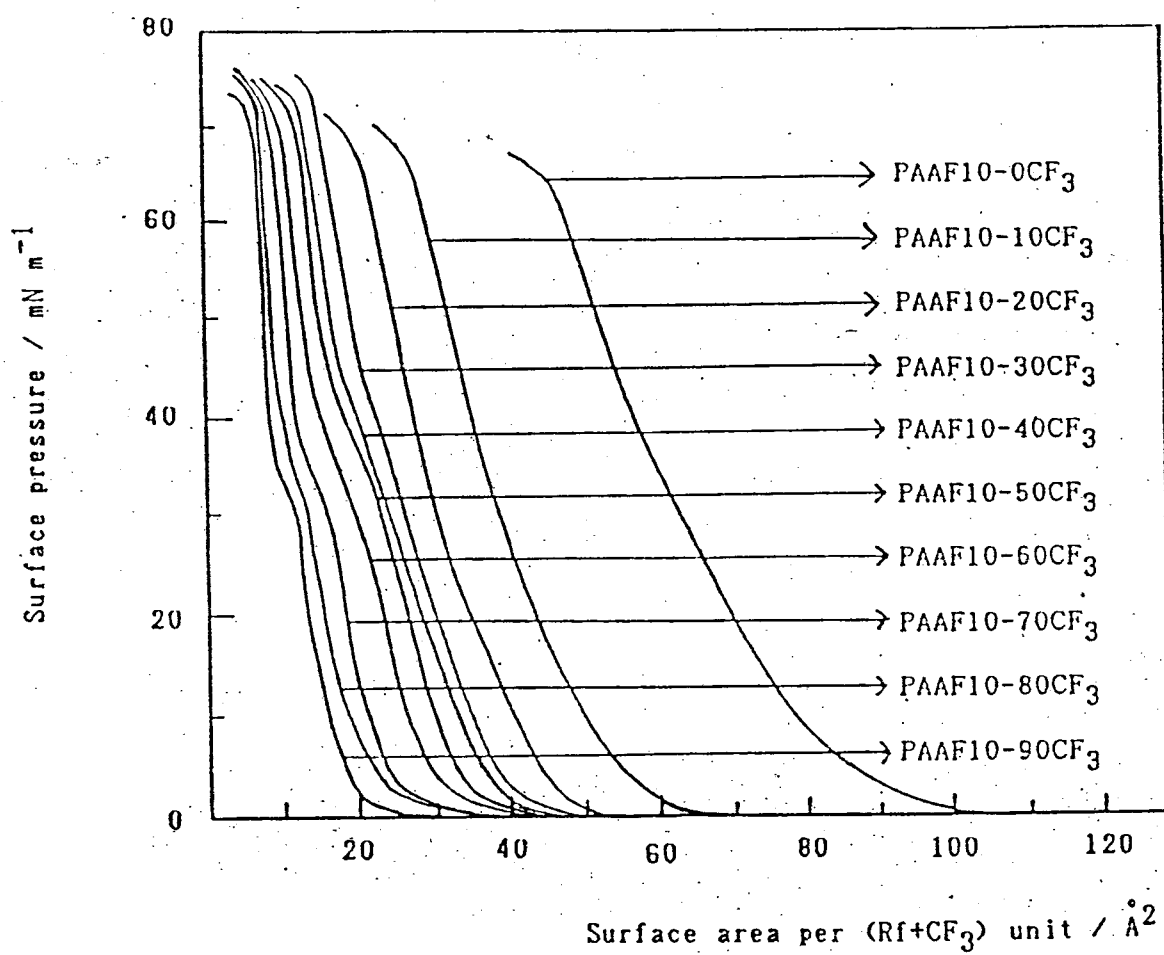


Figure 1. F-A Isotherms of PAAF10-nCF₃ on pure water at 17°C.

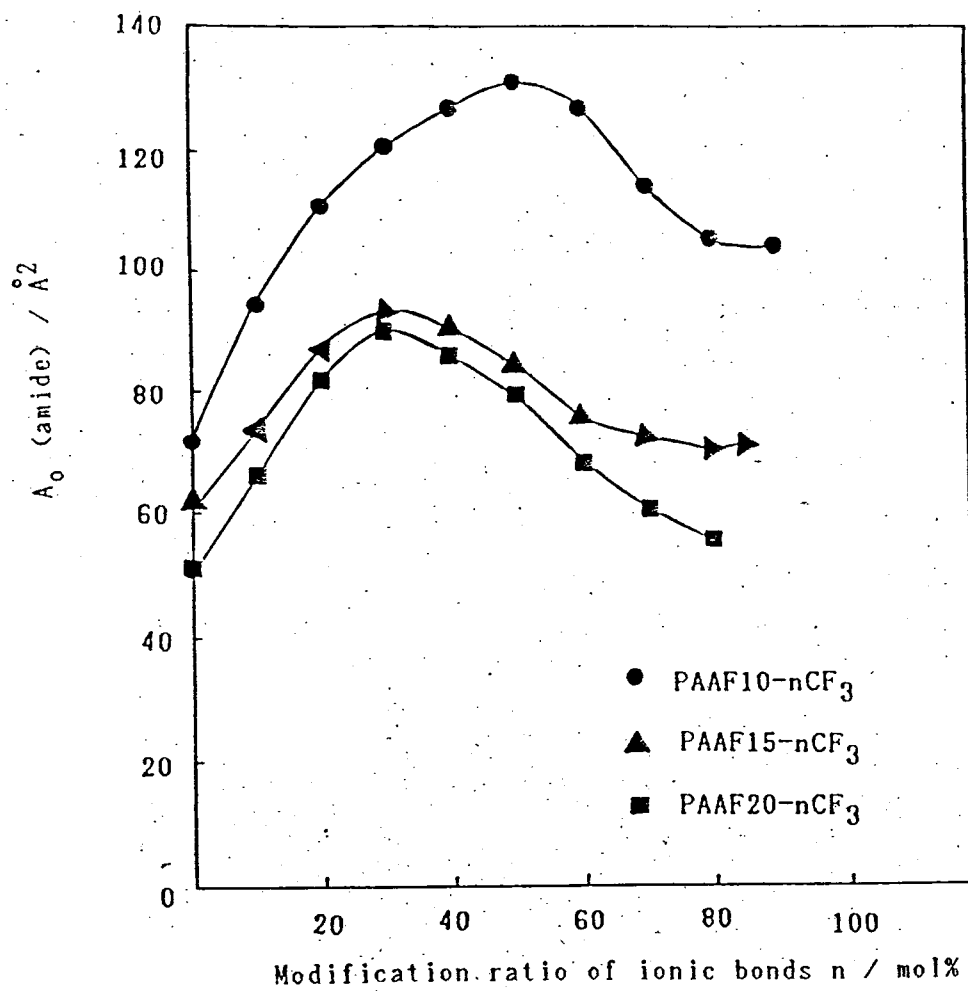


Figure 2 Relationship between A_0 (amide) and modification ratio of ionic bonds n .

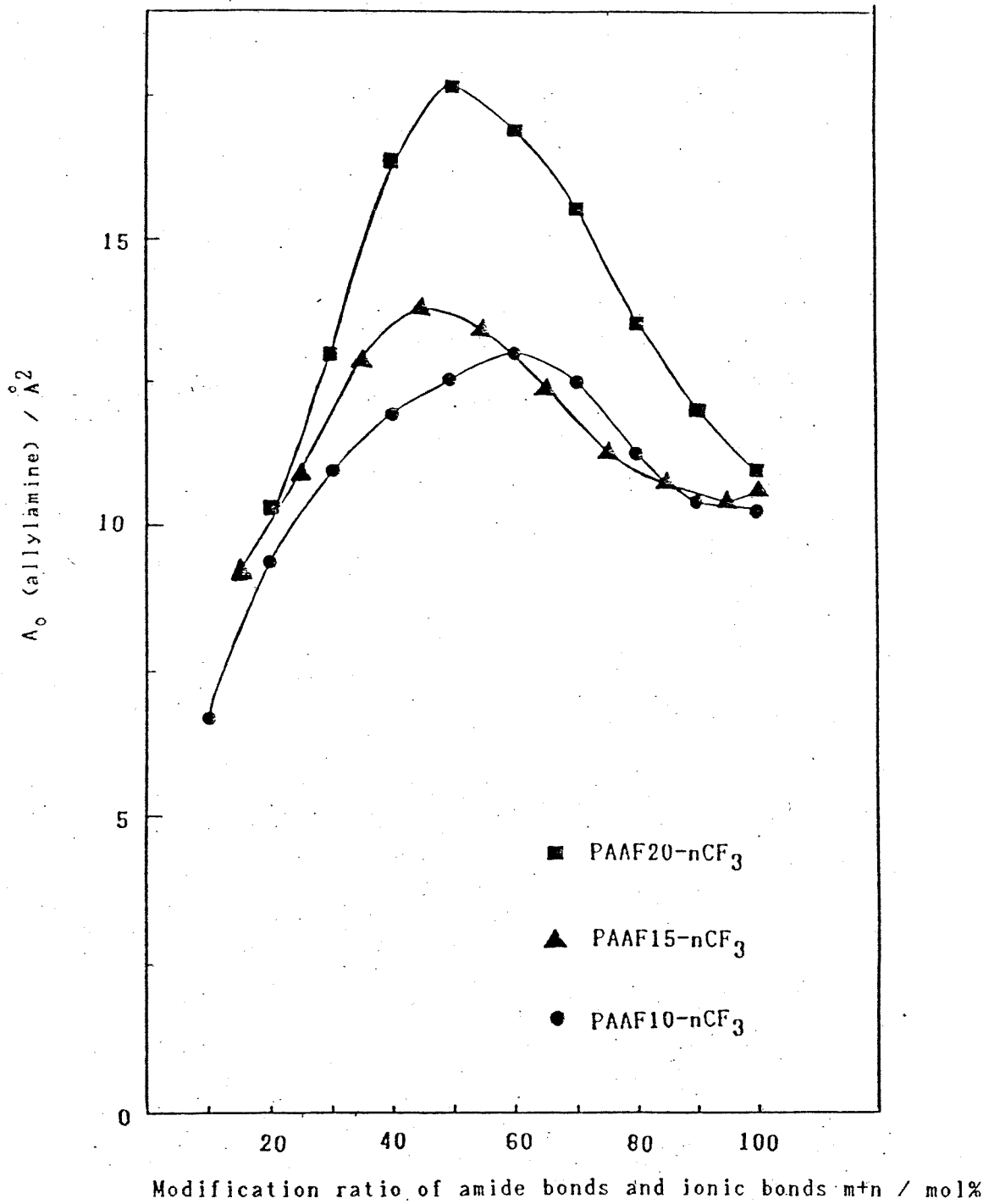


Figure 3. Relationship between A_0 (allylamine) and modification ratio of amide bonds and ionic bonds $m+n$ / mol%.

A STUDY OF THE PERMEABILITY OF IONS TO ORGANIC COATING

Cynthia R. Habana, Toshiaki Kodama, Ph.D.

ABSTRACT

This work is concerned with the study of the permeability of sodium and chloride ions through detached films of white alkyd, clear epoxy, and polyurethane paint with thickness ranging from 6 - 50 μm when exposed to 3% NaCl solution.

In this experiment, conductivity measurements have been used to investigate ion uptake and diffusivity of ions into the coating. Impedance measurements were carried out on detached film and attached film on steel substrate. It is aimed that the information gathered in this experiment may help explain the behavior of a coating when attached to a substrate.

PRESENT PAPER

"THE OVERALL CORROSION MONITORING SYSTEM"

PRESENT BY

MR. CHAICHAREARN ATIBAEDYA

DEPUTY DIRECTOR TECHNICAL SERVICE DEPARTMENT

NATURAL GAS OPERATION

PETROLEUM AUTHORITY OF THAILAND

THAILAND HAD A VERY LONG HISTORY; WE BUILT THIS COUNTRY MANY YEARS AGO. BASIC LIFE IS AGRICULTURE. TO ME THIS IS ONE OF THE FACTOR THAT PEOPLE OR THAI PEOPLE MIGHT FORGET WHEN WE MOVE INTO INDUSTRIALIZATION. THIS FACTOR OF CHANGING IS VERY IMPORTANT AND PLAYS A BIG RULES IN PEOPLE'S MIND AND HOW TO MANAGE.

THAI PEOPLE LIKE TO BUILD, LIKE ARCHITECTURAL, WE HAD BEAUTIFUL TEMPLES. INFACT: A LOT OF TEMPLES MORE THAN A GOOD SCHOOL IN MY COMMUNITY. AGAIN A LOT OF THEM START WITH A BEAUTIFUL DECORATION AND VERY NICE TRADITIONAL STYLE, BUT THOSE SEEMS HAD A SHORTER LIFE MORE THAN I EXPECTED. THE CONCLUSION TO THIS; IS "THAI PEOPLE LIKE TO BUILD BUT DID NOT CARE MUCH ABOUT MAINTAIN" I DON'T KNOW ANY ONE OF US HERE WILL AGREE WITH ME OR NOT.

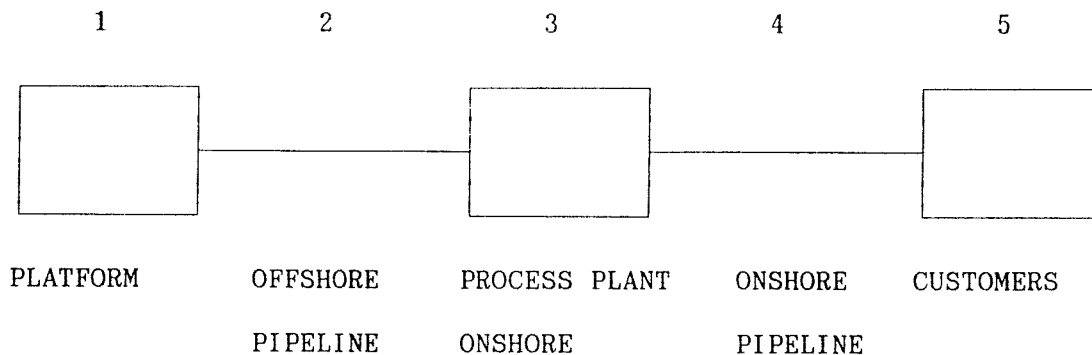
THIS ALSO THE FACT OF MY 10 YEARS OPERATION EXPERIENCE. IF YOU TALK ABOUT MAINTENANCE OR INSPECTION, OF COURSE, CORROSION IS ONE OF THE MAJOR DIFFICULT THINGS PEOPLE EVER INTERESTING IN IT. BECAUSE OF THE LONG LEAD TIME EFFECT, A LOT OF FACTORS INVOLVED AND SO ON; AS EVERY BODY IN THIS CONFERENCE ACKNOWLEDGE ABOUT IT.

I AM WORKING IN THE AREA OF ONE OF THE MOST ADVANCE ELECTRONIC AND COMPUTER CONTROLS ENVIRONMENT WHICH OF COURSE, CONSISTS OF OVER 98 % MADE OUT OF STEEL. THIS IS THE FIRST NATURAL GAS PIPELINE TRANSMISSION OF THAILAND. THIS IS IN OPERATION DAY AND NIGHT OVER 10 YEARS OF AGES. A LOT OF MODIFICATION, A LOT OF ADDITIONAL INTO THE ORIGINAL SYSTEM. WE FACED A CORROSION PROBLEMS, STARTED WITH HIGH VELOCITY ERROSION, CHEMICAL CORROSION, VIBRATION, BACTERIALIZE CORROSION ETC. BOTH INSIDE AND OUTSIDE OF THE PIPES AND VESSELS.

WHEN WE TALK ABOUT CORROSION. NOT MANY PEOPLE PAY ATTENDTION; OR GIVE PRIORITY, WHY? DID ANY BODY HERE CAN ANSWER THIS QUESTION? BECAUSE WE WILL TALK IN MIL PER YEAR OF MILIMIL PER MONTH. IT IS TOO SMALL! MY WIFE ALWAYS SAID THAT, THEN FORGET ABOUT IT.

WE INVESTED A LOT OF MONEY IN GETTING THE KNOWLEDGES, A TOOLS, INSTRUMENTS, CONSULTANTS FOR THE PAST, BUT THESE SO FAR NOT A GOOD EFFECTIVE

CORROSION CONTROL SYSTEM. THE FACT OF THIS IS WE ARE NOT SURE ABOUT THE DATA,
THE FIGURE IS TOO SMALL. HOW MUCH THE ERROR?



WHAT WE DID WRONG IN THE PAST IS WE DID NOT INTEGRATE OR RELATE THE
CORROSION DATA OF. 1 AND 2 AND 3 AND 4 TOGETHER AND THEN ANALYZE FOR: WHY'S
EFFECT, WHAT SHOULD BE DONE, HOW MANY FOR OPTIMIZATION AND SO ON.

HOPE THIS COMING 1991'S. THE FIRST PHASE OF "THE OVERALL CORROSION
MONITORING SYSTEM" FOR US WILL BE IN OPERATION. THESE WILL INCLUDE:

- STUDY WHERE, HOW TO PUT THE MONITORING INSTRUMENTS ALONG THE
PIPES, VESSELES; FROM UPSTREAM TO DOWNSTREAM.
- INSTALLATION AND MAKE ADJUSTMENT.
- DISTRIBUTE SAME METHOD OF" HOW TO GET THE CORROSION DATA".
- GATHERING AND INTEGRATE THE INFORMATIONS TO THE COMPUTER CENTER
WHICH WILL INCLUDES INFORMATIONS OF THE FOLLOWING:
 - . GAS; LIQUID, PRODUCTS QUALITY.; MILL SCALE ANALYSIS
 - . PHYSICAL DATA: TEMP, VELOCITY, PRESSURE OR OPERATION PHILOSOPHY
CHANGE
 - . ULTRASONIC READ OUT, THICKNESS DATA, VIBRATION DATA
 - . DATA FROM ONLINE/OFFLINE MONITORING POINTS ALONG THE PIPELINES
& VESSELS
 - . CATHODIC PROTECTION DATA

- . OTHER SUSPECT SUCH AS: PIPELINE MOVEMENT, INHIBITOR INJECTION RATE ETC.
- . COMPUTER SOFTWARE WILL COMPARE THE UP TO DATE DATA TO THE HISTORICAL DATA LOG AND THE ORIGINAL DESIGN.

GENTLEMAN; SO FAR WE STILL IN PROGRESS IN CORROSION MONITORING AND CONTROLS. IN FACT WE SHOULD NOT STOP EVEN TO THINK HOW TO DO IT BETTER?, AS EVERY CORROSION GUYS KNEW THAT "CORROSION WILL NEVER STOP" MY TARGET IS I WOULD LIKE TO SEE WE OPERATE THE SYSTEM MORE THAN THE DESIGNED'S LIFE.

WELL, BEFORE I CLOSE UP MY PRESENTATION I WOULD LIKE TO WELCOME ALL DELEGATE TO THAILAND. HOPE THERE WILL BE A NEXT TRIP TO BANGKOK AGAIN.

THANK YOU VERY MUCH FOR YOUR ATTENTION.

The Determination of Film Resistance by Means of the Frequency at the Maximum Phase Angle and the Estimation of the Degradation of the Coating Film

Isao SEKINE,* Kazuhiko SAKAGUCHI, and Makoto YUASA*

Department of Industrial Chemistry, Faculty of Science and Technology,
Science University of Tokyo, 2641 Yamazaki, Noda, Chiba 278

(Received August 25, 1989)

Synopsis. The determination of film resistance (R_f) was investigated by means of the frequency at the maximum phase angle ($f_{\theta_{\max}}$), as obtained from electrochemical impedance measurements. $f_{\theta_{\max}}$ was linearly correlated with R_f . The degradation of the coating film was obviously and rapidly evaluated from $f_{\theta_{\max}}$ by comparison with R_f .

Recently, the degradation of coating films and under-film corrosion have been widely investigated by means of electrochemical impedance measurements.^{1–6)} To evaluate the degradation of coated steels, a method utilizing the break point frequency (f_b) was proposed by Tsuru et al.⁷⁾ It is based on the theory that the break point frequency (phase shift=45°) is proportional to the area of delamination. Using this theory we have been evaluating the corrosion protective property of coating films by means of the film resistance (R_f) values.^{6,8–14)} When a coating system has a large film resistance, however, this evaluation method can not be used. Such a condition can be seen when the initial stage is immersed in test solution and in the case of highly insulated binders. In order to estimate the R_f values in such a case, we attempted to use a new parameter of a frequency at a maximum phase angle ($f_{\theta_{\max}}$). The $f_{\theta_{\max}}$ is not easily affected by radio ham noise (50 Hz), for it is observed on the high frequency side in comparison with f_b . In this paper, the R_f value was determined by the use of the $f_{\theta_{\max}}$ value obtained by means of electrochemical impedance measurements in order to estimate the degradation of the coating film.

Experimental

Steel plates coated with boiled linseed oil were prepared. The specimen was a cold rolled steel plate (JIS G 3141, SPCC-SB) coated at a thickness of 40 μm and with an exposed area of 9 cm^2 . It was immersed in an aqueous 3% NaCl solution.

Electrochemical impedance measurements were carried out by using a frequency response analyzer, FRA (NF Electronic Instruments, 5020) and a potentiostat (Toho Technical Research, 2000). They were conducted using a standard three-electrode configuration at the immersion potential. The applied signal amplitude was 9 mV (RMS) in the frequency range from 20 kHz to 10 mHz.

Results and Discussion

Figure 1 shows Bode plots of the electrochemical impedance spectra obtained from the coated steel. After immersion for 30 minutes, the Bode plots of the electrochemical impedance spectra were disordered below 500 Hz, because the paint film was sound and radio ham noise occurred. The film resistance (R_f) was determined by the extrapolation of the frequency-

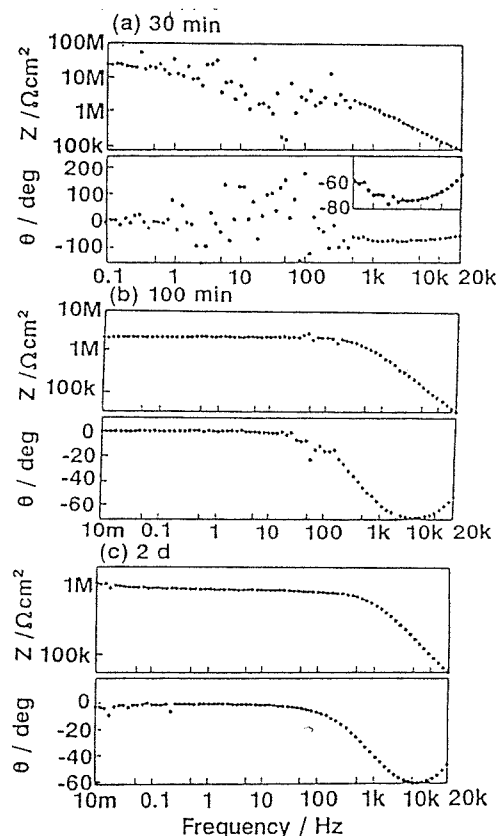


Fig. 1. Bode plots of impedance data obtained from coated steel. (a) after 30 minutes, (b) after 100 minutes, and (c) after 2 days.

independent horizontal line to the Z axis and reading off the value of Z . It was difficult to obtain the R_f value exactly because the paint film was sound. After 100 minutes, the Z decreased and the Bode plot became comparatively stable. It can be seen from these impedance spectra that a parallel resistor/capacitor combination is present in the high frequency range. The R_f value obtained was 1.7 $\text{M}\Omega\text{cm}^2$. After immersion for 2 days, the degradation of the film proceeded more than that after 100 minutes, judging from the decrease in the Z value and phase angle ($\theta \neq 0^\circ$) at 10 mHz. The various electrochemical parameters, R_f , the immersion potential (E), the maximum phase angle (θ_{\max}), and the $f_{\theta_{\max}}$ value were determined by the analysis of the Bode plot at various immersion times (Fig. 2). The R_f value after 30 minutes is represented in Fig. 2. As the Nyquist and Bode plots could not be

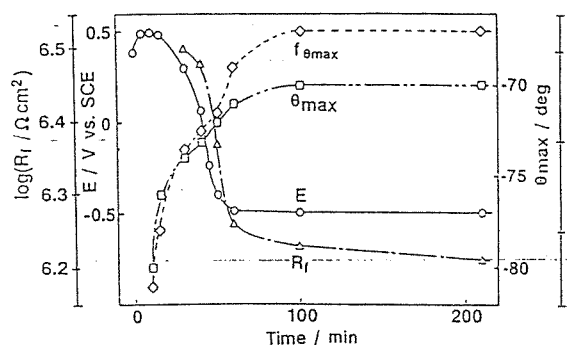


Fig. 2. Electrochemical parameters (E , R_f , θ_{\max} , and $f_{\theta_{\max}}$) vs. immersion time curves. E ; immersion potential, R_f ; film resistance, θ_{\max} ; maximum phase angle, and $f_{\theta_{\max}}$; frequency at θ_{\max} .

described clearly for 30 minutes after immersion, the R_f value could not be obtained. The E value was kept at ca. 0.4 to 0.5 V vs. SCE after immersion for 20 minutes after the initial immersion; thereafter it gradually shifted to a negative potential in the figure until it remained constant at ca. -0.5 V vs. SCE. In connection with the R_f value, the tendency for the E value to change is similar to that of the R_f value at an initial immersion. However, the E value is influenced by the substrate and so can not reflect the film condition directly. It is thought, therefore, that it is unsuitable to evaluate the degradation of paint film by means of the E value instead of the R_f value.

The other parameters—that is, θ_{\max} and $f_{\theta_{\max}}$ —could be determined. The θ_{\max} and $f_{\theta_{\max}}$ values increased with the immersion time; this behavior corresponded to that of the R_f . The parameters of θ_{\max} and $f_{\theta_{\max}}$ are superior to that of E , in that these parameters enable us to understand the difference between the two time constants concerned with the paint film and the substrate; they can be determined after an initial immersion for 10 minutes. The $f_{\theta_{\max}}$ is, then, related to Z (or resistance (R)) and the capacitance (C) as follows: $f_{\theta_{\max}} = 1/2\pi Z_{\theta_{\max}} C$, where $Z_{\theta_{\max}}$ is Z at θ_{\max} .¹⁵⁾ The parameter of $f_{\theta_{\max}}$ can be evaluated for the degradation of the coating film in comparison with that of θ_{\max} . Figure 3 shows the relationship between R_f and $f_{\theta_{\max}}$. The R_f decreased linearly in logarithms with the increase in $f_{\theta_{\max}}$. The calculated data in such a relationship were also shown in the same figure; they were determined by an equivalent circuit model in this figure. The values of R' and C_f are of the pseudoresistance (apparent resistance), containing both the solution resistance (R_{sol}) and the resistance on the measuring system (R_c), and the film capacitance, respectively ($R' (=R_{\text{sol}} + R_c) = 2.7 \times 10^4 \Omega \text{ cm}^2$ and $C_f = 3.0 \times 10^{-10} \text{ F cm}^{-2}$). The values of R' and C_f in this calculation were assumed to be constant, because they are not very variable. The impedance Z of the equivalent circuit shown in Fig. 3 is given by:

$$Z = R' + R_f / (1 + j\omega C_f R_f) \\ = \frac{R'(1 + \omega^2 C_f^2 R_f^2) + R_f}{1 + \omega^2 C_f^2 R_f^2} - j \frac{\omega C_f R_f^2}{1 + \omega^2 C_f^2 R_f^2} \quad (1)$$

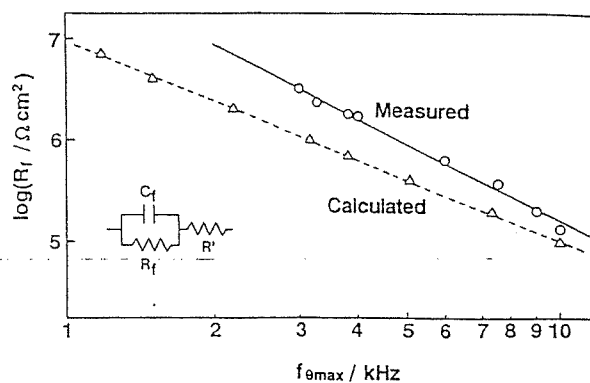


Fig. 3. Relationship between $f_{\theta_{\max}}$ and R_f .

where ω is related to the frequency f by this relationship: $\omega = 2\pi f$ and where $j = (-1)^{1/2}$. Hence, the phase of the impedance θ is expressed by:

$$\theta = -\tan^{-1} \left(\frac{\omega C_f R_f^2}{R' + R_f + \omega^2 C_f^2 R_f^2 R'} \right) \quad (2)$$

The maximum of θ with respect to ω is given by the relationship of $d\theta/d\omega = 0$ as follows:

$$\frac{d\theta}{d\omega} = \frac{C_f R_f^2 (R' + R_f + \omega^2 C_f^2 R_f^2 R') - \omega C_f R_f^2 (2\omega C_f^2 R_f^2 R')}{(R' + R_f + \omega^2 C_f^2 R_f^2 R')^2 + (\omega C_f R_f^2)^2} = 0 \quad (3)$$

From Eq. 3 we obtain:

$$\omega_{\max}^2 = (R' + R_f) / (R_f^2 R' C_f^2) = 4\pi^2 f_{\theta_{\max}}^2 \quad (4)$$

where ω_{\max} is the maximum radial frequency. From Eq. 4 we get:

$$f_{\theta_{\max}} = \frac{1}{2\pi} \left(\frac{R' + R_f}{R_f^2 R' C_f^2} \right)^{1/2}$$

By taking logarithms of both sides of this equation, we obtain:

$$\log f_{\theta_{\max}} = -\log 2\pi + 0.5 \log (R' + R_f) \\ - 0.5 \log R_f^2 - 0.5 \log R' C_f^2 \\ = -\log 2\pi - 0.5 \log R' C_f^2 \\ + 0.5 \log (R' + R_f) - \log R_f \quad (5)$$

If $R' \ll R_f$, the $(R' + R_f)$ term of Eq. 5 can be replaced by R_f . Substituting the values of R' ($= 2.7 \times 10^4 \Omega \text{ cm}^2$) and C_f ($= 3.0 \times 10^{-10} \text{ F cm}^{-2}$) into Eq. 5 yields the following equation:

$$\log R_f = 13 - 2 \log f_{\theta_{\max}} \quad (6)$$

Equation 6 indicates the calculated line in Fig. 3. The relationship between $\log R_f$ and the $f_{\theta_{\max}}$ value determined by the use of the calculated data is also linear; the experimental values have the same correlation as the calculated values. The straight line of $\log R_f$ vs. $f_{\theta_{\max}}$ obtained by the use of the experimental value was shifted upward in comparison with that obtained by the use of the calculated value. Such a shift may be ascribed to the fact that the center of the semicircle in the Nyquist plot was below the real axis.

That is, it seems to be caused by increased surface roughness or by geometrical effects leading to a non-uniform, repartitioning of the current density on the surface.^{16,17)} In this case, the relation between R_f and $f_{\theta_{max}}$ based on the measured and calculated values showed the same tendency. The R_f value can be determined by the measurement of the $f_{\theta_{max}}$ value, while the $f_{\theta_{max}}$ can be measured rapidly in the high frequency range. The precision of the electrochemical impedance measurements by means of FRA rises as the integration time increases.

At any rate, the relationship of R_f with $f_{\theta_{max}}$, as is shown in Fig. 3, can be regarded as a calibration curve. The R_f value is speedily and exactly determined by the measurement of the $f_{\theta_{max}}$ value and its relationship. The degradation of the coating film can easily be predicted by the use of the estimation method described above.

References

- 1) M. W. Kendig and H. Leidheiser, Jr., "Corrosion Protection by Organic Coatings," Electrochemical Society (1987).
 - 2) L. M. Callow and J. D. Scantlebury, *J. Oil Col. Chem. Assoc.*, **64**, 83 (1981).
 - 3) F. Mansfeld, M. W. Kendig, and S. Tsai, *Corrosion*, **38**, 478 (1982).
 - 4) T. Tsuru, H. Sudoh, and S. Haruyama, *Denki Kagaku*, **51**, 159 (1983).
 - 5) J. Hubrecht, J. Verecken, and M. Piens, *J. Electrochem. Soc.*, **131**, 2010 (1984).
 - 6) I. Sekine, "Corrosion Control by Organic Coatings," ed by H. Leidheiser, Jr., National Association of Corrosion Engineers, Houston (1981), p. 130.
 - 7) T. Tsuru, M. Asari, and S. Haruyama, *Kinzoku Hyomen Gijutsu*, **39**, 2 (1988).
 - 8) I. Sekine and T. Kato, *Ind. Eng. Chem. Prod. Res. Dev.*, **25**, 7 (1986).
 - 9) I. Sekine, T. Kato, and H. Suda, *Shikizai Kyokaishi*, **59**, 525 (1986).
 - 10) I. Sekine and T. Kato, *J. Oil Col. Chem. Assoc.*, **70**, 256 (1987).
 - 11) I. Sekine, T. Kato, and H. Suda, *Boshoku Gijutsu*, **36**, 487 (1987).
 - 12) I. Sekine and H. Suda, *Boshoku Gijutsu*, **37**, 485 (1988).
 - 13) I. Sekine and K. Sakaguchi, *Boshoku Gijutsu*, **38**, 3 (1989).
 - 14) I. Sekine, K. Moriya, and M. Yuasa, *Boshoku Gijutsu*, **38**, 365 (1989).
 - 15) G. W. Walter, *Corros. Sci.*, **26**, 681 (1986).
 - 16) a) K. S. Cole and R. H. Cole, *J. Phys. Chem.*, **9**, 341 (1941), b) *ibid.*, **10**, 98 (1942).
 - 17) I. Epelboin and M. Keddam, *J. Electrochem. Soc.*, **117**, 1052 (1970).
-

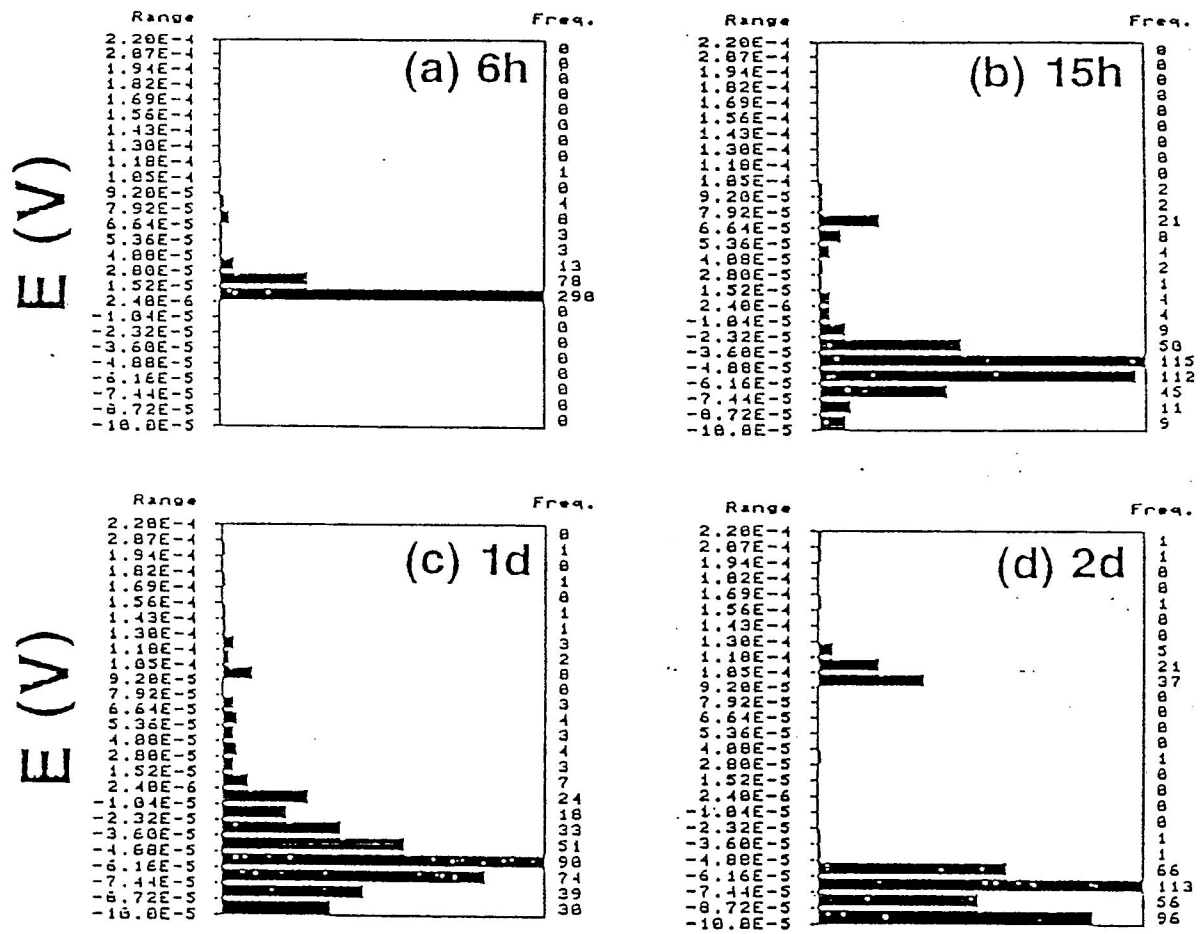


Fig.5 Distribution of E for Ep paint film.
Immersion time: a;6h, b;15h, c;1d, d;2d

Corrosion Resistance of Various Coating Materials on Steels Buried in Soil*

Isao SEKINE[†], Toshimasa KOBAYASHI and Hideaki SUDA

Department of Industrial Chemistry,
Faculty of Science and Technology,
Science University of Tokyo

The corrosion resistance of various coating materials on steels used in retaining walls was investigated using electrochemical measurements and the weight-loss test over five years. In addition, the early evaluation of corrosion resistance in various corrosion environments was tested in the laboratory.

In the field test, the aluminum spray coatings on steel plate and the nontar epoxy paint bolt/nut samples showed the best corrosion resistance for five years; the appearances of these specimens changed little and the weight loss was small. Cathodic protection further enhanced the corrosion resistance of the anchor.

In the laboratory test of various corrosion environments, the aluminum spray coating on steel plate showed the best corrosion resistance, as it had in the field test. However, the more economical hot-dip galvanizing on steel plate did not retain its excellent corrosion resistance in sea sand, the severest environment. The corrosion resistance of uni-chrome plating on bolt/nut samples also did not last in sea sand.

1. INTRODUCTION

Several studies have already been published on the corrosion resistance of steels in soil. According to the results obtained by the NBS test¹⁾ and by Kobayashi²⁾, the corrosion rates of steels in the same soil are not very critically affected by the chemical compositions of the steel, but are mainly affected by the quality of the surface coatings and by the nature of the soil.

The aim of the present study was to evaluate the corrosion resistance of several potential coating materials on steels used for retaining walls. Surface-coated steel test pieces were buried in the soil outdoors and their natural electrode potential

(NEP) and $\tan \delta$ were measured during a period of five years. These test pieces were occasionally dug up from the soil for observation of their appearance and for measurement of weight loss. In addition, several laboratory tests were carried out in conjunction with these outdoor tests in order to assess the validity of the laboratory tests.

2. EXPERIMENTAL

2.1. Materials

The plate test piece (50 × 60 × 2.3 mm), anchor (2 m × 22 mm ϕ) and anchor plate (400 × 400 × 8 mm) were made of SS41 steel plate. The bolt (16 mm ϕ) and nut (22 mm ϕ) were made of SRW3 steel. The anchor was subjected to cathodic corrosion protection by a Mg sacrificial anode (400 × 30 × 8 mm).

2.2. Coatings

Four different types of surface coatings were tested:

*Originally presented at 32nd Joint Symposium on Corrosion Science and Technology held at Hokkaido University, Sapporo, in 1985.

[†]To whom correspondence should be addressed. 2641, Yamazaki, Noda, Chiba, 278 Japan.

TABLE 1
Specimens subjected to various surface treatments.

Plate (SS 41)	1 No treatment 2 Rust-preventing agent and nontar epoxy paint 3 Nontar epoxy paint 4 Aluminum flame-spraying 5 Hot-dip galvanizing
Bolt/nut (SRW-3)	1' No treatment 2' Rust-preventing agent and nontar epoxy paint 6 Etching primer and nontar epoxy paint 7 Uni-chrome plating
Anchor (SS 41)	1' No treatment 2' Rust-preventing agent and nontar epoxy paint 6' Etching primer and nontar epoxy paint

1) *rust + rust preventing agent + nontar epoxy paint*

Rust was prepared over the SS41 steel plate as follows. First, the surface was polished with # 180 emery paper. Then the plate was dipped into 3% NaCl aqueous solution for 1 hr and dried for 2 hr in air at room temperature. This dipping and drying cycle was repeated 12 times so that a layer of rust was formed. A rust preventing agent was

then painted over it to about 30 μm thickness, and it was dried for about 6 hr. Finally, it was coated twice with nontar epoxy paint to a thickness of about 200 μm .

2) *nontar epoxy paint*

The steel plate was polished with # 180 and # 240 emery papers, successively. Then it was degreased by tetrachloroethylene. Nontar epoxy

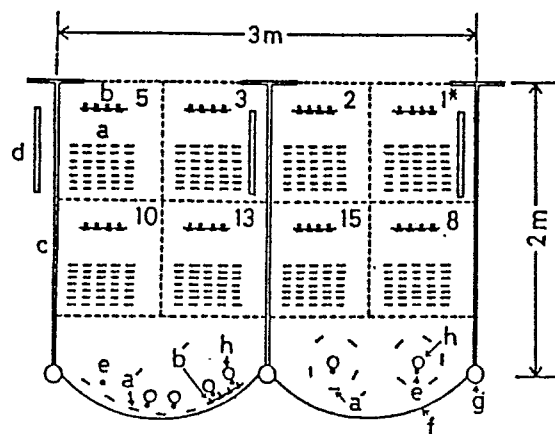


FIGURE 1 Arrangements of specimens in soil of retaining wall. a) test piece for weight-loss measurement, a') test piece for electrochemical measurement, b) bolt/nut for weight-loss measurement, b') bolt/nut for electrochemical measurement, c) anchor, d) Mg sacrificial anode, e) Zn reference electrode, f) steel sheet for retaining wall, g) steel pipe for retaining wall, h) vinyl pipe for setting SCE in soil, *)Numbers (1~15) in each section show the length of the buried period (years) of specimens in soil.

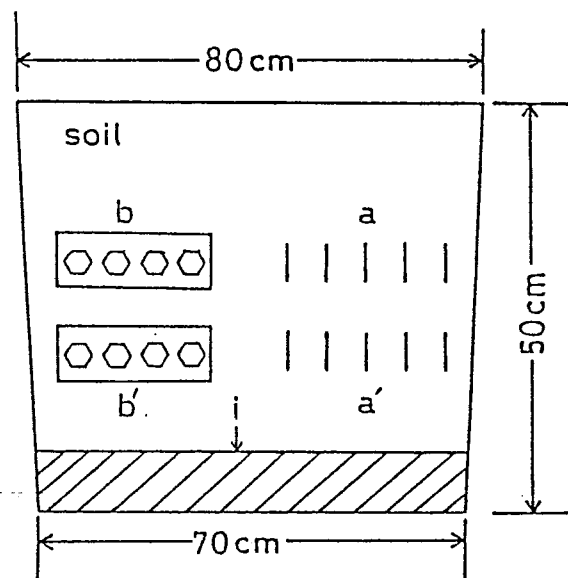


FIGURE 2 Arrangements of specimens in soil in laboratory test. a) test piece for weight-loss measurement, a') test piece for electrochemical measurement, b) bolt/nut for weight-loss measurement, b') bolt/nut for electrochemical measurement, i) water.

TABLE 2
Properties of soil in various corrosion environments.
Surface treatment conditions

Experimental condition	Specific resistance ($\Omega \cdot \text{cm}$)	Water content (%)	pH	Temperature ($^{\circ}\text{C}$)
Soil of retaining wall outdoors	66700	48.9	6.2	7 ~ 23
Soil of retaining wall in laboratory (A)	15200	51.3	6.4	1 ~ 23
Soil submerged by 0.3% NaCl aq in laboratory (B)	3030	59.8	6.4	
River's mud in laboratory (C)	11900	53.3	6.7	
Sea sand in laboratory (D)	480	20.0	7.3	

paint was painted over it twice to a thickness of about 200 μm .

3) aluminum flame-spraying

The primary surface treatment of the test pieces was performed according to the JIS-norm. Aluminum (99.85%) was flame-melt-sprayed to a thickness of 120–200 μm . Treatment by etching primer followed, and the surface was finished according to JIS-K5682.

4) hot-dip galvanizing

A zinc-plated layer of about 80 μm was prepared over the test pieces.

2.3 Corrosion environments

2.3.1. Outdoor test in retaining wall

The schematic arrangement of the outdoor test is shown in Fig. 1. Plate samples (a) were placed vertical to the ground at intervals of 5 cm on the southern side of each section. Bolt/nut samples (b) were attached to an SS41 steel plate standing vertical to the ground. These samples were covered by about 1 m of soil. Test pieces for weight loss (a, b) were dug up at 0, 1, 2, 3, 5, 8, 10, 13, and 15 years after being buried. Electrochemical measurements for test pieces a' and b' were performed every two weeks for 15 years.

2.3.2. Laboratory test

The schematic arrangement of the laboratory test is shown in Fig. 2. The container has double bottom layers. The bottom part is always filled with specified aqueous solutions so that the soil in the upper part is always wet.

The samples were tested under the following four conditions:

- i) in soil from the outdoor test site, with water, for 2 years,
- ii) in mud from the river (Toné river), with water, for 2 years,
- iii) in sea sand (from Kuju-kuri beach), with sea water, for 1 year,
- iv) in soil from the outdoor test site, submerged in 0.3% NaCl aqueous solution, for 1 year.

2.3.3. Quality of soils

Several characteristic parameters of the soils are summarized in Table 2.

One of the common measures of the corrosive nature of soil is specific resistance.³⁾ When specific resistance is lower than the order of 10^3 ($\Omega \cdot \text{cm}$), the soil is classified as strongly corrosive; when it is around the order of 10^4 , the soil is classified as moderately corrosive; when it is greater than the order of 10^5 , the soil is classified as weakly corrosive. Judging from these criteria, the soil of

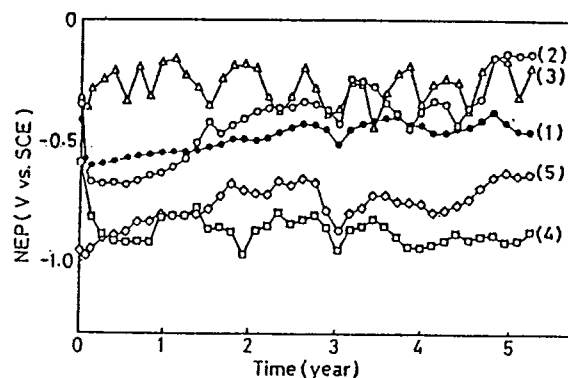


FIGURE 3 NEP vs. time curves of test steel plates.

the retaining wall (both outdoors and in the laboratory (A)) and the mud from the river (C) are weakly corrosive, the soil submerged in 0.3% NaCl aqueous solution in the laboratory (B) is moderately corrosive, and the sea sand (D) is highly corrosive.

2.4. Measurements

Measurements were made for the following terms; natural electrode potential (NEP), $\tan \delta$, polarization resistance, and weight loss.

A saturated calomel electrode (SCE) was used as the reference electrode for the electrochemical measurements. A steel retaining wall was used as the counter electrode for the measurements of $\tan \delta$ and polarization resistance. Measurement of $\tan \delta$ was performed for those plate sample pieces coated by nontar epoxy paint and those coated by rust + rust-preventing agent + nontar epoxy paint with a fixed frequency of 1 kHz.

3. RESULTS AND DISCUSSION

3.1. Outdoor test in retaining wall

3.1.1. Steel plates

The values of NEP are plotted as a function of

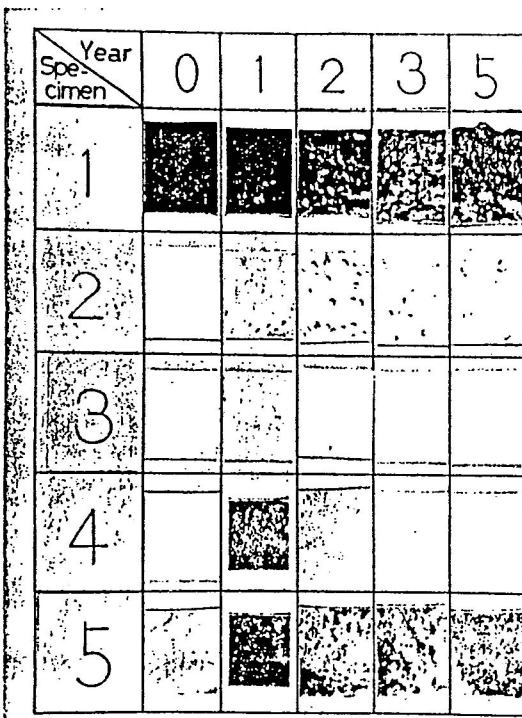


FIGURE 4 Appearances of test steel plates.

time in Fig. 3, and the appearances of the surfaces of the tests pieces are shown in Fig. 4.

Specimen (1) had no surface coating. The value of NEP of this specimen was about -0.5 vs. SCE around 1.6 years after burial, and, thereafter, no significant variations in NEP were observed, as shown in Fig. 3. The surface of specimen (1) after 1 year was covered by islands of red rusts, and after 2 years the red rusts extended uniformly over the entire surface area, as can be seen in Fig. 4.

Specimen (4) had a flame-sprayed aluminum coating. The value of NEP of this specimen appeared to be stable at around -0.9 V (Fig. 3). The surface of this specimen maintained the silver-white color typical of alumina (Al_2O_3). Thus, the non-soluble alumina film appeared to be functioning as a corrosion-protective layer on the surface.

On the other hand, the NEP of the Zn-coated sample piece (5) turned toward the noble side as time passed (Fig. 3), and the surface became mottled (Fig. 4.)

Specimen (3) had a single-layer coating of nontar epoxy paint, while specimen (2) had a multi-layer coating including a rust-preventing agent under a nontar epoxy layer. The NEP values of these two test pieces appeared almost to converge after 3 years and were about -0.2 V after 5 years.

Figure 5 shows the variations of $\tan \delta$ with time for specimens (2) and (3). A larger value of $\tan \delta$ implies better ionic conductivity of the layer,

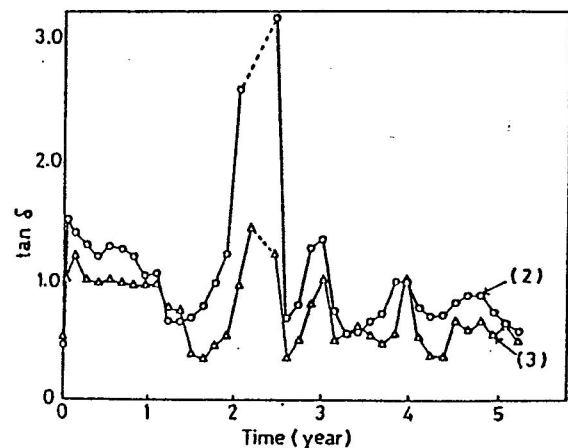


FIGURE 5 $\tan \delta$ vs. time curves of painted steel plates.

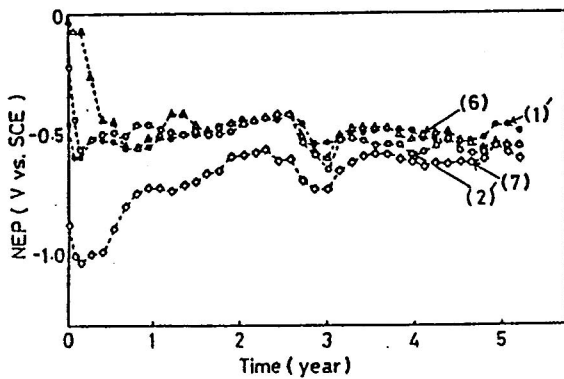


FIGURE 6 NEP vs. time curves of bolt/nut samples.

which eventually leads to a faster corrosion rate.^{4) 5)}

Significant peaks are observable for $\tan \delta$ curves of both specimens (2) and (3) during the period from 1.5 to 2.5 years. These peaks imply that serious degradation of the coating layers occurred. The trigger for this degradation may have been the flooding of the test site during the rainy season of that year.

The surface of specimen (2), with an intermediate layer of rust-preventing agent, showed appreciable blistering after only 1 year. There appeared to be some correlation between the blistering and the peak of $\tan \delta$ of this specimen. The rust-preventing agent used for the intermediate layer of the surface coating appeared to accelerate the corrosion rate of the base steel plate.

On the other hand, no such blistering was ob-

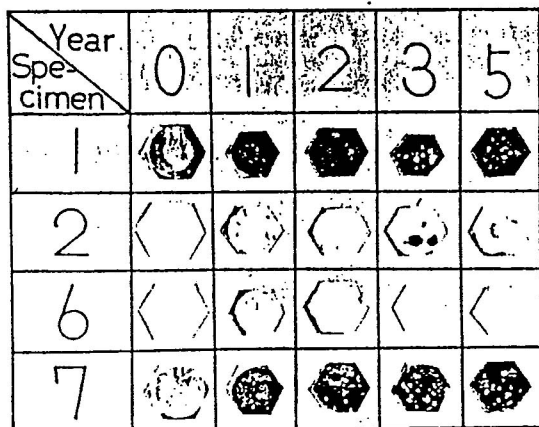


FIGURE 7 Appearances of bolt/nut samples.

served for specimen (3) with a single coating of nontar epoxy paint, even after 5 years. Thus, while the $\tan \delta$ curve of specimen (3) also showed a smaller peak around 1.6 years, its corrosion resistance should be superior to that of specimen (2). This view was also supported by the high specific resistance value ($3 \times 10^5 \Omega \text{ cm}$) of the coating layer of specimen (3).

3.1.2. Bolt/nut samples

The variations of NEP as a function of time are plotted in Fig. 6 and the appearances of the specimens are shown in Fig. 7.

Specimen (1') had no surface coating. The NEP value of this specimen stabilized at around -0.5 V, which was almost the same as that for the non-surface-treated plate specimen (1) (cf., Fig. 3).

Variations in the NEP values of specimens (2') and (6) appeared to follow the same pattern as specimen (1'). Blistering was observed for specimens (2') and (6) after 5 years.

The surface of specimen (7) was uni-chrome-plated. The NEP of this specimen tended to shift toward the noble side for 2 years and, thereafter, stabilized around -0.6 V. Observation of the surface of this specimen showed that rust had begun to appear after only 2 years and completely covered the surface after 3 years. Thus, the corrosion protection effect of plated Cr on the steel surface lasted only 2 years.

3.1.3. Corrosion rate

Figure 8 shows the corrosion rate calculated from weight loss. Among the plate specimens, the aluminum flame-sprayed specimen (4) showed the

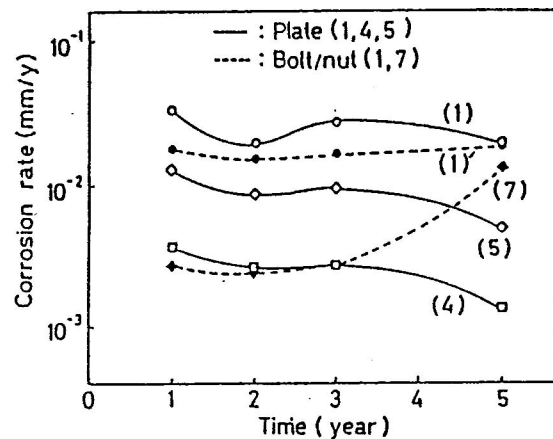


FIGURE 8 Corrosion rate vs. time curves of steel plates and bolt/nut samples.

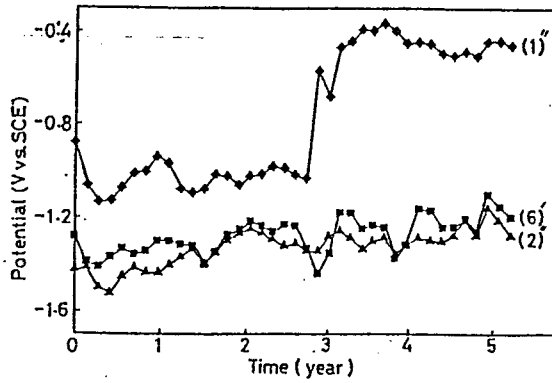


FIGURE 9 Potential vs. time curves of anchors under cathodic protection.

best result, which is in accordance with the conclusion derived from the NEP measurement. For the first three years the corrosion rate of the uni-chrome-plated bolt/nut specimen (7) was as small as that of specimen (4). However, after 5 years the weight loss was three times greater than it had been after three. This appreciable increment in the corrosion rate of specimen (7) between the 3rd and 5th years may be attributable to the flooding of the test site in the 2nd year, which eventually destroyed the Cr-plated coating.

3.1.4. Anchor

Figure 9 shows the potential vs. time curves and Fig. 10, the protective current density vs. time curves for the anchors.

Specimen (1'') had no surface treatment. The protective current density (Fig. 10) of this speci-

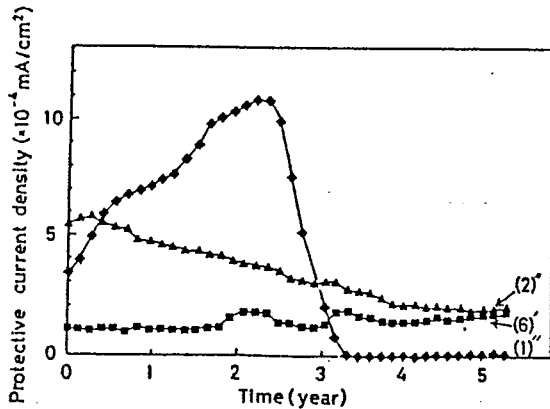


FIGURE 10 Protective current density vs. time curves under cathodic protection.

men increased gradually to 1×10^{-3} mA/cm² in the first 2 years. During the same period, the potential (Fig. 9) was almost stable at approximately -1.0 V. Thus, the cathodic protection appeared to have been effective during that period. However, after 2.5 years a drastic reduction of the protection current density was observed, which was associated with the shift of potential toward the noble side. This drastic degradation of the non-surface-treated anchor may be explained by the loss of the effect of the Mg sacrificial anode as a result of flooding of the site in the 2nd year. In fact, the Mg sacrificial anode was almost completely corroded and had lost its original shape after the 5-year test was completed.

On the other hand, the protection current densities of the anchors with the rust-preventing agent (2'') and with nontar epoxy paint (6') were appreciably smaller than that of specimen (1''), and the potential of (2'') and (6'), -1.2v, was less noble than that of (1''). Thus, the corrosion resistance of the surface-coated anchors with cathodic protection was efficiently enhanced. In addition, the life of the Mg sacrificial anode was prolonged.

3.2. Laboratory tests

3.2.1. Steel plates

Figure 11 shows the corrosion rate of the plate specimens in terms of weight loss. Group (A) was in the soil from the outdoor test site and water; (B), the mud from the river and water; (C), sea sand with sea water; and (D), the soil from the

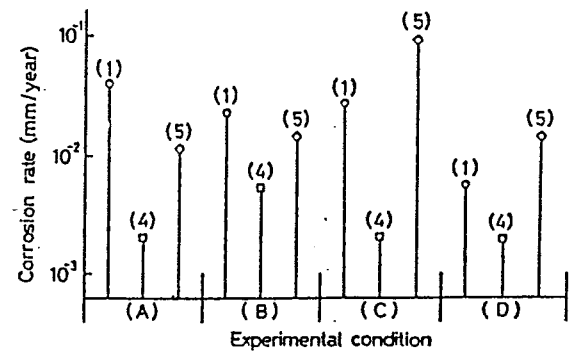


FIGURE 11 Corrosion rate of steel plates in laboratory test in various corrosion environments. A) soil of retaining wall, B) mud in rivers, C) sea sand, D) soil submerged by 0.3% NaCl aq.

outdoor test site in 0.3% NaCl aqueous solution.

It is clear that under all of these testing conditions, the aluminum flame-sprayed coated specimens (4) exhibited the best corrosion resistance.

The corrosion rates of specimens (1), which had no surface treatment, under testing conditions (A), (B), and (C) were essentially the same (Fig. 11). The corrosion rate of specimen (1) in (D) was appreciably lower. These results appear to suggest that the lack of oxygen under condition (D), in which the test piece was submerged in NaCl aqueous solution, eventually suppressed the corrosion rate. These observations do not contradict earlier reports²⁾ that the determining factor for the corrosion rate of steels in soil is aeration, rather than the content of NaCl in the soil.

The corrosion rates of the Zn-plated specimen (5) were lower than those of (1) under circumstances (A) and (B), but the order was reversed in (C) and (D).

Figure 12 shows the variation of NEP with time of the steel plate specimens in sea sand. The NEP of the Zn-plated specimen (5) at first shifted quickly to the noble side, but after 100 days stabilized at about -0.6 V, which corresponds to the corrosion potential of Fe. The rapid shift of NEP toward the noble side was, therefore, attributable to the quick loss of the plated Zn in the early stage, which led to the loss of the sacrificial anode effect.

On the other hand, the NEP of the aluminum

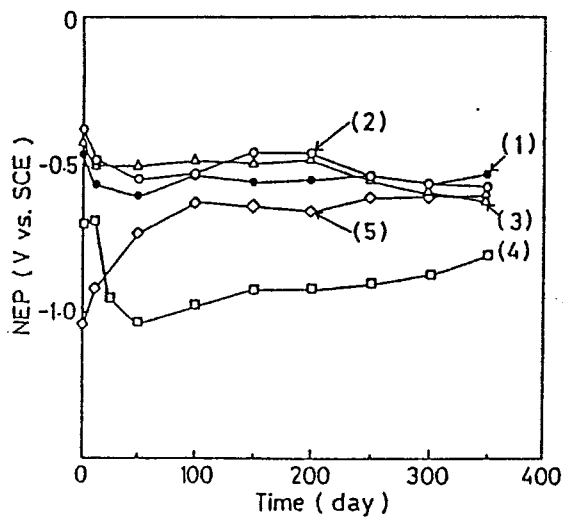


FIGURE 12 NEP vs. time curves of steel plates in sea sand.

flame-sprayed specimen (4) shifted only very slowly toward the noble side, (Fig. 12), but after 400 days still remained below the corrosion potential of Fe. The surface of this specimen remained silver-white, which is typical of aluminum. Thus the alumina film functioned effectively as a corrosion protective surface, even in severely corrosive sea sand.

The NEP of specimens (2) and (3) appeared to vary almost in parallel with that of non-surface-treated specimen (1), (Fig. 12), suggesting that in sea sand the coatings applied to specimens (2) and (3) were no better than no treatment at all (specimen (1)). These observations were also supported by the results of $\tan \delta$ measurements. That is, the $\tan \delta$ of specimens (2) and (3) increased rapidly, reaching a value of 1-2, while the corrosion resistance of surface-coated steels in NaCl aqueous solution is considered good when $\tan \delta$ is in the range 0.1-0.2.⁶⁾ Thus, the coatings of specimens (2) and (3) in sea sand degraded very rapidly by blistering and decrease of bonding to the base steel

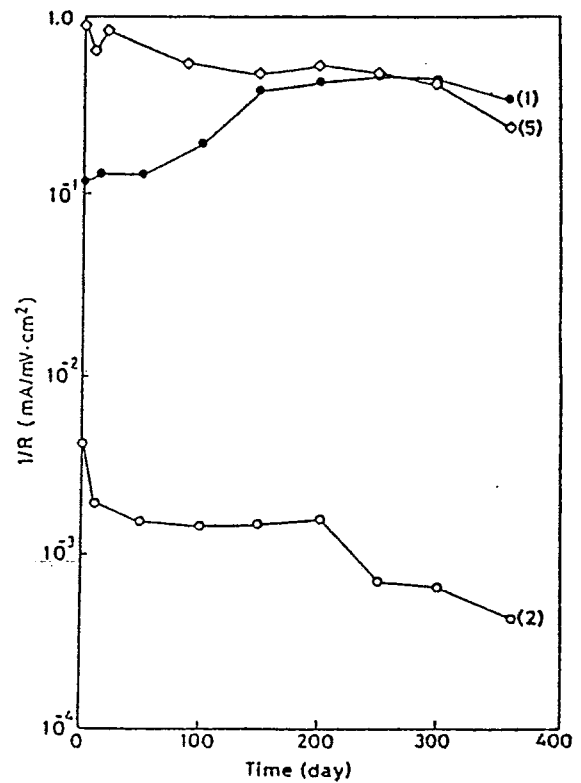


FIGURE 13 Polarization resistance vs. time curves of steel plates in sea sand.

even in the very early stages, and no longer provided a good corrosion-protective surface.

Figure 13 shows the polarization resistance ($1/R$) of the steel plate in sea sand as a function of time. The value of $1/R$ of the non-surface-treated specimen increased monotonously with time, implying corrosion was progressing. The value of $1/R$ of specimen (2) with rust-preventing agent decreased with time, which may be attributed to the accumulation of corrosion products formed from Fe under the coating. The value of $1/R$ of the Zn-coated specimen (5) was originally 8–9 times that of specimen (1), then decreased gradually until around 100 days. This decrease of $1/R$ may have been caused by the formation of $Zn(OH)_2$ on the steel. The decrease of $1/R$ after 300 days may be ascribed to the accumulation of corrosion products from Fe after the surface coating was destroyed. The results obtained from $1/R$ measurements did not contradict those obtained from NEP.

3.2.2. Bolt/nut samples

Figure 14 shows the corrosion rates of bolt/nut samples calculated from weight loss.

It is apparent in this figure that the corrosion rate of the uni-chrome-plated specimen (7) was lower than that of the non-surface-treated specimen (1') under testing conditions (B) and (D), while under (A) and (C) no significant difference in corrosion rates is noticeable. The corrosion rate of specimen (7) appeared to be highest in the sea sand (D).

Figure 15 shows the NEP vs. time curves of

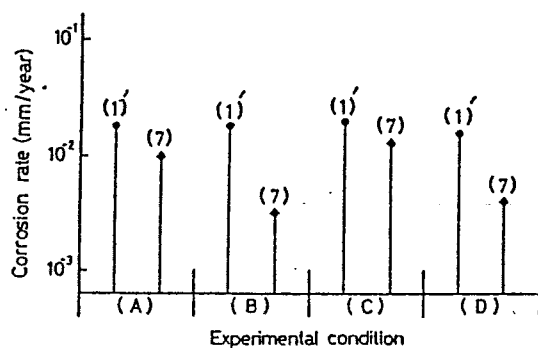


FIGURE 14 Corrosion rate of bolt/nut samples in laboratory test of various corrosion environments. A) soil of retaining wall, B) mud in rivers, C) sea sand, D) soil submerged by 0.3% NaCl aq.

bolt/nut samples in sea sand. This figure shows that the corrosion potential of the uni-chrome-plated specimen (7) shifted to the corrosion range within 50 days and, thereafter, followed the same pattern as that of non-surface-treated specimen (1'). These results reveal clearly that the corrosion resistance of uni-chrome plating is rather poor, especially under severely corrosive conditions as in sea sand. The NEP values of painted specimens (2') and (6) shifted gradually toward the corrosion range.

Polarization resistance $1/R$ of the uni-chrome plated bolts/nuts in sea sand varied from the initial value of $1.6 \times 10^{-1} \text{ mA/mV}\cdot\text{cm}^2$ to 9×10^{-2} at day 50, which may be attributable to the formation of chromium oxide. Thereafter, $1/R$ increased with time, which may be a result of the destruction of the surface chromium oxide, followed by the corrosion of Fe. These observations obtained for $1/R$ appear to support the results for NEP.

On the other hand, the $1/R$ value of specimen (2) with rust-preventing agent increased from the initial value of $1.5 \times 10^{-4} \text{ mA/mV}\cdot\text{cm}^2$ to 4×10^{-3} within 200 days. This observation may imply that the degradation of the coatings and the corrosion of Fe proceeded concurrently in sea sand.

4. CONCLUSIONS

4.1. Outdoor test

(1) Corrosion resistance of the plate specimen

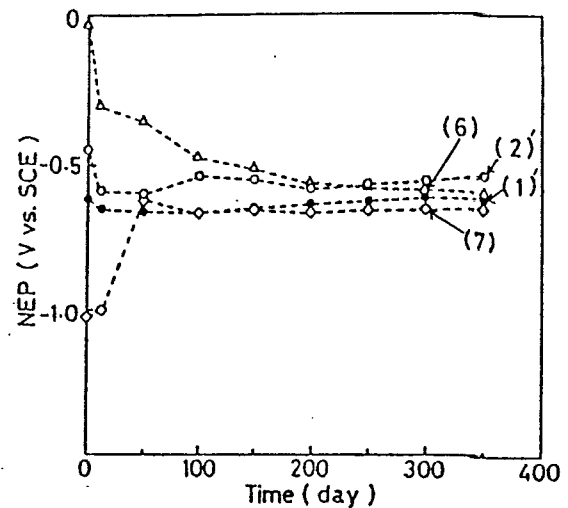


FIGURE 15 NEP vs. time curves of bolt/nut samples in sea sand.

during a 5-year test period proved to be as follows: aluminum flame-sprayed > nontar epoxy paint > hot-dip galvanized > (rust + rust-preventing agent + nontar epoxy paint) > non-surface treated.

(2) The results for bolt/nut samples were as follows: nontar epoxy paint > uni-chrome-plated > (rust + rust preventing agent + nontar epoxy paint) > non-surface treated.

(3) Corrosion resistance of the anchor was further enhanced by cathodic corrosion protection.

4.2. Laboratory tests

(1) The best corrosion resistance was observed in the aluminum flame-sprayed plate specimen.

(2) The hot-dip galvanized plate specimen showed reasonable corrosion resistance under mild corrosion conditions. In sea sand, however, corrosion resistance of this specimen was not good.

(3) Corrosion resistance of uni-chrome-plated bolt/nut samples in sea sand was rather poor.

ACKNOWLEDGEMENTS

Kansai Paint Co., Ltd., Kan-meta Engineering Co., Ltd., Oh-em Engineering Co., Ltd., and Nakagawa Corrosion Protection Co., Ltd. are gratefully acknowledged for the preparation of specimens. Mr.

Hiroyuki Chino of Oh-bayashi Engineering Co., Ltd. is appreciated for the analyses of soils.

REFERENCES

- 1) H. H. Uhlig: "Corrosion and Corrosion Control", Wiley, New York (1962). (Japanese translation by S. Matsuda and I. Matsushima, Sangyo Tosho Publ., Tokyo (1972) p. 142).
- 2) a) T. Kobayashi, S. Yamamoto, T. Kato, T. Maekita and K. Oda: *Proc. 26th. Joint Symp. Corros. Sci. and Technology*, JSCE, Osaka, (1979) p. 82.
b) T. Kobayashi, S. Yamamoto, T. Kato, T. Kanamura and K. Oda: *Proc. '82 Spring Meeting of JSCE, Tokyo, (1982) p. 305.*
- 3) JSCE (ed.): "Handbook of Metallic Corrosion" (*Kinzoku Boshoku Gijutsu Binran*), Nikkan Kogyo Shinbun Publ., Tokyo, (1977) p. 224.
- 4) Y. Ohyabu, H. Kawai and S. Ikeda: *Shiki-zai Kyokai-shi (Bulletin of Japan Society of Color Materials)*, 37, 90 (1964).
- 5) R. Sano: *Shiki-zai Kyokai-shi*, 46, 593 (1973).
- 6) G. Okamoto, T. Morozumi and T. Yamashina: *Kogyo-kagaku Zasshi (Bulletin of Chemical Engineering Society of Japan)*, 61, 291 (1958)

E R R A T A

Corrosion Engineering (Bōshoku Gijutsu), Vol. 36, 3–11 (1987).

Corrosion Resistance of Various Coating Materials on Steels Buried in Soil

Isao SEKINE, Toshimasa KOBAYASHI and Hideaki SUDA

Page	Column	Line	Reads	Should read
3	Right	5	In addition, several laboratory tests were carried out in conjunction with these outdoor tests in order to assess the validity of the laboratory tests.	In addition, several laboratory tests were carried out in conjunction with these outdoor tests in order to achieve the early evaluation of corrosion resistance in various corrosion environments.
4	Table 1	10	1'	1''
4	Table 1	11	2'	2''
7	Left	14	Add sentence	The corrosion rate of the specimen (2) increased with increasing degradation of the coating layers.
9	Right	5	remained silver-white, which is typical of aluminum.	remained silver-white, which is typical of alumina.
10	Left	32	in sea sand (D).	in sea sand (C).
10	Right	15	at day 50,	at 50 days,
10	Right	23	initial value of 1.5×10^{-4} mA/mV·cm ⁻³ ,	initial value of 1.5×10^{-4} mA/mV·cm ² ,

DETERIORATION OF VARIOUS PAINTS IN AQUEOUS ACETIC ACID SOLUTION

Isao Sekine,* Kazuyoshi Moriya, and Makoto Yuasa*
Department of Industrial Chemistry, Faculty of Science & Technology,
Science University of Tokyo, Noda, Chiba 278, JAPAN

Abstract

Deterioration behaviour of five paints of epoxy (Ep), phenol (Ph), polyester (Es), polyurethane (Ur) and polyvinyl chloride (Vc) resins was investigated in 30% aqueous acetic acid solution at 40°C by physicochemical measurements. High values of paint film resistance (R_f) in Ph and Ep systems were observed for a long time by electrochemical impedance measurement. The R values for Es, Ur and Vc decreased at early immersion times. Distributions of potential gradient in various paint films were measured by scanning vibrating electrode technique (SVET) to determine the difference of potential gradient (ΔE), which corresponds to corrosion current. The ΔE values in Ph and Ep systems were smaller to those in Es, Ur and Vc systems. The ΔE value by SVET was correlated with the reciprocal value of the time of breaking time ($1/t_b$) by electrochemical impedance measurement. From this correlation, it was found that the life prediction of the paint film is possible. The deterioration of Ph and Ep paints was slower than that of the other paints; Ph and Ep paint films had an effective corrosion protective property.

1. Introduction

Drum cans made of mild steel are used to store various organic acid solutions. Such drum cans are frequently corroded by their acids, and the degree of the corrosion is comparatively rapid. (1,2) The corrosion brings about some troubles as to quality control and safety in storage and transportation of their acids. To inhibit the corrosion of drum cans at present, drum cans with stainless steel and of special structure were used in above environment. On the other hands, inner coating of drum cans has been investigated by use of

paints having good durability against organic acids. If the coating has good corrosion protection against organic acids, the cost of such can will become cheaper in comparison with that of specially made-drum can.

To obtain inner coating technique with good durability against organic acids, it is necessary that the corrosion protective ability and deterioration behavior of paint films are accurately evaluated in organic acid solutions. The evaluation of deterioration for various paint films is studied by many researchers and find practical application. (3,4) Recently, some nondestructive evaluation methods have been studied and developed, that is, current interrupt method (5), electrochemical impedance method (6-8), acoustic emission method (9), photo-acoustic spectroscopy (10) and so on. The authors have also reported some techniques of this evaluation. (11,12)

In this work, the deterioration of five different paint films was investigated in 30% aqueous acetic acid solution at 40°C by electrochemical impedance-measurement and a novel method of scanning vibrating electrode technique (SVET) for the paints of epoxy resin (Ep), phenol resin (Ph), polyester resin (Es), polyurethane resin (Ur) and polyvinyl chloride resin (Vc) in order to obtain the fundamental knowledge selecting effective paint with good durability against organic acids.

2. Experimental

2. 1. Materials and Preparations

Paints used were Ep, Ph, Es, Ur and Vc paints without pigment. Table 1 shows the composition of these paints. The cold rolled steel plate (JIS G3141 SPCC SB, Nippon Test Panel) was polished with emery paper up to #1200 before degreasing by reagent grade tetrachloroethylene and reagent grade ethanol to obtain the specimens of coated steels. Every paint was coated by a barcoater with film thickness of 10 μm on the cold rolled steel plate. They were baked for 10 min at 150°C. A 30% aqueous acetic acid solution for immersion was prepared from reagent grade acetic acid and water distilled three times.

2. 2. Electrochemical Impedance Measurements

The measurement cell was composed of working, counter and reference electrodes; the measurement area of the working electrode was 2.0 cm^2 and regulated by O-ring made of silicone on a coating steel plate, the counter electrode was a platinum plate (surface area; 40 cm^2) and the reference electrode was a saturated calomel electrode (SCE). The measurement of electro-chemical impedance was carried out at the natural electrode potential by using a potentiostat (Toho

Technical Research, P/G-2000) and a frequency response analyzer (NF Circuit Design Block, FRA-5020) in the frequency range from 20 kHz to 10 MHz at 40°C. The reference signal voltage of the sinusoidal wave was 9 mV (RMS).

2. 3. Scanning Vibrating Electrode Technique (SVET)

In SVET, the edge and reverse side of samples were shielded with epoxy adhesive agents except for the measurement area (2.5 x 2.5 cm). Paint films of samples were artificially cut (cutting length; 0.5 cm) at the centre of the measurement area by the cutter in conformity with a method of the cross cut test regulated by Japanese Industrial Standard (JIS).

The potential gradient caused by current between local anode and local cathode on the samples was measured at 400 points ((x, y) = (0, 0) to (20, 20), 1.0 x 1.0 cm²) including the scribe in 30% aqueous acetic acid solution at room temperature by the SVET system (Nisshin Steel/NF -Circuit Design Block, Figure 1). The vibrating frequency was 220 Hz, amplitude about 150 μm, and distance between centre of amplitude and coating steel surface about 150 μm.

3. Results and Discussion

3.1. Electrochemical Impedance Measurements

Figure 2 shows the change of the Cole-Cole plot against immersion time in the Ph paint film system. The curves until 430 h were not described as the shape of semi-circle, but as one of a straight line because the paint film resistance (R_f) is fairly high. The R_f values were determined by the approximate program of semi-circle from Cole-Cole plots. For immersion times up to 430 h, the R_f values were not possible to calculate as the curve was seen as too small of a semi-circle, or it was similar to a part of a straight line.

The relation of R_f value with immersion time is shown in Figure 3. The Ph paint film had a high resistance for a long time. The R_f value of Ep paint film also remained high until 900 h of immersion, but was one order of magnitude lower than that of the Ph one. The R_f value of the Es paint film was similar to (or higher than) that of the Ep paint film at early immersion time, but the R_f value became as those of Ur and Vc after ca. 100 h. The R_f values of the Ur and the Vc paint films showed the low one of ca. 100 Ω from early immersion time, whose value corresponded to that of undercoating steel plate. This suggested that the insulation ability of paint film failed in early immersion time. Therefore, the deterioration of the Ph and the Ep paint films is slower than that of Es, Ur and Vc films under this experimental condition. It was thought that the Ph and the Ep paint films have a good corrosion protective property in comparison with Es,

Ur and Vc ones as the Ph and the Ep have a high insulation ability for a long time.

3.2. Scanning Vibrating Electrode Technique (SVET)

When a local cell forms and the metal corrodes, the potential gradient appears around the corroded metal surface in the solution by current (I)-resistance (R) drop. The degree of the potential gradient is proportional to the current density of corrosion, i.e., corrosion rate. The SVET is a method for determining the distribution of current density (i) for the corroded metal surface in solution. (14,15) In general, it is difficult to measure the potential gradient caused by corrosion of the metal in solution of high conductivity for SVET measurement. (16) The conductivity of 30% acetic acid solution used in this work was 1.64 mS/cm at 25°C; i.e., the conductivity of this solution was reasonable for SVET as reported in the literature. (12) In this work, the distribution of corrosion (rate) indicated the distribution of relative potential gradient corresponding to current density.

Figure 4 shows the solid graph (three-dimensional map) of SVET data for the Ep paint film after immersion for 6 h in 30% aqueous acetic acid solution at room temperature. The centre-peak and the flat parts show the artificial defected in the paint film which acts as local anode and intact part of the paint film which acts as a local cathode, respectively. It is thought that the current flowed from local anode to local cathode from a broad intact region.

The distribution data of potential gradient (E) were shown in Figure 5 for some immersion time in the Ep paint film system. The distribution of E at the intact part changed from a narrow distribution to a broad one with immersion time. The frequency of E at the anodic part increased with immersion time. The distribution at the anodic part became independent against the total distribution. It seems that the deterioration of paint film proceeds with growth of the anodic part.

To evaluate the deterioration of paint films, the degree of growth of the anodic part is given by the difference of potential gradient (ΔE) as follows;

$$\Delta E = E_a - E_c \quad (1)$$

where E_a is an average value of the top 10 potential gradients at the anodic part and E_c is an average of potential gradients at cathodic regions (intact region), i.e., base line value. Assuming that the distribution of E at the cathodic part would conform to the regular distribution, the value of E_c was computed as shown in Figure 6. First average (μ_1) and first standard deviation (σ_1) were calculated by using total measured values (E values at 400 plots). The E values within $\pm 3 \sigma_1$ were adopted. The second average (μ_2) and the second standard deviation (σ_2) were calculated by using surviving

and effective E values. If neither μ_1 was equal to μ_2 nor σ_1 was equal to σ_2 , this process was repeated (μ_n and σ_n). When the values of μ and σ converged, the μ value adopted the E_c value. The E_c approximated E at 50% point on the cumulative relative frequency of the potential gradient. This result suggests that the E_c value is effective as the base line value for statistical calculation.

The relation of ΔE with immersion time is shown in Figure 7 for the Ep paint film. The ΔE increased with increasing immersion time. This result means the deterioration of the paint film. Figure 8 shows the ΔE for various paint films after immersion for 6 h. In the Vc paint film system, the distribution of E was not able to be measured by SVET, and the ΔE value could not be determined because a large number of blisters and peels were formed. The ΔE values of the Ph and the Ep paint films were smaller than those of the Es and the Ur ones. Therefore, it was found that the Ph and the Ep paint films have a good corrosion protective property. This result corresponded to the result obtained by the electrochemical impedance measurement.

The life-time of paint films was able to be predicted by ΔE . In the plot of $\log R_f$ vs. immersion time (Figure 3), the time of breaking point (t_b) showed the rapid decrease of R_f value predicts the deterioration of the coating film. The life-time of the paint film can be determined by measuring the t_b value, but the t_b value is difficult to determine in the coating film system deteriorating for short immersion time. By application of the SVET and use of the ΔE vs. R_f , the plot of ΔE vs. $1/t_b$ is described in Figure 9; this plot gave a straight line, and this empirical equation was obtained as follows;

$$\log(\Delta E) = 0.530 \log(1/t_b) - 2.61 \quad (2)$$

Thus the ΔE value was correlated with the $1/t_b$ value. It predicts that the life of the paint film becomes larger as the ΔE value becomes smaller.

4. Conclusions

(1) Both the Ph and the Ep paint films showed high paint film resistance (R_f) for a long time in 30% aqueous acetic acid solution. But the R_f values in the Vc and the Ur systems were low from early immersion time, and kept to lower value in comparison with the Ph and the Ep films. The Ph and the Ep paint films were deteriorated more slowly than the Vc, the Ur and the Es ones, and had a good corrosion protective property.

(2) The evaluation for deterioration of various paint films was determined by the scanning vibrating electrode technique (SVET). The deterioration was quantitatively evaluated by the difference of potential gradient (ΔE) of peak (defective and anodic part) and flat area (intact and cathodic part) based on the statistical analysis; the ΔE value of paint film increased with increasing immersion time.

The corrosion protective property in the Ph and the Ep systems was superior to that in the other systems.

(3) The ΔE value by the SVET was correlated with $1/t_p$ obtained from the electrochemical impedance measurement. From this correlation, the life prediction of the paint film became possible.

Acknowledgment.

Authors are grateful to Mr. H. Fukumoto, Mr. H. Mizuki, and Mr. T. Murakami of Nisshin Steel Co., Ltd. for use of SVET apparatus.

References

- (1) E. Heits, "Advance in Corrosion Science and Technology," Eds. by M. G. Fontana and R. W. Staehle, Vol. 4, p. 149, Plenum Press, New York (1974).
- (2) I. Sekine, Boshoku Gijutsu, 36, 735 (1987).
- (3) M. W. Kendig and H. Leidheiser, Jr. (Eds.); Corrosion Protection by Organic Coatings (Electrochemical Society, 1987).
- (4) Y. Sato, "Bosei Boshoku Toso Gijutsu," Kogaku Tosho (1981).
- (5) Y. Sato, S. Hoshino, and H. Tanabe, Boshoku Gijutsu, 28, 444 (1979).
- (6) L. M. Callow and D. J. Scantlebury, J. Oil Col. Chem. Assoc., 64, 83 (1981) and reference therein.
- (7) M. Kendig and F. Mansfeld, Corrosion, 39, 466 (1983) and reference therein.
- (8) M. Asari, T. Tsuru, and S. Haruyama, Iron and Steel, 72, S422 (1986) and reference therein.
- (9) T. Tsuru, A. Sagara, and S. Haruyama; Corrosion, 43, 703 (1987).
- (10) T. Tsuru, Nippon Kinzoku Gakkaihou, 25, 856 (1986).
- (11) I. Sekine, K. Moriya, and M. Yuasa, Boshoku Gijutsu, in press.
- (12) M. Yuasa, M. Ichikawa, K. Moriya, I. Sekine, H. Fukumoto, H. Mizuki, and T. Murakami, DENKI KAGAKU, in press.
- (13) D. M. Brasher and A. H. Kingsbury, J. Appl. Chem., 4, 62 (1954).
- (14) Y. Ishikawa and H. S. Isaacs, Boshoku Gijutsu, 33, 147 (1984).
- (15) T. Shibata and S. Fujimoto, Boshoku Gijutsu, 35, 566 (1986).
- (16) H. Fukumoto, H. Mizuki and K. Masuhara, Iron and Steel, 73, S406 (1987).

Table 1 Composition of various paints.

Epoxy resin paint (Ep)	
Epoxy #1100 clear (Dainippon Toryo Co.)	
Epoxy resin varnish	60.0 wt%
Phenol resin varnish	24.0
Additive	1.0
Aromatic solvent	7.0
Glycolic solvent	8.0
Phenol resin paint (Ph)	
4A (Toyo Ink Co.)	
Phenol resin varnish	33.5 wt%
Additive	0.3
Alcoholic solvent	25.0
Ketonic solvent	15.2
Aromatic solvent	26.0
Polyester resin paint (Es)	
Highmel varnish (Dainippon Toryo Co.)	
Phtalic acid resin varnish	87.0 wt%
Dryer & Additive	3.0
Solvent	10.0
Polyurethane resin paint (Ur)	
V-top clear (Dainippon Toryo Co.)	
(Main agent)	
Polyolic acid resin varnish	60.0 wt%
Solvent & Additive	2.0
(Hardener)	
Isocyanate resin varnish	20.0
Polyvinyl chloride resin paint (Vc)	
Vinyllose clear (Dainippon Toryo Co.)	
Vinyl chloride resin varnish	83.0 wt%
Plasticizer & Additive	2.0
Solvent	15.0

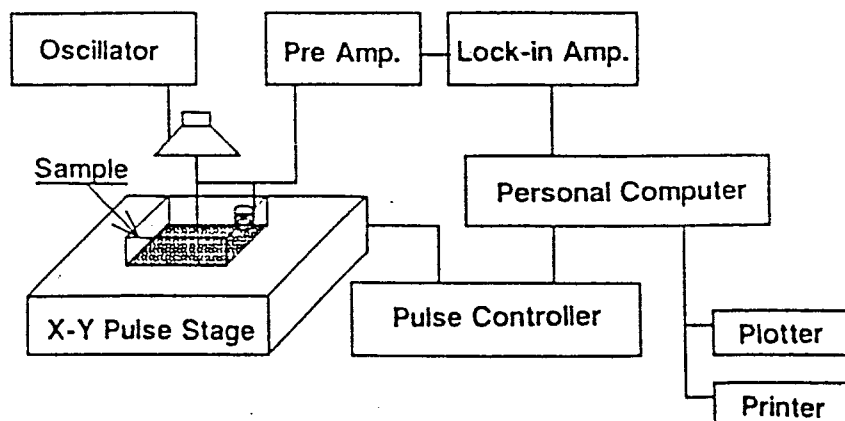


Fig. 1 Block diagram of scanning vibrating electrode technique.

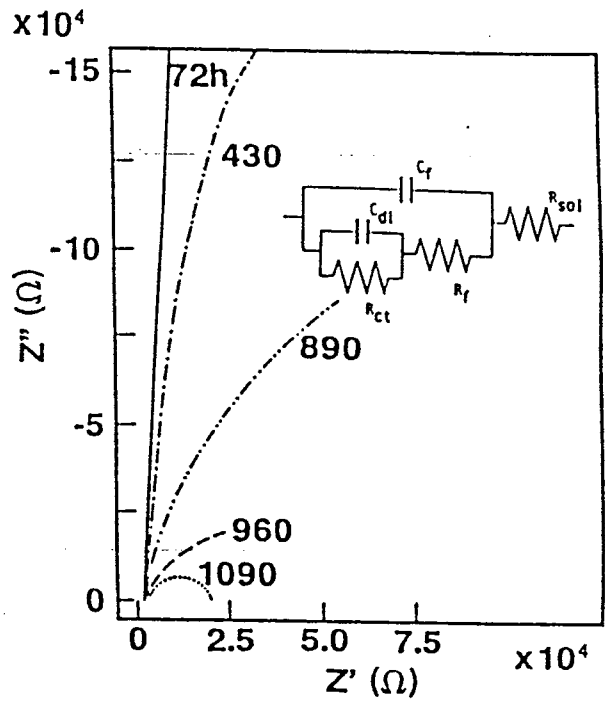


Fig. 2 Time change of Cole-Cole plots for steel plates coated by Ph paint.

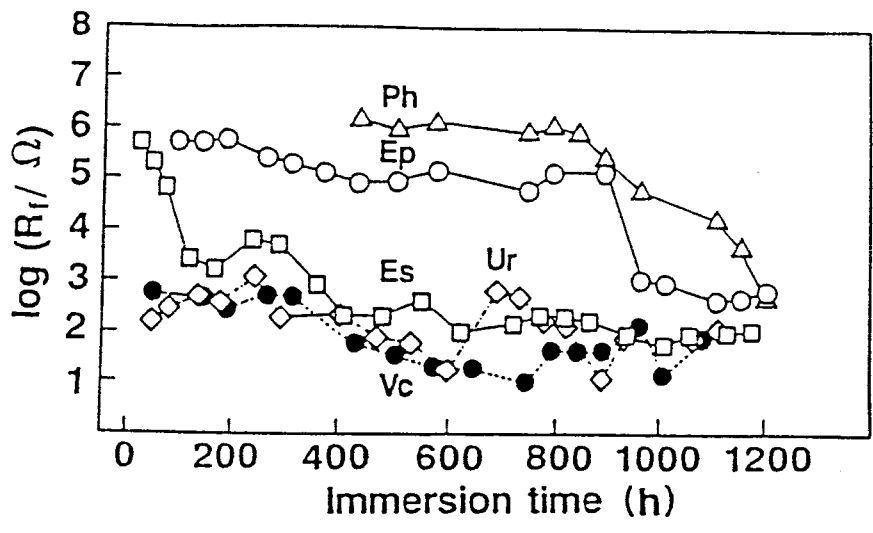


Fig. 3 $\log (R_f)$ vs. immersion time curves of steel plates coated by various paints in 30% aqueous acetic acid solution at 40°C.

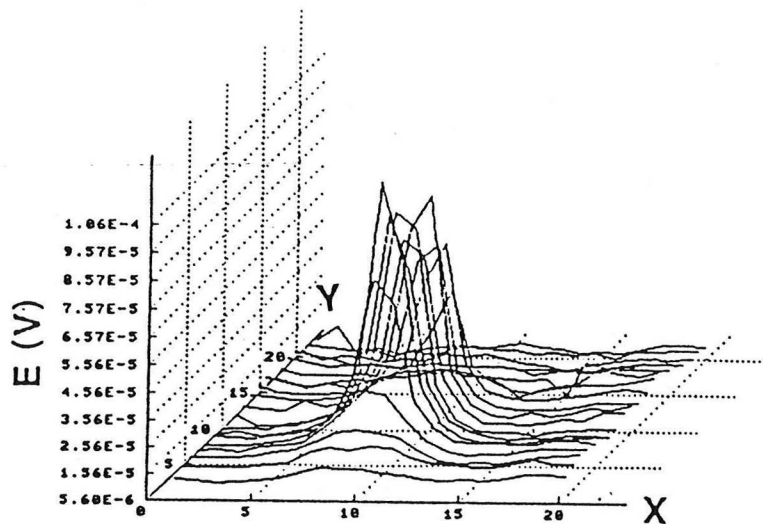


Fig. 4 Solid graph of SVET data of Ep paint film after immersion for 6 h in 30% aqueous acetic acid solution at room temperature.

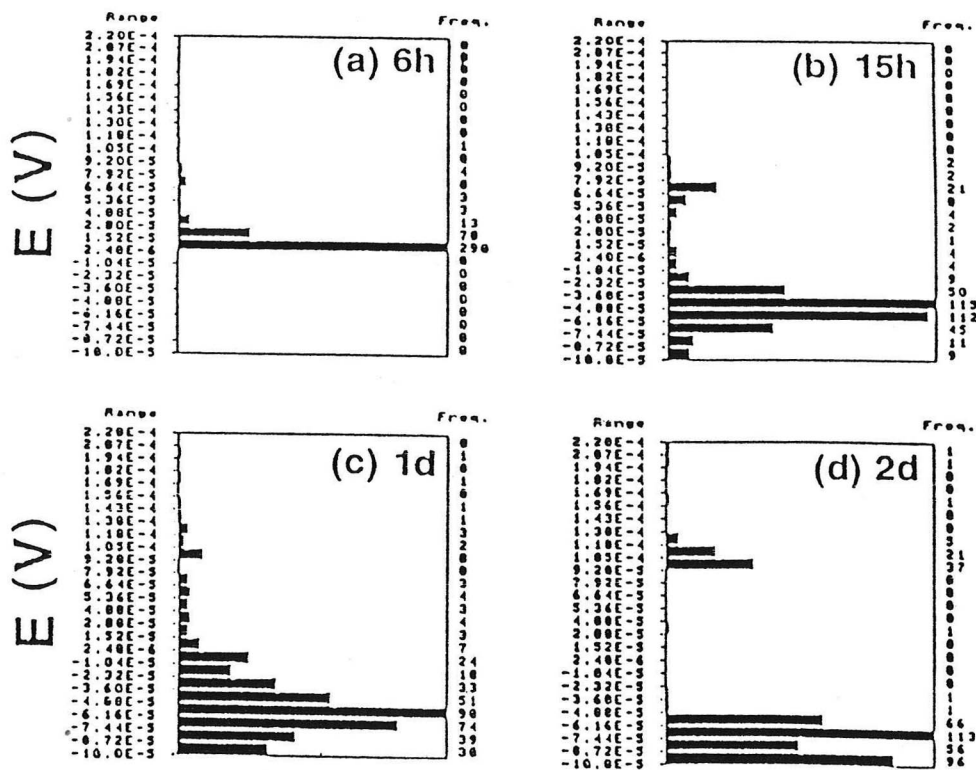


Fig. 5 Distribution of E for Ep paint film. Immersion time; a; 6 h, b; 15 h, c; 1 d, d; 2 d.

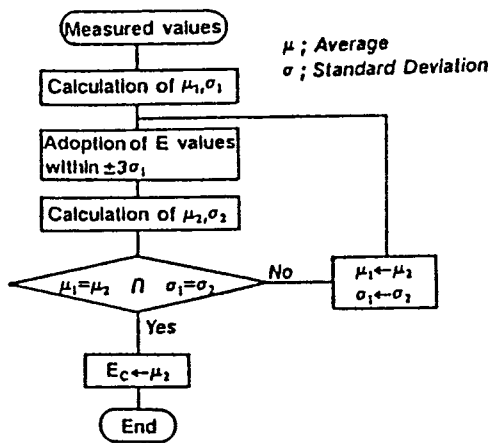


Fig. 6 Flow chart of E_c calculation.

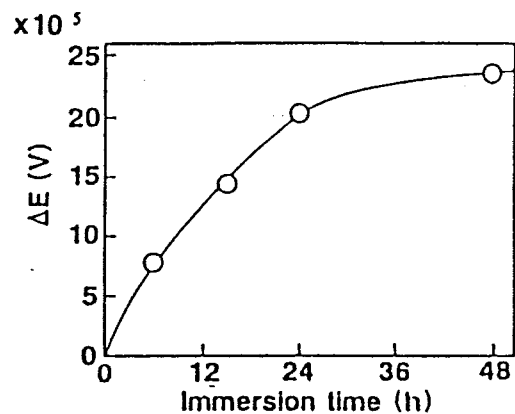


Fig. 7 ΔE vs. immersion time curve of Ep paint film.

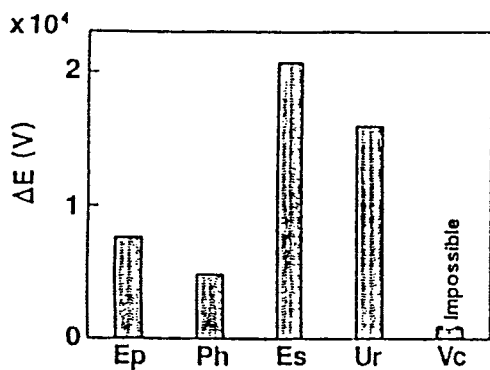


Fig. 8 Comparison of ΔE values of various paint films after immersion for 6 h.

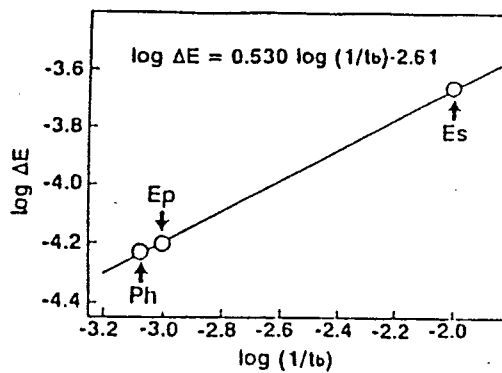


Fig. 9 Prediction curve of life-variant vs. ΔE value.

Corrosion Problems in Petroleum Refinery

Abstract

Case examples of typical corrosion problems encountered in petroleum refinery will be presented. The cause and corrective measures of each case will be discussed.

Corrosion Problems in Petroleum Refinery

Abstract

Case examples of typical corrosion problems encountered in petroleum refinery will be presented. The cause and corrective measures of each case will be discussed.

"Ambient Acid Rain Precursor Concentration and Emission
in Samutprakarn Industrial District"

by

Dr. Supat Wangwongwatana
Office of the National Environment Board, Thailand

CORROSION OF STEEL REINFORCING BARS IN MARINE ENVIRONMENT

Abstract

Concrete structures all over the world use steel reinforcing for added strength.

The early deterioration of concrete is the accelerated corrosion of the steel reinforcing bars (rebar) due to salts in marine environment.

The corrosion makes its more and more volume than the original steel. The resultant pressure is cracks in concrete.

The reinforcing steel, rusted completely, leaves the concrete structure destroyed before its designed lifetime.

CORROSION OF STEEL REINFORCING BARS IN MARINE ENVIRONMENT

BACKGROUND INFORMATION

The deterioration of concrete bridge decks has become a major problem during the last decade. One of the reasons for this early deterioration is the accelerated corrosion of the steel reinforcing bars due to the increasing use of deicing salts (calcium chloride and sodium chloride) in the northern parts of North America.

A few years ago the U.S.A. Federal Highway Administration undertook a feasibility study of organic coatings, especially epoxies, on corrosion protection of steel reinforcing bars embedded in concrete of bridge decks.

Why do I pick this problem out for presentation in this Seminar because of Asian Countries have many construction in coastal area.

WHAT IS CONCRETE?

As I am sure you all know, concrete consists of cement, ballast (sand and sand-like materials), water and (in some cases) additives to give specific properties. To obtain increased mechanical strength, it is common to reinforce the concrete with steel. The properties of the concrete is determined by the relative amount of the components and the way the mixture is treated.

The concrete is bound (glued) by the cement component, that reacts chemically with part of the water, and by this reaction the composite becomes hard. This process is called hydration. It is important to know that the gelled matrix that is formed, is alkaline, with a pH higher than 11.0 (usually between 12.5 and 12.8). This results in formation of a passive layer of iron oxide (Fe_2O_3) at the iron surface, and the material is rendered in a passivated (non-corrosive) stage.

When cement curing is taking place with a mixture of cement, water, sand and stone, the sand- and stone particles are held together in the firm and strong building material that we call CONCRETE.

CONCRETE CORROSION - CORROSION OF REINFORCEMENT STEEL MATERIAL.

The reinforcement steel material is - as all iron materials - unstable under most natural conditions. Iron will corrode and produce iron oxide components. This happens when iron is brought into contact with oxygen and water. The presence of salts (like chlorides) will enhance this

process. Luckily, iron has the ability to stabilize itself by forming a thin layer of Fe_2O_3 at the surface, and this layer will under certain conditions prevent further oxidation. The main condition for this passivated state is alkaline conditions, i.e. pH higher than 12.5.

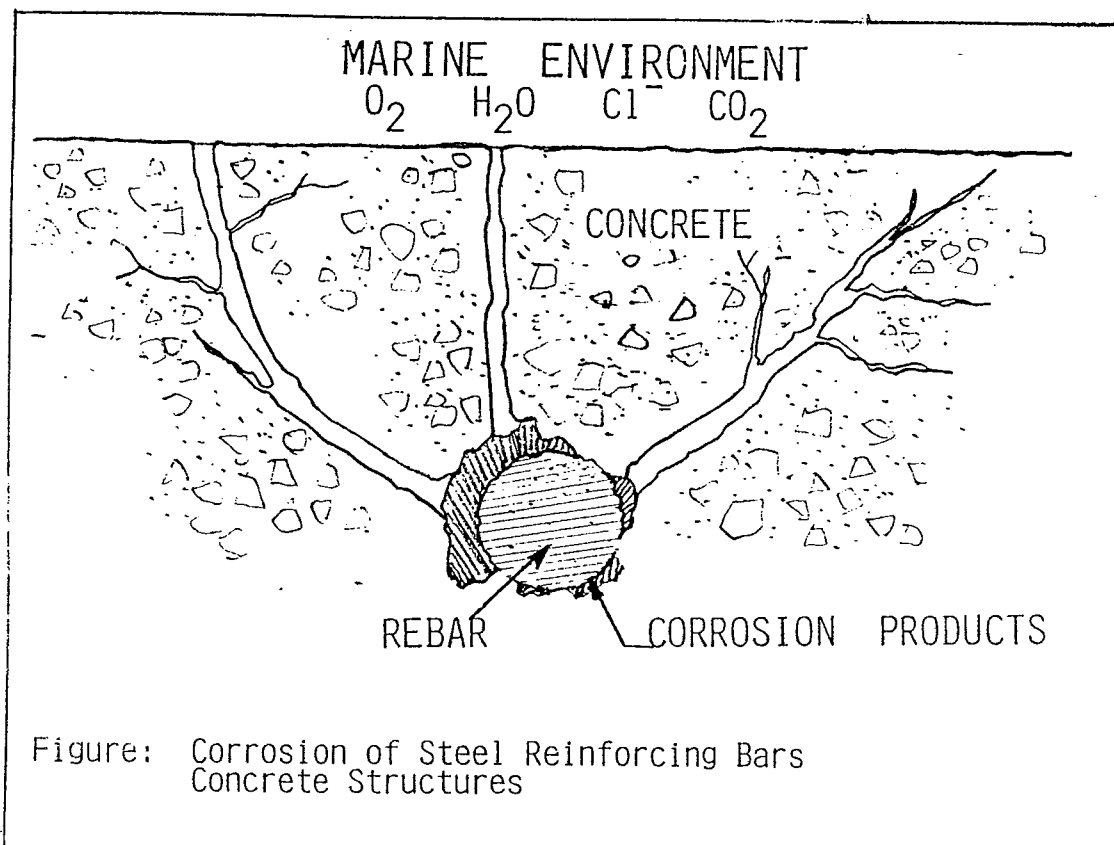
Freshly made concrete is strongly alkaline and will efficiently prevent corrosion even when oxygen and water is present.

So far - all is well.

Upon ageing of concrete, however, the alkalinity of concrete will be reduced, due to following reasons:

1. Water transport will remove water soluble alkaline salts and thereby lower the pH value.
2. Acids from industry and acid rain water will neutralize the alkalinity.
3. Carbonation is a process where CO_2 (and SO_2) from the atmosphere reacts chemically with the $\text{Ca}(\text{OH})_2$ in the concrete and forms inert carbonates. This is usually a slow process that is starting at the concrete surface and spreading inwards towards the steel at a constant rate.

After a time the alkalinity will be reduced to a value where iron oxidation start. The iron oxide products that are formed, have volume 5-8 times that of the iron. After some time the concrete will crack and disintegrate. As a result of this, structural strength is gradually (or acutely) lost.



We would like to propose, in this Seminar, the following way to counteract or prevent concrete and reinforcing steel bars corrosion.

1. The quality of the concrete is of importance. Good quality concrete has higher resistance. Poor quality can corrode quickly.
2. The thickness of the concrete layer over (around) the reinforcement material.
3. Low chloride concentration in the concrete (sands with low salt content).
4. Surface treatment (paint) can reduce the system permeability and thereby reduce corrosion velocity.
5. Organic coatings on reinforcing steel bars.

Examples of corrosion in varied stages are shown in slides.

Effect of Crack Width on Corrosion of
Reinforced Concrete Structures Subjected to Marine Environment

by

Dr. Ekasit Limsuwan

Synopsis

Cracks in reinforced concrete structures are absolutely un-avoidable due to the structural behaviors, but the performance can be controlled by crack width or its distribution. These structures when subjected to marine environment which is one of the most severe condition, will actively be corroded as highly attracted by oxygen, water and chloride. Even several measures have been introduced for protection such as increasing concrete cover, improving concrete quality, coating of rebars or using of cathodic protection, but none will be perfectly assured unless crack width or crack control had taken into consideration.

This paper paid much attention on crack widths and were selected as major variables to conduct various tests in real condition in the gulf of Siam. Twenty four specimens with different concrete covers, mixed aggregates, mixed designs, and crack widths, were directly exposed to tidal zone at Chulalongkorn University Marine Research Center in Ang-Sila, Chonburi, at periods of 6 and 12 months. The results have shown severe corrosion of concrete of aggregate with chloride content higher than 0.15%. For regular concrete with river sand and fresh water, the crack width should be less than 0.02 mm., concrete cover should be more than 50 mm. and the W/C ratio must less than 0.45, to assure protection against corrosion of rebars in tidal zone of marine environment.

"Material Selection of Fiber Reinforced Plastics (FRP)
for Corrosion Resistance."

by Dr.Somsak Naviroj

ABSTRACT

Chemical attacks of fiber reinforced plastics (FRP) and result of such attacks are discussed in order to provide understanding for material selection. Properties of resins and glass fiber which are the main components in FRP are pointed out. Criteria for material selection and purchasing of FRP products for corrosion resistance are also provided.

INTRODUCTION

For many centuries, man has been using metals such as iron and bronze in various applications such as containers, tools, etc. Engineering materials such as composites for corrosion resistance are known to corrosion engineers about 20 years ago. Due to the fact that the glass fiber was discovered and put in commercial and being commercialized in 1937, the development of polyester resins in 1935 gave the reinforced plastic industries a break through in corrosion resistant composites.

To understand corrosion characteristics, we have to understand the nature of chemical attacks. We may classify into board categories, namely,

1. Metallic attack and
2. Reinforced plastic attack.

METALLIC ATTACK

The common type of metallic corrosion shows deterioration by a number of methods:

- i.) General corrosion; General degradation of the metal, which may be accelerated in localized areas and cause perforations. Rusting is a typical phenomenon.
- ii.) Galvanic corrosion; A flow of current between two dissimilar metals which results in the deterioration of the least noble metal.
- iii.) Aerobic corrosion; Generally bacterial in nature.

Other types of common metallic corrosion which occur may include pitting, dezincification, and intergranular corrosion. It is interesting to note that reinforced plastics are not subject to any of these symptoms, so prevalent in metals. This does not mean, however, that reinforced plastics are not subject to attack. They certainly are, but in a completely different manner.

REINFORCED PLASTICS ATTACK

When FRP are misapplied, chemical attack, which is a relatively complicated phenomenon for these materials, may occur in several ways. These may be broadly classified as follows:

1. Disintegration of degradation of a physical nature due to absorption, permeation, solvent action, etc.
2. Oxidation, where chemical bonds are attacked.

3. Hydrolysis, where ester linkages are attacked.
4. Dehydration (rather uncommon)
5. Radiation.
6. Thermal degradation, involving depolymerization and possibly repolymerization.
7. Combinations of these mechanism, and possibly others.

As a result of such attacks, the material itself may be affected, softened, crazed, delaminated discolored, dissolved, blistered, swelled, etc. Although all polyesters will be attacked in essentially the same manner, certain chemical-resistant types suffer negligible attack, or exhibit significantly lower rates of attack, under a wide variety of severely corrosive conditions, due primarily to the unique molecular structure of the resins, including built-in steric protection of ester groups, etc.

Cure, of course, plays an important part in the chemical resistance developed by a polyester or epoxy, as does the construction of the laminate itself and the type of glass or reinforcing used. The degree and nature of the bond between the resin and the glass or other reinforcement also plays an important role.

In order to consider any material as a potential solution to the corrosion problem, the engineer must be intimately familiar with the material to be applied. He needs to know its strong points and its weaknesses and, above all, the limits on its successful application. We must therefore determine, first, with the general classes of reinforced plastic material available, where each can be used successfully and where it should be avoided.

Many different types of polyester and epoxy chemical resistant resins are being manufactured today. Although, for the purposes of illustration, a specific resin may be referred to occasionally, this mention is for the purpose of illustration. However, it is not meant to imply that other resins, manufactured by other vendors, are not equally good or equally acceptable.

There are various services/applications of FRP for corrosion resistance. Some of the common applications are listed below ...

- o Tanks
- o Pipes
- o Ducts
- o Floor Grating
- o Hoods
- o Cooling Towers
- o Housing for pumps
- etc.

Aside from the corrosion resistant properties of FRP, there are other advantages which engineers look for such as low maintenance cost, high strength/weight ratios, ease of installation. The lower modulus of elasticity of FRP virtually eliminates the use of expansion joints which are commonly required with metals. Most composite materials now being manufactured are in the form of glass fiber. Due to the low softening point of resins, most of the composite materials remain strong at the temperatures not in excess of 400 C. Careful selection of reinforcing materials and resins may introduce the working temperatures beyond 400 C. Reinforcing materials such as boron, carbon, or silicon carbide together with epoxy resins can produce a very strong combination in composite materials.

RESINS

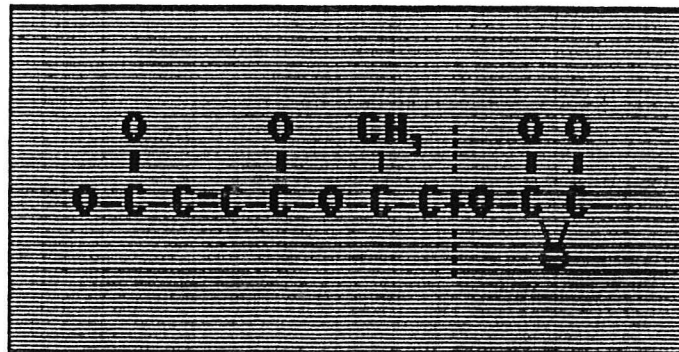
Generally, we are dealing with families of resins which have the following characteristics:

1. Resistance to many of the oxidizing acids, up to fairly strong concentrations.
2. Potentially, superior alkaline resistance.
3. Good solvent resistance in some areas but limited resistance in other.
4. Most useful in the areas of low pressure or vacuum.
5. Can provide complete piping systems at relatively high operating pressures and in most of the common sizes up to 150 psig
6. Can be tailor-made for abrasive conditions where service under extended temperatures for short periods of time is desired.
7. Low thermal and electrical conductivity so that use can be made of these properties.

General purpose polyester

- mild corrodents
- low cost

uses : boats

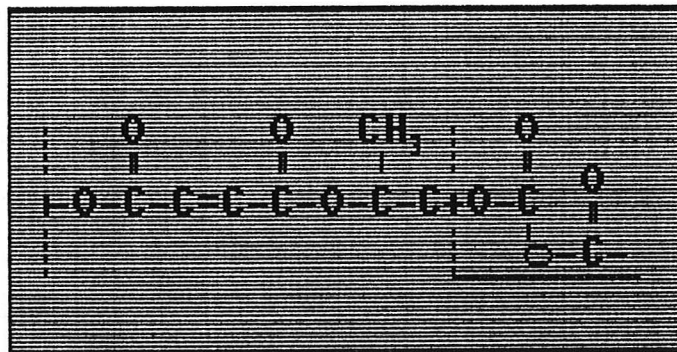


GENERAL-PURPOSE POLYESTERS, are normally not recommended for use in chemical process equipment. These resins are generally adequate for use with non-oxidizing mineral acids and corrodents that are relatively mild. This is the resin which predominates in boat, building, so that, obviously, its resistance to water of all types, including sea-water, is more than adequate.

Isophthalic polyester

- good chemical resistance

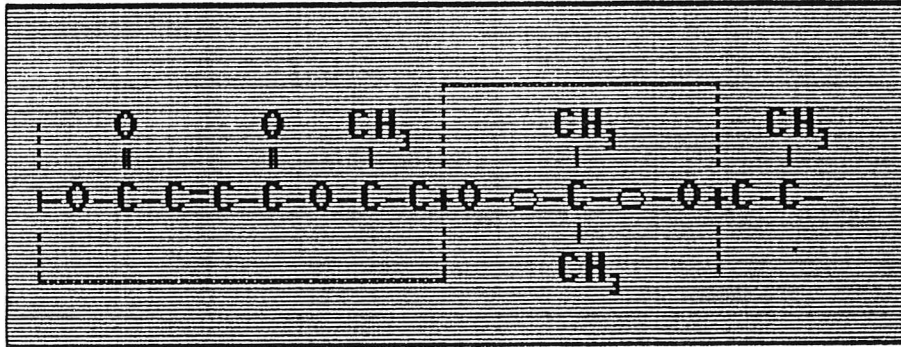
uses : chemical tanks,
gasoline tanks



ISOPHTHALIC POLYESTERS, they definitely show much better resistance to attack in the solvent areas, and are used extensively in the manufacture of underground gasoline tanks, where a satisfactory service life in the storage of gasoline and under the varied conditions of ground-soil corrosion are not successfully.

Bisphenol polyester

- excellent chemical resistant
uses : piping, tanks, structure



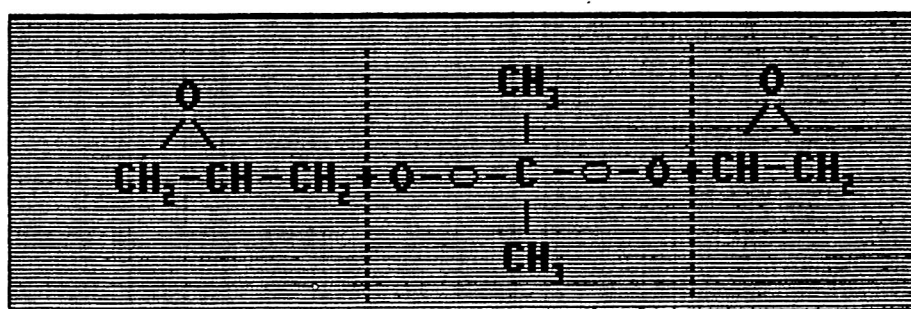
BISPHENOL AND HYDROGENATED BISPHENOL POLYESTERS

The bisphenol and hydrogenated bisphenol polyesters have an exceptionally high degree of chemical resistance, superior to both the general-purpose and isophthalic classes of polyester resins. They show superior acid resistance to the epoxies. The bisphenol-type resins show good performance with moderate alkaline solution and excellent resistance to the various categories of bleaching agents. However, all the polyesters and the epoxies break down under highly concentrated acids or alkalis, such as 93% H₂SO₄ and 73% NaOH. Failure with the concentrated acid is by dehydration.

Epoxy

- good chemical resistance
- more expensive

uses : good solvent resistance
piping, tanks



EPOXY. Many different epoxy resins will provide outstanding service in chemical-process equipment under severe conditions. Piping systems in reinforced epoxy have been well engineered, and their use is prevalent. Flanged and adhesive assembled systems are commonly used.

TYPE OF RESINS. Recommended areas of application are as follows:

General-Purpose Polyester

Acids

10% acetic acid
Citric acid
Fatty acids
1% lactic acid

Oleic acid
Benzoic acid
Boric acid

Salts

Aluminum sulfate
Ammonium chloride
10% ammonium sulfate
Calcium chloride(saturated)
Calcium sulfate
Copper sulfate(saturated)
Ferric chloride
Ferric nitrate
Ferric sulfate

Ferrous chloride
Magnesium chloride
Magnesium sulfate
Nickel chloride
Nickel nitrate
Nickel sulfate
Potassium chloride
Potassium sulfate
10% sodium chloride

General-purpose resins have been found to be unsatisfactory in:

Oxidizing acids
Alkaline solutions, such as calcium hydroxide, sodium hydroxide, and sodium carbonate
Bleach solutions, such as 5% sodium hypochlorite
Solvents such as carbon disulfide, carbon tetrachloride, gasoline, distilled water

Isophthalic Polyester

Acids

10% acetic acid
Benzoic acid
Boric acid
Citric acid
Fatty acids

Oleic acid
25% phosphoric acid
Tartaric acid
10% sulfuric acid
25% sulfuric acid

Salts

Aluminum sulfate
10% ammonium carbonate
Ammonium chloride
Ammonium nitrate
Ammonium sulfate
Barium chloride
Calcium chloride(saturated)
Copper chloride
Copper sulfate

Iron salts
5% hydrogen peroxide
Magnesium salts
Nickel salts
Sodium and potassium salts
which do not have a high
alkaline reaction
Dilute bleach solutions

Isophthalic resins have been found to be unsatisfactory
in:

Acetone
Amyl acetate
Benzene
Carbon disulfide
Solutions of alkaline salts of potassium and sodium
Hot distilled water
Higher concentrations of oxidizing acids

Vinyl Ester Resin

Acids

Benzene sulfonic acid	Lactic acid
Benzoic acid	25% maleic acid
Boric acid	10% nitric acid(to 150° F)
25% butyric acid	Oxalic acid
5% chromic acid	Phosphoric acid(0-80%)
Citric acid	50% sulfuric acid (to 150° F)
Fatty acids	Tannic acid
50% hydrobromic acid	Tartaric acid
Hydrochloric acid(0-30%)	Trichloroacetic acid
Hypochlorous acid, 10% (to 150° F)	

Bisphenol and Hydrogenated Bisphenol Polyester

Acids, to 200° F

25% acetic acid	Maleic acid
Benzoic acid	Oleic acid
Boric acid	Oxalic acid
Butyric acid	80% phosphoric acid
25% chloroacetic acid	Stearic acid
5% chromic acid	50% sulfuric acid
Citric acid	Tannic acid
Fatty acids	Tartaric acid
10% hydrochloric acid	50% trichloroacetic acid
Lactic acid	

Salts, solution to 200° F

All aluminum salts	Low sodium and potassium salts, except the high alkaline salts
Most ammonium salts	
Calcium salts	
Copper salts	Zinc salts
Iron salts	Most plating solutions

Epoxy

Acids

10% acetic acid(to 150° F)
Benzoic acid
Boric acid
50% butyric acid
25% chloroacetic acid
5% chromic acid
Citric acid
Fatty acids
25% hydrochloric acid
Hypochlorous acid
10% nitric acid(to 150° F)
Oxalic acid
30% perchloric acid(to 75° F)
Phosphoric acid(80%)
25% sulfuric acid

Salts

Aluminum
Most ammonium salts
Barium
Calcium
Iron
Magnesium
Potassium
Sodium

Chlorinated Chemical-Resistant-Type Polyester

<u>Environment</u>	<u>Remarks</u>
Water: demineralized, distilled, deionized, steam, and condensate	Lowest absorption of any polyester. Resistant to 212° F.
Alkaline solutions: pH greater than 10	Not ordinarily recommended for continuous exposure, but resistant to 20% ammonium and 10% sodium hydroxides, to about 150° F.
pH greater than 10, intermittent pH less than 10	Suitable to about 200° F, depending upon exposure. Resistant to, and often higher than, about 200° F.
Amines: aliphatic, primary aromatic	Can cause severe attack, depending upon conditions.
Amides, other alkaline organics	Can cause severe attack, depending upon conditions.
Salts: alkaline, such as sodium sulfide, trisodium phosphate	Can cause severe attack, depending upon conditions.
Salts, neutral	Resistant to, and in some instances higher than, about 250° F.
Salts, acid	Resistant to, and in some instances higher than, about 250° F.
Acids: mineral, nonoxidizing	Resistant to, and in some instances higher than, about 250° F.

Acids, organic	Resistant to, and in some instances higher than, about 250°F, including glacial acetic to about 120°F.
Acids: organic; certain high-molecular-weight acids; sulfonic, amino, and sulfinic acids	Can cause severe attack, depending upon conditions.
Phenol and phenols	Not ordinarily recommended.
Acid halides	Not ordinarily recommended.
Mercaptans	Resistant to about 180°F.
Ketones	Resistant to about 180°F.
Aldehydes	Resistant to about 180°F.
Alcohols	Resistant to about 180°F.
Glycols	Resistant to about 180°F.
Esters, organic	Resistant to about 180°F.
Fats and oils	Resistant to about 180°F.
Solvents: aliphatic, aromatic, and chlorinated	Resistant to about 200°F. Uniquely resistant to many such as CCl ₄ to 110°F; trichlorethylene to 180°F; monochlorobenzene to 150°F; petroleum ether, benzene, toluene, heptane, CS ₂ , dimethyl sulfoxide, polyvinylidene chloride at room temperature.
Oxidizing acids and solutions.	Uniquely resistant to many; such as 35% HNO ₃ to 140°F; 70% HNO ₃ at room temperature; 40% chromic at 210°F; chlorine water to 285°F; wet Cl ₂ and ClO ₂ to 220°F; 15% hypochlorites to 110°F; 6% hypochlorites to 140°F. Concentrated H ₂ SO ₄ is severely destructive.
Gases: wet and dry	Resistant to about 350°F, with intermittent exposure to as high as 425°F. SO ₃ can cause severe attack.

CRITERIA FOR MATERIAL SELECTION

In selecting a material for an application, a designer has several factors to consider such as cost, ease of installation, expected service life, ease of modification or repair, delivery, safety, especially strength and corrosion resistance. In material selection, engineers have to distinguish between the strength and corrosion resistance required to withstand operating pressure and physical abuse while providing maximum corrosion resistance. Thermal and oxidative stabilities are also to be considered in material selection. The following figures show the properties of glass reinforced polyester composites in various conditions.

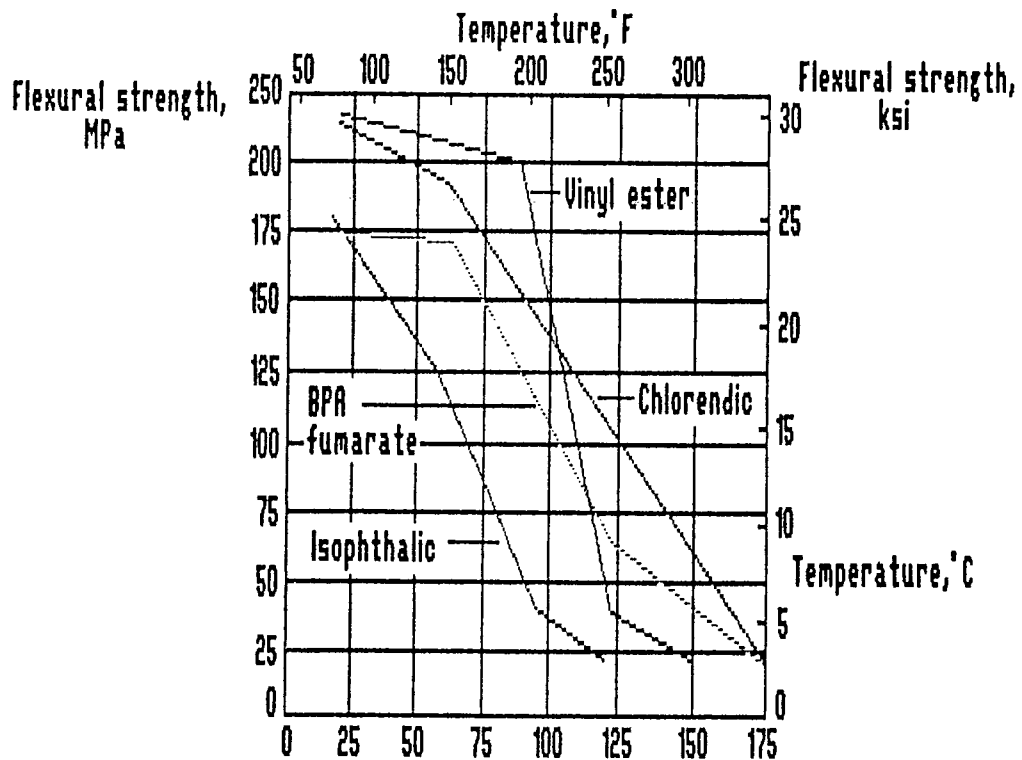


Figure: Flexural strength versus temperature, glass-polyester composites of 40% glass

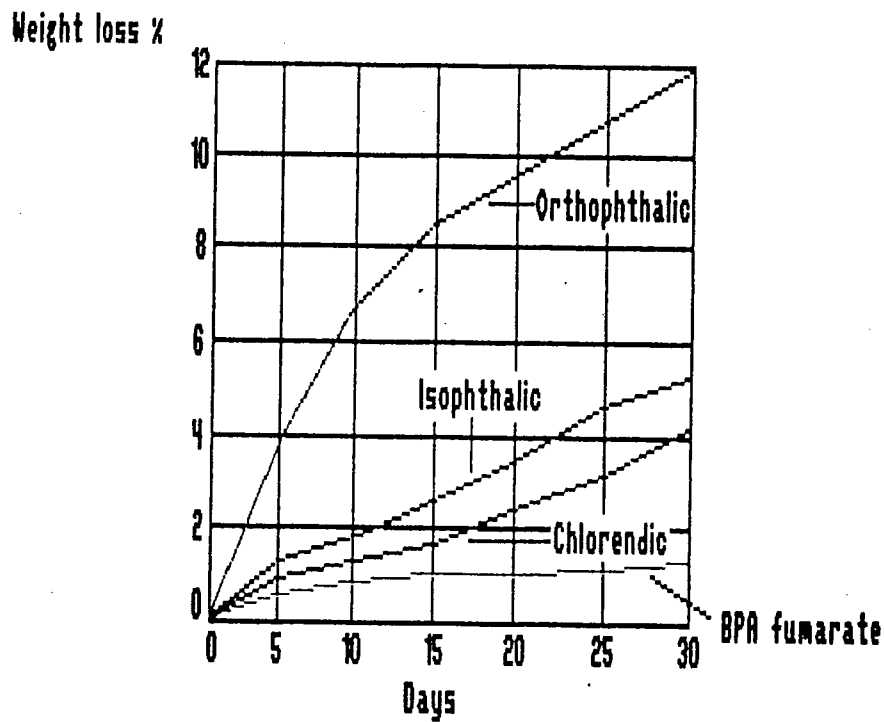


Figure : Thermal stability of glass-polyester composite at 180°C (355°F)

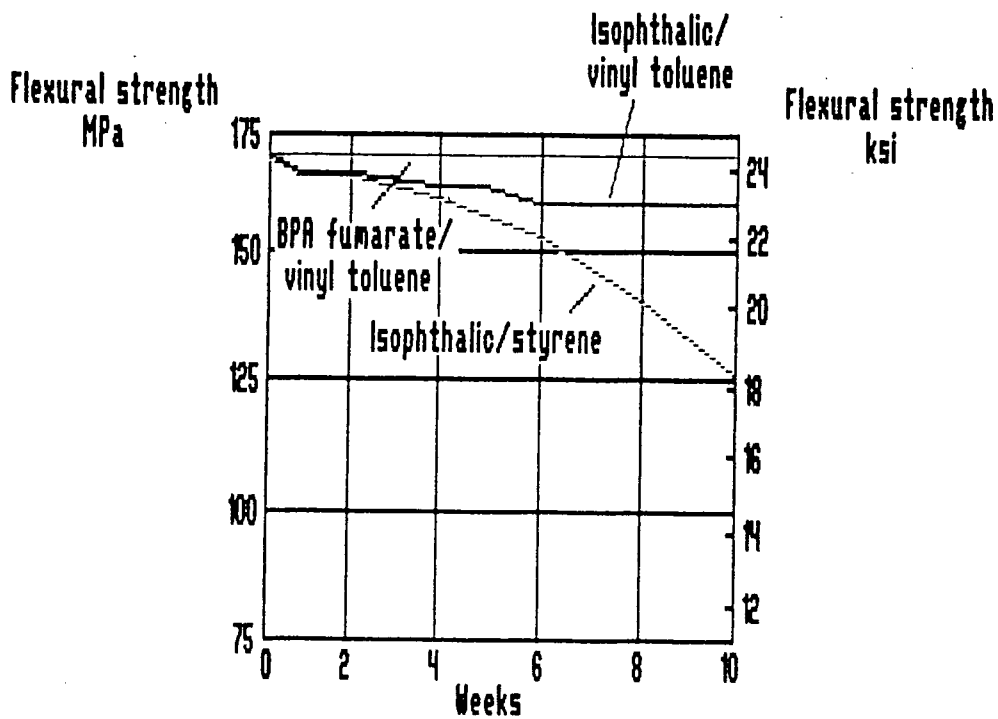


Figure : Flexural strength retention of glass-polyester composite when aged at 200°C (390°F), tested at room temperature

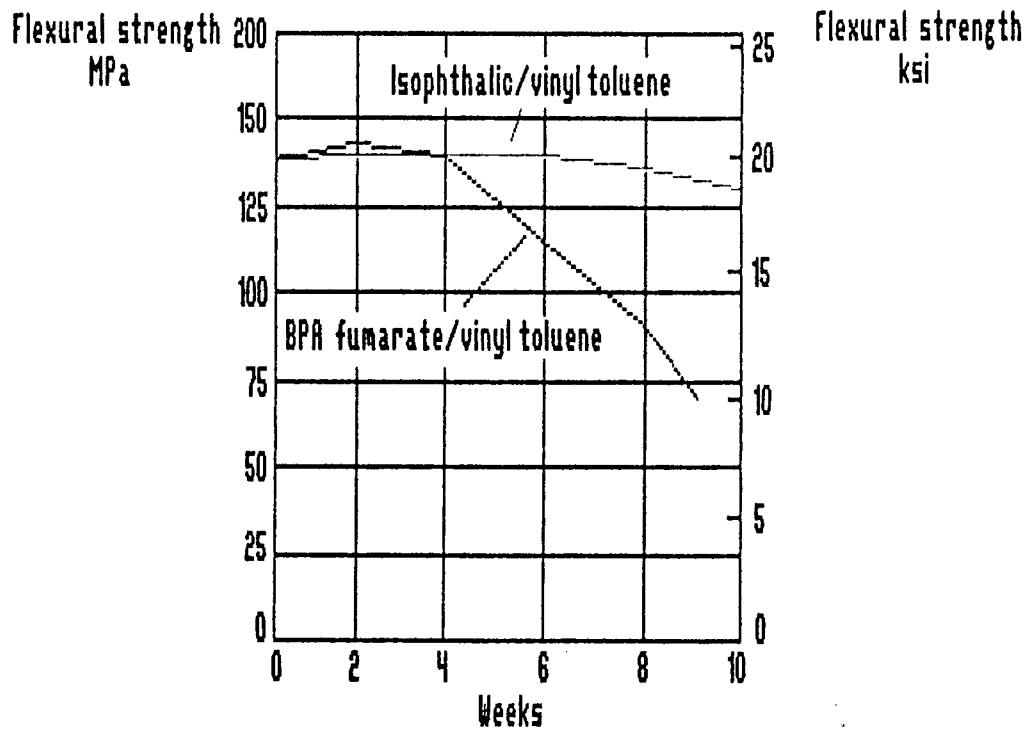


Figure : Flexural strength retention of glass-polyester composite
When aged at 220°C (430°F) tested at room temperature

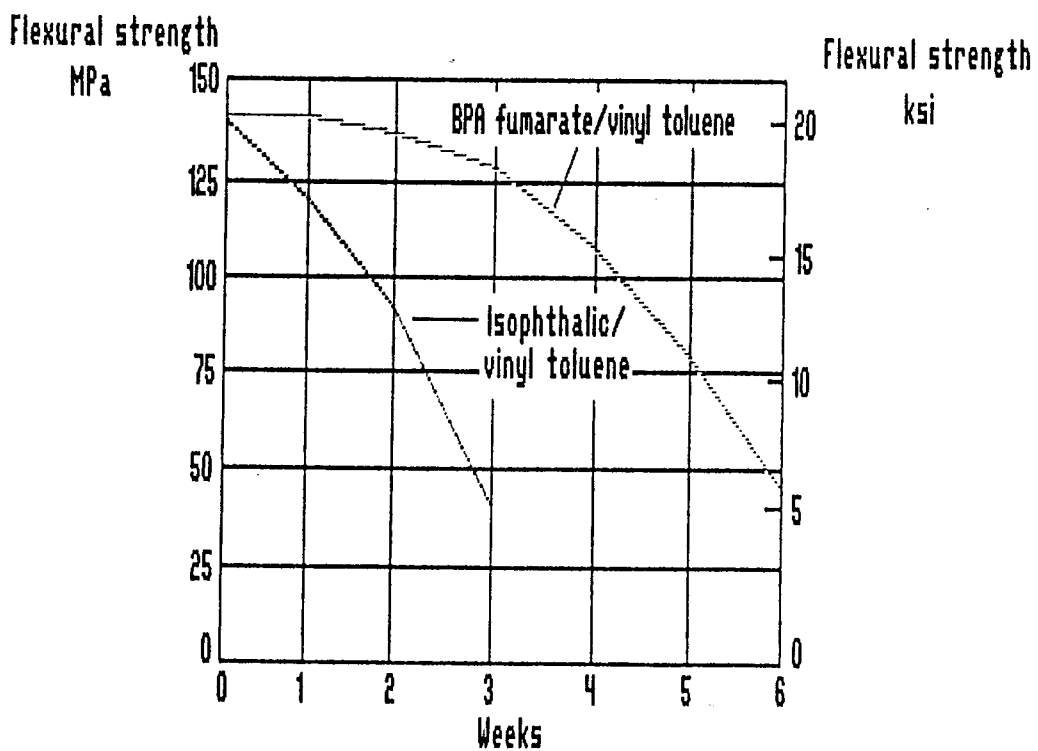


Figure : Flexural strength retention of glass-polyester composite
When aged at 240°C (465°F), tested at room temperature

MANUFACTURING METHODS

There are many methods in manufacturing FRP composite materials. The first and most well-known method is hand lay-up method. In this method, fiber is hand laid into a mold. Liquid resin is poured onto the fiber. Curing of the resin occurs at room temperature after the catalyst is mixed into the resin. Air bubbles are eliminated from the work piece by action of rolling a tool. This method can provide a structure with large dimension, for example, tanks, ducts, etc. The hand lay-up method is not used in strength/weight critical application since the glass fiber loading is only up to 30%-35%.

Filament winding method is achieved by wrapping continuous strands of glass fiber roving around the outside of a mandrel in a predetermined pattern. The roving may be impregnated with a liquid polyester resin or other types of resin. A resin rich inner layer which forms an integral part of the product structure provide excellent corrosion resistance. Subsequent polymerization of the resin is obtained by post curing of the product to ensure reproducible strength of the product. Some product may be lined with thermoplastic or rubber materials in order to provide suitable corrosion resistance. The filament winding method can provide the fiber loading up to 65%-70%. Consequently, products such as piping, can bear a tremendous level of pressure.

GLASS FIBER REINFORCEMENT

The major consumption of reinforcing materials is glass fiber. In the application of corrosion resistance, various compositions of glass can be used if the product requirement is critical. Fabrication technique can affect the product performance drastically. The compositions of glass fiber are ...

1. Chemical resistant glass, called "C" glass is often used for composites which will be in contact with acidic materials, for example tanks in electro-painting industries.
2. Alkaline resistant glass, called "A" glass can also be used in some application especially for reinforcing cement.
3. Electric "E" glass which has a large portion of total market has become standard for most uses. "E" glass has superior strength than "C" glass or "A" glass. Due to its lower cost and acceptable, corrosion resistant properties, "E" glass is widely use in the corrosion resistant industries.

SURFACING SYSTEM

To prepare a good corrosion resistant composite materials, surfacing systems have to be understood. There have many types of surface layer ...

1. Gel coat Commonly used in many epoxy piping systems. Little used in hand-laid-up polyester construction. Less resistance to cracking and crazing than with a reinforced laminate.

2. Type C Surface mat Most commonly used with reinforcement, for chemical plant applications. Particularly necessary on tanks, ductwork, etc. Commonly used in polyester piping. About 10% glass/90% resin.

3. Organic veil Good weathering characteristics. Improves abrasion resistance and impact strength in many cases. Some provide complete transparency. Standard specification in HF work or caustic applications. About 10% veil/90% resin.

4. Asbestos mat Good acid and alkaline resistance. Used as an inner liner in some commercial epoxy pipe. Could equally be used with polyesters. Good solvent resistance.

CONCLUSION

Now materials such as FRP on composites play an important role in today's corrosion resistant industries. There are various applications of such materials. With careful selection of resins, glass, manufacturing method, an engineer can successfully design products which possess desirable properties. Filament winding method provides a product with high load bearing factor.

REFERENCE

Mallinson, J. H., Reinforced Plastic Pipe: A User's Experience, Chemical Engineering, Dec 20, 1965.

Mallinson, J. H., Chemical Plant Design with Reinforced Plastics, McGraw-Hill Book Company, 1969.

Szymanski, W. A. Hooker Chemical Corp., Durez Div., North Tonawanda, N. Y., Personal Communication, Jan 17, 1967.

THE CHLORINATION AND OXIDATION PROCESS OF NICKEL AND NICKEL BASED ALLOYS
AT ELEVATED TEMPERATURE

M.J. McNallan, Y.Y. Lee

Department of CEMM, University of Illinois at Chicago, Chicago, IL 60680.

and

S.Thongtem

Faculty of Science, Chiang Mai University, Chiangmai 50002.

ABSTRACT

The corrosion process of nickel and nickel based alloys in environments containing 0-50 % oxygen, 0-3 % chlorine and argon over the temperature range of 970-1275 degrees kelvin was studied by the use of scanning electron microscope (SEM) equipped with an energy dispersive x-ray analysis (EDX) system and thermogravimetric analysis. It was found that the volatilization process was controlled by the diffusion of volatile species in the gas phase. Temperature, corrosive gas potentials and composition of alloys that controlled the corrosion kinetics. For alloys containing aluminium, low vapor pressure of aluminium chloride over the alumina was the result for them to show the least attack in all environments of this study.

INTRODUCTION

Gas mixtures containing chlorine at high temperature are among the most corrosive environments which are encountered in a number of important industrial energy conversion and metallurgical processes [1]. These include the use of low quality coal [2], the disposal of toxic and municipal waste products containing polyvinyl chloride (PVC) [3,4] and many others. The corrosion behavior of most commercial alloys in these environments is not clearly understood. The presence of chlorine in environments is an important factor to accelerate the corrosion rate of the metals although they are considered to be corrosion resistant [5,6].

The main purpose of this experiment is to determine the mechanisms on corrosion of nickel and nickel based alloys and to explain the effect of chromium and aluminium additions to nickel on corrosion resistance.

OPTICAL MICROGRAPHS AND EDX ANALYSIS

When the alloys were exposed to a mixture of 0-50 % oxygen, 0-3 % chlorine and balance argon at elevated temperatures of 970-1275 °K. The results are then given and discussed on according to the following.

Microstructures of corrosion product formed on nickel in 50 % O₂ - 1.5 % Cl₂ - Ar at 1000 °K are shown in Fig. 1. It was found that the corrosion product composed of fine particles with size of approximately 100 microns. Therefore, the general morphology of the corroded sample shows rough surface. During cooling, stress in the corrosion product was developed which resulted to the cracking and spallation of the product.

When alloy C15 was exposed to 600 ppm Cl_2 - Ar at 1100 °K, the corrosion product was rich of both chromium and nickel as shown in Fig. 2. It indicates that both chromium and nickel were chlorinated in this environment. The EDX analysis on the corrosion product shows higher concentration of chromium than that of nickel. At the beginning of each run, chlorine diffuses into the alloy matrix [7,8], then spot of chlorides of nickel and of chromium gradually show up and spread all over the surface of the samples [9,10]. These chlorides are able to volatile even at a temperature lower than their melting points [10-12].

The structures of the corrosion products of alloys C1 and A1 in 600 ppm Cl_2 - Ar at 1200 °K are shown in Fig. 3 and 4. The products are characterized by dense-faceted compounds spread over the whole surface of the samples. During the chlorination, chlorides of the products can also evaporate. At the beginning, chlorine gas diffuses through the alloy matrix [7,8] and chlorinates the alloys to form chloride products, then the evaporation of the chlorides is initiated [10-12]. As long as the chlorides are supplied to the corrosion products, the evaporation process can thus keep going on.

At the beginning of each run, the chlorination process goes very fast and gradually keeps constant afterwards. On the other hand, the evaporation rate of the corrosion products starts from zero and gradually increases to a constant value. When the rate of chlorination equals to the rate of evaporation, the process is then in equilibrium.

At the end of each run, the sample is slowly cooled down to room temperature. The chlorination and the evaporation processes are slow down. Some of the chloride products are then left as thin film on the samples. Moreover, some chloride vapors surrounding the samples can also condense to form solid compounds. Therefore, some chlorides are left on the samples.

Fig. 5 shows the morphology of corrosion products of alloy A5 in 600 ppm Cl_2 - Ar at 1200 °K. The products are crystalline structure.

Fig. 6 shows the morphology and EDX analysis of the corrosion product of alloy C15 in 0.25 % Cl_2 - 20 % O_2 - Ar at 1200 °K. The EDX analysis shows that the corrosion product mostly contains chromium.

At the beginning, the sample is covered with a film of chlorides then the spot of oxides gradually originates and spreads across the whole surface of the sample [9-10]. Therefore, the corrosion process is related to the formation of oxide scale with further transformation to chlorides. The chlorides can evaporate even the temperature lower than their melting points [10-12]. At equilibrium, the scale contains both chlorides and oxides which are on evaporation. At the end of the corrosion process, the products are thus a mixture of chlorides and oxides.

From Ellingham diagram [13,14], ΔG° of Cr_2O_3 is lower than that of NiO ; therefore, chromium is oxidised faster than nickel. It is consistent with the EDX analysis on the corrosion products in Fig. 6 which shows the highest concentration of chromium.

According to this experiment, it also shows that the corrosion products of alloys containing chromium compose of particles of blunt edges but that those of alloys containing aluminium compose of particles of sharp edges as shown in Figs. 2-5 for alloys C15, C1, A1 and A5 respectively.

Fig. 7 shows the morphology and EDX analysis of corrosion product of alloy 600 in 2.8 % Cl_2 - 20 % O_2 - Ar at 1200 °K. The result shows that the corrosion product consists of different kinds of metal compounds.

MASS CHANGE RESULTS

Mass change results of nickel based alloys exposed in environment of 0.25 % Cl_2 - 20 % O_2 - Ar at the temperature range of 973-1273 °K are shown in Figs. 8-11. Mass change of all alloys increases with the test temperatures and is linearly dependent of the experimental time. As compared among them, alloys 600, C-276 and S show mass change with almost at the same rate. For these environments, alloy 214 is corrosion resistance by forming Al-rich oxide scale [15]. It shows that vapor pressure of aluminium chloride over the alumina is extremely low. However, alloys 600 and 214 at 973 °K show their mass increase with the time. It indicates that the rate of oxidation is higher than that of evaporation. Thus, the oxidation scale is thickened at this temperature.

SUMMARY AND CONCLUSIONS

1. The corrosion products of alloys C1 and C15 compose of particles of blunt edges but those of alloys A1 and A5 are crystalline in nature.
2. Alloys in these environments are corroded by the formation of oxides with subsequent evaporation of chlorides.
3. As compared among commercial superalloys, alloys 600, C-276 and S are corroded at the highest rates.
4. Alloy 214 forms alumina protective scale to resist corrosion in these environments.

REFERENCES

1. M.H. Rhee, M.J. McNallan and M.F. Rothman : High Temp. Corr. in Energy Syst. , M.F. Rothman, ed., The Metall. Soc. of AIME, Warrendale, PA., 1985, p.483.
2. A.L. Plumley and W.R. Roczniak : Trans. ASMZ, J. Engi. for Power, Vol. 124, 1982, p. 874.
3. G. Marsh and P. Elliot : High Temp. Tech., Vol. 1, 1982, p. 115.
4. P.D. Miller, H.H. Krause, D.A. Vaughan and W.K. Boyd : Corr., Vol. 28, 1972, p. 274.
5. M.J. McNallan, M.H. Rhee, S. Thongtem and T. Hensler : CORR./85, paper no. 11.
6. S. Thongtem, M.J. McNallan and G.Y. Lai : CORR./86, paper no. 372.
7. S.N.S. Reddy and R.A. Rapp : Met. Trans. B, Vol. 9B, 1978, p. 559.
8. S.N.S. Reddy and R.A. Rapp : Met. Trans. B, Vol. 11B, 1980, p. 99.
9. K. Hauffe and J. Hinrichs : Oxid. of Met. and All., ASM, 1970, p. 87.
10. P. Elliott, C.J. Tyreman and R. Prescott : J. of Met., Vol. 37, no. 7, 1985, p. 20.
11. Y. Ihara, H. Ohgame, K. Sakiyama and K. Hashimoto : Corr. Sci., Vol.22, no. 10, 1982, p. 901.

12. E. Ruedl, F. Coen-Porisini, T. Sasaki and C. De Asmundis: J. of Nucl. Mat., Vol. 101, nos. 1&2, 1981, p. 135.
13. D.R. Gaskell : Intro. to Metall. Therm., Mat. Sci. and Engi. Series, 2nd ed., McGraw-Hill Book Co., 1981, p. 272.
14. C.H.P. Lupis : Chem. Therm. of Mat., North-Holland, NY., Elsevier Sci. Publ. Co., Inc., 1983, p. 133.
15. W.W. Smeltzer, H.M. Hindam and F.A. Elrefaie : High Temp. Corr., NACE, 1983, p. 251.

Table I Compositions (wt %) of alloys in present study.

Alloy Designation	Ni	Cr	Fe	Co	Mo	W	Al
C1	Bal.	0.58	-	-	-	-	<0.01
C15	Bal.	13.85	-	-	-	-	<0.01
A1	Bal.	-	-	-	-	-	2.95
A5	Bal.	0.14	-	-	-	-	4.34
600	Bal.	16	8	-	-	-	<0.35
C-276	Bal.	15.5	5.5	<2.5	16	4	-
S	Bal.	15.5	<3	<2	14.5	<1	0.2
214	Bal.	16	4	-	-	-	4.5

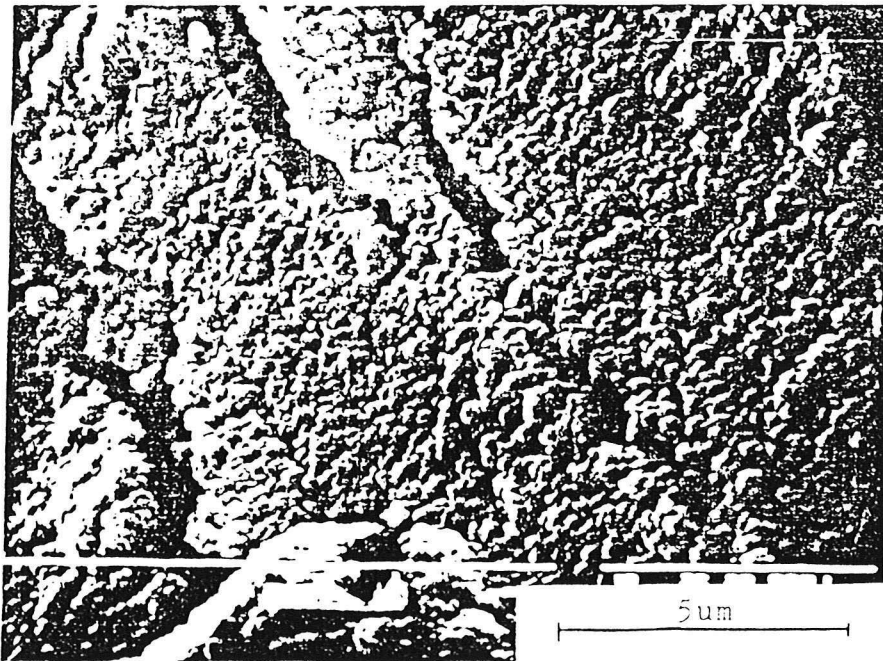
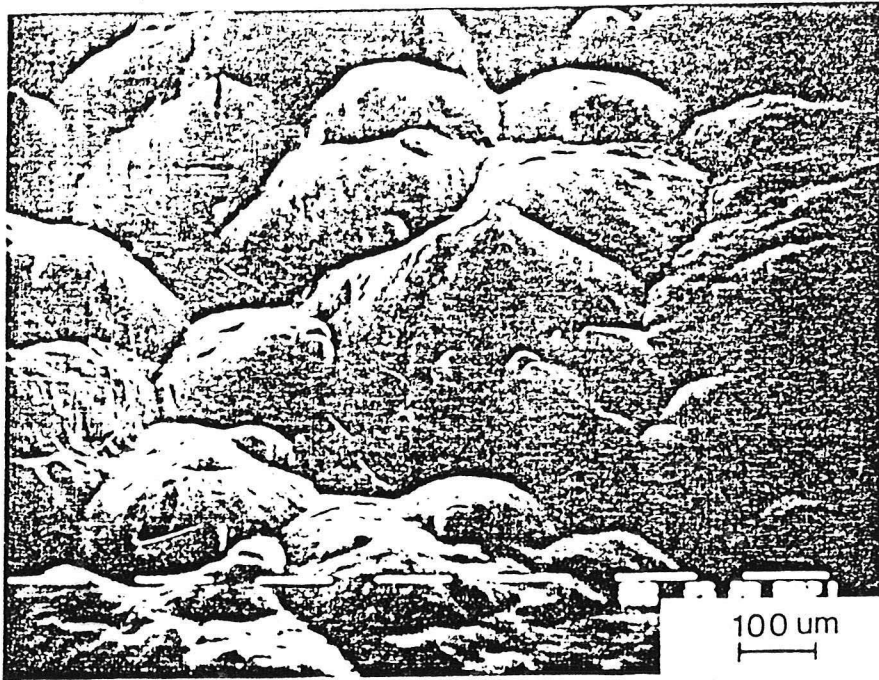


Fig. 1. Microstructures of corrosion product of Ni in 50 % O_2 - 1.5 % Cl_2 - Ar at 1000 °K.

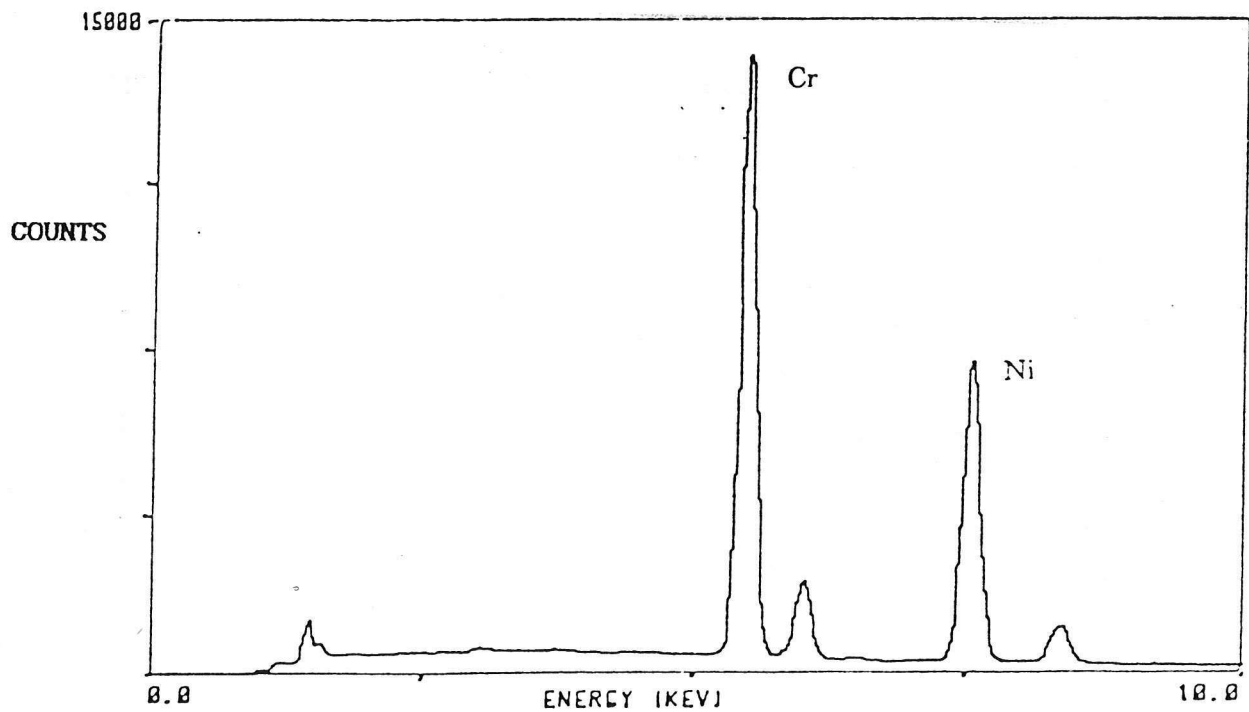
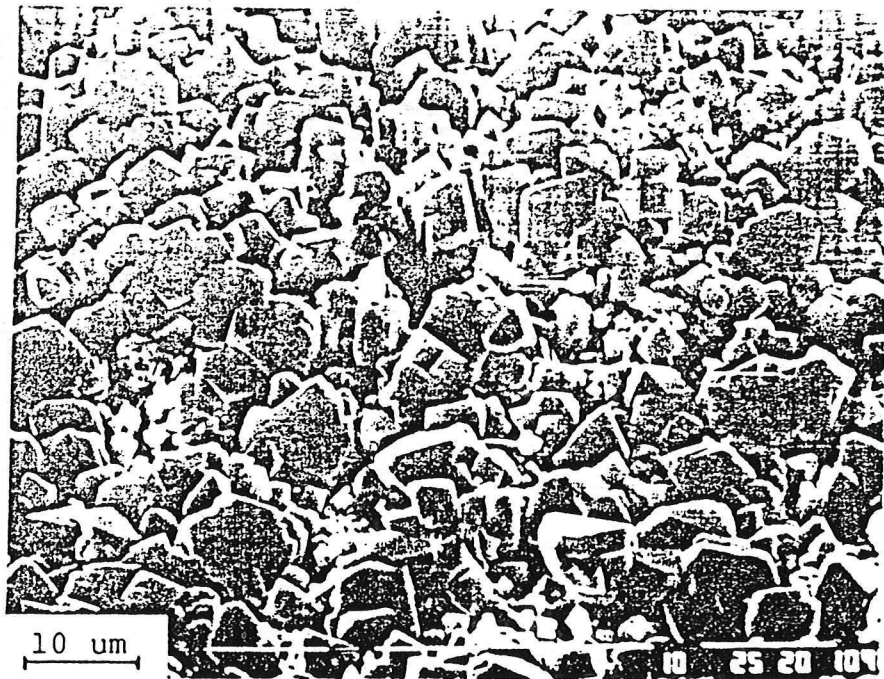


Fig. 2. Microstructures and EDX analysis of corrosion product of alloy C15 after 100 hours exposure to 600 ppm Cl_2 - Ar at 1100 °K.

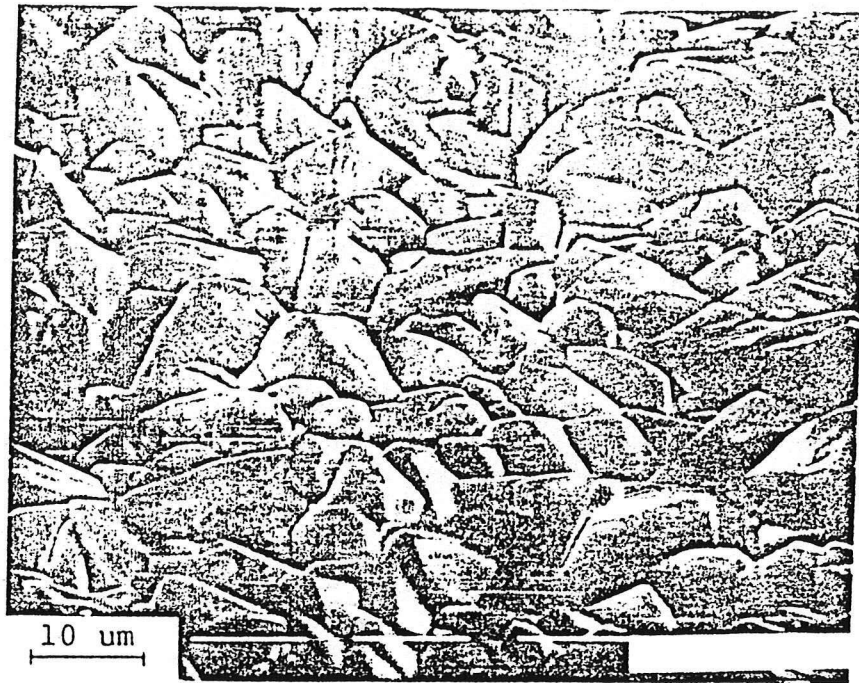


Fig. 3. Microstructures of corrosion product of alloy C1 after 24 hours exposure to 600 ppm Cl_2 - Ar at 1200 °K.

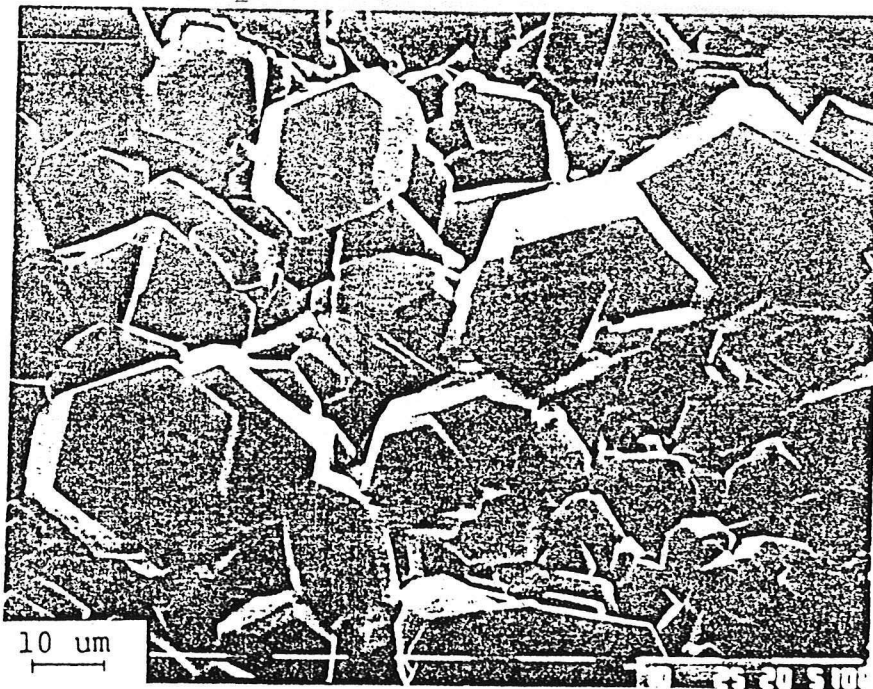


Fig. 4. Microstructures of corrosion product of alloy A1 after 24 hours exposure to 600 ppm Cl_2 - Ar at 1200 °K.

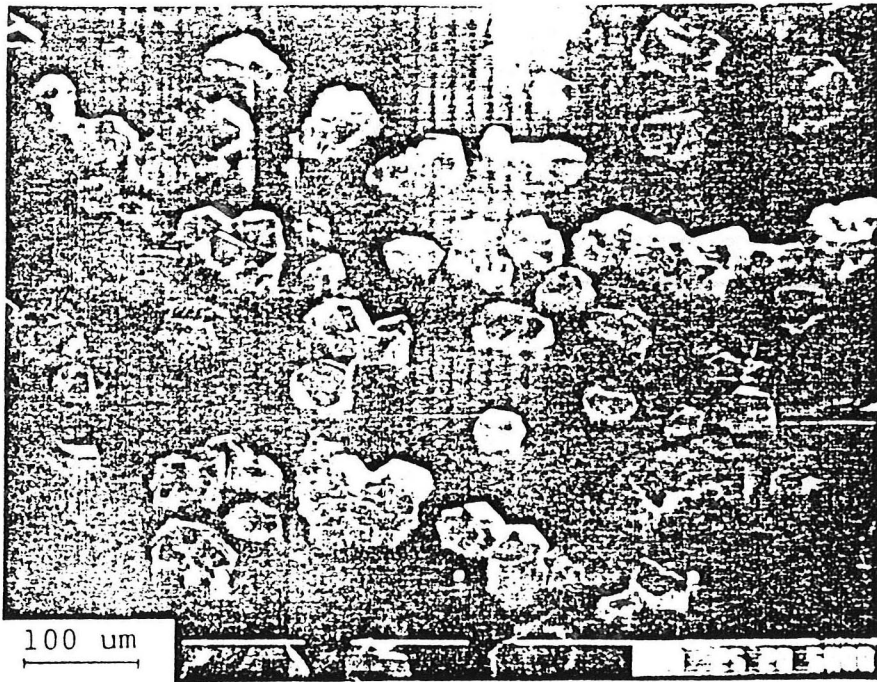


Fig. 5. Microstructures of corrosion product of alloy A5 after 24 hours exposure to 600 ppm Cl_2 - Ar at 1200 °K.

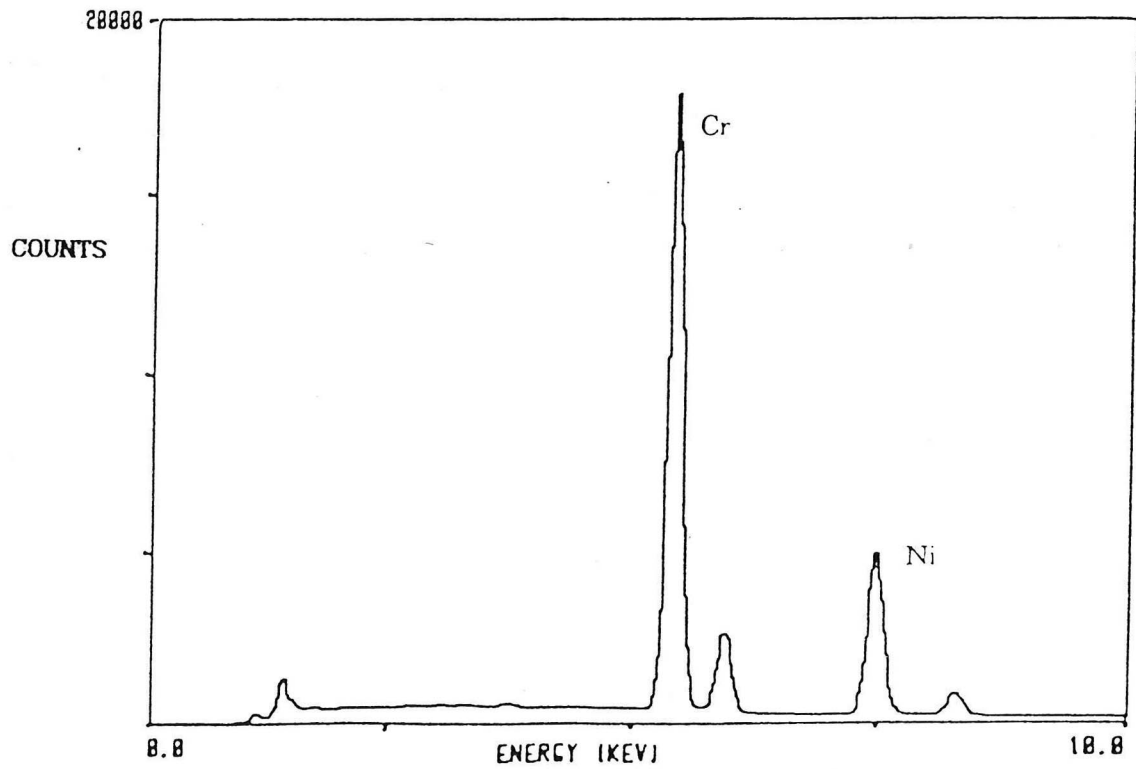
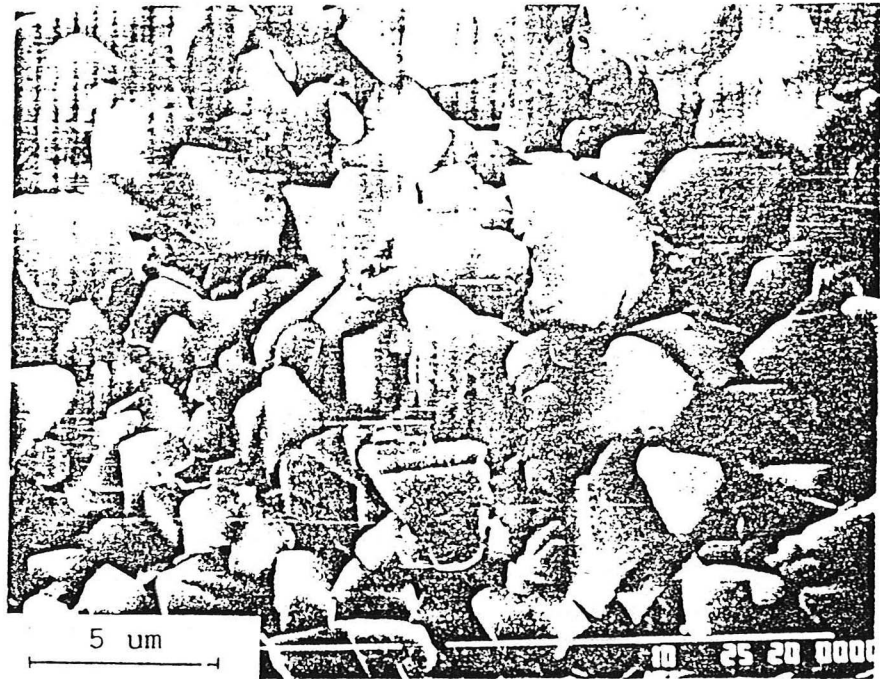


Fig. 6. Microstructures and EDX analysis of corrosion product of alloy C15 after 400 hours exposure to 20 % O₂ - 0.25 % Cl₂ - Ar at 1200 °K.

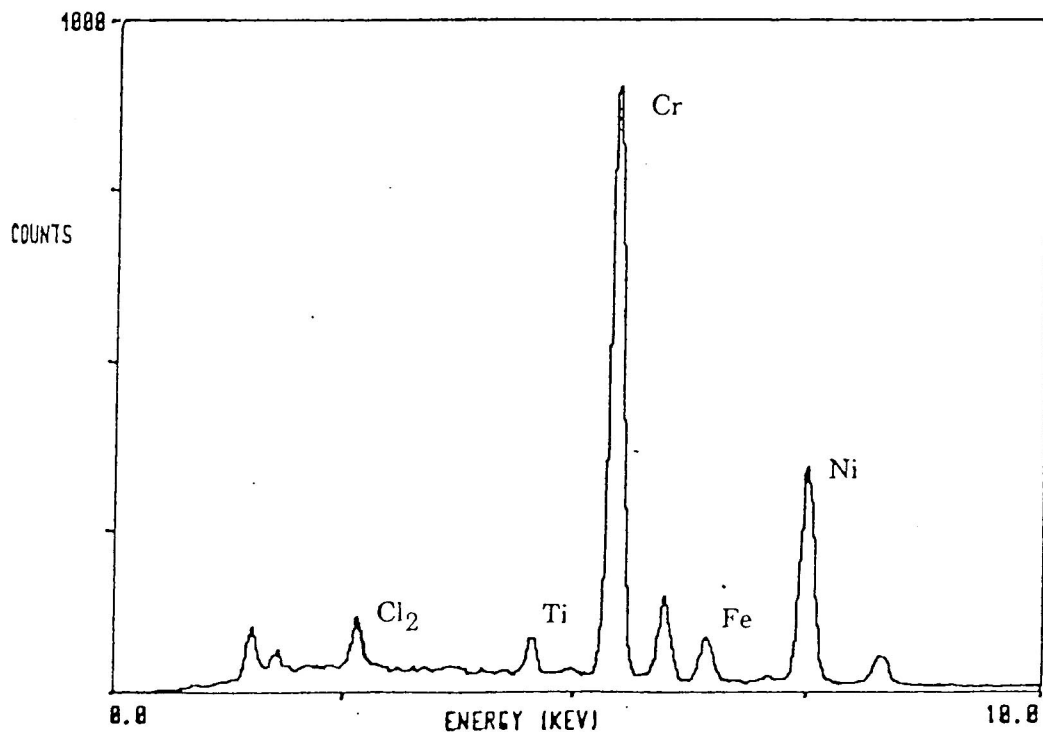
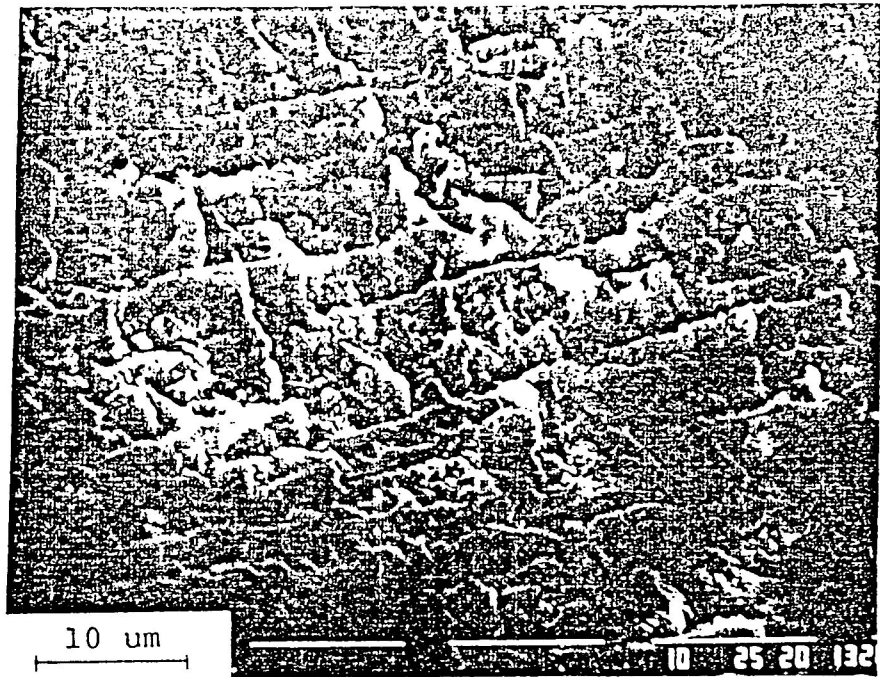


Fig. 7. Microstructures and EDX analysis of corrosion product of alloy 600 in 20 % O₂ - 2.8 % Cl₂ - Ar at 1200 °K.

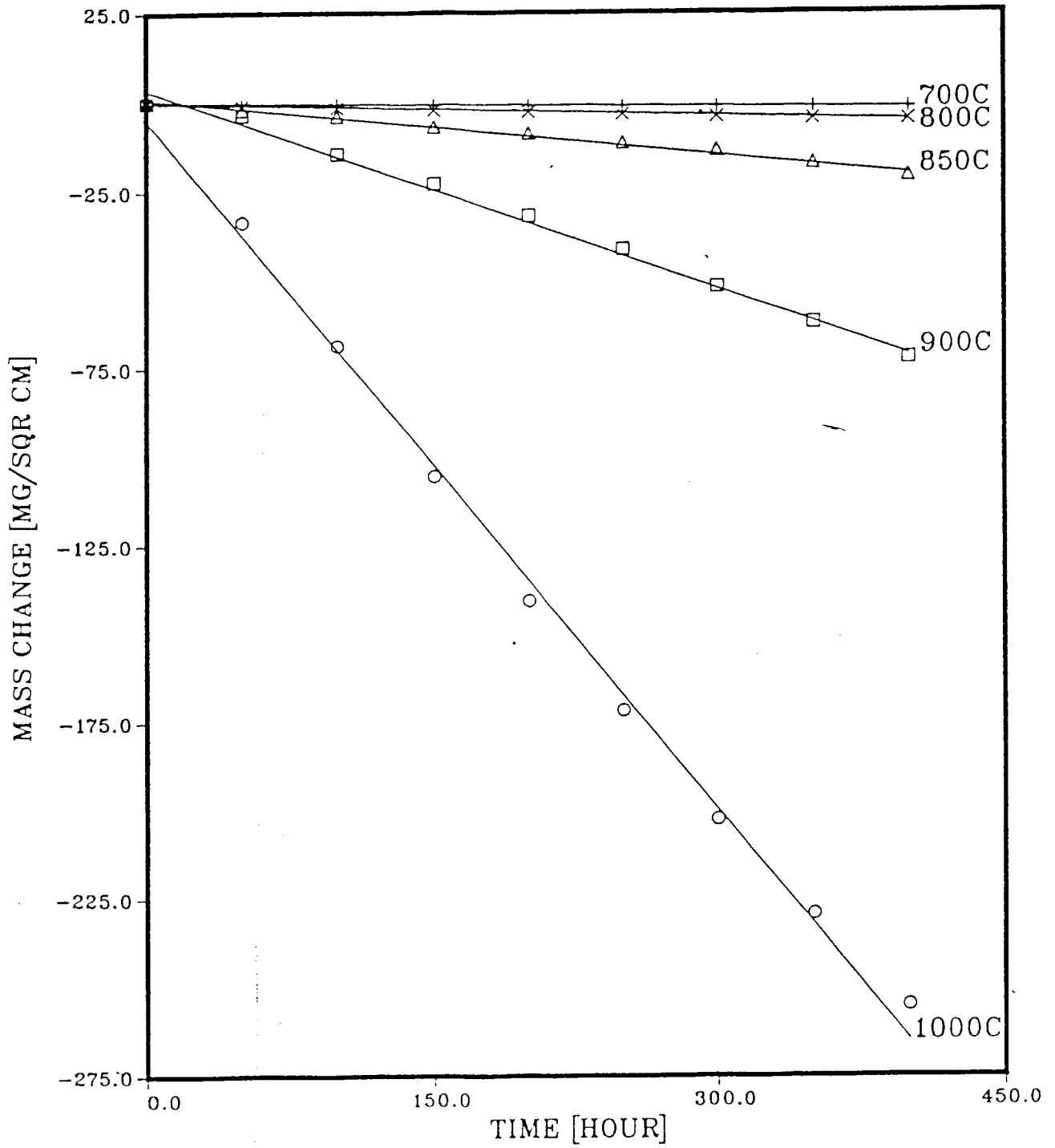


Fig. 8. Mass change of alloy 600 in 20 % O₂ - 0.25 % Cl₂ - Ar at high temperature.

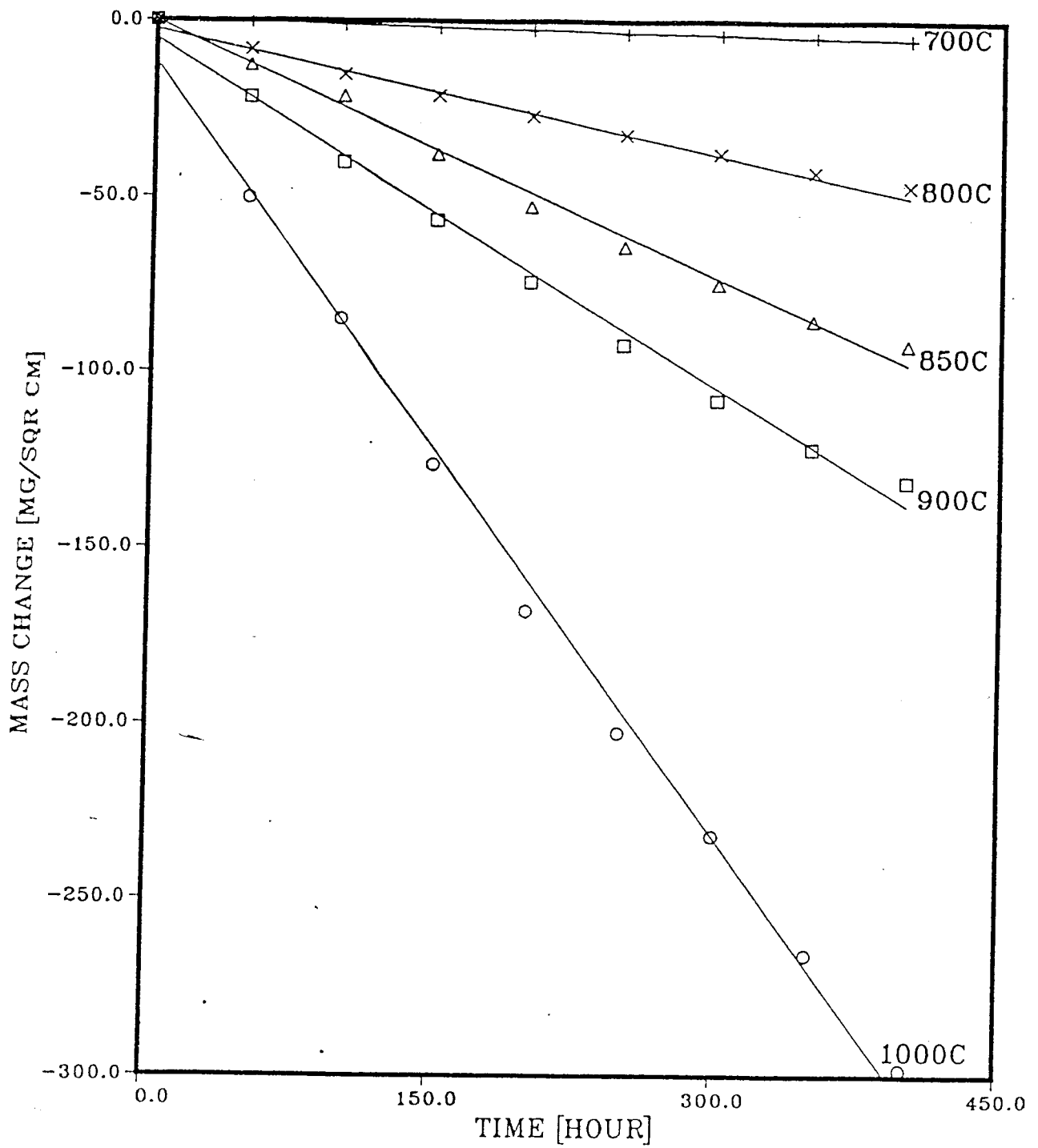


Fig. 9. Mass change of alloy C-276 in 20 % O₂ - 0.25 % Cl₂ - Ar at high temperature.

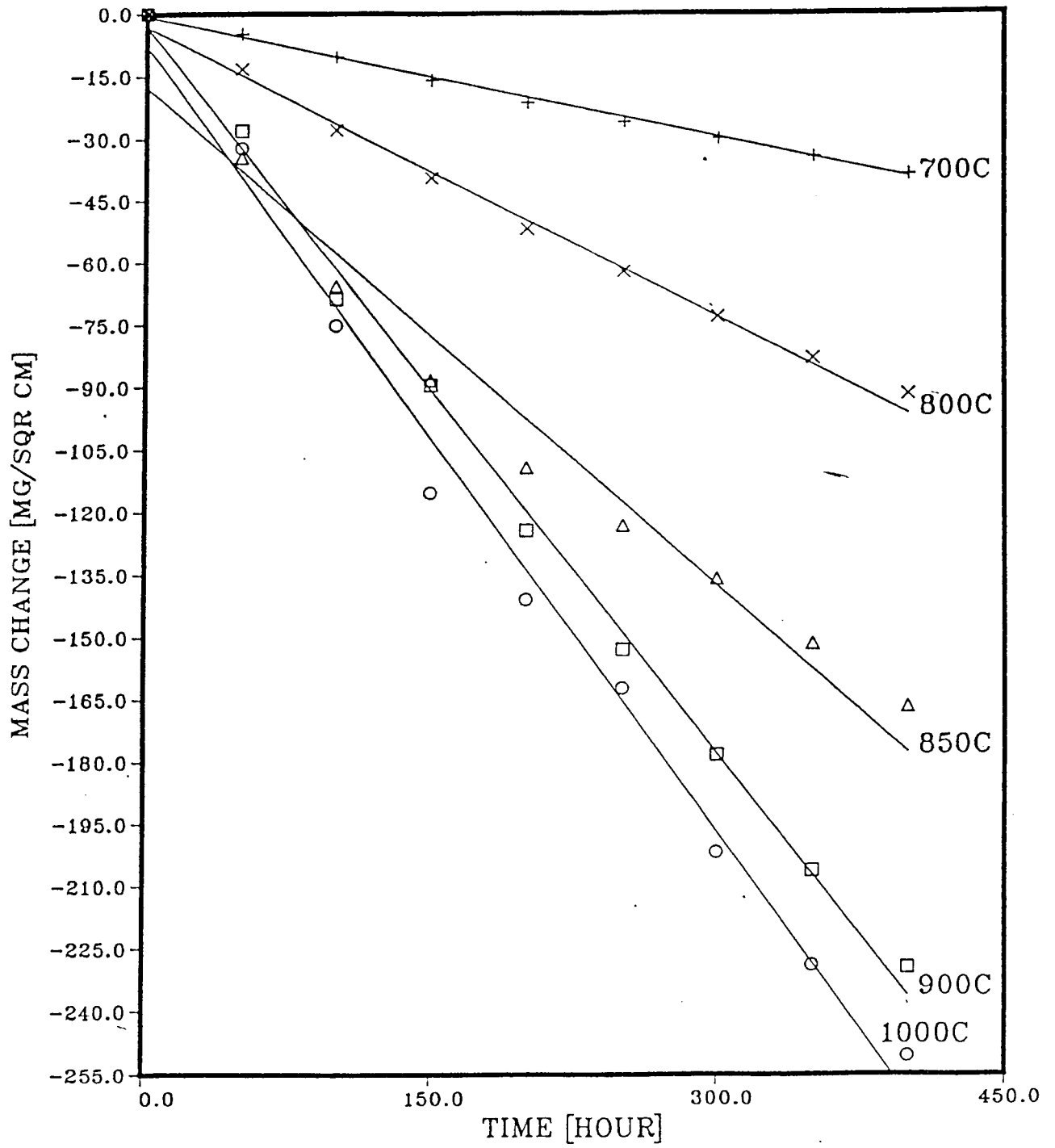


Fig. 10. Mass change of alloy S in 20% O₂ - 0.25% Cl₂ - Ar at high temperature.

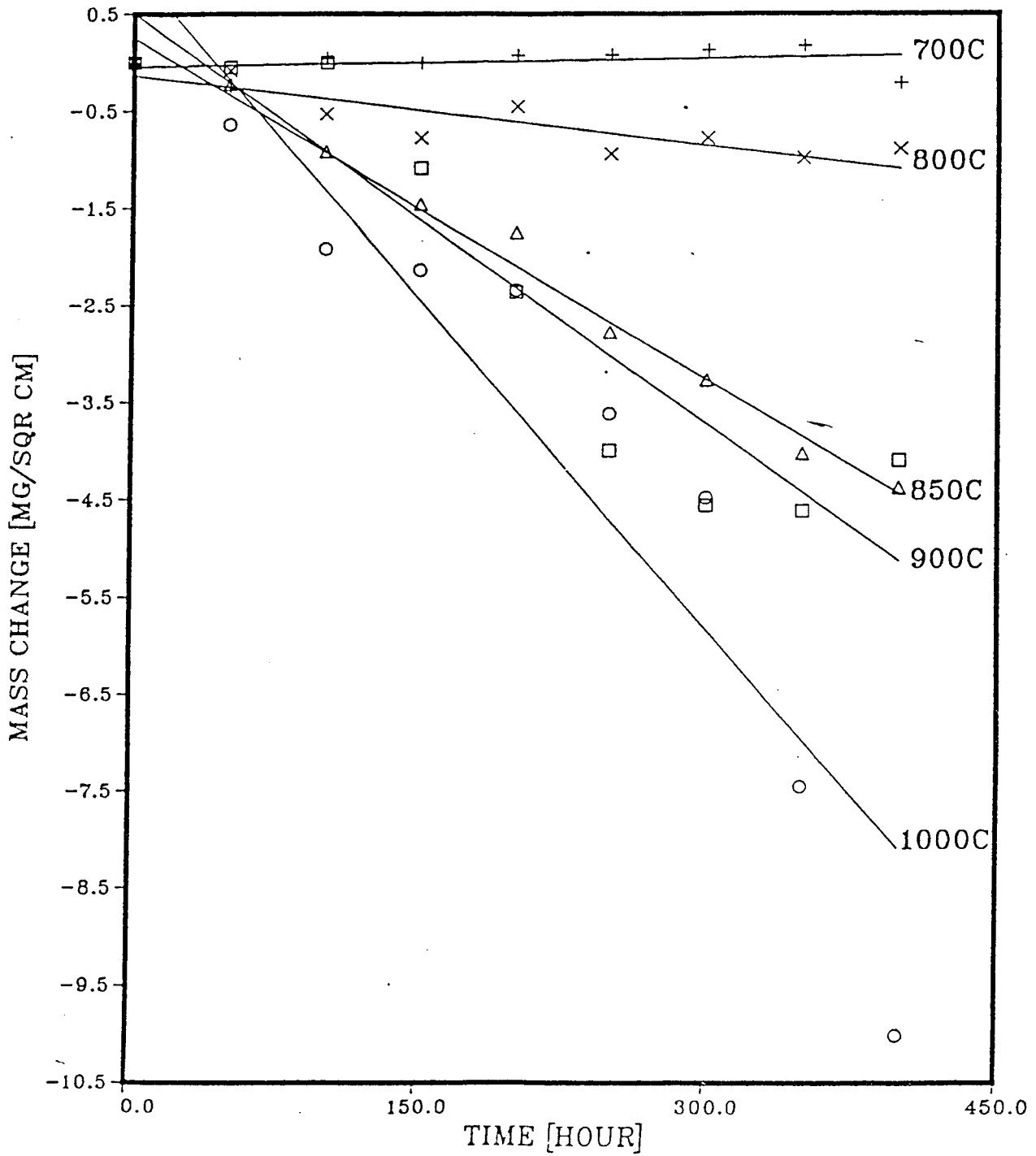


Fig. 11. Mass change of alloy 214 in 20 % O_2 - 0.25 % Cl_2 - Ar at high temperature.

Painting Systems for Heavy Duty Coatings

I. Steel Pipeline Coatings

1. Alkyd Coating Systems

A. ALL milscale, rust and foreign matter are to be removed. Wire brushing to a standard of min. st 2

a.) 2 Coats Alkyd Anticorrosive Primer (2 × 35 microns)

2 Coats Alkyd Enamel (2 × 30 microns)

Total film thickness 130 microns

b.) 1 Coat Etching Primer (1 × 15 microns)

2 Coats Alkyd Anticorrosive Primer (2 × 35 microns)

2 Coats Alkyd Enamel (2 × 30 microns)

Total film Thickness 145 microns

B. ALL milscale, rust and foreign matter are to be removed. Sand blasting or shot blasting or gritblasting to a standard of min. Sa 2.5

1 Coat Epoxy Zinc Rich Primer (1 × 18 microns)

2 Coats Alkyd Anticorrosive Primer (2 × 35 microns)

2 Coats Alkyd Enamel (2 × 30 microns)

Total film Thickness 148 microns

2. Chlorinated Rubber Coating Systems

A. ALL milscale, rust and foreign matter are to be removed. Wire brushing to a standard of min. St 3

1 Coats Etching Primer (1 × 15 microns)

2 Coats Chlorinated Rubber Anticorrosive Primer (2 × 40 microns)

2 Coats Chlorinated Rubber finish (2 × 35 microns)

Total film Thickness 165 microns

B. ALL milscale, rust foreign matter are to be removed, Sand blasting or shot blasting or grit blasting to a Standard of min. Sa 2.5

1 Coat Epoxy Zinc Rich Primer	(1 × 18 microns)
2 Coats Chlorinated Rubber Anticorrosive Primer	(2 × 40 microns)
2 Coats Chlorinated Rubber finish	(<u>2 × 35 microns</u>)

Total film Thickness	<u>168 microns</u>
----------------------	--------------------

3. Vinyl Coating Systems

A. ALL milscale, rust and foreign matter are to be removed Wire brushing to a standard of min. St 3

1 Coat Etching Primer	(1 × 15 microns)
3 Coats Vinyl Anticorrosive Primer	(3 × 25 microns)
2 Coats Vinyl finish	(<u>2 × 25 microns</u>)

Total film Thickness	<u>140 microns</u>
----------------------	--------------------

B. ALL milscale, rust and foreign matter are to be removed, Sand blasting or shot blasting or grit blasting to a standard of min. Sa 2.5

1 Coat Epoxy Zinc Rich Primer	(1 × 18 microns)
3 Coats Vinyl Anticorrosive Primer	(3 × 25 microns)
2 Coats Vinyl finish	(<u>2 × 25 microns</u>)

Total film Thickness	<u>143 microns</u>
----------------------	--------------------

4. Epoxy Coating Systems

A. ALL milscale, rust and foreign matter are to be removed. Wire brushing to a standard of min. St 2

a.) 1 Coat Etching Primer	(1 × 15 microns)
2 Coats Epoxy Anticorrosive HB Primer	(2 × 100 microns)
1 Coats Epoxy Undercoat	(1 × 60 microns)
1 Coats Epoxy finish	(<u>1 × 40 microns</u>)
Total film Thickness	<u>315 microns</u>

b.) 1 Coat Etching Primer	(1 × 15 microns)
2 Coats Epoxy Anticorrosive HB Primer	(2 × 100 microns)
1 Coat Epoxy Undercoat	(1 × 60 microns)
1 Coat Acrylic Modified Epoxy finish	(<u>1 × 35 microns</u>)
Total film Thickness	<u>310 microns</u>

c.) 1 Coat Etching Primer	(1 × 15 microns)
2 Coats Epoxy Anticorrosive HB Primer	(2 × 100 microns)
1 Coat Epoxy Undercoat	(1 × 60 microns)
1 Coat Polyurethane finish	(<u>1 × 35 microns</u>)
Total film Thickness	<u>310 microns</u>

B. ALL milscale, rust and foreign matter are to be removed. Sand blasting or shot blasting or grit blasting to a standard of min. Sa 2.5

a.) 1 Coat Epoxy Zinc Rich Primer	(1 × 18 microns)
2 Coats Epoxy Anticorrosive HB Primer	(2 × 100 microns)
1 Coat Epoxy Undercoat	(1 × 60 microns)
1 Coat Epoxy finish	(1 × 40 microns)
Total film Thickness	<u>318 microns</u>

b.)	1 Coat Epoxy Zinc Rich Primer	(1 × 18 microns)
	2 Coats Epoxy Anticorrosive HB Primer	(2 × 100 microns)
	1 Coat Epoxy Undercoat	(1 × 60 microns)
	1 Coat Acrylic Modified	(<u>1 × 35 microns</u>)

Total film Thickness 313 microns

c.)	1 Coat Epoxy Zinc Rich Primer	(1 × 18 microns)
	2 Coats Epoxy Anticorrosive HB Primer	(2 × 100 microns)
	1 Coat Epoxy Undercoat	(1 × 60 microns)
	1 Coat Polyurethane finish	(<u>1 × 35 microns</u>)

Total film Thickness 313 microns

II. Steel Tank Coatings

A. Crude Oil Tank

1. Tar - Epoxy Coating Systems

ALL milscale, rust and foreign matter are to be removed. Sand blasting or Shot blasting or Grit blasting to a standard of min. Sa 2.5

a)	1 Coat Epoxy Zinc Rich Primer	(1 × 18 microns)
	2 Coats Coal Tar Epoxy	(<u>2 × 125 microns</u>)

Total film Thickness 268 microns

b)	1 Coat Epoxy Zinc Rich Primer	(1 × 18 microns)
	1 Coat Coal Tar Epoxy HB	(<u>1 × 250 microns</u>)

Total film Thickness 268 microns

2. Bleached Tar - Epoxy Coating Systems (or Non - bleedTar - Epoxy Coating Systems)

ALL milscale, rust and foreign matter are to be removed. Sand blasting or Shot blasting or grit blasting to a standard of min. Sa 2.5

a) 1 Coat Epoxy Zinc Rich Primer	(1 × 18 microns)
2 Coats Non - bleedTar-Epoxy	(<u>2 × 125 microns</u>)
Total film Thickness	<u>268 microns</u>
b) 1 Coat Epoxy Zinc Rich Primer	(1 × 18 microns)
1 Coat Non - bleedTar-Epoxy HB	(<u>1 × 250 microns</u>)
Total film Thickness	<u>268 microns</u>

3. Epoxy Coating Systems

ALL milscale, rust and foreign matter are to be removed. Sand blasting or shot blasting or grit blasting to a standard of min. Sa 2.5

1 Coat Epoxy Zinc Rich Primer	(1 × 18 microns)
1 Coat Special Epoxy Anticorrosive Primer HB	(1 × 112.5 microns)
1 Coat Special Epoxy finish HB	(<u>1 × 112.5 microns</u>)
Total film Thickness	<u>268 microns</u>

B. Lubricating Oil Tank

1. Inorganic Zinc Coating Systems

ALL milscale, rust and foreign matter are to be removed. Sand blasting or Shot blasting or grit blasting to a standard of Sa 3

2 Coat Inorganic Zinc	(<u>2 × 20 microns</u>)
Total film Thickness	<u>40 microns</u>

2. Epoxy Coating Systems

ALL milscale, rust and foreign matter are to be removed, Sand blasting or Shot blasting or grit blasting to a standard of min. Sa 2.5

1 Coat Epoxy Zinc Rich Primer	(1 × 18 microns)
1 Coat Special Epoxy Anticorrosive Primer HB	(1 × 75 microns)
1 Coat Special Epoxy Undercoat HB	(1 × 75 microns)
1 Coat Special Epoxy finish HB	(<u>1 × 75 microns</u>)
Total film Thickness	<u>243 microns</u>

C. Fresh Water Tank

1. Vinyl Coating Systems

ALL milscale, rust and foreign matter are to be removed Wire brushing to a standard of min. St 3

1 Coat Etching Primer	(1 × 15 microns)
4 Coats Special Vinyl Anticorrosive Primer	(4 × 20 microns)
2 Coats Special Vinyl Finish	(<u>2 × 25 microns</u>)
Total film Thickness	<u>145 microns</u>

2. Epoxy Coating Systems

ALL milscale, rust and foreign matter are to be removed Sand blasting or Shot blasting or grit blasting to a standard min. Sa 2.5

1 Coat Epoxy Zinc Rich Primer	(1 × 18 microns)
1 Coat Special Epoxy Anticorrosive Primer HB	(1 × 75 microns)
1 Coat Special Epoxy Undercoat HB	(1 × 75 microns)
1 Coat Special Epoxy Finish HB	(<u>1 × 75 microns</u>)
Total film Thickness	<u>243 microns</u>

III. Steel Structural Coatings

1. Alkyd Coating System.

ALL milscale, rust and foreign matter are to be removed. Wire brushing to a standard of min. St 2

1 Coat Etching Primer	(1 × 15 microns)
2 Coats Alkyd Anticorrosive Primer	(2 × 35 microns)
2 Coats Alkyd Enamel	(<u>2 × 30 microns</u>)
Total film Thickness	<u>145 microns</u>

2. Chlorinated Rubber Coating System.

ALL milscale, rust and foreign matter are to be removed. Sand blasting or Shot blasting or grit blasting to a standard of min. Sa 2.5

1 Coat Epoxy Zinc Rich Primer	(1 × 18 microns)
2 Coats Chlorinated Rubber Anticorrosive Primer	(2 × 40 microns)
2 Coats Chlorinated Rubber Finish	(<u>2 × 35 microns</u>)
Total film Thickness	<u>168 microns</u>

3. Vinyl Coating System.

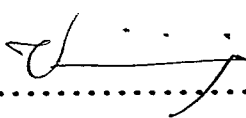
ALL milscale, rust and foreign matter are to be removed. Sand blasting or Shot blasting or grit blasting to a standard of min. Sa 2.5

1 Coat Epoxy Zinc Rich Primer	(1 × 18 microns)
3 Coats Vinyl Anticorrosive Primer	(3 × 25 microns)
2 Coats Vinyl Finish	(<u>2 × 25 microns</u>)
Total film Thickness	<u>143 microns</u>

4. Epoxy Coating Systems

ALL milscale, rust and foreign matter are to be removed. Sand blasting or Shot blasting or grit blasting to a standard of min. Sa 2.5

a) 1 Coat Epoxy Zinc Rich Primer	(1 × 18 microns)
2 Coats Epoxy Anticorrosive HB Primer	(2 × 100 microns)
1 Coat Epoxy Undercoat	(1 × 60 microns)
1 Coat Epoxy Finish	(<u>1 × 40 microns</u>)
Total film Thickness	<u>318 microns</u>
b) 1 Coat Epoxy Zinc Rich Primer	(1 × 18 microns)
2 Coats Epoxy Anticorrosive HB Primer	(2 × 100 microns)
1 Coat Epoxy Undercoat	(1 × 60 microns)
1 Coat Acrylic Modified Epoxy Finish	(<u>1 × 35 microns</u>)
Total film Thickness	<u>313 microns</u>
c) 1 Coat Epoxy Zinc Rich Primer	(1 × 18 microns)
2 Coats Epoxy Anticorrosive HB Primer	(2 × 100 microns)
1 Coat Epoxy Undercoat	(1 × 60 microns)
1 Coat Polyurethane Finish	(<u>1 × 35 microns</u>)
Total film Thickness	<u>313 microns</u>


.....

(Mr. Vinij La-onsuwan)

STRESS CORROSION CRACKING IN STAINLESS STEEL

PIPING MATERIALS 304 AND 321 AND WELDMENT

NARONG SUKAPADDHI

ABSTRACT

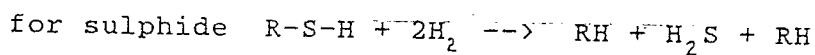
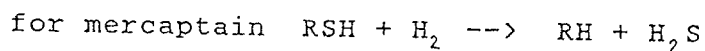
In November 1988, the stainless steel linework grade AISI 304 and 321 from hydrodesulphurizer reactor R-1401 to effluent exchangers E-1401C failed during start up by leaking from two cracked weldjoints on pressurizing the unit. The cracks which were detected at weldmetal and fusion zone could be largely attributed to original weld defects, which had been slowly growing over the 17 years of operation due to thermal stresses and/or environmentally assisted stress cracking (Polythionic acid SCC).

These cracks were intergranular in nature resembling hot-crack or solidification cracking since it occurred at the center of the weld in fully austenitic material which is prone to this type of cracking. Upon the renewal of all weldjoints, further cracks were found in piping and fittings of the new weld preparations appearing to be transgranular and showing numerous branches, typical of chloride stress corrosion cracking. The cracks in the fusion zone propagating into parent metal were transgranular in nature.

Conclusion can be drawn that the internal cracks in piping material and weld deposit of 310 material most probably originated from hot cracking and stress cracking induced by chloride/sulphide and polythionic acid. While the external cracks at piping and fitting could attributed to chloride and/or sulphide stress corrosion cracking from insulation and atmosphere via rain water ingress.

INTRODUCTION

The hydrodesulphurization unit is designed for treatment of gas oil using hydrogen. During this treatment the sulphur in the sulphur compounds is converted into H₂S which is removed to the sulphur plant according to the reactions. :



Some of unsaturated hydrocarbons also become saturated paraffin.

Olefin + H₂ ---> paraffin

Cyclo-olefin + H₂ ---> naphthene

Diolifin + 2H₂ ---> paraffin

Thai Oil Refinery operates HDS for treating unsaturated and sulphur contaminated gas oil from fluid catalytic cracking (FCC) and thermal cracking (TC) units. The reactor circuit piping of the unit has been upgraded from low alloy to AISI 321 piping since 1972 (commissioning in 1970) because of too high corrosion rates of the low alloy piping. The unit which has been operated in the on and off mode developed a leak in the reactor circuit piping on starting up (Nov.88).

Because of the nature of the cracking all existing welds were radiographed resulting in the discovery of further defective weldjoints. Based on this result the decision was taken to renew all welds of the reactor circuit, except the heater section welds, which proved to have been made with 347 weld consumable. Before repair but sometime after opening the unit, the piping concerned was given a neutralizing wash with soda ash and nitrate solution (5% Na₂CO₃ + 2% NaNO₃). Upon weld metal checking with our Texas nuclear (Model 9266) it was found that the effluent line P-14006 was made of AISI 304 instead of AISI 321 as was supposed to be the case. With LPI checking of weld bevel and the vicinity base metal cracking was found externally in 8" elbow and 4" return bends of the convection bank of heater H-1401. On the basis of this it was decided to renew effluent line P-14006.

PRELIMINARY INSPECTION

1. Radiographical inspection was carried out after leaking on the reactor circuit and in total 5 welds were found to be defective. All cracks started in the root run and remained in the austenitic 310 weld deposit. Crack propagation in circumferential direction showed to be much faster than in through thickness direction. There were two joints in which the cracks were wall penetrating i.e. No.5 and 6 located at the elbow connecting (see attached diagram) the horizontal line to vertical section running to exchanger E-1401 C.
2. This line (P-14006) is for flexibility reasons hanging from pipe rack between reactor and heat exchanger structure (Figure 1). Crack length in joint No.5 was internal 225 mm. external two cracks 5 and 10 mm. separately. RT on joints 3, 4 and 13 revealed cracks which were not wall penetrating.

3. LPI inspection was carried out on weld bevel preparations and immediate vicinity during the replacement of AISI 310 weld deposit by AISI 347. Texas nuclear instrument was used to check complete removal of AISI 310 weld deposit. The followings were found.
 - 3.1 Most of piping material at P-14006 was AISI 304 except for elbows which were AISI 321.
 - 3.2 Close to the weld in pipe material straight cracks perpendicular to the weld, none of which showed to be wall penetrating yet, some 1/2 - 2/3 of weld thickness deep.
 - 3.3 At random areas but also in the vicinity of weld small wavy, numerously branched cracks were found at random orientation also not wall penetrating yet.
 - 3.4 Elbow in P-14006 (Figure 2) and return bend in convection bank of H-1401 in several cases suffer from superficial hairline crack but 2 of return bends were severely cracked.
 - 3.5 Areas where during construction temporarily pieces have been welded to the piping and fittings, showed a wavy type of superficial cracking at these locations.
 - 3.6 On rehydrotest after the complete preliminary weld repair of joint Nos 3,4,5,6 and 13 one of the original weld failed (No.11).

FAILURE ANALYSIS

Two samples were cut for failure analysis in order to determine the cause and mechanism of failure pipe. They as follows :

- First sample was removed from a 8" diameter pipe at the location of the weldment to elbow (Point No.5) in line from the hydrodesulfurisation (HDS) Reactor to feed/effluent heat exchanger. Dye-penetrant check was conducted prior to cutting.
- Second sample was removed from a 90 degree elbow (between point No.10 and 11) in line from the hydrodesulfurisation (HDS) Reactor to feed/effluent heat exchanger.

These samples were sent to Veritec Laboratory, Singapore for further thorough investigation of the cause of failure.

METHOD OF INVESTIGATION.

The following work scope was carried out.

- Visual Inspection.
- Macro-examination.
- Metallography.
- Micro-hardness Check.
- Energy Dispersive Spectrometry/Scanning Electron Microscopy.
- Chemical Composition Analysis.

RESULT OF FIRST SAMPLE.

VISUAL INSPECTION.

The as-received sample is shown in Figure 3. Pin hole was observed at the weld toe of both internal and external surface. A reference portion was removed before other non-destructive tests were carried out to avoid further contamination and also be used as a calibration reference for analysis. Dye penetrant test gave pin-hole surface defect indication both on internal and external surface. No other significant defect was observed. The sample was further sectioned for other analysis. The dye-penetrant test and the cut samples are shown in Figure 4.

MACRO-EXAMINATION.

The cut samples as in Figure 4 (C) were ground, polished and etched electrolytically with oxalic acid. The macro sections of the various cut sections are shown in Figure 5 (a) and Figure 5 (b). In general, the weldment contained the following defects :

- Slight under-cut at weldment.
- Pitting and cracking at weld surface.
- Lack of root fusion at root toe between weld and 9 mm. thick pipe materials.
- Weld contains micro-intergranular cracks.
- Porosity of size 0.2 mm to 1.1 mm.

METALLOGRAPHY.

The etched surface of macro 3 sample was selected for further study. The micrographs are shown in Figure 6 to Figure 8. The metallographic observation is tabulated in Table 1.

Table 1 - Metallographic Observation.

Location	Microstructure	Reference Figure
12mm pipe	- Coarse austenitic grains with annealing twins.	6a
9 mm pipe	- Deformation resulting from dislocation within each grain along the rolling direction. - Numerous precipitation observed at grain boundaries. - Elongated inclusion along rolling direction.	6b
Fusion zone 9mm/weld	- Lack of fusion and also lack of inter-run fusion in weld adjacent to fusion line. - Numerous intergranular corrosion attack at 9mm pipe internal surface adjacent to root toe.	7
Weld	- Numerous intergranular cracks.	8

ENERGY DISPERSIVE SPECTROMETRY (EDS)/SCANNING ELECTRON MICROSCOPY.

Scanning Electron Microscopy was carried out on the etched surface of macro 3 sample. The Scanning Electron Microscope was coupled to the Energy Dispersive Spectrometer where selected location on the etched surface could be analysed for type of elements present. The EDS spectrums at various locations are shown in Figure 9 to Figure 12.

The intermetallic phase in the 12.5 mm pipe material was found to contain titanium (Figure 9). This is titanium cubonitride. However, the stabilizing effect seems not to be sufficient because chromium carbides are clearly visible at the grain-boundaries. The 9 mm. pipe material (Figure 10) contain silicate slag stringers in addition to clearly visible grain-boundary precipitation (normally is chromium carbides, Cr₄C).

The scale layers in the root crack tip contained chromium with traces of silicon and sulphur (Figure 12).

HARDNESS TEST.

Hardness measurement was carried out on macro 2 sample, using Zwick hardness tester. The locations and readings are shown in Figure 13 and Figure 14.

The summary of the results is tabulated in Table 2.

Table 2 - Hardness Reading in HV5.

Location	Range	Average
9mm pipe	201 - 224	210
HAZ 9mm/weld	211 - 243	227
Weld	243 - 298	266
HAZ Weld/12.5mm	204 - 242	215
12.5mm pipe	196 - 218	209

CHEMICAL ANALYSIS.

Chemical analysis was carried out on the sample, using inductive coupled plasma and combustion method. The results are tabulated in Table 3.

Table 3 - Chemical Composition in Percentage.

Element	Pipe Materials			Weld Materials	
	9.0mm	12.5mm	SS321 Specification	Weld	SS310 Specification
C	0.05	0.04	0.08 max.	0.12	0.25 max.
Mn	1.63	1.70	2.00 max.	2.19	2.00 max.
Si	0.36	0.37	1.00 max.	0.37	1.50 max.
Cr	19.4	18.8	17.0 - 19.00	25.9	24.0 - 26.0
Ni	9.3	11.3	9.0 - 12.0	17.7	19.0 - 22.0
P	< 0.010	< 0.010	0.045 max.	< 0.010	0.045 max.
S	< 0.010	0.015	0.03 max.	< 0.010	0.03 max.
Ti	< 0.01	0.20	0.20 min.	0.01	0.60 min.

The chemical analysis shows that the weld metal does not comply with stainless steel type 310 (carbon, nickel and titanium are out of specification). The 9.0 mm thick pipe material is of stainless steel type 304, which confirmed Thairoil field chemical analysis by Alloy Detector (Texas Nuclear).

RESULTS OF SECOND SAMPLE.

VISUAL INSPECTION.

The as-received sample is shown in Figure 15. The ground surface was observed to have dye penetrant stain (Preliminary check at site) exhibiting cracks. A confirmative dye penetrant test (Figure 16) was conducted and it was found that the cracks on the ground surface were of branching nature. This surface is the external surface. No crack was observed on the internal surface. The through thickness view in Figure 16 showed clearly propagating crack from external surface towards internal surface.

METALLOGRAPHY.

The as-received sample was cut as shown in Figure 17. The cut plates was ground, polished and etched electrolytically with 10% oxalic acid. The micrographs are shown in Figure 18 and Figure 19.

The metallography at these cut sections showed severe branching cracks initiated at the external surface and propagating inwards into the internal surface.

The microstructure exhibited austenitic grains with annealing twins.

ENERGY DISPERSIVE SPECTROMETRY (EDS).

The EDS spectrum at various locations of the cracks is shown in Figure 20.

The scale layers in the crack contained traces of calcium, chloride and sulphur.

HARDNESS TEST.

Hardness measurement was carried out on the cut and etched section using Zwick hardness tester. The locations and readings are shown in the figure below.

Calibration	:	242	HV
Load	:	5	kg

All readings in HV.

No significant variation in hardness was observed in the parent material and at the crack vicinity.

The average hardness is 135 HV.

CHEMICAL ANALYSIS.

Chemical analysis was carried out on the sample, using inductive coupled plasma and combustion method.

The results are tabulated below :

Chemical Composition in Percentage.

Element	Elbow Materials	SS 321 Specification
C	0.06	0.08 max.
Mn	1.74	2.00 max.
Si	0.38	1.00 max.
Cr	19.00	17.0 - 19.0
Ni	11.70	9.0 - 12.0
P	0.010	0.045 max.
S	0.010	0.03 max.
Ti	0.22	0.20 min.

The chemical analysis shows that the elbow material complies with stainless steel type 321.

DISCUSSION.

Two distinctive morphologies of crack in these two samples are clearly distinguishable. The welding cracking found in fusion zone and in welding material are intergranular in nature meanwhile in the pipe fitting cracks are transgranular in nature and branching, propagating from external to internal surface. This suggested that the mechanism of cracking of each sample should be different.

The problem occurred in the weldment and at the fusion zone between the weld and the 9 mm thick pipe material, namely pin hole and microcrystalline cracking.

The 9mm thick pipe material itself has some degree of internal residual stress carried over from manufacturing technique which can be evidenced by the deformation in the rolling direction (Figure 6b). With the presence of numerous elongated silicate rich inclusions present, the 9 mm thick pipe material is highly susceptible to formation of sigma phase during welding especially at the fusion zone.

The welding of fully austenitic welding material 310 is prone to have such hot cracking on solidification. From Schaeffler diagram, the chromium and nickle equivalent as computed from chemical content of weld deposit show risk of hot cracking and σ -phase embrittlement (Figure 21).

The analysis of corrosion deposit showed sulphur on internal surface crack. Some of them had been washed away by neutralizing solution before the unit was shutdown. A very small amount of O and moisture ingress into the unit the polythionic ($H_2S_2O_x$, $x = 3-5$) can form at the metal surface. It is noted that this unit has never been neutralized when idle up to failure date. Therefore the austenitic stainless steel piping likely to suffer from stress corrosion cracking by polythionic acid (1).

As negligible titanium element is present in the weld material and 9mm thick pipe material, chromium carbides precipitated at grain boundaries were evident. With depletion chromium at the grain boundary vicinity, the material is susceptible to the intergranular corrosion attack (2).

In the investigation of the weld longitudinal crack was detected at fusion zone. Perpendicular to this crack, small branching cracks were found in pipe base material (304), transgranular in nature (Figure 20). This cracking could be attributed to chloride SCC. The source of chloride is from the platformer unit as organic chloride is injected to activate the catalyst and hydrogen by product rich gas is routed to HDS unit. The HCL removal (V-1616) has been installed in 1984, probably H₂S gas from platformer which is already contaminated with HCL may be the source of Cl and cracking may have possibility to start before installation of this vessel.

Halide stress corrosion cracking is a serious problem in the chemical industry. Perhaps the most significant environments producing SCC in austenitic steels are SCC in austenitic steels in aqueous solutions of chlorides at elevated temperatures. In practice it is rare for failures to occur below 70-80 C (3-4). Even small concentrations of chlorides may cause SCC provided there is oxygen. A sample of U-bend specimens of Type 321 will crack within 8 days in 70 ppm O₂ is present in a 0.02 % NaCl solution at pH2 and 150 C (5) (Figure 22).

The possible cause of external surface cracking at elbow, based on the investigation result, chloride/sulphide could possibly be attributed to the cracking.

The presence of sulphur and chloride element may be from the insulating material/and probably existed as atmospheric hydrogen sulphide gas trapped in the insulation via rain water ingress.

The chloride and hydrogen sulphide accumulation at the surface together with high temperature and operating stresses with on and off mode of operation, thermal stress or low cycle high strain fatigue can superimpose on the piping system and initiate SCC.

CONCLUSION.

- The leaks in weldment and fusion zone were caused by weld defect, with the environment stress corrosion assisting.
- The piping material 304 of non-stabilized grade had internal crack extending from weldjoint due to chloride/polythionic stress corrosion cracking.
- The external surface of fitting had cracking caused by the chloride/sulphide stress corrosion cracking.

CORRECTIVE AND PREVENTIVE MEASURE.

With the type of cracking mentioned the estimation of the remaining servicability becomes virtually impossible, because of the many variations in possible crack propagation rates. The linework of 304 piping (P-14006) was totally renewed with 321 material except for the reactor reducer, 10" lapjoints and branch nipple as no material were available. The reducer was ground till crack free by LPI check. The deep excavations were fill welded and ground smooth. Because those lineworks in the heater circuit found to be 321 material, the original weldjoints of 310 were totally renewed with type 347. Some parts of cross over section particularly for elbow which contained surface crack were renewed.

The complete weld and pipe renewal were accomplished and followed by hydrostatic test. Aluminium silicone paint system and low chloride insulation were applied as specified in DEP 30.48.00.31 GEN (painting and coating) and 30.46.00.31 GEN (insulation) respectively.

After inspection and repair as planned, Thai Oil intends to operate the plant and to replace the pipe system, 8"-P14002, 4" & 8" P-14004 and 8"P-14006 in about 8 months.

In future every shutdown will have to be followed by a neutralizing wash in case of possible ingress of air and moisture (6).

REFERNCES

1. Takeo Kudo, Yoshio Tarutani, Minoru Miura, Yoshiatsu Sawaragi and Michio Nishi :
347 AP Stainless Steel With High Resistance To Polythionic Acid SCC for Furnace Tubes : The Sumitomo Search No.36 May 1988.
2. J.L Robinson : Preferential Corrosion of Welds. Part 2. Austenitic Stainless Steels : The Welding Institute Research Bulletin, February 1979.
3. Honeycombe J and Gooch TG : Metal Construction and British Welding Journal 1973 5 (4) 140.
4. Truman J.E in ISI Publication 117 : Stainless Steels 1969.
5. Heinz Spahn : Performance Requirements for Stainless Steels in the Chemical Process Industry : Climax Molybdenum Publication ; Stainless Steels 77 : 1977.
6. NACE - Standard RP-01-70
7. DEP 30.48.00.31 GEN
8. DEP 30.46.00.31 GEN

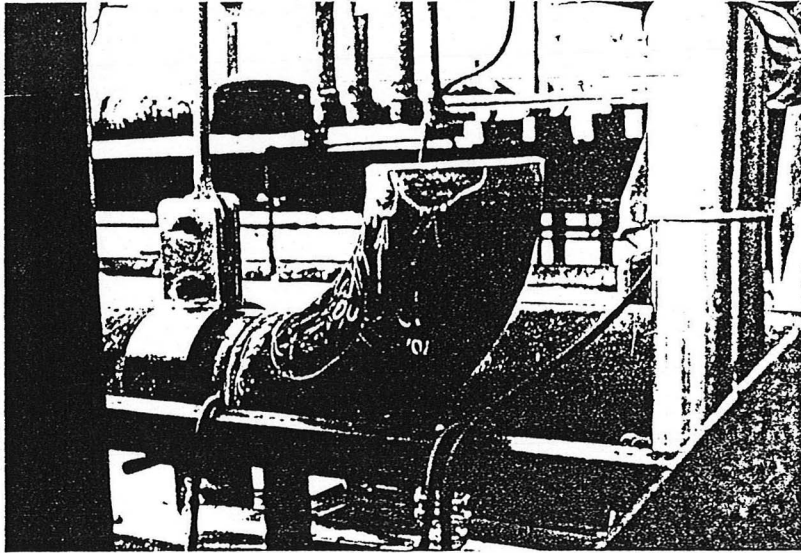


Figure 1 Run pipe between outlet R-1401 to E-1401 C

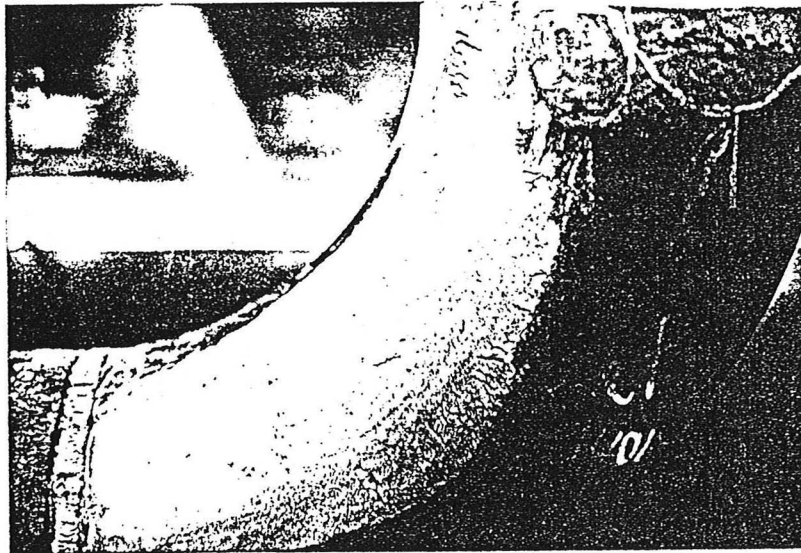
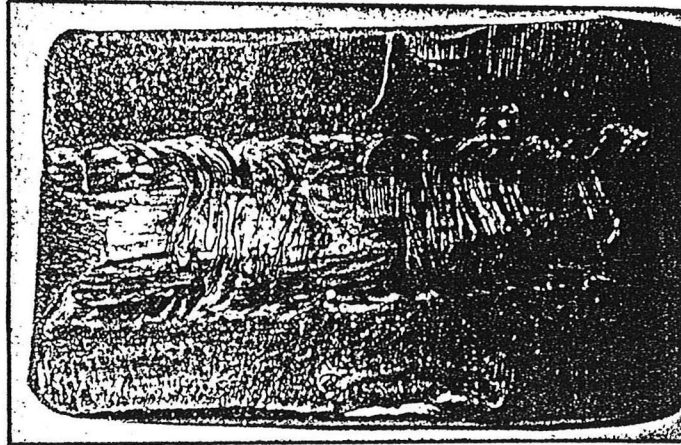
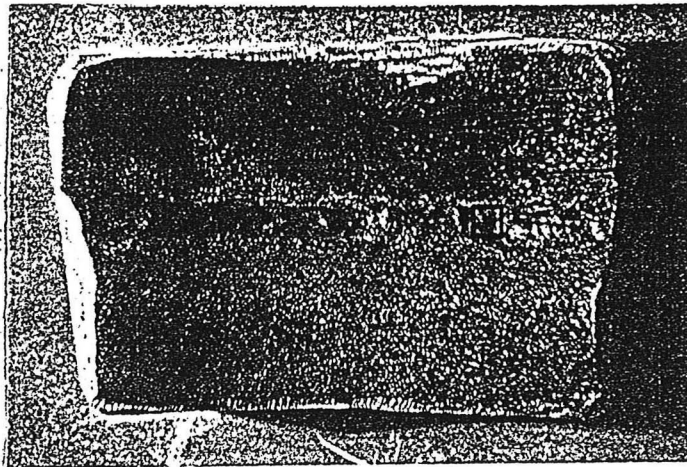


Figure 2 Close up of elbow in Figure 1 to show surface cracks.



(a) External surface



(b) Internal surface

Figure 3 - As-received sample

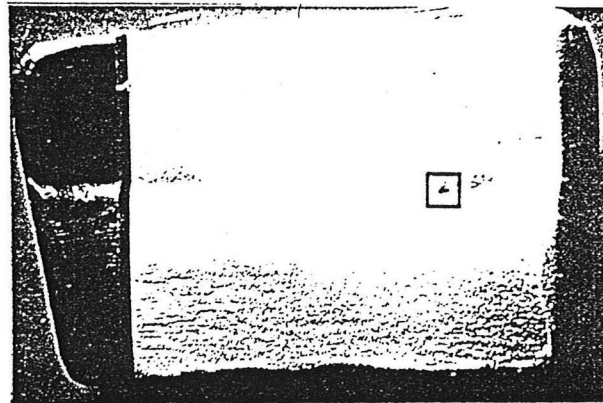
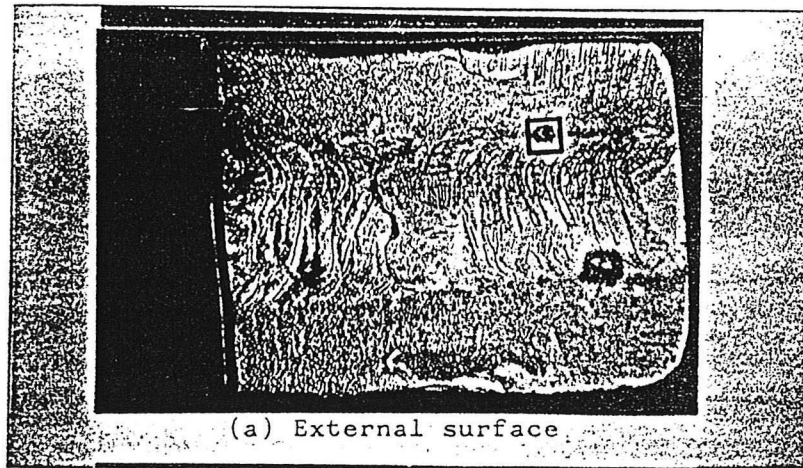


Figure 4 - (a) Dye-penetrant test on external surface giving defect indication.
(b) Dye-penetrant test on internal surface giving surface defect indication.
(c) Cut samples with arrows showing section plane for macro-examination. Note that "ref" was cut before test were carried out to avoid further contamination and also be used as a calibration reference for analysis.

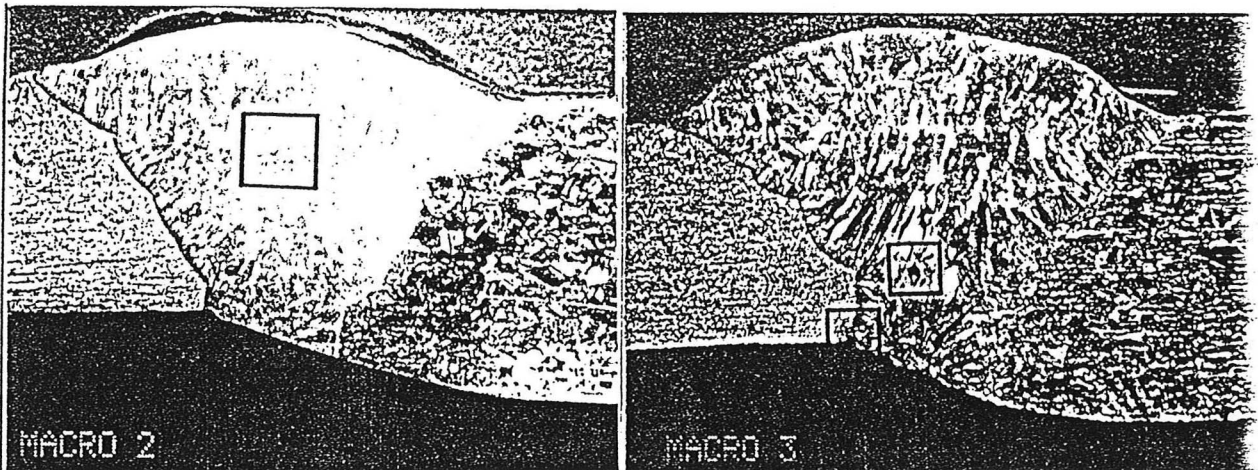
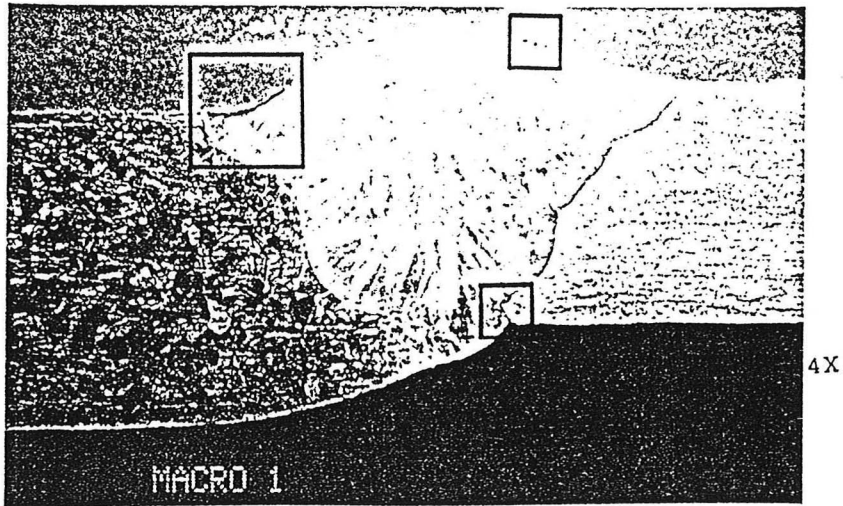


Figure 5 (a) - Macro-examination of weldment.

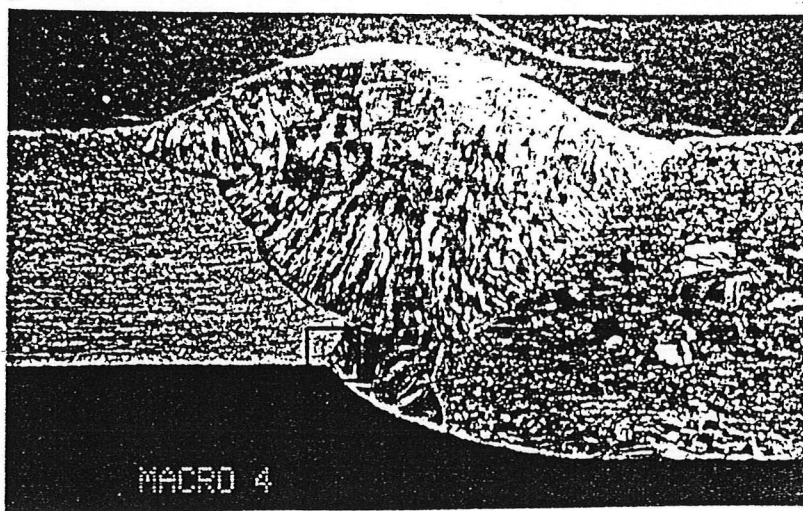
See also Figure 2c.

Macro 1 - Slight under-cut on top-left of weld.
 - Also pitting/crack at weld surface.
 - Lack of root fusion (right side) about 0.5mm.

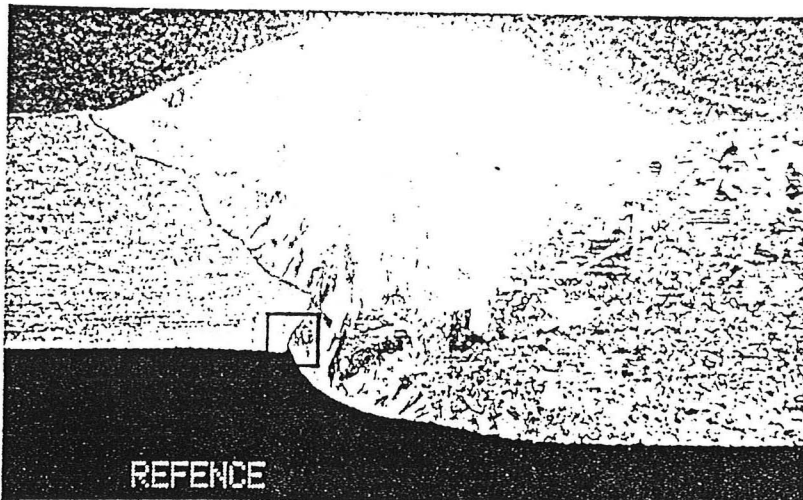
Macro 2 - Lack of inter-run fusion in weld.

Macro 3 - Porosity about 1.1mm in size.
 - Lack of fusion (left side).
 - Several micro cracks intergranular in nature in weld.

4X



4X

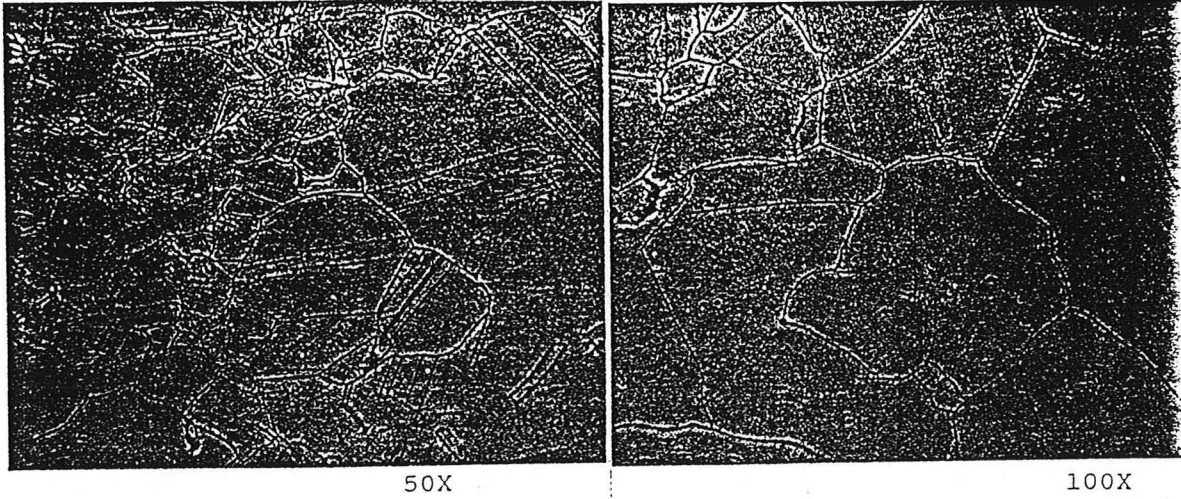
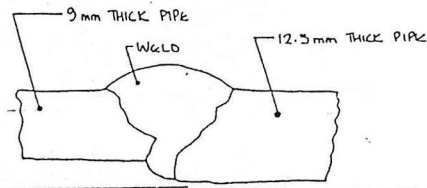


4X

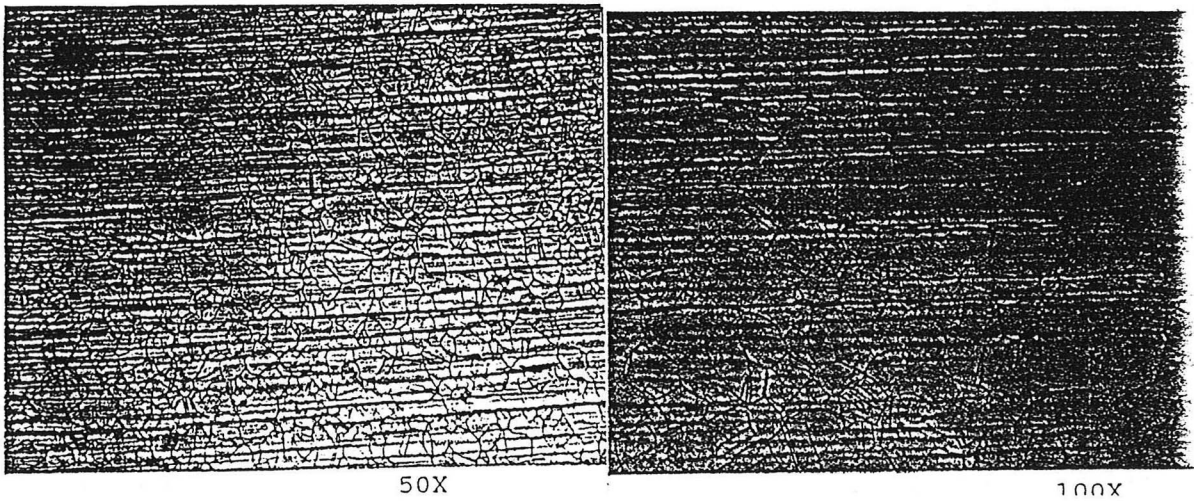
Figure 5 (b) - Macro-examination of weldment. See also Figure 4c.

Macro 4 - Lack of fusion (left side).
 - Porosity about 0.2mm in size.
 - Several micro-cracks intergranular in nature in weld.

Reference- Lack of fusion (left side).
 - Porosity about 0.2mm in size.
 - Several micro-cracks intergranular in nature in weld.



(a) 12.5mm thick pipe materials



(b) 9.0 mm thick pipe materials

Figure 6 - Metallography of pipe materials.

(a) Coarse austenitic grains with annealing twins.

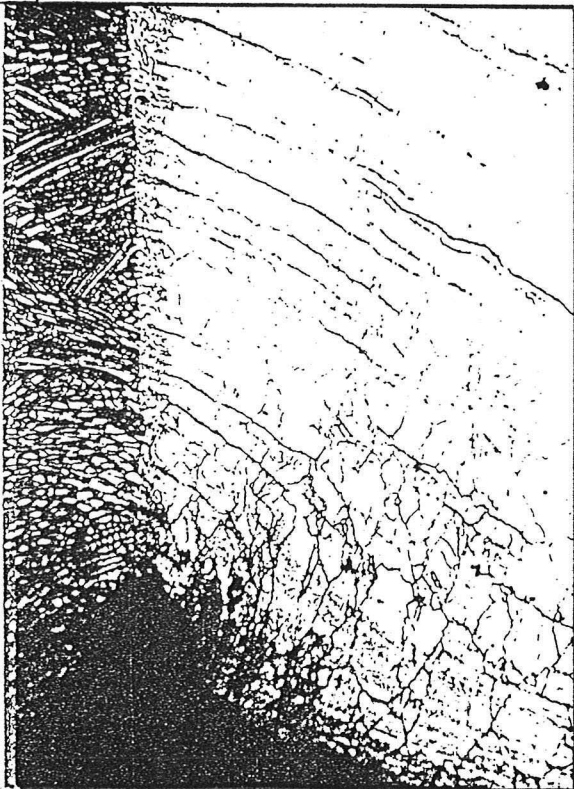
(b) Fine austenitic grains with annealing twins.

Micrograph exhibits degree of deformation resulting from dislocation within each grain along the rolling direction. Numerous precipitations and elongated inclusions are observed.

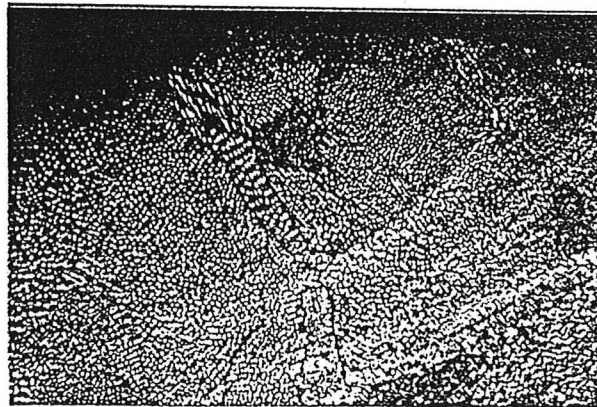
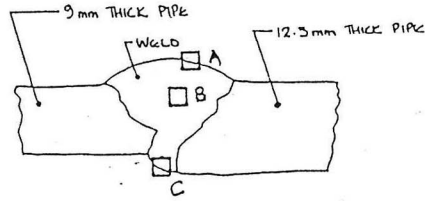


Location
A
200X

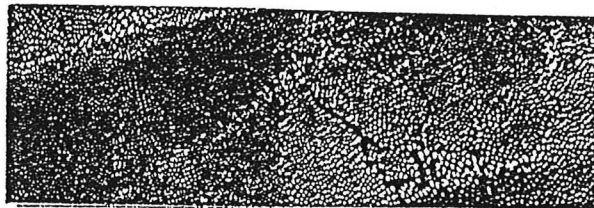
Figure 7 - Metallographic micrographs exhibiting defects at the fusion zone between the weldment and the 9mm thick pipe material. Besides root toe defect, intergranular corrosion is observed adjacent to the defect.



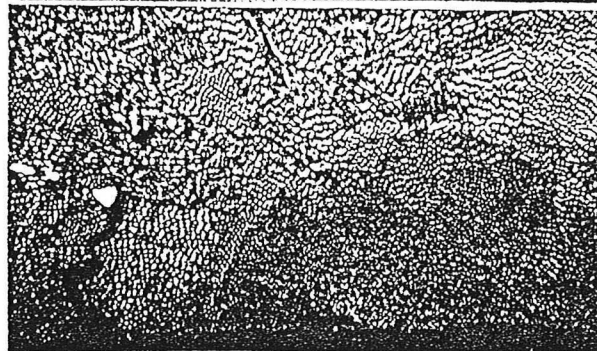
Location
B
100X



Location A
50X

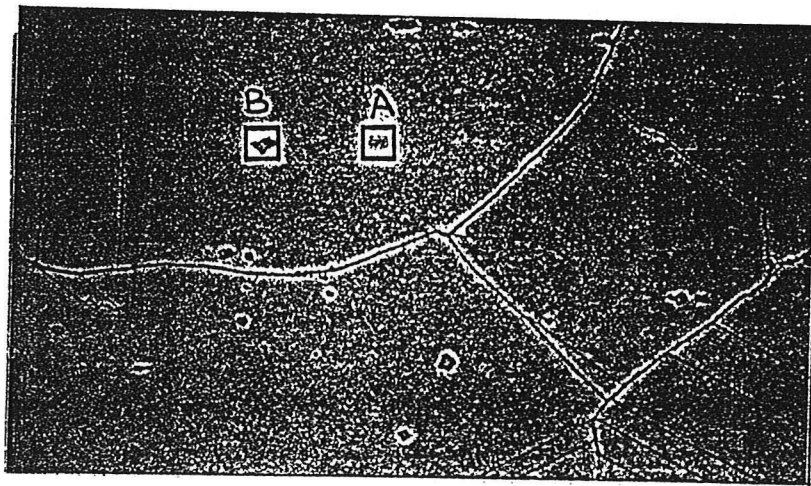
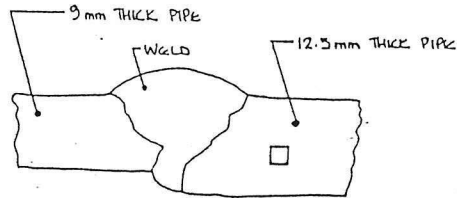


Location B
50X



Location C
50X

Figure 8 - Metallography exhibits weld defects.
Intergranular cracks found at the external surface, internal surface and internal of weld.



321 CNT 3480 EU 20 1K FE: A
Link Systems 840 Analyser 28-Dec-88

313 CNT 3480 EU 20 1K FE: A
Link Systems 840 Analyser 28-Dec-88

Location A

Location B

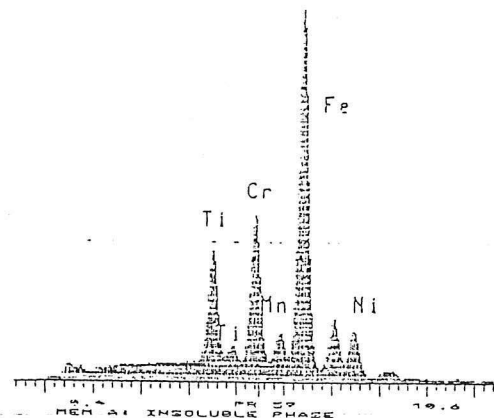
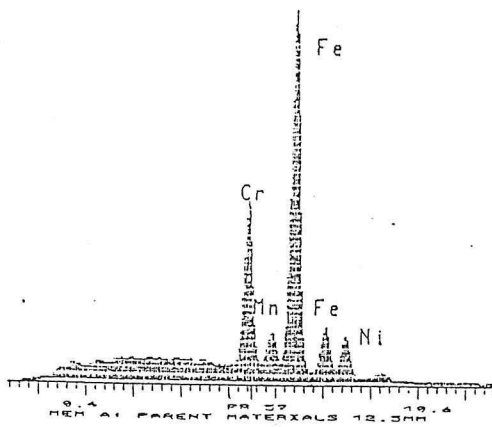
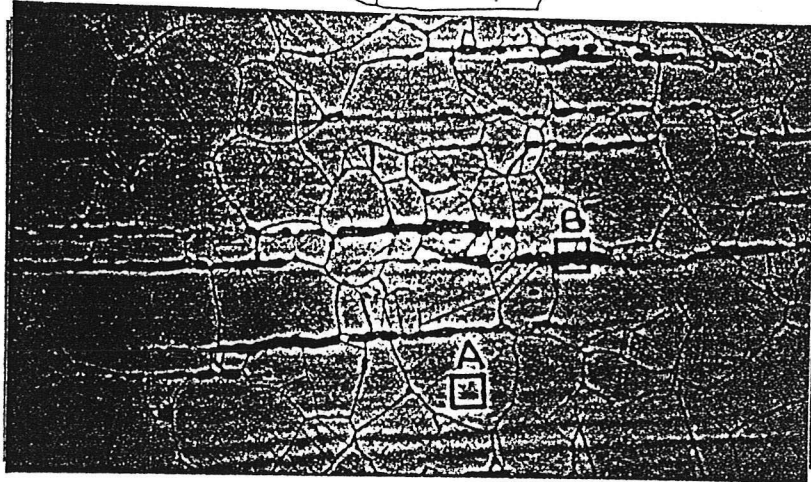
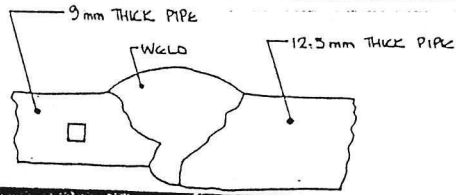


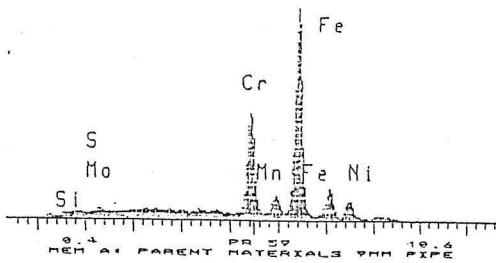
Figure 9 - Energy Dispersive Spectrum (bottom) showing presence of Ti in intermetallic phase of 12.5mm thick pipe. Metallographic micrograph (top) shows the intermetallic phase and grain-boundary probably chromium carbides.



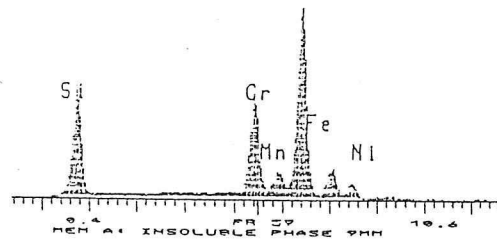
200X

181 CNT 5489 EV 20 1K FSI A
Link Systems 868 Analyser 28-Dec-88

189 CNT 5489 EV 20 1K FSI A
Link Systems 868 Analyser 28-Dec-88

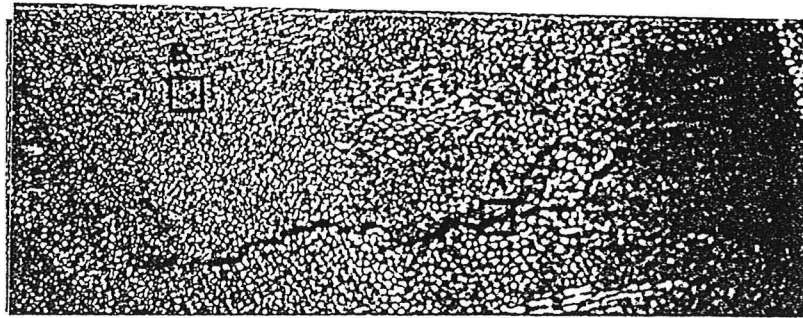
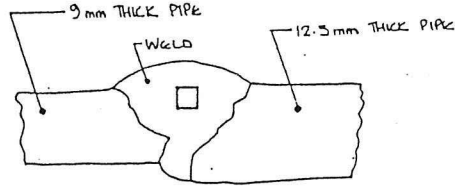


Location A



Location B

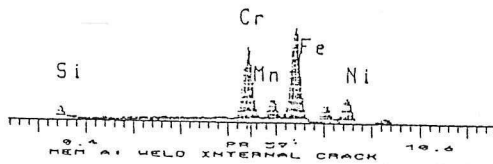
Figure 10 - Energy Dispersive Spectrum showing presence of Si in slag stringers of 9mm thick pipe. Metallographic micrograph (top) shows the slag stringers in addition to grain-boundary precipitates (probably Chromium carbides).



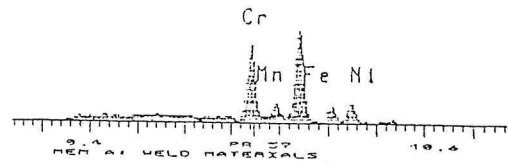
50X

131 CNT 5489 EU 20 1K FSI 2
Link Systems 488 Analyser 28-Dec-98

107 CNT 5489 EU 20 1K FSI 2
Link Systems 488 Analyser 28-Dec-98

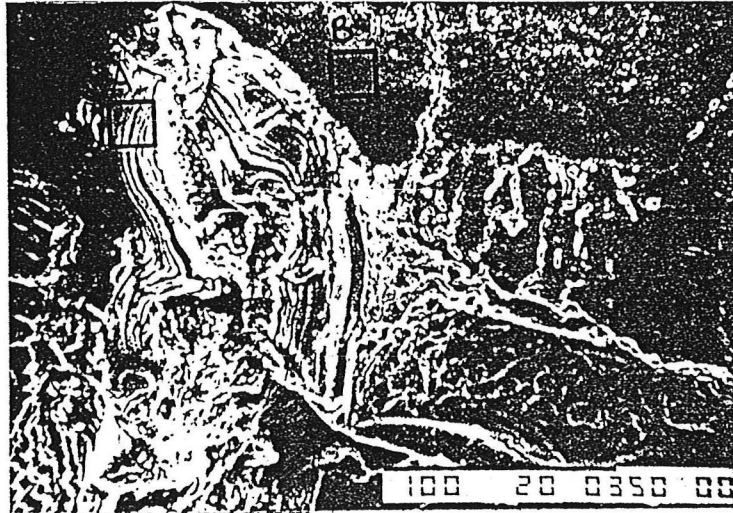
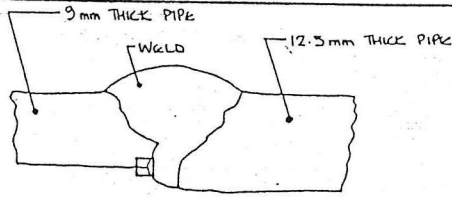


Location A



Location B

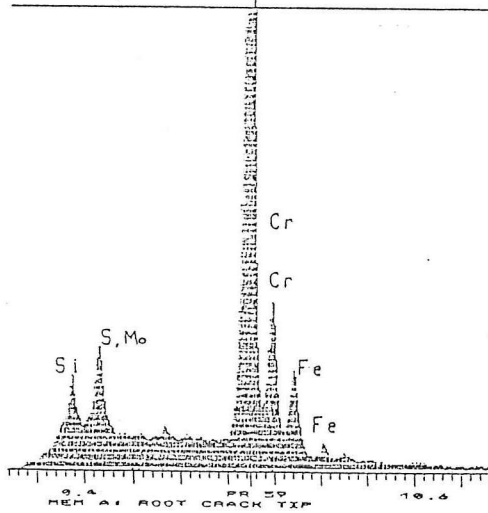
Figure 11 - Energy Dispersive Spectrum showing presence of Si, Cr, Mn, Fe and Ni in scale layer at weld micro-crack. The intergranular weld microcrack is shown in the metallographic micrograph (top).



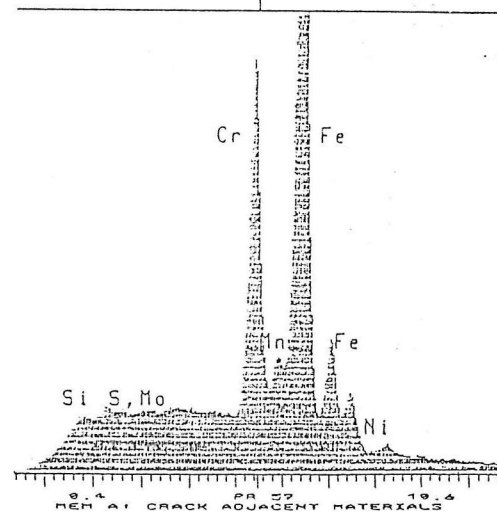
350X

781 CNT 5489 EU 20 1K PDI A
Link Systems 868 Analyser 28-Dec-88

784 CNT 5489 EU 20 1K PDI A
Link Systems 868 Analyser 28-Dec-88

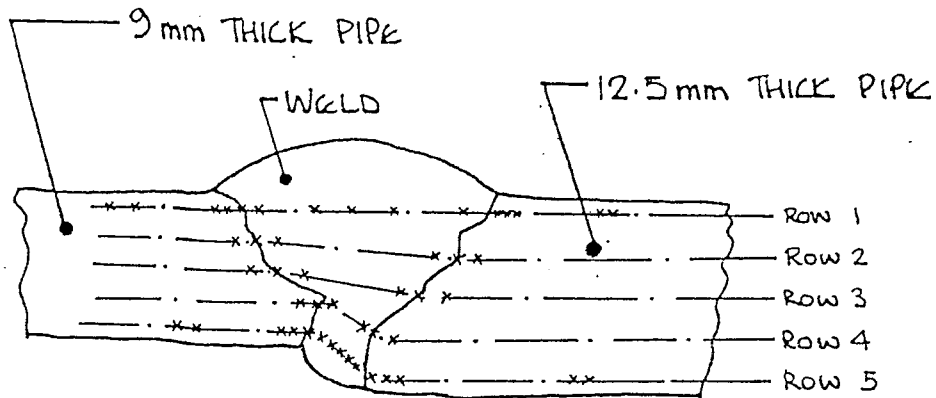


Location A



Location B

Figure 12 - Energy Dispersive Spectrum showing presence of Si, S, Cr and Fe at crack tip located at fusion zone indicated by \square . Scanning electron micrograph of crack revealed layers of scale form crack surface. Detailed macro-sections are documented in Figure 5.



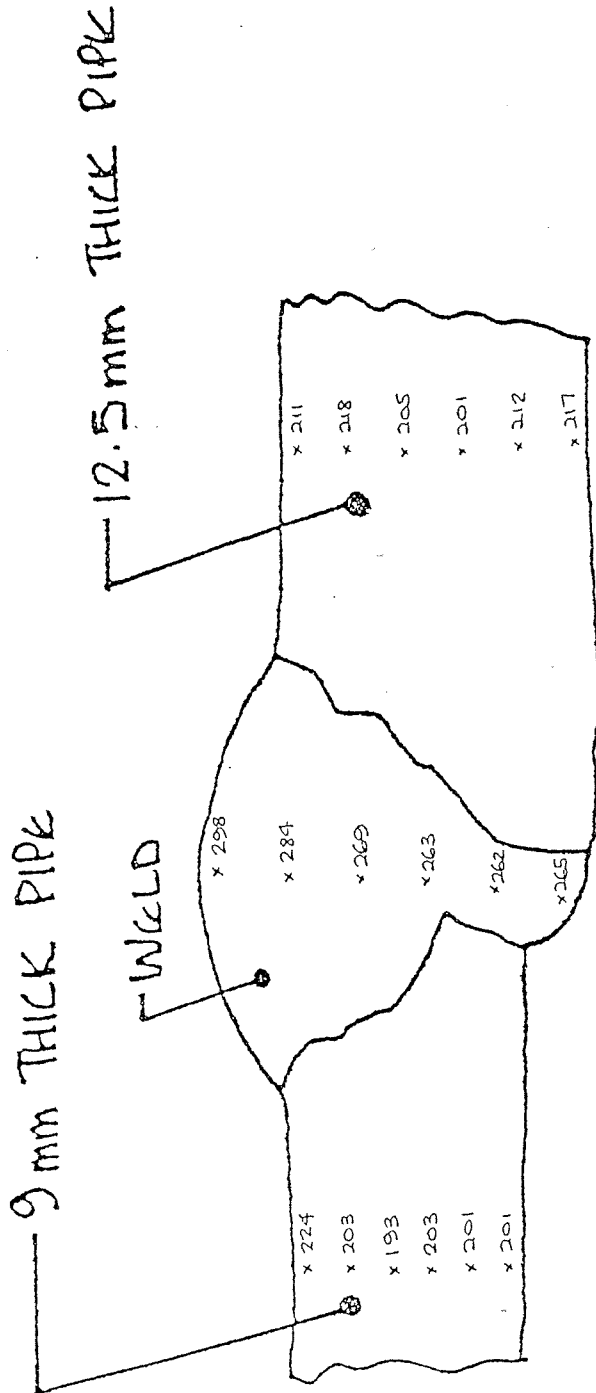
HARDNESS TAKEN FROM LEFT TO RIGHT

Load : 5 kgs

INDENTATION	ROW 1	ROW 2	ROW 3	ROW 4	ROW 5
1	218	244	213	211	221
2	216	243 HAZ	221 HAZ	230 HAZ	221
3	227	273	257	257	225
4	235 HAZ	267 Weld	281 Weld	243 Weld	219 HAZ
5	240	234	231	223	225
6	280	211 HAZ	204 HAZ	206 HAZ	258
7	257				265
8	262 Weld				260 Weld
9	273				243
10	286				253
11	226				242
12	195 HAZ				211 HAZ
13	200				207
14	199				196
15	216				217

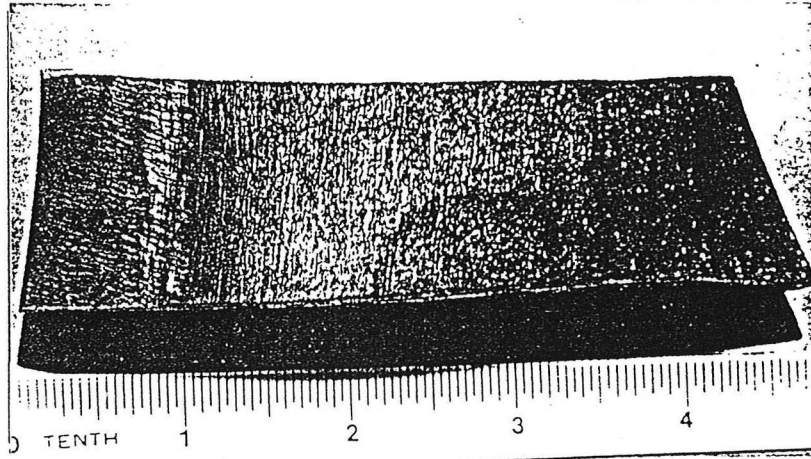
Reading in HV5.

Figure 13 - Hardness measurement on macro sample no. 2.



LOAD : 5 KGS
READING IN HV5

FIGURE 14 - HARDNESS MEASUREMENT ON MACRO SAMPLE NO. 2



Internal Surface

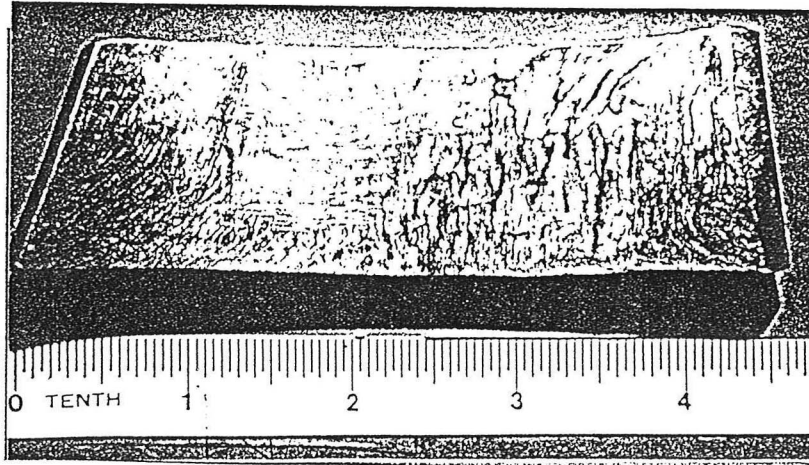
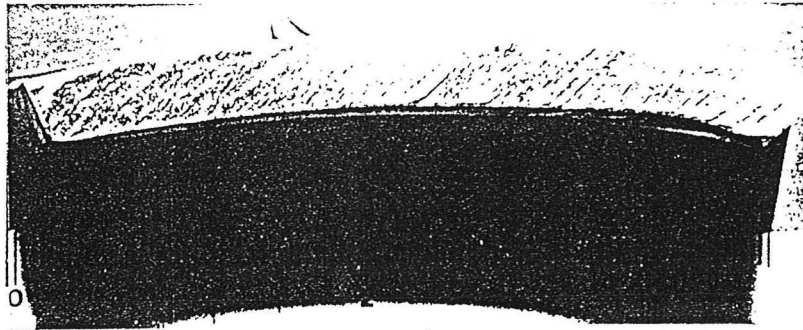


Fig 15 As received sample.

Report No.:

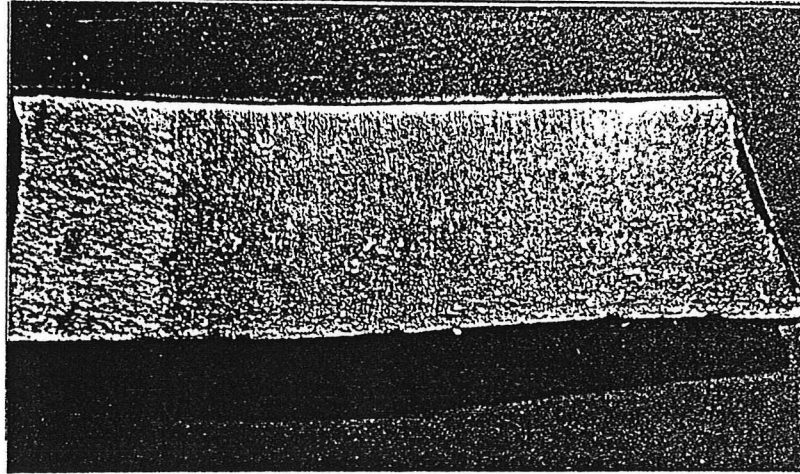
VT/MC/89013



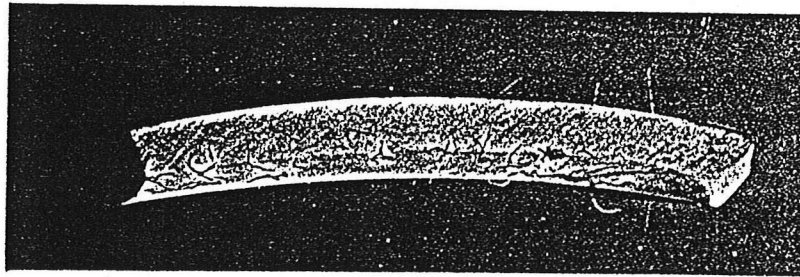
VERITEC
DnV Technology and Services Pte Ltd

Page No.:

7



Internal Surface



External Surface

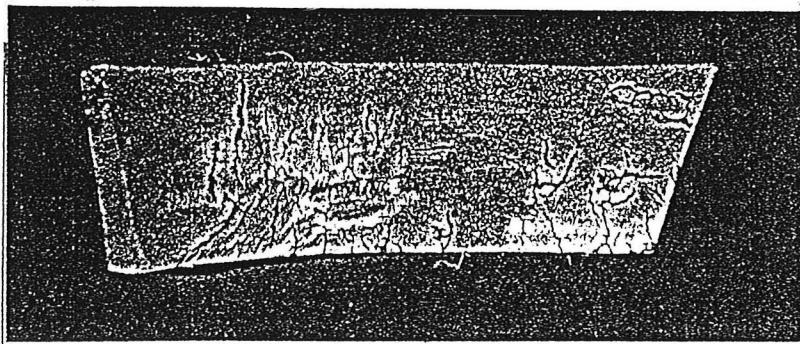
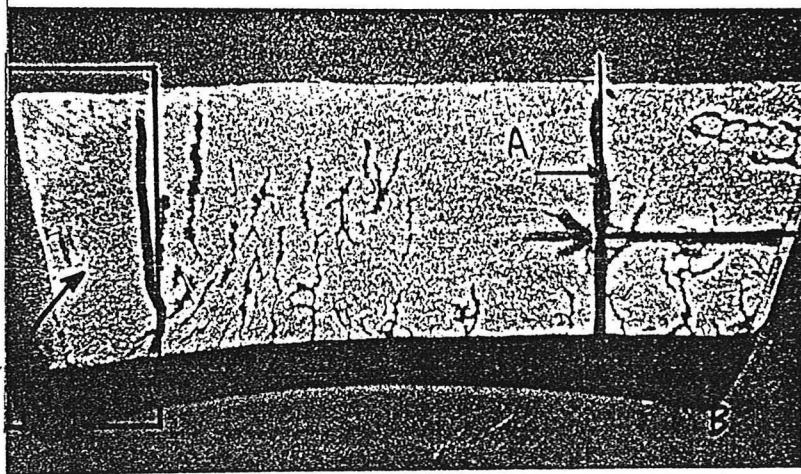


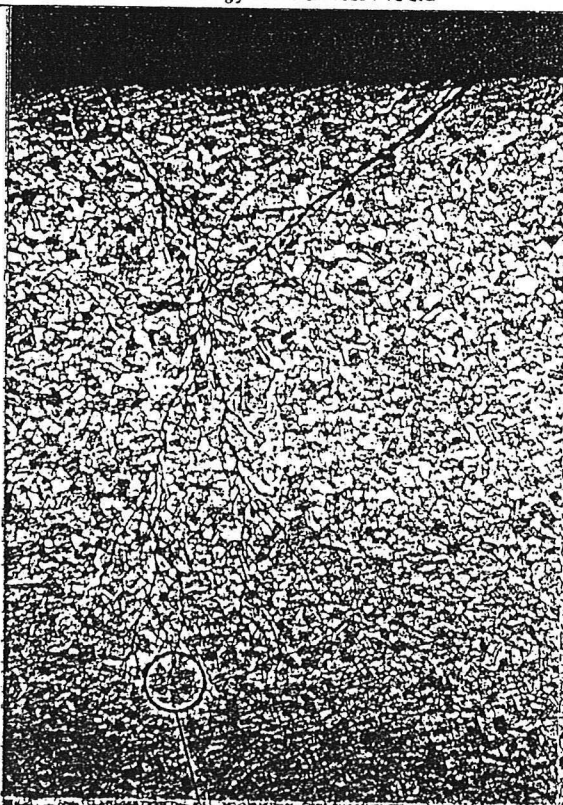
Fig 16 Dye Penetrant Test on as-received sample showing numerous branching cracks on external surface.



Material removed
from here for chemical analysis.



Fig 17 Cut section for further analysis.
Face A and face B for metallography.



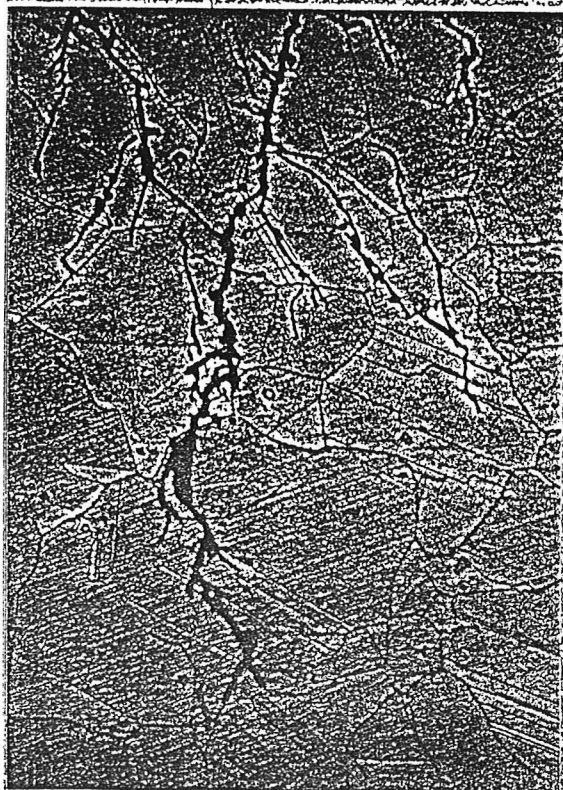
External
surface



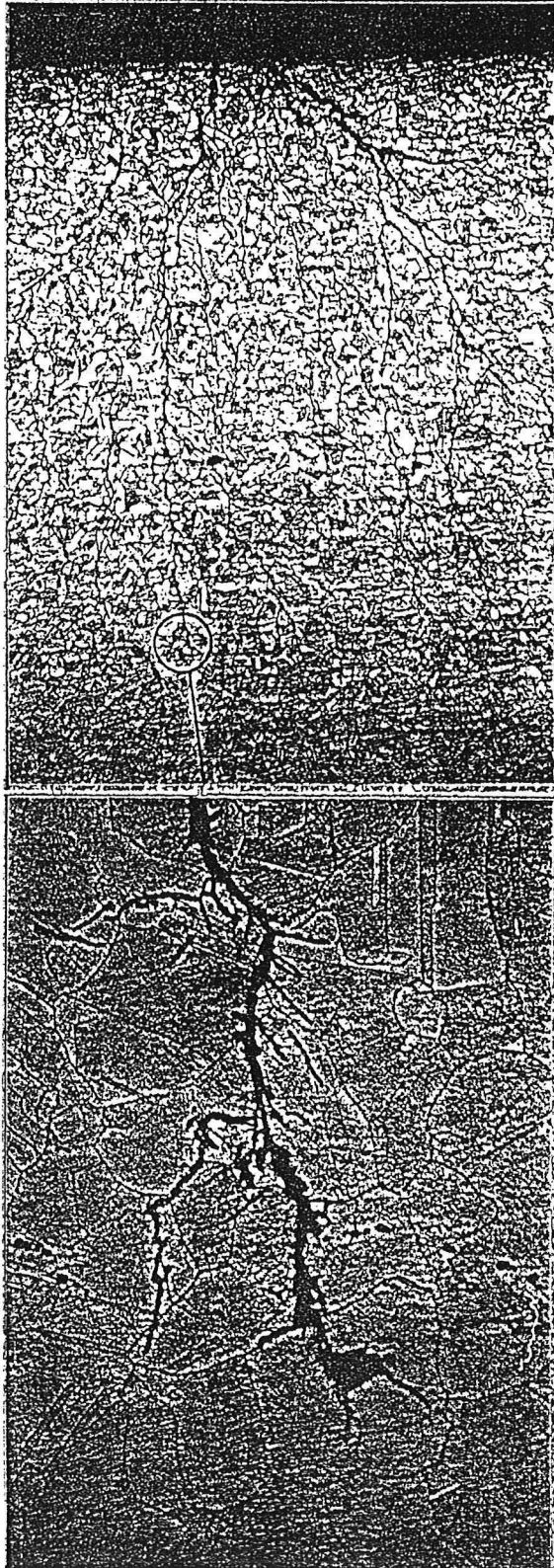
Towards
internal
surface

20X

Fig 18 One typical
branching crack
found on face A.



200X



External
surface

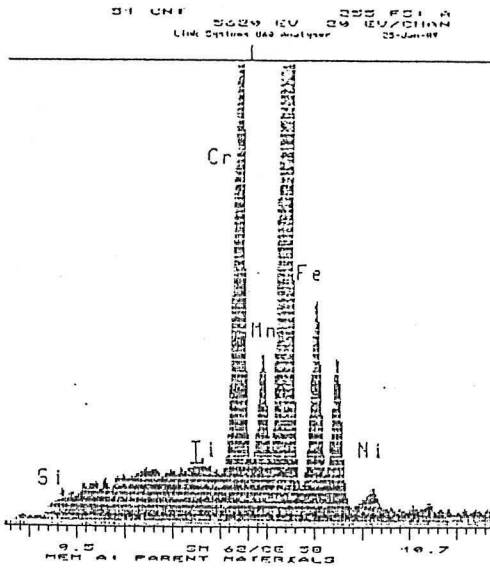
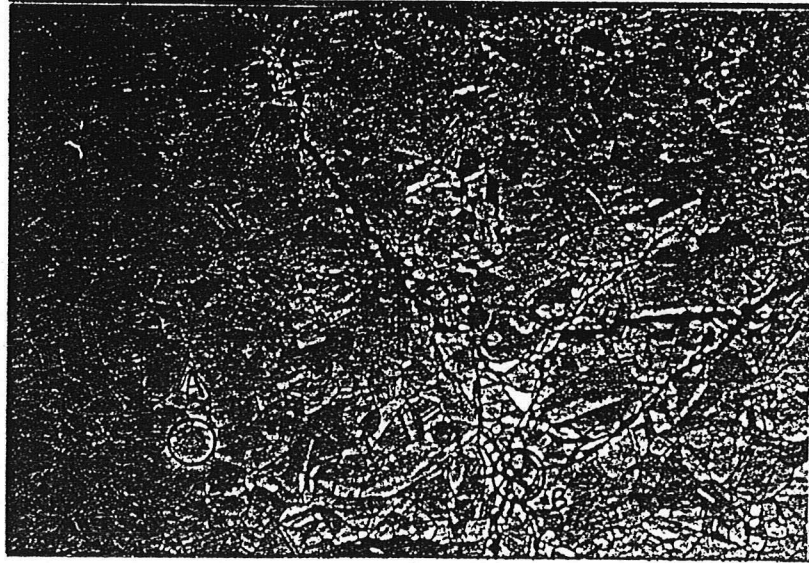


Towards
internal
surface

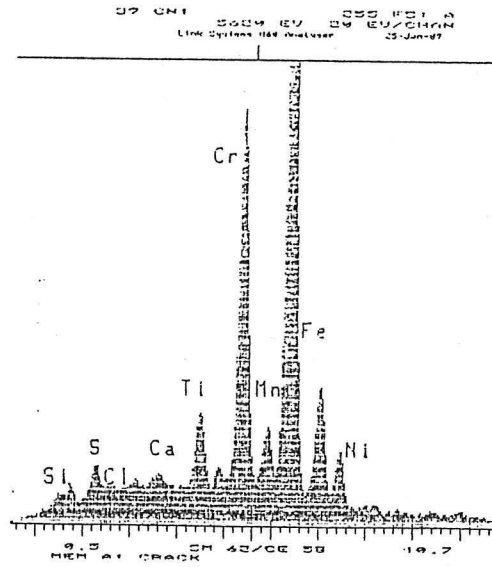
20X

Fig 19 One typical
branching crack
found on face B.

200X



Location A



Location B

Fig 20 EDS spectrum on parent materials (area A) and crack location (area B).

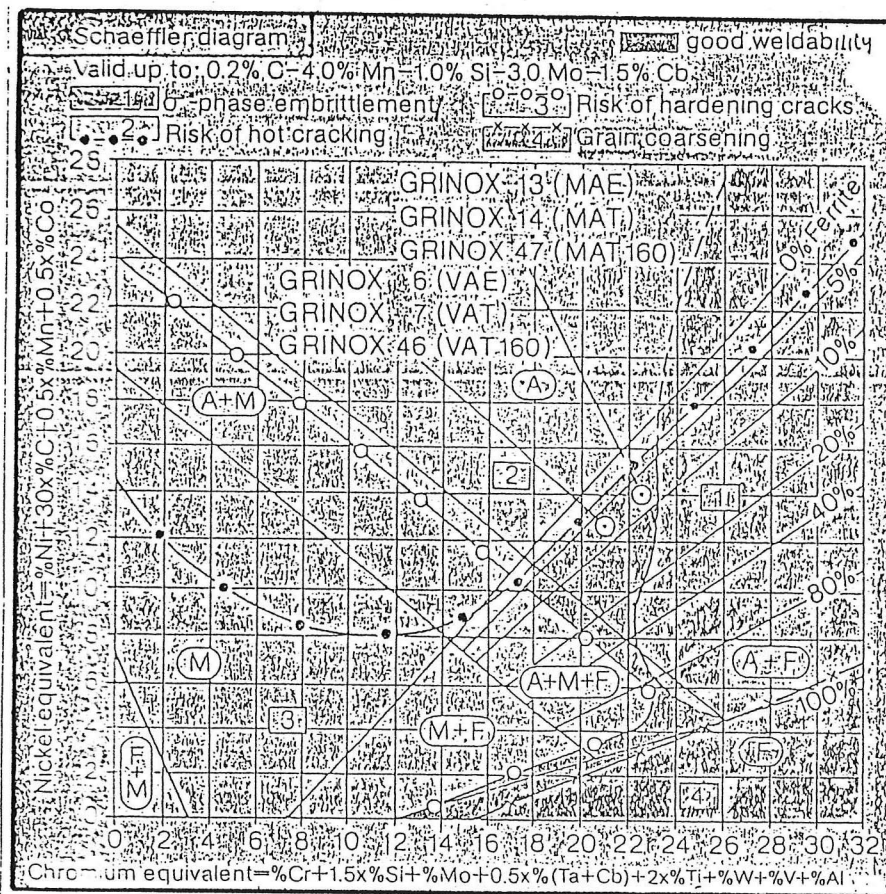
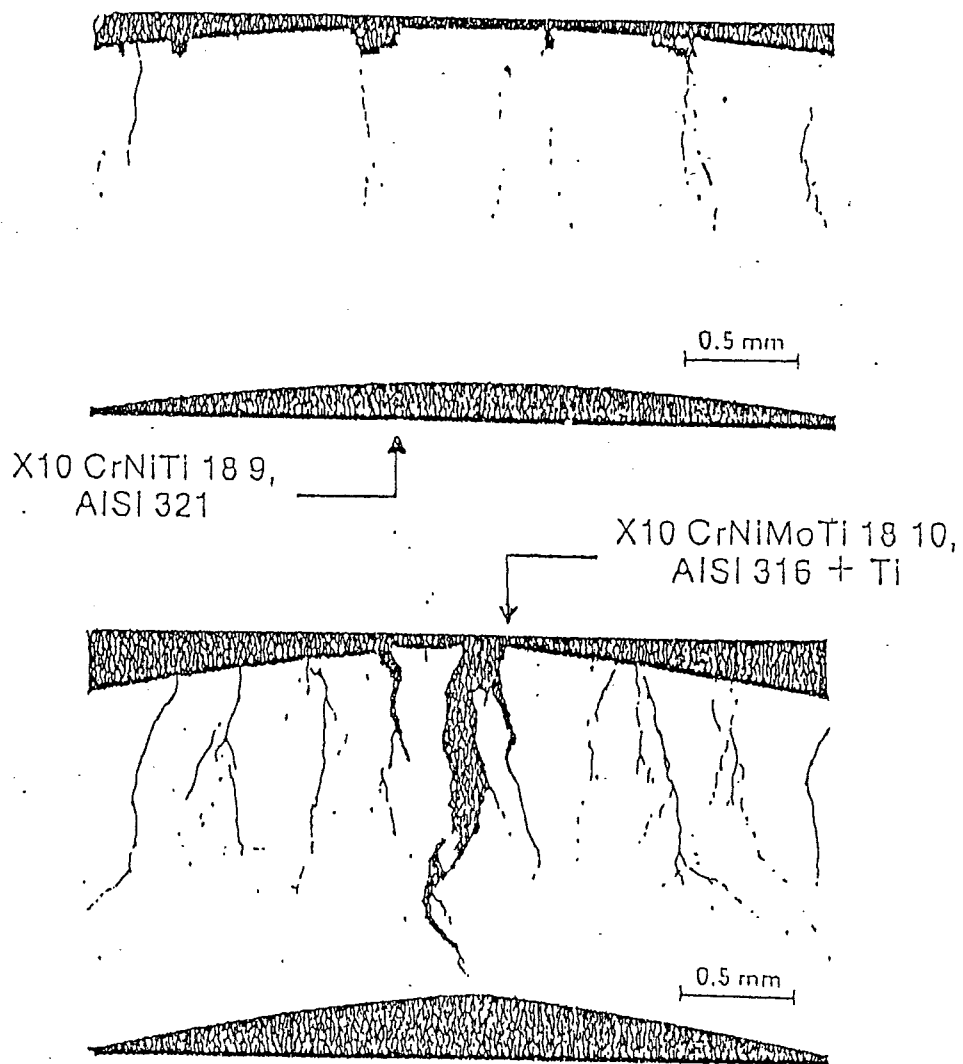
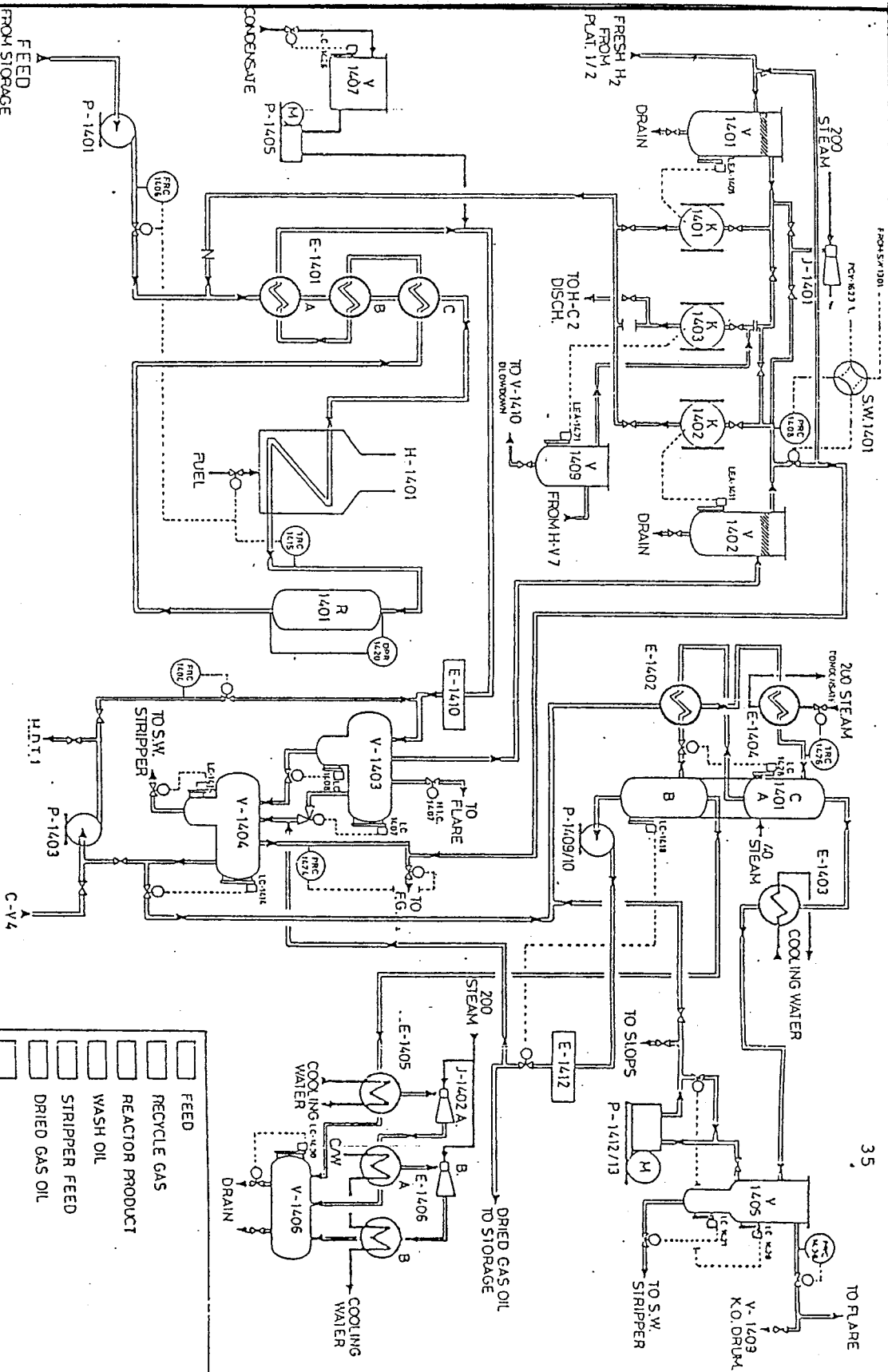


Figure 21. Schaeffler Diagram



SCC Conditions: Autoclave, 150 C (300 F),
70 ppm O_2 , Exposure Time 8 Days

Figure 22. Stress Corrosion cracking in 0.02% aqueous NaCl at pH 2.



- FEED
- RECYCLE GAS
- REACTOR PRODUCT
- WASH OIL
- STRIPPER FEED
- DRIED GAS OIL

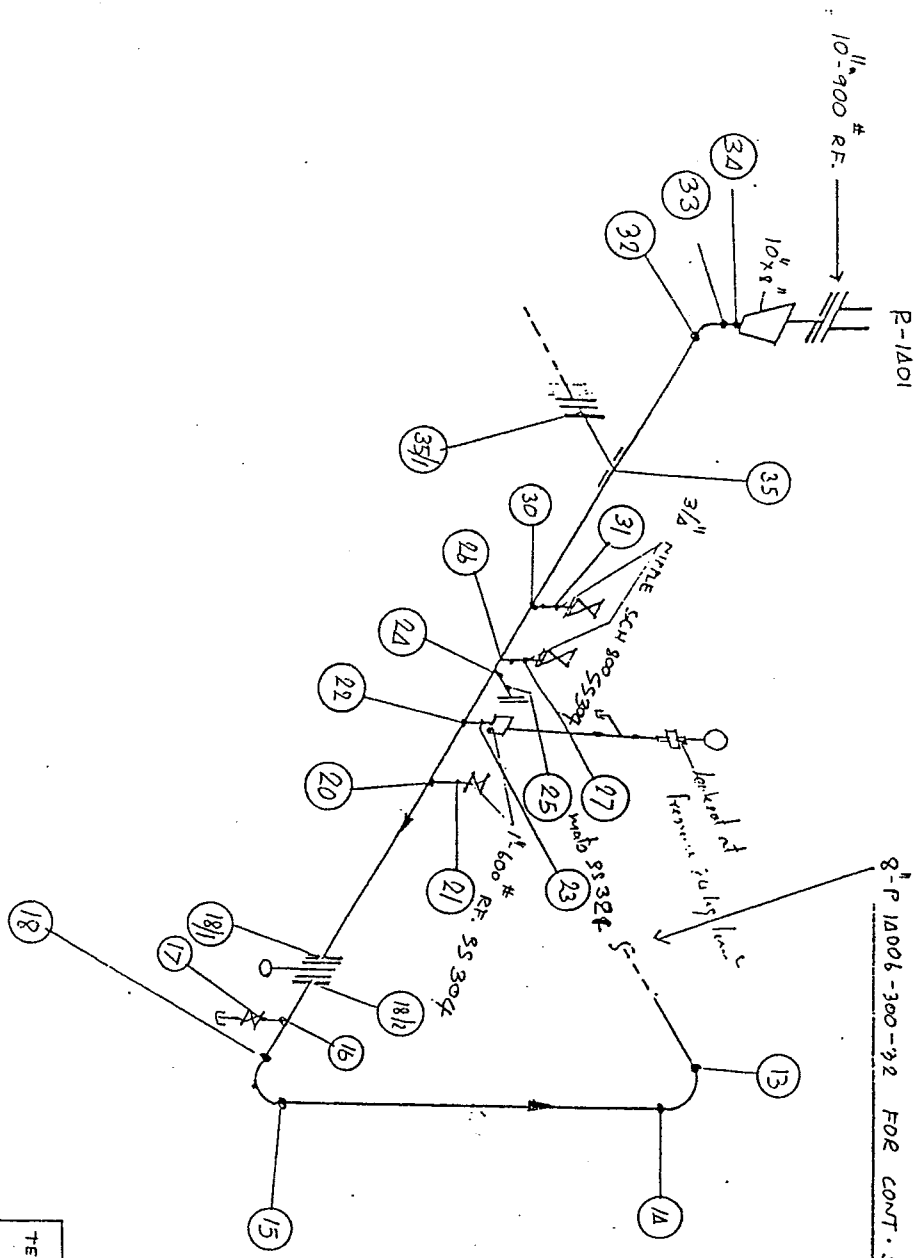
Appendix 1

NO.	DATE	REVISION	BY

DATE	APPROVED	THE THAI OIL REFINERY CO., LTD.	THANACHA	THANACHA

DATE	SCALE	DRAWING NO.
7 Dec '82	SCALE	TRAINING - 1400

HYDROSULPHURISER

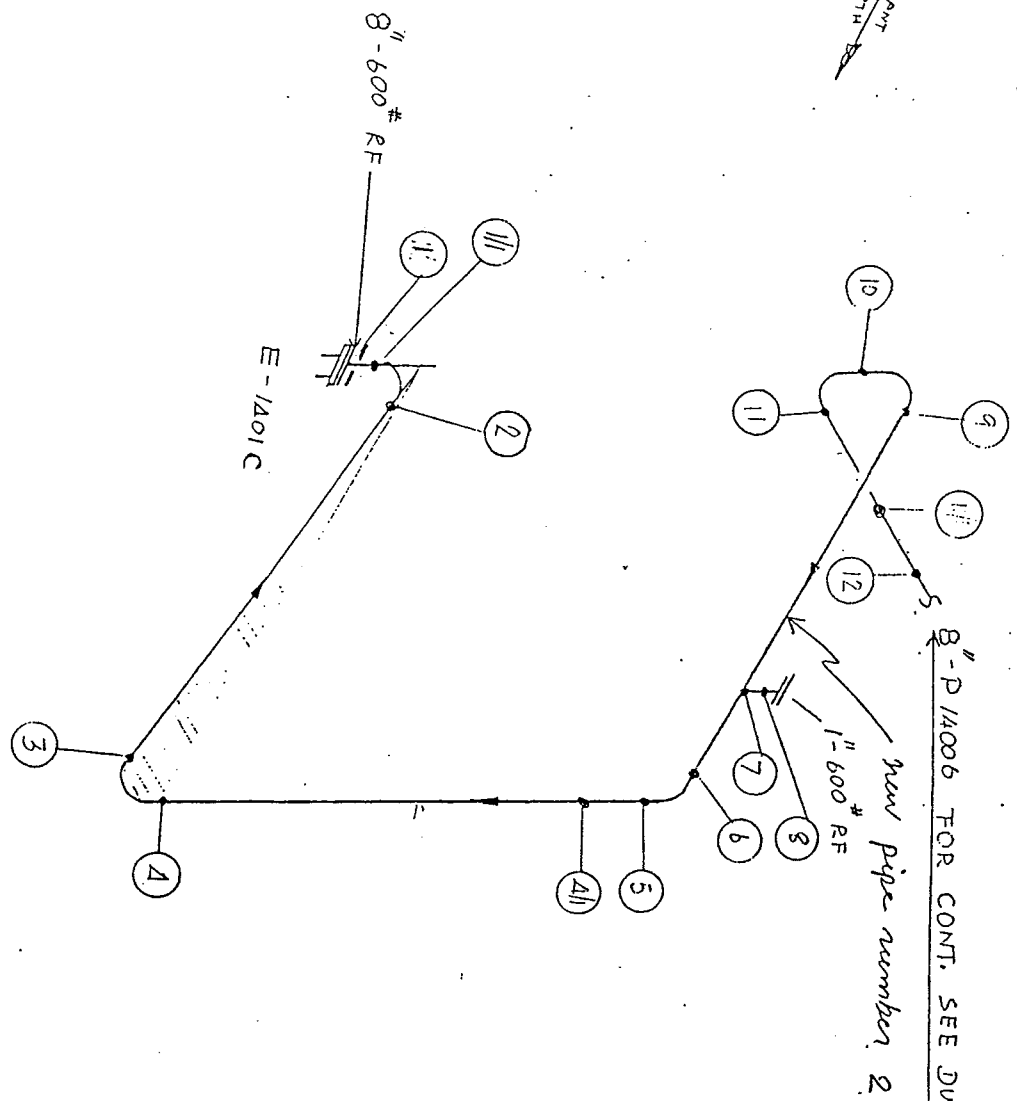


8" P 1A006-300-32 FOR CONT. SEE DWG, R 1738-10-11-19-J

Appendix 2a

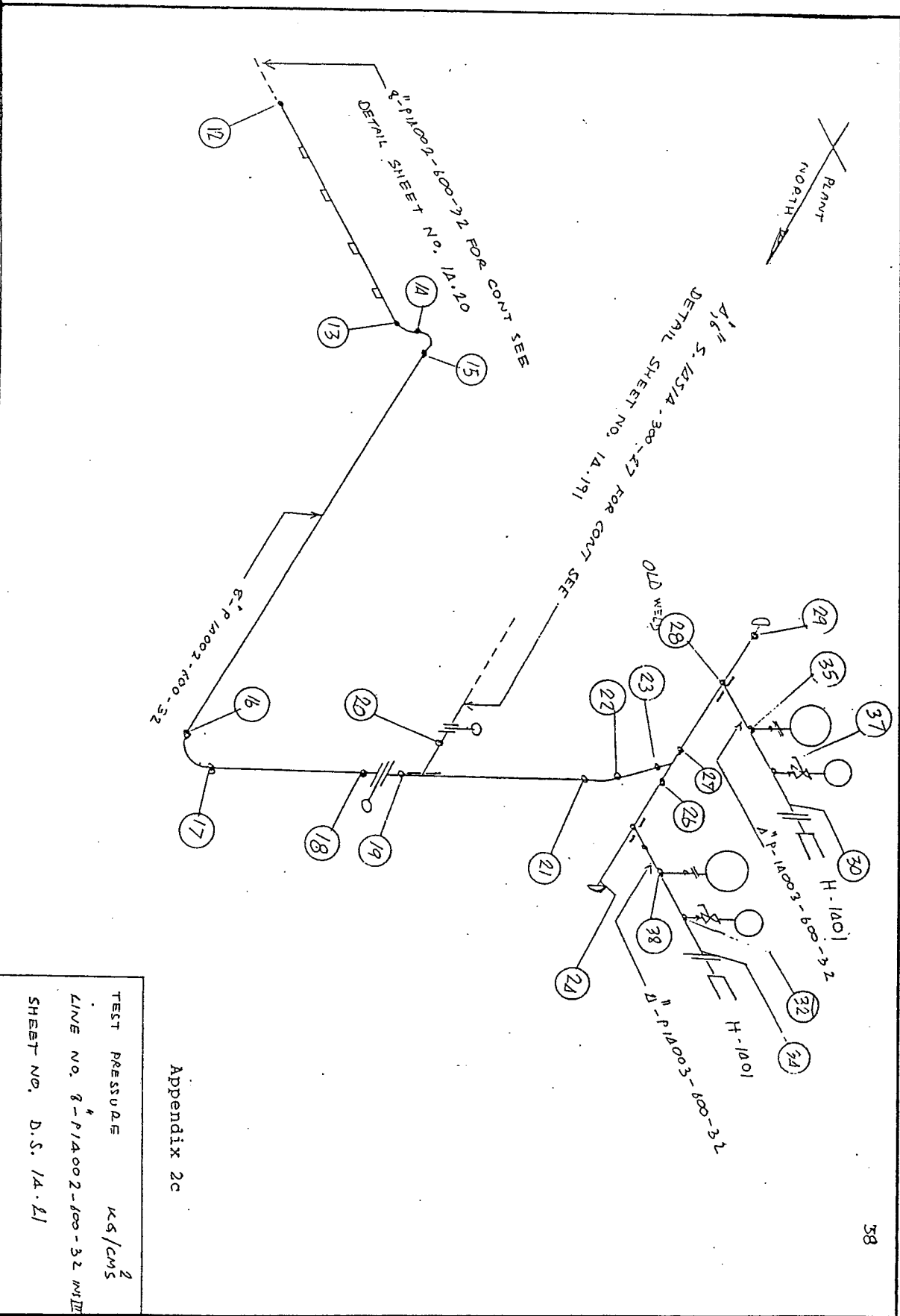
TEST PRESSURE	85.3 kg/cm ²
LINE NO.	8"-P1A006-300-32 INSTM
SHEET	D.S. 1A.05

PLAN
NORTH



Appendix 2b

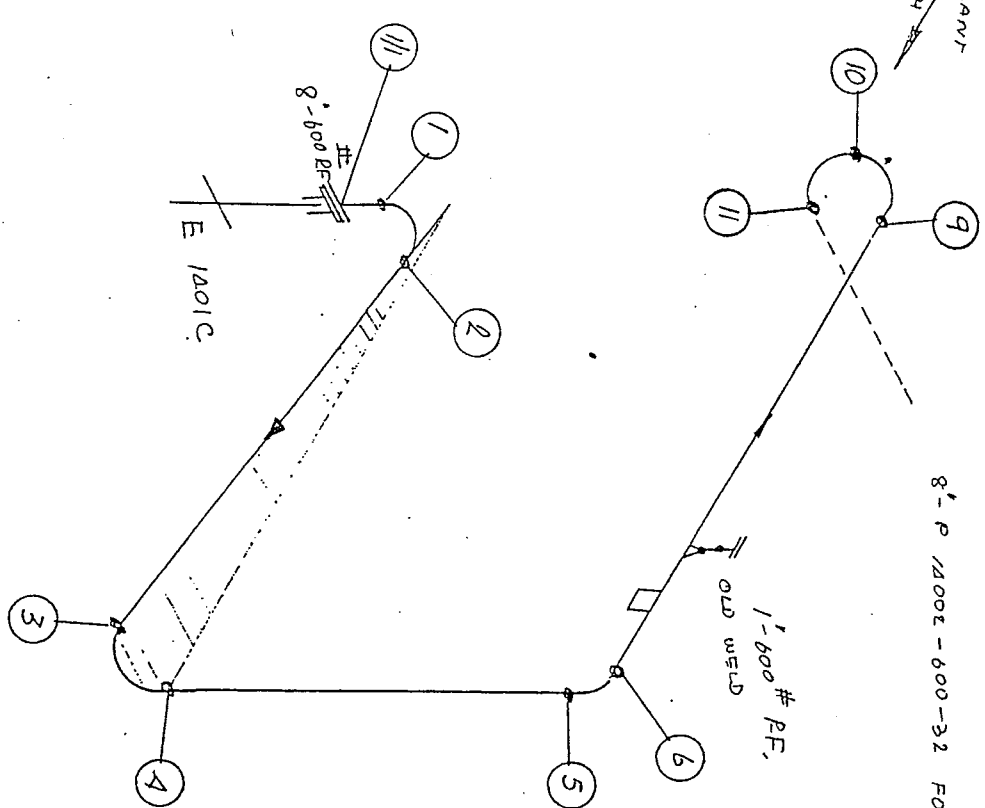
TEST PRESSURE	84 kg/cm ²
LINE NO.	8" P 1A006-600-32-1A
SHEET NO.	DS. 1A.06.



TEST PRESSURE 145 CM/S
 LINE NO. 8-P1A002-600-32 INT III
 SHEET NO. D.S. 1A.21

Appendix 2c

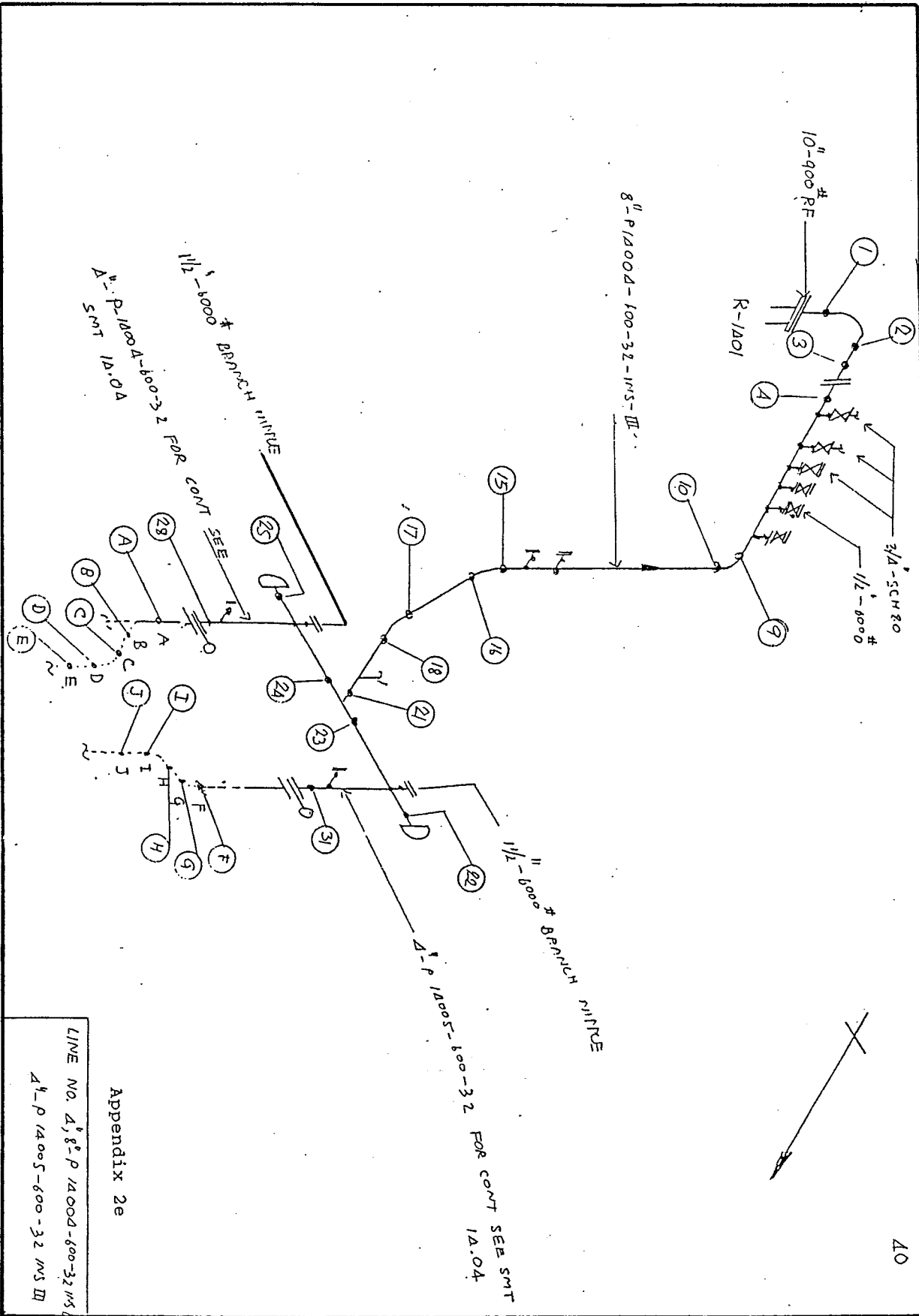
PLANT NORTH



8-1 P 12002-600-32 FOR CONT. SEE DETAIL SHEET NO. 16.21

Appendix 2d

TEST PRESSURE kg/cm^2
 LINE NO. 8'-P12002
 SHEET NO. DS. 12.20



Appendix 2e

LINE NO. 4, 8" P 1400D-100-32 1MS III
 4" P 1400S-100-32 1MS III

Using of Amino tri(methylene phosphonic acid) and 1 - hydroxyethylene
-1,1-diphosphonic acid as chemical cleaning on condenser tube.

K.Chudthong.

Dept. of Chemical Analysis, Electricity Generating Authority of Thailand

Abstract

Organic polyphosphonic acids are usually strong chelating agents and react with iron or copper oxide to be complexes compounds. The condenser scale at Krabi power station was composed of copper, iron and some metals, which were impurity in Aluminum brass. The cleaning chemical would be recirculated for a long time more than 12 hours, while MBT. added in process to be copper corrosion inhibitor. The deposits were removed about 80 % in form of iron oxide and copper oxide.

I. Introduction

Amino tri (methylene phosphonic) acid and 1-hydroxyethylene-1,1-diphosphonic acid are organic polyphosphoric acid. Its water soluble salt, polyphosphonate, have been thermal and chemical stability with C-P bond. So they are suitable to become dispersant or corrosion inhibitor in cooling water system. Since these compounds readily form stable complexes with many cations such as iron and copper ions, it was applied to be cleaning chemicals for metals oxide scale. Especially, some chelating agents may be added to cooperate in process.

In case of the operated condenser all content foulants are consists of organics and inorganics compounds. Hence, cleaning chemical types should be selected depend on foulants compositions to illustrate as in table I.. The chemical structures are shown as in figure I..

Addition to chemical composition of seale are consists of

Iron oxide	as Fe_2O_3	24.1 %
Copper oxide	as CuO	52.2 %
Other		23.7 %

Hence, the cleaning chemicals would recommend to be mixing chelating chemicals which are amino tri (methylene phosphonic acid) and 1-hydroxyethylene-1,1-diphosphonic acid. Actually, the cleaning chemicals should be operated with corrosion inhibitors.

The tested turbine condenser has been once through cooling system at water flow rating to be 5,500 tons per hour. The condenser tube made by admiralty brass and aluminum brass and tube sheet made by noval brass. However, this turbine condenser was operated more than one year metal surfaces were coated by some foulant and metal oxides.

II. Procedure

Tolyl Triazole was selected to be copper corrosion inhibitor and prepared as solution concentrating about 50 mg/l. This solution was recirculated more 30 minutes for film forming on bare metal surface. Amino tri (methylene phosphonic acid) and 1-hydroxyethylene-1, 1-diphosphonic acid were added continuously in concentrating about 1,000 mg/l after first recirculation step. The cleaning solution was recirculated until iron and copper concentration in cleaning solution were constant which chemical composition analysis had been done continuously between process operation. However the cleaning solution should be recirculated at least 12 hours, the chemical had reacted with metal oxide completely. When process was operated continuous, the pH of solution must be controlled between 4.5 - 5.0 with sulfamic acid and sodium hydroxide. The chemical parameter was interested to be pH turbidity conductivity, iron and copper ions which had indicated scale removal capability. When the process had arrived to finish, the continuous flushing was beginning. The drainage are always adjust the pH

with sodium hydroxide before leave its. Between the continuous flushing process are operating, turbidity has been checked on time. When turbidity was constants, the solutions had been drained to neutralizing pit. And fill up fresh water were second water flushing. Final process are passivated with tolyl triazole to concentrate about 40 ppm and recirculating at 30 minute.

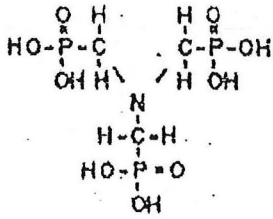
III. Result and Discussion

Condenser tubes before cleaning and after cleaning are shown in figure 2 and 3. Removal scales are Fe_2O_3 in quantity 2.49 kgs. and Cu_2O in quantity 3.37 kgs. which is 80 % of all scale. However the foulants are removed in form of colloids and become as turbidity. Some ions concentration are presented in figure 4, copper metals are eluted to solution as copper ion which are rapidly increased in the final. Actually, iron scale are soluted after recirculating in more than 2 hrs and increasing on slowly rate until it is constant at 60 ppm. The result is presented that some corrosion are created during the process are in operation. Hence, corrosion inhibitor should be added to concentration of 50 ppm.

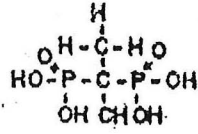
IV. Bibliography.

1. T. Notoya and T. Ishikawa, 4th Asian - Pacific Corrosion Control Conference, May 26 - 31, 1965, P. 982 -988
2. L. Show-chum, and et al., 4th Asian - Pacific Corrosion Conference, May 26-31, 1965, P. 1013-1019
3. Z. Wang and X. Shou-Chang, 4th Asian - Pacific Corrosion Control Conference, May 26-31, 1965, P. 1020
4. J,W.Macoy, Industrial Chemical Cleaning, 1984, Chemical Publishing Co.N.Y.
5. L.L. Shreir, Corrosion, 1979 Newnes - Butterworths, London.
6. P.A.Thomas, J.S.Beecher, and J.R.S Stinger, Cleaning and Passivating Open Recirculating Cooling Water System, 43th International Water Conference, 1982 pp. 533-544

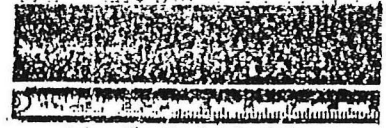
Figure 1 - Illustration of AMP and HEDP Structure Formula



AMP
Ammonium tri(methylene phosphonic acid)



HEDP
1-hydroxyethylidene-1,1-diphosphonic acid



ใช้สารเคมีแต่ไม่ได้อ่าง

Figure 2 - Tube before cleaning

TABLE 1 CLEANING PROCEDURE SUMMARY

TYPE OF FOULANT	CHEMICAL REQUIREMENTS	pH	MONITOR
MICROBIOLOGICAL, BIL	CHLORINE - 2.0 ppm FAC.	6 - 7	CHLORINE LEVEL, SUSPENDED SOLIDS, MICROBIAL COUNTS
IRON OXIDES	NTA - 1000 ppm TOTAL EDTA AMP OR HEDP	4.5	IRON
CALCIUM CARBONATE, CALCIUM SULFATE	NTA - 250 ppm AMP - 100 ppm PMAORFA - 250 ppm	4.5	CALCIUM
CALCIUM PHOSPHATE	AMP - 500 ppm PMA - 500 ppm NTA - 500 ppm	4.5	CALCIUM, PHOSPHATE
SUSPENDED SOLIDS	AQUIONIC POLYMER 100 ppm	7.0	SUSPENDED SOLIDS TURBIDITY

NOTE: LEVELS OF CLEANING CHEMICALS ARE GIVEN IN PPM ACTIVE MATERIAL.

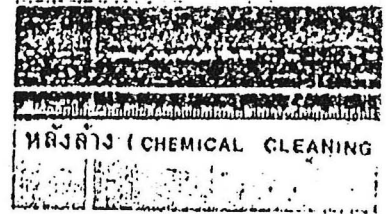
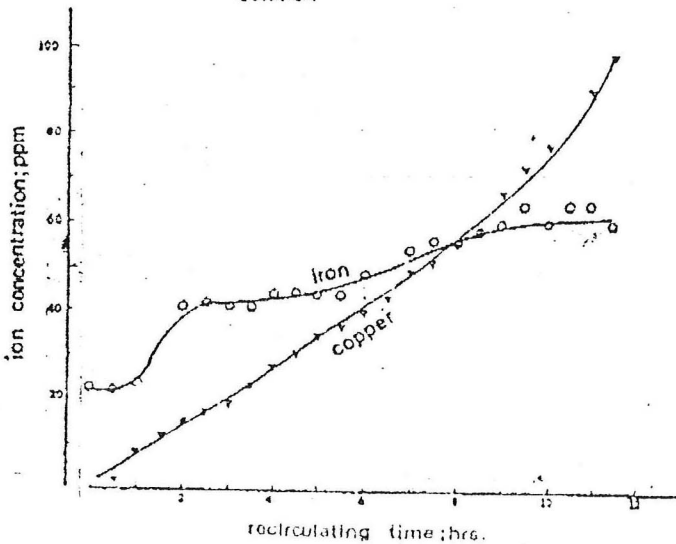


Figure 3 - Tube after cleaning

Figure 4 illustration of ion concentration in cleaning solution



620.193:620.197

29000

A8

ASEAN - JAPAN COOPERATION ON
MATERIALS SCIENCE & TECHNOLOGY.
SEMINAR ON CORROSION AND PROTECTION
(1990 ; BANGKOK).

CORROSION AND PROTECTION : A SEMINAR
HELD IN BANGKOK, 17-19 OCTOBER 1990.

620.193

:620.197

A8

ศูนย์บริการเอกสารวิจัยฯ



BE29000

Corrosion and